The physics of black-hole microstates : what is the fate of the horizon?

Yixuan Li

université
PARIS-SACLAY

The physics of black-hole microstates: what is the fate of the horizon?

La physique des micro-états de trous noirs : quelle destinée pour l'horizon ?

Thèse de doctorat de l'université Paris-Saclay

École doctorale n° 564 : physique en Île-de-France (PIF)
Spécialité de doctorat: Physique
Graduate School : Physique, Référent : Faculté des sciences d'Orsay

Thèse préparée à l'**Institut de Physique Théorique** (Université Paris-Saclay, CNRS, CEA),
sous la direction de **Iosif BENA**, Directeur de Recherche

Thèse soutenue à Paris-Saclay, le 2 juin 2022, par

Yixuan LI

Composition du jury

Dieter LÜST Professeur, Max-Planck Institute for Physics & Ludwig-Maximilian University of Munich	Président
Rodolfo RUSSO Professeur Associé, Queen Mary University of London	Rapporteur & Examinateur
Ángel URANGA Professeur de Recherche, CSIC/Autonomous University of Madrid, Instituto de Física Teórica	Rapporteur & Examinateur
Monica GUICA Ingénieure de Recherche CEA, Université Paris-Saclay, CNRS, CEA, Institut de Physique Théorique	Examinatrice
Emil MARTINEC Professeur, University of Chicago, Kadanoff Center for Theoretical Physics & Enrico Fermi Institute	Examinateur
Ruben MINASIAN Directeur de Recherche CNRS, Université Paris-Saclay, CNRS, CEA, Institut de Physique Théorique	Examinateur
Eran PALTI Professeur Associé, Ben-Gurion University of the Negev	Examinateur
Iosif BENA Directeur de Recherche CEA, Université Paris-Saclay, CNRS, CEA, Institut de Physique Théorique	Directeur de thèse

THESE DE DOCTORAT
NNT : 2022UPASP050

université PARIS-SACLAY | ÉCOLE DOCTORALE Physique en Île-de-France (PIF)

Titre: La physique des micro-états de trous noirs: quelle destinée pour l'horizon?
Mots clés: Théorie des Cordes, Trous noirs, Supergravité, Paradigme des Fuzzballs, Géométries de micro-états

Résumé: Les trous noirs sont des objets astrophysiques qui se forment par l'effondrement gravitationnel d'étoiles supermassives. Elles peuvent être décrites par des solutions de la Relativité Générale (RG) : l'horizon indique l'endroit à partir duquel rien ne peut échapper. Les considérations de la mécanique statistique montrent que le trou noir a une entropie proportionnelle à l'aire de son horizon. Cependant, la RG n'a pas assez de degrés de liberté pour décrire les micro-états qui représentent l'entropie du trou noir. La théorie des cordes fournit une description des micro-états en tant qu'états liés de branes à faible couplage de cordes.

À fort couplage, l'hypothèse des Fuzzballs s'attend à ce qu'individuellement, les micro-états de trou noir diffèrent de la solution de trou noir à l'échelle de l'horizon. Cette hypothèse introduit un changement de paradigme : puisque l'on ne devrait plus se fier à notre intuition issue de la RG, les micro-états de trous noirs pourraient ne pas avoir d'horizon. Motivée par la construction en Supergravité de solutions similaires aux trous noirs et sans horizon – les géométries de micro-états –, l'hypothèse de Fuzzball a également l'avantage de résoudre, presque par définition, le paradoxe de l'information de trou noir et le problème de la singularité de trou noir. Cette thèse vise à étudier plusieurs aspects de l'hypothèse des Fuzzballs et des géométries de micro-états.

Title: The physics of black-hole microstates: what is the fate of the horizon?
Keywords: String Theory, Black holes, Supergravity, Fuzzball paradigm, Microstate geometries

Abstract: Black holes are astrophysical objects formed from the gravitational collapse of supermassive stars. They can be described by solutions in General Relativity (GR): the horizon indicates the locus from which nothing can escape. Considerations from Statistical Mechanics show that the black hole has an entropy proportional to the area of its horizon. However, GR does not have enough degrees of freedom to describe the microstates accounting for the black-hole entropy. String Theory on the other hand, provides a description of the microstates as brane bound-states at weak string (and gravitational) coupling.

At strong gravitational coupling, the Fuzzball hypothesis expects the individual black-hole microstates to differ from the black-hole solution at the scale of the horizon. It introduces a paradigm shift: Because one should not rely on its intuition from GR, black-hole microstates may not have a horizon. Motivated by the construction of black-hole-like horizonless solutions in Supergravity – the microstate geometries –, the Fuzzball hypothesis has also the advantage to solve, almost by definition, the black-hole information paradox and the problem of the black-hole singularity.

This thesis aims to study several aspects of the Fuzzball hypothesis and of microstates geometries. In particular we will:
1) introduce the Fuzzball hypothesis and some of its main challenges.
2) investigate the notion of distance on the space of solutions of a class of microstate geometries – the bubbling solutions.
3) analyse a family of non-supersymmetric extremal black holes and their horizonless microstate geometries in four dimensions, and compute the gravitational multipole structure.
4) compute the tidal effects on a string following infalling null geodesics in a family of black hole microstate geometries – the superstata.
5) construct solutions with zero horizon area that have the same charges as a three-charge F1-NS5-P Type-IIA black hole and preserve the black hole's spherical symmetry.

Acknowledgments

First and foremost, let me thank Iosif for being my PhD supervisor. My PhD journey has been scientifically really fascinating, and this is largely thanks to Iosif, who taught me so much interesting physics that I had not even previously dreamt of. Iosif always managed invent enthralling projects that were tailored to my knowledge and my level, even at the start of my PhD. I would like thank Iosif for having encouraged me to write my first paper in the field as a single-author paper. The task was not easy but as a result I gained much autonomy and confidence. Thanks to Iosif, I felt like that my lack of knowledge in the field was not always a handicap; that despite all my shortcomings, I can contribute to physics at my level. Besides, Iosif always encouraged me to set high objectives that seemed impossible. But he could also communicate his belief that the objective was possible; thanks to that I always surpassed myself and achieved things that I thought I couldn't. Finally, I am also grateful to Iosif for his support during the whole postdoc application time, thanks to which I did not experience too much pressure.

I would like to thank Monica Guica, Dieter Lüst, Emil Martinec, Ruben Minasian, Eran Palti for having accepted to be part of my PhD defense committee, and more particularly Rodolfo Russo and Ángel Uranga for also taking the "rapporteur" role. I would like to thank Ángel for everything he has taught me, back in Madrid before I started my PhD.

I would like also to thank the numerous collaborators I had and still have the chance to work with. I would like to thank (in the chronological order of collaborations): Daniel Mayerson for helping me to understand a lot of things in the field in the first phase of my PhD; Pierre Heidmann for being a really efficient collaborator; Ibou Bah for showing us rigour and high standards: I appreciated a lot all Ibou's insights. Next thanks go to Nejc Ceplak and Shaun Hampton for having completed two papers together, including one during Covid and lockdown times. I have learned really much with Shaun and Nejc. I appreciated every single blackboard discussion we had together; we make a great "optimistic-neutral-pessimistic" team. Additional thanks go to Nick Warner and Dimitris Toulikas, with whom we completed one of the most interesting projects I ever had. I would really like to thank Nick for organising a regular sub-group meeting in Covid times; I learned so much from Nick and Iosif's insights during these meetings.

I have really been lucky to complete my PhD at IPhT, where I met so many people in my field. I am grateful to the permanent members of the String Theory group – Iosif, Mariana Graña, Monica Guica, Ruben Minasian, Eric Perlmutter and Nick Warner – to have brought so many postdocs and students into the group. In the a rough chronological order: Ruben Monten, Severin Lüst, Adam Bzowski, Pierre Heidmann, Lilian Chabrol, Yi Zhang, Lucía Córdova, Ana Garbayó Peón, Daniel Mayerson, Ander Retolaza, Eva Llabres, Chiara Toldo, Gabriele Lo Monaco, Andrea Galliani, Alessandro Bombini, Felicity Eperon, Valentí Vall Camell, Anthony Houppe, Peng

Cheng, Bernardo Fraiman, Stavros Mougiakakos, Robert Walker, Peter Weck, Alvaro Herraez, Shaun Hampton, Bogdan Ganchev, Dimitris Toulikas, Callum Brodie, Nejc Ceplak, Nicolas Kovensky, Héctor Parra de Freitas, Silvia Georgescu, Gabriele Di Ubaldo, Hynek Paul, Veronica Collazuol, Antoine Bourget, Soumangsu Chakraborty, Bin Guo, Himanshu Raj, Yiannis Tsiares and Etienne Ligout. I hope I haven't forgotten anyone. Thank to the 48 people of this paragraph – who are not only colleagues, but also friends –, I enjoyed every single day I spent at the Institute (even though I need a two-hour round trip to get there), I always learned something, whether it was about physics or anything else.

I am thankful to the administration, IT team and head of IPhT, especially: Loïc Bervas, Emmanuelle De Laborderie, Camille Flouret, François Gelis, Philippe Girault, Maxime Leroy, Caroline Meysson, Grégoire Misguish, Catherine Pépin, Laure Sauboy and Laurent Sengmanivanh (who saved me so many times with computer problems).

It has been a great pleasure teaching at the Physics Department at Paris-Saclay University. I would like to thank all the colleagues I collaborated with for this purpose: Gilles Abramovici, Mireille Bordelais, Witse Herreman, Daniele Nutarelli, Evangelos Papalazarou, Loëva Remita and Jacques Robert.

With conferences, "summer" schools and other activities linked to research, I also met quite a lot of fellow PhD students and early postdocs, and quite a lot of them turned out to be good friends. From Paris: François Rondeau, Grégoire Josse, Vassilis Papadopoulos, Carlo Branchina, Giulia Isabella, Wenqi Ke, Dongsheng Ge, Yorgo Pano; from Madrid: Ginevra Buratti, José Calderón, Florent Baume, Michael Fuchs, Llorenç Espinosa Portalés, Max Wiesner, Walter Riquelme, Joan Quirant; from elsewhere: Vincent Van Hemelryck, Vasko Dimitrov, Damian Van De Heisteeg, Koen Stemerdink, Johannes Lahnsteiner, Dora Nikolakopoulou, Evita Verheijden, Carlos Duaso Pueyo, Tomas Reis, Cesc Cunillera, Bruno Balthazar, and many more.

I would like to thank my parents, for the education they gave me, for their courage to have ventured in a foreign country and for always having encouraged me in the professional path I want to follow.

Finally, I would like to thank Ioana, for all her support, for all her tenderness, for her happiness and the happiness she brings to me; for being part of my simple life – and being simply my life.

Publications

Published papers

- **Black holes and the swampland: the deep throat revelations,**
  Yixuan Li
  JHEP 06 (2021) 065, [arXiv:2102.04480]

- **Gravitational footprints of black holes and their microstate geometries,**
  I. Bah, I. Bena, P. Heidmann, Y. Li, D. Mayerson
  JHEP 10 (2021), 138, [arXiv:2104.10686]

- **Toroidal tidal effects in microstate geometries,**
  N. Ceplak, S. Hampton and Y. Li
  JHEP 03 (2022) 021, [arXiv:2106.03841]

Preprints

- **An Alliance in the Tripartite Conflict over Moduli Space,**
  Yixuan Li
  [arXiv:2112.03281].

- **Resolving Black-Hole Microstructure with New Momentum Carriers,**
  I. Bena, N. Ceplak, S. Hampton, Y. Li, D. Toulikas and N. P. Warner
  [arXiv:2202.08844].

Contents

Chapter 0

Introduction en Français

0.1 L'énigme des trous noirs

Les trous noirs sont des objets astrophysiques formés à partir de l'effondrement gravitationnel d'étoiles supermassives. Elles peuvent être décrites par des solutions en Relativité Générale : l'horizon indique le lieu d'où rien ne peut s'échapper.

Dans les années 1970, la découverte que le trou noir est un objet statistique a été une percée qui allait changer dans les décennies suivantes notre compréhension de la Relativité Générale et de la mécanique quantique. En effet, le trou noir, en tant que solution de la Relativité Générale, suit des lois thermodynamiques [1,2]. On peut donc lui associer une température et une entropie thermodynamique (l'entropie de Bekenstein-Hawking), cette dernière étant proportionnelle à la surface de l'horizon, A_H [3,4]:

$$S_{\text{Bekenstein}-\text{Hawking}} = \frac{A_H}{4G_N}\,, \tag{0.1.1}$$

où G_N est la constante de Newton, et où nous prenons des unités comme $c = \hbar = k_B = 1$.

La température du trou noir vient du fait que lorsque l'on applique la théorie quantique des champs sur un fond de trou noir, le calcul de Hawking [5] montre que le trou noir est un corps noir qui radie à une certaine température T. Ainsi, l'analogie avec les lois thermodynamiques ne peut donc pas être considérée comme une simple coïncidence : *Le trou noir a (physiquement) une température ; c'est d'ailleurs une machine thermique, caractérisée notamment par une entropie, et elle satisfait aux lois de la thermodynamique comme tout autre système thermodynamique !*

En tant qu'objet statistique et thermique, le trou noir soulève de nombreuses questions. Énumérons les trois principales énigmes concernant les propriétés de gravité quantique des trous noirs.

1. **L'origine microscopique de l'entropie du trou noir.**

   Quels sont les degrés de liberté microscopiques qui caractérisent les micro-états individuels des trous noirs? Et à quoi ressemblent les micro-états responsables de l'entropie du trou noir? (0.1.2)

2. Le paradoxe de l'information du trou noir.

L'entropie du rayonnement sortant suit-elle la courbe de Page, comme le préconise l'unitarité ? Si oui, quel processus induit ce phénomène ? (0.1.3)

3. La singularité du trou noir.

Quels sont les degrés de liberté permettant de résoudre la singularité du trou noir ? Et si ces degrés de liberté se trouvent au voisinage de la singularité, comment l'horizon – qui se situe dans son passé causal – est-il au courant de ces degrés de liberté, comme le suggère la formule de Bekenstein-Hawking (0.1.1)? (0.1.4)

0.2 Trous noirs en théorie des cordes, fuzzballs et géométries de micro-états

0.2.1 La réponse de la théorie des cordes à la question de l'entropie

En tant que théorie de la gravité quantique, la théorie des cordes devrait fournir une réponse aux énigmes des trous noirs de la section précédente.

L'idée de base de la théorie des cordes est que les particules élémentaires (comme l'électron, le photon, les quarks, etc.), que nous considérons généralement comme ponctuelles, sont en fait différents modes de vibration d'un objet fondamental étendu : la corde. Un avantage d'avoir des cordes au lieu de particules ponctuelles est que toutes les divergences UV possibles dans les amplitudes de diffusion en physique des particules sont automatiquement apprivoisées. En particulier, les divergences impliquant le graviton sont résolues par l'invariance conforme de la feuille d'univers (*world-sheet*) de la corde, ce qui fait de la théorie des cordes une théorie UV-complète de la gravité quantique.

Les cordes en théorie des cordes peuvent être fermées ou ouvertes. Les cordes fermées et les cordes ouvertes génèrent différents spectres de champs. L'oscillation des cordes fermées génère notamment le graviton, alors que les cordes ouvertes génèrent par exemple des champs vectoriels dans leur spectre sans masse. Les cordes fermées sont des boucles de cordes se terminant sur elles-mêmes, alors que les extrémités des cordes ouvertes se terminent sur des solutions solitoniques de la théorie des cordes : les D-branes.

La théorie des cordes est une théorie perturbative de la gravité quantique, dependant en deux paramètres : la longueur de la corde, l_s, et le couplage de cordes, g_s.

La longueur de la corde, l_s, vient du fait que la corde fondamentale a une tension, τ, qui peut être exprimée en termes de longueur, la longueur de la corde :

$$\tau \equiv \frac{1}{2\pi\alpha'} = \frac{1}{l_s^2}\,. \tag{0.2.1}$$

La longueur de la corde, l_s, définit l'énergie à laquelle on mesurerait les modes harmoniques supérieurs de la corde : $M_s \propto \frac{1}{l_s}$. En revanche, si l'on sonde les cordes à une énergie $E \ll M_s$, on ne sonderait que les modes sans masse de la corde et on ne verrait pas la partie du

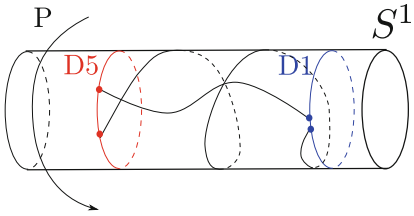

Figure 1 – Représentation de cordes ouvertes s'étendant entre une brane D1 et une brane D5 dans le cercle y, S^1. La taille du tore T^4 est supposé paramétriquement plus petit que celui du cercle S^1_y, donc la physique est décrite par une corde D1-D5 effective dans S^1_y. L'image est issue de [6].

spectre correspondant aux modes massifs de la corde. Dans cette limite, on ne peut pas exciter d'oscillations sur les cordes et les cordes se comportent comme des particules ponctuelles.

Le couplage de la corde, g_s, contrôle l'expansion en genre de surface de la feuille d'univers de la corde. A basse énérgie, $E \ll M_s$, le nombre de trous dans ces diagrammes correspond au nombre de boucles dans les diagrammes de Feynman. De plus, le couplage de cordes définit la constante de Newton, G_N, en D dimensions:

$$G_N \propto g_s^2 \, l_s^{D-2} \, . \tag{0.2.2}$$

La réponse que fournit la théorie des cordes sur la première énigme des trous noirs est la suivante : En variant la constante de couplage des cordes g_s, on peut interpoler entre certaines configurations particulières de D-brane définies à $g_s N \ll 1$, et une solution de trou noir en supergravité définie à $g_s N \gg 1$. De plus, dans les configurations supersymétriques, en utilisant des théorèmes d'indice, on peut montrer que le nombre de micro-états est le même dans les deux régimes. Par conséquent, on peut apprendre beaucoup de choses sur les trous noirs (en supergravité) à partir de la physique des cordes ouvertes des D-branes.

En effet, l'entropie du trou noir est principalement donné par le nombre de possibilités pour les cordes ouvertes de s'étendre entre une D1-brane qui entoure N_1 fois le cercle et une brane D5 qui entoure N_5 fois, pour induire la charge de quantité de mouvement N_P. Voir Figure 1.

0.2.2 Le paradigme des Fuzzballs

Nous savons maintenant comment décrire les micro-états dans le régime des cordes ouvertes. Cependant, le trou noir est défini comme une solution de supergravité, et le paradoxe de l'information est pertinent dans le régime de validité de la supergravité. Nous pouvons maintenant reformuler notre question (0.1.2), que nous avons auparavant listée dans la section Section 1, sous la forme suivante:

> *Peut-on décrire les micro-états dans le régime de paramètres où la solution du trou noir est définie (i.e. dans le régime $g_s N \gg 1$)? dans quelle mesure et en quoi diffèrent-ils du trou noir?* (0.2.3)

Une hypothèse formulée pour répondre à cette question est la suivante:

L'hypothèse des Fuzzballs [7–11]
A $g_sN \gg 1$, les micro-états individuels des trous noirs diffèrent de la solution classique des trous noirs à l'échelle de l'horizon ; elles n'ont d'ailleurs pas d'horizon et pas de singularités. De tels micro-états sans horizon sont appelés "Fuzzballs".

La différence impliquée ici entre les micro-états et le trou noir est d'ordre de $\mathcal{O}(1)$, et non pas de l'ordre de $\mathcal{O}(e^{-S})$ ni de $\mathcal{O}(e^{-S/2})$. Cela doit être mis en contraste avec le point de vue naïf, où les micro-états ne diffèreraient de la solution du trou noir qu'au voisinage de la singularité.

L'hypothèse ci-dessus introduit un *changement de paradigme*. Parce que les micro-états et la solution classique du trou noir diffèrent d'une quantité non négligeable à l'échelle de l'horizon, on ne peut plus se fier à l'intuition de la Relativité Générale. En particulier, les micro-états de trous noirs peuvent ne pas avoir d'horizon, même si la relativité générale elle-même reste une bonne approximation à l'échelle de l'horizon.

Du point de vue de l'hypothèse des fuzzballs, les micro-états individuels n'ont pas d'entropie; par conséquent, ils n'ont pas d'horizon dans le régime de couplage fort ($g_sN \gg 1$).

De plus, cela n'a pas de sens de parler de l'intérieur du trou noir pour les micro-états du trou noir, car l'horizon est remplacé par une autre phase de la matière qui supporte l'effondrement gravitationnel qui conduirait à un trou noir.

Nous avons introduit l'hypothèse Fuzzball comme une réponse naturelle à la question sur les micro-états (0.1.2): *Les micro-états de trou noir sont des solutions sans horizon qui sont similaires à la solution de trou noir dans la région asymptotique, mais diffèrent de la solution de trou noir à l'échelle de l'horizon.* Ainsi, la réponse à la question de la singularité du trou noir (0.1.4) suit immédiatement: *L'expression "résoudre la singularité du trou noir" n'a pas de sens, car les micro-états du trou noir n'ont pas de singularité, et les degrés de liberté distinguant les micro-états se situent à l'échelle de l'horizon.*

À propos du paradoxe de l'information (0.1.3), l'absence d'horizon pour les micro-états des trous noirs change complètement le problème. La création de paires de particules de Hawking ne se produit pas avec une géométrie sans horizon. Au lieu de cela, le rayonnement du corps noir d'un fuzzball (non extrême) se produit comme celui d'une étoile ou d'un morceau de charbon [12]. Par conséquent, le processus d'évaporation est toujours unitaire et aucun paradoxe de l'information ne se produit. Le changement de paradigme introduit par l'hypothèse Fuzzball est de comprendre que la réponse à la question (0.1.2) peut impliquer que les questions (0.1.3) et (0.1.4) sont mal définies.

Afin de soutenir l'hypothèse des Fuzzballs, de nombreuses solutions sans horizon ont été trouvées dans la théorie des cordes. En particulier, le *Programme des Geometries de Micro-états* [13, 14] s'efforce de trouver des solutions sans horizon à la supergravité ; de telles solutions sont appelées *géométries de micro-états*. Voir Figure 2.

0.2.3 Contributions de ce manuscrit

Dans le Chapitre 1, nous présentons une introduction en anglais plus complète du sujet.

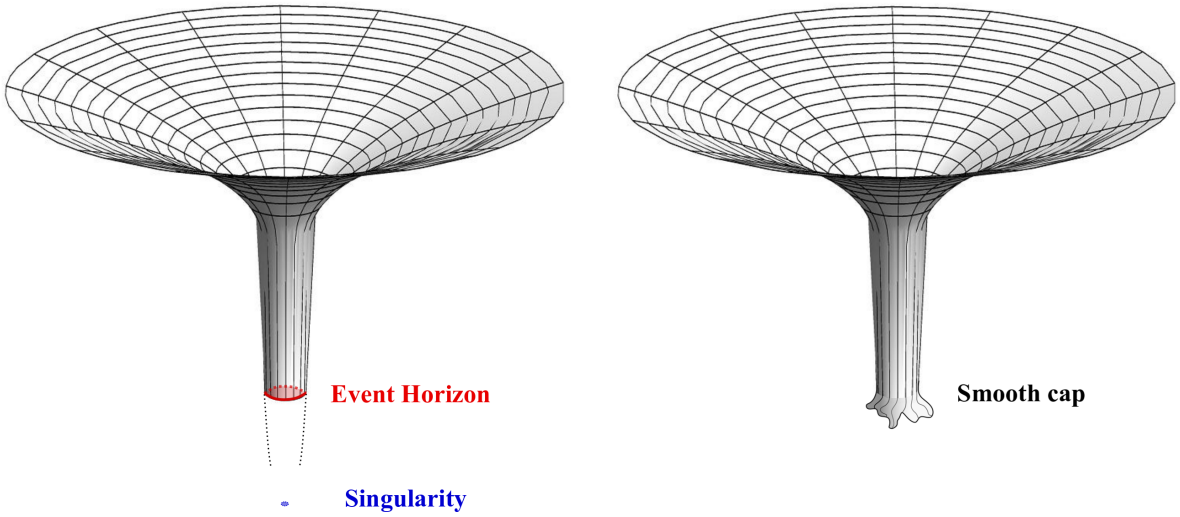

Figure 2 – Image schématique d'un trou noir classique (à gauche) et d'une géométrie de micro-état (à droite). Du point de vue de l'observateur asymptotique, au lieu de l'horizon des événements situé au fond d'un cou de longueur infinie, une géométrie de micro-états le remplacerait par une "capsule" lisse située au fond d'un cou de longueur finie. Les images sont issues de [15].

Dans les Chapitres 2 et 3, nous étudions la notion de distance sur l'espace des solutions d'une classe de géométries de micro-états – les solutions à bulles. D'une part, l'espace des modules des géométries de micro-états est considéré comme un espace de phase classique sur lequel la *quantification géométrique* donne le nombre de micro-états quantiques du trou noir. D'autre part, l'espace des modules des compactifications de Calabi-Yau est un espace de théories de champ effectives dont le domaine de validité peut être délimité par des notions de Swampland.

En nous appuyant sur [16], nous étudions la connexion entre ces deux points de vue, dans la région de l'espace des modules où les *solutions multicentriques* dégénèrent dans le trou noir – la *limite d'échelle*. Nous montrons, à partir de la structure Kähler de l'espace des phases de la solution et en utilisant le *carquois mécanique quantique*, que bien que la composante métrique dans l'espace des modules explose près de la limite d'échelle, la distance à la limite d'échelle est étonnamment *finie*.

En outre, en nous appuyant sur [17], nous confirmons ces résultats en calculant une distance de DeWitt appliquée à la limite d'échelle. Cependant, à partir d'une autre distance de DeWitt qui est utilisée dans le cadre du programme Swampland, la distance de la limite d'échelle est *infinie*. Cette distance infinie semble naturelle du point de vue de Swampland, car dans la limite d'échelle, une tour infinie de modes de Kaluza-Klein devient sans masse. Nous commentons les implications physiques possibles de cette inadéquation.

Dans le Chapitre 4, nous étudions les *moments multipolaires gravitationnels* qui sont une classe d'observables permettant de distinguer les géométries de micro-états avec des trous noirs de la relativité générale. En nous appuyant sur [18], nous analysons une famille de trous noirs extrémaux non-supersymétriques ainsi que leurs géométries de micro-états sans horizon en quatre

dimensions, qui fournissent des prototypes intéressants pour étudier les déviations par rapport aux solutions de Kerr causées par la nouvelle physique à l'échelle de l'horizon. Nous inventons ensuite une méthode pour calculer analytiquement les multipôles gravitationnels d'une nouvelle famille de trous noirs rotatifs non supersymétriques à quatre charges et de leurs géométries de micro-états. Nous montrons en outre que ces trous noirs que nous avons construits à partir du modèle *supergravité STU* peuvent avoir la même masse, les mêmes charges et le même spin qu'un trou noir de Kerr-Newman presque neutre, mais avec une tour très différente de multipôles gravitationnels. Par conséquent, ce travail met en lumière d'éventuels observables pouvant être détectés dans un futur proche par le détecteur eLISA.

Dans le Chapitre 5, nous calculons les effets de marée sur une corde suite à sa chute selon une géodésique nulle dans une famille de géométries de micro-états de trous noirs – les superstata. En effet, une différence notable entre les corrélateurs holographiques dans un fond de trou noir et ceux dans une géométrie de micro-états est que ces derniers affichent des échos gravitationnels dus à la présence de la capsule lisse à la place de l'horizon. Cependant, comme le montre la littérature antérieure, les corrections de cordes à ces corrélateurs peuvent être importantes, car les *forces de marée* excitent les modes massifs d'une corde sans masse tombant dans la géométrie depuis l'infini, interdisant à la sonde de revenir à l'infini.

Une question intrigante est de comprendre quel est le dual holographique de ces forces de marée ; la première étape pour résoudre cette énigme est de caractériser leurs effets sur la corde. Les résultats de la littérature antérieure suggèrent qu'il n'y a pas de forces de marée le long des directions toroïdales. Cependant, en nous appuyant sur [19], nous montrons qu'il s'agissait d'un artefact d'une géodésique particulière. Sur une géodésique plus générique, nous prouvons, en utilisant les *limites de Penrose*, que la corde subit des contraintes de marée le long de *toutes* les directions possibles. De plus, nous montrons que les effets de marée alternent entre compression et étirement, alors que dans la littérature antérieure, les effets étaient soit l'un soit l'autre.

Dans le Chapitre 6, en nous appuyant sur [20], nous mettons en évidence, en utilisant des *techniques de génération de dualité de cordes*, des *nouveaux degrés de liberté* qui empêchent la formation d'un horizon macroscopique dans la limite où les superstrates semblent dégénérer en trous noirs. Pour ce faire, nous construisons des solutions avec une aire d'horizon nulle qui ont les mêmes charges qu'un trou noir à trois charges F1-NS5-P de Type-IIA, et qui préservent en plus la symétrie sphérique du trou noir. Les solutions ont des degrés de liberté qui correspondent aux modes locaux de densité de branes le long du cercle commun F1-NS5, et sont des porteurs d'impulsion qui n'ont pas d'extension dans les directions spatiales non compactes. Nous soutenons que ces solutions doivent être interprétées comme la limite à long cou des superstrates. L'existence de ces géométries indique donc qu'un horizon de taille finie n'apparaît pas même dans les coins singuliers de l'espace des modules des géométries de micro-états à trois charges.

Chapter 1

Introduction

1.1 Quantum gravity puzzles about black holes

Black holes are astrophysical objects formed from the gravitational collapse of supermassive stars. They can be described by solutions in General Relativity: the horizon indicates the locus from which nothing can escape.

In the 1970s, the discovery that the black hole is a statistical object was a breakthrough that would change in the following decades our understanding of General Relativity and Quantum Mechanics. Indeed, the black hole, as a solution of General Relativity, follows thermodynamic laws [1,2]. One can therefore associate to it a temperature and a thermodynamical entropy (the Bekenstein-Hawking entropy), the latter being proportional to the area of the horizon, A_H [3,4]:

$$S_{\text{Bekenstein}-\text{Hawking}} = \frac{A_H}{4G_N}\,, \tag{1.1.1}$$

where G_N is Newton's constant, and where we take units such that $c = \hbar = k_B = 1$.

Relating the horizon area with an entropy comes from the following fact. Take a stationary black hole of mass M, electric charge Q, and angular momentum J. Besides, the black hole rotates with angular velocity, Ω_H, and charged up to an electric potential, Φ_H. If some external work – like someone from outside the black hole sending light rays or matter into the black hole with a certain angle – forces a small change, $(\delta M, \delta Q, \delta J)$, in the black hole mass, charge and angular momentum, then the changes must verify the constraint [4]

$$dM = \frac{\kappa}{8\pi G_N} dA_H + \Omega_H dJ + \Phi_H dQ\,, \tag{1.1.2}$$

where the constant κ is the surface gravity. By associating a temperature, T and an entropy, S, as

$$T = \alpha \frac{\kappa}{8\pi}\,, \qquad S = \frac{A_H}{\alpha}\,, \tag{1.1.3}$$

both defined up to some numerical factor, α, the relation (1.1.2) is rewritten as the first thermodynamic law:

$$dE = TdS + +\Omega_H dJ + \Phi_H dQ\,. \tag{1.1.4}$$

This relation suggests that the black hole behaves as a thermal machine.

Applying quantum field theory on a black-hole background, Hawking's calculation [5] found that the black hole is a black body that radiates at a temperature of

$$T = \frac{\hbar\kappa}{2\pi}\,, \tag{1.1.5}$$

incidentally fixing the constant α in the temperature (1.1.3) and in the Bekenstein-Hawking entropy (1.1.1). (We have restored Planck's constant, $\hbar$.) Therefore, the analogy with the thermodynamic laws cannot be considered as a mere coincidence: *The black hole has (physically) a temperature; it is besides a thermal machine, characterised in particular by an entropy, and it satisfies the laws of thermodynamics like any other thermodynamic systems!*

Before going further, one should stress that the Bekenstein-Hawking entropy (1.1.1) can be generalised to take into account the matter and gravitons outside of the black hole:

$$S_{\rm gen} = \frac{A_H}{4\hbar G_N} + S_{\rm outside}\,. \tag{1.1.6}$$

Strictly speaking, in presence of matter and gravitons outside of the black hole, the quantity obeying the second law of thermodynamics is in fact the generalised entropy, $S_{\rm gen}$, and not simply the Bekenstein-Hawking entropy [21]:

$$\Delta S_{\rm gen} \geq 0\,. \tag{1.1.7}$$

As a statistical and thermal object, the black hole raises numerous questions. Let us enumerate the three main puzzles about the quantum-gravity properties of black holes.

1. The microscopic origin of the black-hole entropy.

The inequality (1.1.7) means that the generalised entropy (1.1.6) is the entropy defined in $19^{\rm th}$-century thermodynamics, or coarse-grained entropy. However, from late $19^{\rm th}$-century thermodynamics, the coarse-grain entropy of a gas of molecules for instance also provides a measure of the total number of degrees of freedom in a given system:

$$S_{\rm coarse-grained} = k_B \log \Omega\,, \tag{1.1.8}$$

where Ω is the number of microstates – microscopic configurations of the molecules – sharing the same thermodynamic properties with the gas.

Similarly, one can wonder whether the Bekenstein-Hawking entropy of the black hole is given by the number of black-hole microstates having the same properties as the black hole: the mass, M, charges, Q, and angular momentum, J – the unique quantities that can define the black-hole solution in General Relativity according to Uniqueness theorems. Crucially, if the answer is yes, then one needs to answer the following intriguing questions:

> *What are the microscopic degrees of freedom that characterise the individual black-hole microstates? And what do the microstates accounting for the black-hole entropy look like?* (1.1.9)

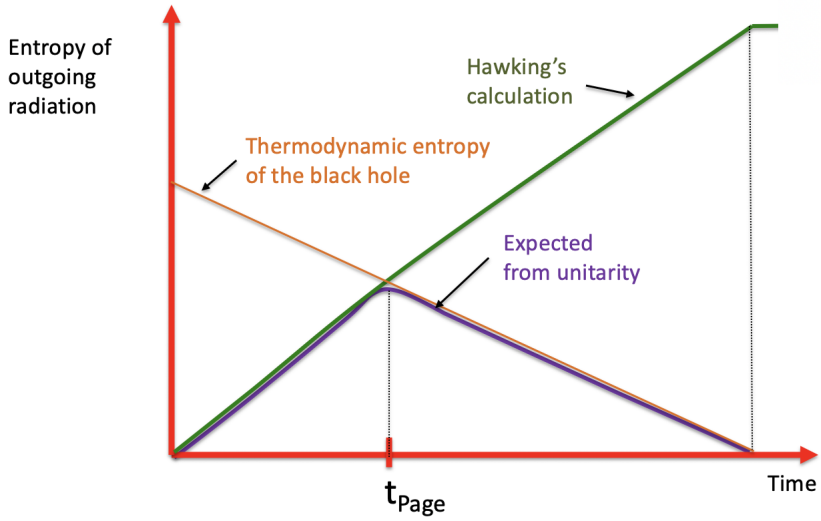

Figure 1.1 – Schematic behaviour of the evolution in time of the entanglement entropy of the outgoing radiation, S_{rad}. In green, Hawking's calculation predicts S_{rad} grows monotonically in time, as the black hole evaporates. In orange, the Bekenstein-Hawking entropy decreases in time, altogether with the area of the black hole. After the Page time, where the two curves cross, it is not possible for all of the outside radiation to be entangled with degrees of freedom inside of the black hole, as the number of those degrees of freedom is bounded from above by $e^{S_{\text{Bekenstein-Hawking}}}$. Therefore, if the evaporation process is unitarity, one expects the entropy of the radiation, S_{rad}, to follow the Page curve, drawn in purple. The figure is from [24].

2. The black-hole information paradox.

The black hole's black-body radiation at the Hawking temperature (1.1.5) forces it to lose energy (and mass) continuously. Eventually, the black hole evaporates (almost) completely – at least up to a point where the semi-classical approximation breaks down.

If the black hole was simply a star or a piece of coal, there would be no issue. However, the black hole has a horizon. From the perspective of General Relativity, there is nothing special happening at the horizon: the Ricci scalar is constant, and there is no matter there, only the vacuum of quantum field theory. As such, in Hawking's calculation [22, 23], the black hole's black-body radiation comes from the creation of a pair of photon modes across the black hole's horizon. While the photon outside of the horizon – these photons constitute the black-body radiation – escapes towards infinity, the photon inside the horizon falls towards the black-hole singularity. Crucially, such a pair of modes – the so-called *Hawking pairs* – are entangled.

Now, one can look at the entanglement entropy (or the so-called *fine-grained entropy*, or *von Neuman entropy*) of the outgoing radiation, S_{rad}. See Figure 1.1. We assume the black hole has been collapsed from a pure state. Because the outgoing radiation is that of a black

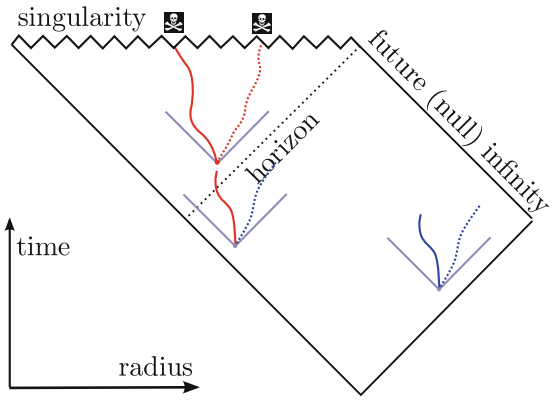

Figure 1.2 – Penrose diagram of a classical Schwarzschild black hole in flat space. From General Relativity, any matter crossing the horizon reaches the singularity in a (proper) time of the scale $\sim M$, i.e. the time for light to cross the scale of the horizon. (It corresponds to $\sim 10^{-5}$ seconds for a solar-mass black hole.) Therefore, it seems that any infalling particle reaches the "end of time" at the singularity. The figure is from [6].

body, the entropy contribution of each photon add up: From Hawking's calculation, the entropy monotonically increases with each photon emitted, until the black hole evaporated completely. However, *if the evaporation process is unitary*, then the entanglement entropy of the system {outgoing radiation + black hole} – that is to say the whole universe – is vanishing. Therefore, the entanglement entropy of the outgoing radiation is equal to that of the black hole: $S_{\text{rad}} = S_{\text{black hole}}$. But the black hole's entanglement entropy is limited by the number of degrees of freedom of the black hole: $S_{\text{black hole}}$ cannot exceed the coarse-grained entropy of the black-hole, $S_{\text{Bekenstein-Hawking}}$. Therefore,

$$S_{\text{rad}} \leq S_{\text{Bekenstein-Hawking}} \,. \tag{1.1.10}$$

As the black hole evaporates, its horizon area and Bekenstein-Hawking entropy decrease – at least as long as the black hole does not reach Planck-mass scale. It follows that the entropy of the radiation cannot increase indefinitely until the end of the Hawking process; this is in contradiction with Hawking's calculation. Instead, the entropy of the radiation should decrease after some time, called the *Page time*, and follow the *Page curve* [25, 26] (see Fig. 1.1).

This paradox leads to the second set of questions, if one assumes that the evaporation process is unitary:

> *Is the entropy of the outgoing radiation following the Page curve, as advocated by unitarity? If yes, what process makes it happen?* (1.1.11)

3. The black-hole singularity.

From General Relativity's perspective, the black-hole solution is a good description up until the neighbourhood of the singularity, where the Ricci scalar diverges. In particular, nothing special should happen at the horizon of large black holes, as the curvature at the horizon is

proportional to M^{-2}, where M is the mass of the black hole. Besides, the black hole's Penrose diagram shows that the singularity implies an end of time at its location. See Figure 1.2. Therefore, the first expectation one generally makes is that General Relativity is fine up until the neighbourhood of the singularity, and this singularity should be resolved by a theory of quantum gravity. Furthermore, understanding the microscopic origin of the black-hole entropy could tell about what degrees of freedom resolve the black-hole singularity. We end up in the following questions:

> *What are the degrees of freedom resolving the black-hole singularity? And if those degrees of freedom lie in the neighbourhood of the singularity, how does the horizon – which lies in its causal past – knows about those degrees of freedom, as suggested by the Bekenstein-Hawking formula (1.1.1)?* (1.1.12)

1.2 The black-hole entropy from String Theory

As a theory of quantum gravity, string theory is expected to provide an answer to the black hole puzzles in the previous section.

The basic idea of string theory that the elementary particles (like the electron, the photon, quarks, etc.), that we usually think of as point-like, are actually different modes of vibration of a fundamental, extended object: the string. An advantage of having strings instead of point-like particles is that all possible UV-divergences in scattering amplitudes in particle physics are automatically tamed. In particular, the divergences involving the graviton are resolved by the conformal invariance of the string's worldsheet, which makes string theory a UV-complete theory of quantum gravity.

The strings in string theory can be closed, or open. Closed strings and open strings generate different spectra of fields. The oscillation of closed strings generate, in particular, the graviton, whereas open strings generate for instance vector fields in their massless spectrum. The closed strings are strings loops ending on themselves, whereas the extremities of the open strings end on solitonic solutions of string theory: the D-branes.

String theory is perturbative theory of quantum gravity, in two parameters: the string length, l_s, and the string coupling, g_s.

The string length, l_s, comes from the fact that the fundamental string has a tension, τ, which can be expressed in terms of a length, the string length:

$$\tau \equiv \frac{1}{2\pi\alpha'} = \frac{1}{l_s^2}\,. \tag{1.2.1}$$

The string length, l_s, sets the energy at which one would measure the higher harmonic modes of the string: $M_s \propto \frac{1}{l_s}$. On the other hand, if one probes the strings at an energy $E \ll M_s$, one would probe only the massless modes of the string and would not see the part of the spectrum corresponding to higher modes of the string. In this limit, one cannot excite oscillators on the strings and the strings behave as point-like particles.

The string coupling, g_s, controls the genus expansion of string world-sheets. At low energies, $E \ll M_s$, the holes strings diagrams become loops in Feynman diagrams. In addition, the string

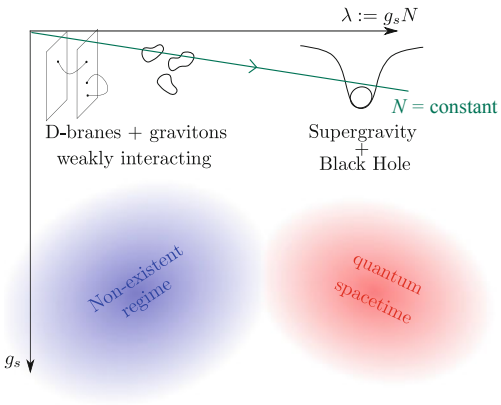

Figure 1.3 – Domains of validity of different descriptions of branes in terms of g_s and $g_s N$. Since $N \geq 1$, the lower-left corner of the diagram (in blue) does not exist. In the upper-left corner, where $g_s \ll 1$ and $g_s N \ll 1$, the D-branes are described by perturbative open-string theory; they do not interact with gravitons, which are closed-string excitations. As one tunes g_s to larger values, keeping N fixed, we follow a linear line in the $(g_s N, g_s)$ plane with a $1/N$ slope, depicted here in green. If N is not large enough, the slope of the line is large and one directly ends up in a quantum spacetime regime ($g_s \gg 1$) that one does not know how to describe. If $N \gg 1$, the constant-N line crosses a regime where $g_s N \gg 1$, but where $g_s \ll 1$: this regime can be described by supergravity. The figure is adapted from [6].

coupling sets the Newton's constant, G_N, in D dimensions:

$$G_N \propto g_s^2 \, l_s^{D-2} \, . \tag{1.2.2}$$

The above equation can be understood as follows: A graviton propagator, in field theory, is proportional to G_N; its interpretation in string diagram corresponds to a string exchange diagram, which involve two factors of g_s, one for emitting the closed string and one for absorbing it.

The end-points of opens strings are labeled by the branes on which the strings end. As such, a stack of N D-branes introduces a degeneracy for one of the open string's end points. Therefore, the expansion parameter that controls the genus expansion of open-string world-sheets is $g_s N$ instead of g_s for closed strings.

The expansion parameter in perturbative open string theory, $g_s N$, controls also the amplitude for D-branes to exchange a graviton. In the regime where $g_s N \ll 1$, the interaction between the D-branes and closed strings is suppressed. Therefore, the D-brane dynamics are described by open strings, and the D-branes do not produce a metric. One the other hand, the closed strings (and graviton) do not feel the source (the D-branes). See Fig. 1.3.

As one increases g_s, keeping N fixed, closed strings interact more and more with the open strings ending on the D-branes, perturbing more and more the dynamics and transverse motion of the branes, so that the support of the branes' wavefunctions spread more and more over the

transverse dimensions of the branes. As a result, one begins to lose the notion of the location of each individual brane; at the same time, the branes begin to back-react gravitationally.

In the regime where $g_s N \gg 1$, the open-string picture has broken down for a long time. But in the regime where we have in addition $g_s \ll 1$, the branes are can described by the theory of closed strings, whose collective excitations create a geometry which satisfies the equations of motions of supergravity.

Crucially, string theory's point of view on the black-hole physics puzzles the following: By dialing the string coupling constant g_s, one can interpolate between some particular D-brane configurations defined at $g_s N \ll 1$ and some black hole solution in supergravity defined at $g_s N \gg 1$. Furthermore, in supersymmetric configurations, using index theorems, one can show that the number of microstates is the same in both regimes. Therefore, one can learn a lot of insights from black holes (in supergravity) from the open-string physics of D-branes.

1.2.1 The three-charge black hole in String Theory

For more concreteness, let us look at the D1-D5-P system. This is a brane configuration composed of D1-branes, D5-branes, and momentum P, corresponding to gravitational waves moving in a given direction in space. In the weak-coupling ($g_s N \ll 1$) regime, start with a flat space-time of topology $\mathbb{R}^{1,4} \times S^1 \times T^4$. Let us label the direction of the circle S^1 by the space-like coordinate y. We wrap the branes and the momentum in the configuration of Table 1.1.

	t	$\mathbb{R}^4$	S^1_y	T^4
D5	–	·	–	–
D1	–	·	–	∼
P	–	·	→	∼

Table 1.1 – Brane configuration of the D1-D5-P system. Here, we use the convention where – indicates that the brane/string is extended in the given dimension(s), · indicates that it is pointlike, and ∼ indicates that the brane is smeared in the given dimension(s). The arrow → indicates that the gravitational wave P is moving in one of the directions (left or right) of the circle, S^1_y.

When the coupling constant g_s is tuned to larger values so that $g_s N \gg 1$, the configuration of Table 1.1 sources a ten-dimensional metric (in the string frame) that depends only on the coordinates of $\mathbb{R}^4$:

$$ds^2 = -\frac{2}{\sqrt{H_1 H_5}}\left[dt^2 + dy^2 + \left(\frac{1}{H_P} - 1\right)(dy - dt)^2\right] + \sqrt{H_1 H_5}\, ds^2_{\mathbb{R}^4} + (H_1 H_5)^{-1/2} ds^2_{T^4}\,, \tag{1.2.3}$$

where

$$H_{1,5,P} = 1 + \frac{Q_{1,5,P}}{r^2}\,. \tag{1.2.4}$$

The supergravity charges can be expressed in terms of the number of branes and momentum quanta:

$$Q_1 = \frac{g_s \alpha'}{v} N_1 \,, \qquad Q_5 = g_s \alpha' \, N_5 \,, \qquad Q_P = \frac{(g_s)^2 \alpha'}{v \rho_y^2} N_P \,, \tag{1.2.5}$$

where $v \equiv \frac{V_4}{(2\pi)^4 \alpha'^2}$ is the volume of the four-torus T^4 measured in units of $2\pi l_s$ and $\rho_y \equiv \frac{R_y}{l_s}$ is the radius of the y circle measured in units of l_s.

What are the regime of validity of the supergravity solution (1.2.3)?

- First, we want to be in a regime where the string loop corrections are small: $g_s \ll 1$.
- Second, we want the stringy α' corrections to the geometry to be small. Thus, we require the curvature invariants to be small everywhere in the geometry. This amounts to constrain the supergravity charges to be large: $Q_{1,5,P} \gg \alpha'$. In other words, the characteristic radius, $r_{1,5,P} \equiv \sqrt{Q_{1,5,P}}$, of each harmonic function appearing in the geometry is large in string units, $r_{1,5,P} \ll l_s$.

The event horizon of the D1-D5-P black hole (1.2.3) lies at $r = 0$. The area of the horizon is given by the size of the orthogonal spatial directions to r, at $r = 0$. The area of the five-dimensional geometry is

$$A_H^{(5)} \sim \sqrt{Q_1 Q_5 Q_P} \sim g_s^2 (l_s)^3 \sqrt{N_1 N_5 N_P} \,, \tag{1.2.6}$$

but the Bekenstein-Hawking entropy is independent of the string coupling and of the string length:

$$S_{\text{Bek.-Hawk.}} = \frac{A_H^{(5)}}{G_N^{(5)}} = 2\pi \sqrt{N_1 N_5 N_P} \,, \tag{1.2.7}$$

where $G_N^{(5)}$ is Newton's constant in five dimensions.

1.2.2 Counting the states of the three-charge black hole

In this subsection, we explain how string theory provides a description of the microstates of the three-charge black hole, in the weak-coupling regime ($g_s N \ll 1$) [27, 28]. Indeed, a configuration of branes as described in Table 1.1 backreacts into a black-hole solution in the strong-coupling regime ($g_s N \gg 1$).

The brane charges, N_1 and N_5, in equation (1.2.5), can appear through different string-theory configurations. For instance, one D1-brane wrapping N_1 times the y circle and N_1 D1-branes each wrapping a single time the y circle account for the same supergravity charge, $Q_1 = \frac{g_s \alpha'}{v} N_1$.

What about the momentum N_p along the y circle? The momentum can be carried by closed strings, open strings, or even D-branes. The dominant contribution to the entropy however, comes from the open strings stretching between D1- and D5-branes, thanks to the phenomenon of *momentum fractionation* [29, 30].

An open string stretching between a singly-wound D1-brane and a singly-wound D5-brane is free of interactions in the regime $g_s N \ll 1$, so its wavefunction is written in the basis of

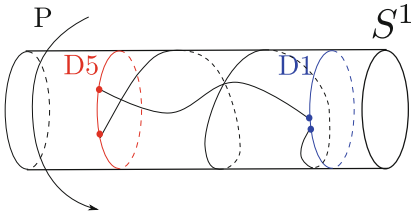

Figure 1.4 – Depiction of open strings stretching between a D1- and a D5-brane in the y circle, S^1. The size of the four-torus T^4 is assumed to be parametrically smaller than that of the circle S^1_y, so the physics is described by an effective D1-D5 string in S^1_y. The figure is from [6].

momentum eigenstates on the S^1_y circle, and has the form

$$\psi(y) = \sum_{n\in\mathbb{Z}} \alpha_n \exp\left(\frac{2i\pi n}{R_y} y\right) . \tag{1.2.8}$$

The smallest value of momentum carried by such an open string is $\frac{1}{R_y}$.

Now, consider a D1-brane wrapping N_1 times the circle S^1_y, and a D5-brane wrapping it N_5 times. See Fig. 1.4. An open string stretching between these two branes has a multi-valued wavefunction on the S^1_y circle: it has to go around $N_1 \vee N_5$ (denoting the least common multiple of N_1 and N_5) times around the S^1_y circle to reach the same point in the two branes' worldvolume again. For simplicity, we will assume that N_1 and N_5 are co-prime; then $N_1 \vee N_5 = N_1 N_5$. The momentum eigenstates of this open string are of the form

$$\psi_n(y) = \exp\left(\frac{2i\pi n}{N_1 N_5 R_y} y\right) , \tag{1.2.9}$$

which means that the momentum on such D1-D5 branes is quantized in units of $\frac{1}{N_1 N_5 R_y}$ – hence the *momentum fractionation*.

Each mode ψ_n carries a momentum amounting to $\frac{n}{N_1 N_5 R_y}$. Let $\mu(n)$ the number of open strings occupying the mode ψ_n. In total, the momentum carried by the open strings is equal to $\frac{N_P}{R_y}$. Then

$$\sum_{n=1}^{\infty} \frac{\mu(n)\, n}{N_1 N_5 R_y} = \frac{N_P}{R_y} . \tag{1.2.10}$$

In other terms, the number of ways for open strings to realize the total momentum it is the number of partitions of $N_1 N_5 N_P$ in integers.

One can show that the entropy corresponding to this number is proportional to $\sqrt{N_1 N_5 N_P}$. One then has to take into account that an open string has four bosonic degrees of freedom corresponding to its free motion along the T^4, and add their four fermionic superpartners, so that one finds the correct numerical coefficient:

$$S_{\text{open strings}} = 2\pi\sqrt{N_1 N_5 N_P} , \tag{1.2.11}$$

which matches the Bekenstein-Hawking entropy (1.2.7).

In a nutshell, the leading order of the black hole's entropy is given by the number of ways for open strings, stretching between a D1-brane wrapping N_1 times the circle and a D5-brane wrapping it N_5 times, to account for the momentum charge N_P.

Let us, for the remaining of the Introduction, denote these D1-D5-P configurations as "*Strominger-Vafa microstates*".

The F1-NS5-P black hole.

Let us note that the brane bound states accounting for the entropy in an other duality frame could be quite different in nature. By S-dualizing the D1-D5-P black-hole solution, we get a F1-NS5-P black hole solution, in Type IIB supergravity. Now, the S-dual of the D1-D5-P microstates gives a D1 brane stretching between a F1 string and an NS5 brane, which is not a stable configuration. The T-dual along one of the torus directions gives a D2 brane stretching between an NS5 brane and ... a smeared density (over that same torus direction) of F1 stings, which is not a stable configuration either.

To account for the entropy of the F1-NS5-P black hole in Type IIA supergravity, one should rather count the momenta of the *little strings* [31] living in the worldvolume of an NS5 brane that wraps the circle S^1_y multiple times. To be more precise, take an NS5 brane wrapping the circle N_5 times. The tension of a string bound to the multiply-wound NS5 brane will become $1/N_5$ times the tension of a normal string, hence the name "little strings" [32, 33]. As such, the momentum of a string wrapping N_1 times the y circle, but bound to the multiply-wound NS5 brane is counted in units of $\frac{1}{N_1 N_5 R_y}$ for the little strings, instead of $\frac{1}{N_1 R_y}$ for normal strings.

The little strings carry the momentum through their transverse motion in T^4, in the NS5 branes' worldvolume. This is to be contrasted with the Strominger-Vafa microstates, where the momentum was carried by open strings stretching between D1- and D5-branes. The moral of the story is that: The object in string theory that "carries the momentum" along the y circle can have different avatars in string theory. In other words, the Strominger-Vafa microstates is just a basis of the Hilbert space of the D1-D5-P black hole. In principle, it is possible to find other bases of the same Hilbert space with different string-theory ingredients.

1.2.3 But what about $g_s N \gg 1$?

We now know how to describe the microstates in the open-string picture. However, the black hole is defined as a solution of supergravity, and the Information Paradox is relevant in the regime of validity of supergravity. We can now reformulate our question (1.1.9) in Section 1 to:

> *Can we describe the microstates in the regime of parameters the black hole solution is defined (i.e. in the $g_s N \gg 1$ regime)? To what extent and how do they differ from the black hole?* (1.2.12)

The standard intuition one learns from Section 1.2.2 is the following.

The standard perspective

The fundamental description of black-hole microstates is from the open-string, or CFT perspective. In the bulk, supergravity is not able to capture the degrees of freedom accounting for the black-hole microstates. Indeed, at $g_sN \gg 1$, the microstates differ from themselves (and to their statistical average, the black-hole solution) only in the vicinity of the singularity. And the vicinity of the singularity is precisely the space-time region which is not captured by supergravity.

This perspective seems appealing from the point of view of General Relativity, whose regime of validity largely contains the horizon region. Nevertheless, this perspective relies on a bias *from* General Relativity, and leads to several questions.

A first question comes from the meaning of horizons in statistical mechanics. In the "standard perspective", all the microstates have a horizon in the $g_sN \gg 1$ regime. But if the individual microstates have a horizon, one could derive the same thermodynamic laws (1.1.2) and (1.1.1) to each microstate. As such, *shouldn't the microstates carry also some (coarse-grained) entropy with them? Is this picture in conflict with what a microstate should be?*

Secondly, the wavefunctions of the brane configurations spreads to the horizon scale as the tuning of the coupling constant g_s interpolates between the open-string and supergravity regimes. But from the "standard perspective", the wavefunctions of different microstates differ only in the singularity region. They differ only in a localized, singularity region, although they have a macroscopic, horizon-scale support. *Is there a top-down argument explaining how this phenomenon happens?*

A collection of N Dp-branes (with $N \gg 1$) sources, after gravitational backreaction, a p-brane solution in supergravity without regions where $g_{tt} < 0$. The three-charge brane configuration sources a geometry, whose metric (1.2.3) is a supergravity solution, in the coordinates corresponding to the viewpoint of an asymptotic observer. It turns out this geometry is not geodesically complete and has a horizon that can be crossed. But do the branes source the geometry inside the horizon? Or is the inside of the horizon acts as an artificial image for the asymptotic observer, like when one applies the method of images in electromagnetism?

1.3 The Fuzzball paradigm

Let us quickly recap what we learned from the previous section. We start, in the regime $g_sN \ll 1$, with a D1-D5-P brane configuration of Table 1.1 that correspond to microstates of the black hole: in this introduction, we call them the *Strominger-Vafa microstates*. As g_s grows up until the regime where $g_sN \gg 1$, the wavefunction of the brane configuration spreads to the horizon scale – and once one backreacts gravity, the horizon scale is captured by the supergravity regime. However, somehow, the Strominger-Vafa microstates become all indistinguishable at the scale of the horizon.

But what if this was only a coincidence?

1.3.1 The growth of branes with Newton's constant

If one starts from a perfectly symmetric brane configuration – point-like in the non-compact spatial dimension, and independent of the compact dimensions –, one will naturally find, at $g_sN \gg 1$, a geometry that is spherically symmetric whose characteristic size is the horizon size.

The Strominger-Vafa microstates correspond to a very particular basis of the Hilbert space of the black hole microstates in the weak-coupling regime, where the precision about the location of the brane system (in the non-compact dimensions) is infinite, and where the D1- and D5-branes are perfectly independent of the compact dimensions. But from Heisenberg's uncertainty principle, the Strominger-Vafa microstates receive a size in the non-compact directions. Then the question becomes: What happens at large g_sN if the brane configurations get some size in the non compact dimensions? What happens if they break a little bit the symmetries?

The computation in [34] provides a toy-model answer to what could happen in a more general instance. The authors considered a three-charge, stringy configurations that make a circular profile in the non-compact dimensions. They showed that as one increases g_s (or G_N), the size of the stringy configuration grows with the same rate as the horizon scale. Moreover, the resulting solution in supergravity has no horizon.

1.3.2 The Fuzzball hypothesis and the paradigm shift

From the previous section, one can naturally formulate the following hypothesis:

> *At $g_sN \gg 1$, generically, the individual microstates differ from themselves and from the classical black-hole solution at the scale of the horizon.*

The difference implied here between the microstates and the black hole is of order $\mathcal{O}(1)$, and not of order $\mathcal{O}(e^{-S})$ or $\mathcal{O}(e^{-S/2})$. This is to be contrasted with the "standard perspective", where the microstates differ from the black-hole solution only in the vicinity of the singularity.

The hypothesis above introduces a *paradigm shift*. Because the microstates and the classical black-hole solution differ by a non-negligible amount at the scale of the horizon, one cannot rely on the intuition from General Relativity anymore. In particular, black-hole microstates may not have a horizon, even if General Relativity itself is fine at the scale of the horizon. The Fuzzball hypothesis, precisely states this.

> **The Fuzzball hypothesis** [7–11]
> *At $g_sN \gg 1$, the individual black-hole microstates differ from the classical black-hole solution at the scale of the horizon; they have furthermore no horizon and no singularities. Such horizonless microstates are called "fuzzballs".*

From the perspective of the fuzzball hypothesis, individual microstates do not carry coarse-grained entropy, therefore, they do not have a horizon in the strong-coupling regime ($g_sN \gg 1$).

Besides, it does not make sense to talk about the black hole interior for black-hole microstates, as the horizon is replaced by another phase of matter that supports the gravitational collapse that would lead to a black hole. But how to evade the theorems from General Relativity, that

stipulate that a horizon and a singularity will form, as soon as matter is compressed in a given radius?

Well, the black-hole horizon and singularity are, within the Fuzzball hypothesis, artefacts of a theory – General Relativity – which do not contain enough degrees of freedom to resolve them. Crucially, one cannot just use General-Relativity theorems to prove that the Fuzzball hypothesis cannot work, because General Relativity will introduce a bias that will imply the presence of horizons and singularities.

The Fuzzball hypothesis understands the horizon of the black hole as some average of the degrees of freedom of string theory describing the microstates ; the interior geometry of the black-hole solution follows as an artefact of the geodesic completion of the averaged black-hole geometry.

If the Fuzzball hypothesis is correct, then the Strominger-Vafa microstates would be one particular basis of the Hilbert space of black-hole microstates at weak coupling. It could be that *generically, a basis of the Hilbert space is composed of horizonless microstates at* $g_s N \gg 1$. But perhaps a weaker statement which could be sufficient for the Fuzzball hypothesis is: One should be able to find (at least) one basis of the Hilbert space composed of only horizonless microstates at $g_s N \gg 1$.

1.3.3 The Fuzzball hypothesis' answer to other black-hole puzzles

We have introduced the Fuzzball hypothesis as a natural answer to the question about the microstates (1.1.9): *The black-hole microstates are horizonless solutions which are similar to the black-hole solution in the asymptotic region, but differ from the black-hole solution at the scale of the horizon.* As such, the answer to the question of black-hole singularity (1.1.12) follows immediately: *The phrase "to resolve the black-hole singularity" does not make sense, as the black-hole microstates do not have a singularity, and the degrees of freedom distinguishing the microstates lie at the scale of the horizon.*

One can also wonder how the collapse of matter leads to the formation of a fuzzball instead of a black hole. In particular, if one collapses a perfectly spherical shell of low-density, infalling matter, how does the matter excite the stringy and non-perturbative degrees of freedom necessary for fuzzballs to exist? Calculation that attempt to answer this question suggests that there is a non-zero probability $\mathcal{P} \sim e^{-S_{\text{Bek.}-\text{Hawk.}}}$ for this collapsing matter to tunnel into one particular fuzzball configuration [35–37]. Therefore, the probability to tunnel into one of the $e^{S_{\text{Bek.}-\text{Hawk.}}}$ fuzzball microstates is of order 1, thus preventing the horizon to form.

Concerning the Information Paradox (1.1.11), the absence of horizon for black-hole microstates changes completely the problem. The pair-creation of Hawking particles does not happen with a geometry without a horizon. Instead, the black-body radiation of a (non-extremal) fuzzball happens like that of a star, or a piece of coal [12]. Therefore, the evaporation process is always unitary, and no Information Paradox arises. The paradigm shift introduced by the Fuzzball hypothesis is to realize that the answer to question (1.1.9) may imply that questions (1.1.11) and (1.1.12) are ill-defined.

It should be stated that the Fuzzball paradigm can be motivated from the bottom-up perspective, as it was originally designed as a solution to the Information Paradox. Indeed, according to

Mathur's "small-corrections theorem" [9], in order to solve the Information Paradox, one should give up (at least) one of the following assumptions [9, 38]:

(1) unitarity of quantum mechanics in the presence of black holes

(2) locality of quantum mechanics in the presence of black holes

(3) smoothness of black-hole horizons.

The Fuzzball hypothesis takes the route of giving up assumption (3), as smooth black-hole horizons are replaced by horizonless microstates.

1.4 The Microstate Geometries programme

In order to support the Fuzzball hypothesis, a lot of horizonless solutions have been found in string theory. In particular, the *Microstate Geometries programme* [13, 14] endeavours to find horizonless solutions of supergravity; such solutions are called *microstate geometries*. One can make the following classification of fuzzballs [39]:

1. A *microstate geometry* is a smooth horizonless solution of supergravity that is valid within the supergravity approximation to string theory and that has the same mass, charge and angular momentum as a given black hole.
2. A *microstate solution* is a horizonless solution of supergravity, or a horizonless, physical limit of a supergravity solution, that has the same mass, charge and angular momentum as a given black hole. Microstate solutions are allowed to have singularities that either correspond to brane sources or can be patch-wise dualized into a smooth solution.
3. A *fuzzball* is the most generic horizonless configuration in string theory that has the same mass, charge and angular momentum as a given black hole. It can be arbitrarily quantum and arbitrarily strongly curved.

Therefore, the set of microstate geometries is contained in the set of microstate solutions, which is itself contained in the set of fuzzballs. From the Fuzzball hypothesis' perspective, all black-hole microstates are fuzzballs, but they do not need to be all microstate geometries or microstate solutions. Indeed, the most entropically dominant fuzzballs could be string or brane condensates, with a wavefunction extending to the horizon-scale and which are not described by supergravity.

Nevertheless, the Microstate Geometries programme surely provides the Fuzzball hypothesis with a concrete mechanism that prevents the gravitational collapse of some phases of matter.

1.4.1 Some families of microstate geometries

Bubbling geometries

To avoid the General-Relativity theorems implying the formation of a horizon when matter is compressed to black-hole size, the trick of the Microstate Geometries programme is to take advantage of the hidden dimensions in string theory [14]. For instance, the Lagrangian of five-dimensional supergravity contains a Chern-Simons term that is inexistent in General Relativity. The addition of this Chern-Simons term changes the equations of motion so that they enable non-trivial topological solitons. More generally, a singular brane source can dissolve into fluxes

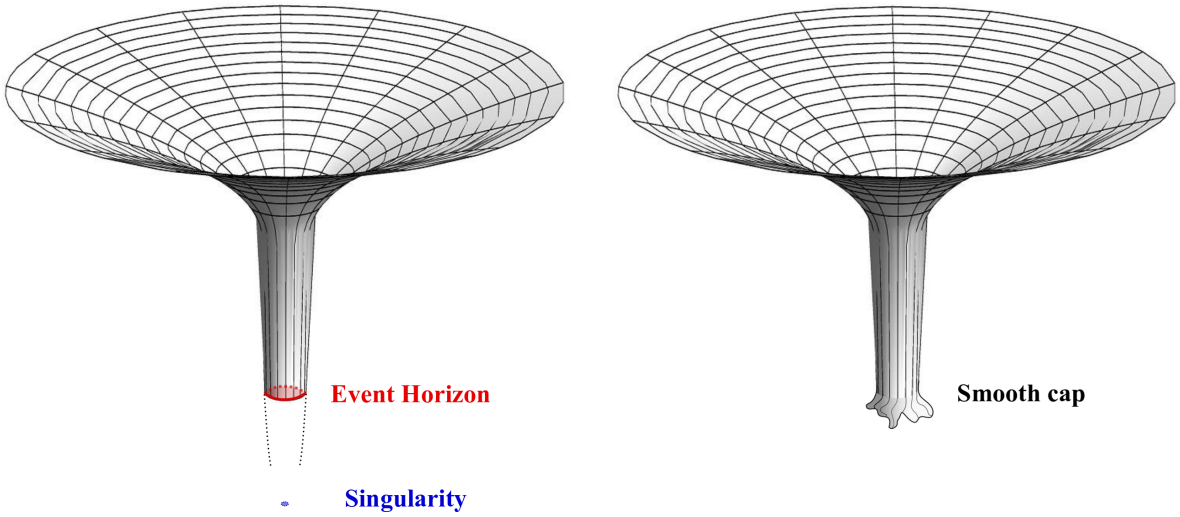

Figure 1.5 – Schematic picture of a classical black hole (left) and a microstate geometry (right). From the asymptotic observer's point of view, instead of the event horizon lying at the bottom of a throat of infinite length, a microstate geometry would replace it with a smooth cap lying at the bottom of a throat of finite length. The figures are from [15].

that thread new topological cycles. The cycles make the geometry smooth and horizonless, and prevent the collapse of matter into a black hole.

Bubbling geometries [40, 41, 14] are smooth, supersymmetric solutions of five-dimensional, ungauged, $\mathcal{N} = 2$ supergravity, coupled to vector multiplets. They have the same asymptotics and asymptotic charges as the three-charge, five-dimensional, supersymmetric black hole (the BMPV black hole [42]). Unlike the extremal black hole whose horizon lies at the bottom of an infinitely-long AdS_2 throat, the bubbling solutions have a smooth cap at the bottom of a long, but finite AdS_2 throat. See Fig. 1.5. Within the Microstate Geometries programme, they are considered as coherent superpositions of the black hole microstates [43, 13]. Much like their corresponding black hole, the bubbling geometries can also be constructed with $\mathbb{R}^{1,3} \times S^1$ asymptotics; reduced to four dimensions, they correspond to a class of *multi-centered solutions* [44–46], which still have the same asymptotics and asymptotic charges as the four-dimensional black hole, but are singular from a 4D perspective. Therefore, they are an interesting top-down model for horizon-scale black-hole phenomenology.

A principle for fuzzballs: the supertube transition

Another principle for making microstate geometries out of black holes in string theory is to make use of the supertube transition [47–49].

Consider a black hole in string theory which is understood at $g_s N \ll 1$ as a brane system put together at a point in the non-compact spatial dimensions (that we will sometimes call the *base space*). At $g_s N \gg 1$, the naïve backreaction of this brane system has a macroscopic horizon.

The idea of the *supertube transition* is to blow up the brane system in a *profile* in the base space. The advantage of this manipulation is that, in the $g_s N \gg 1$ regime, the fields

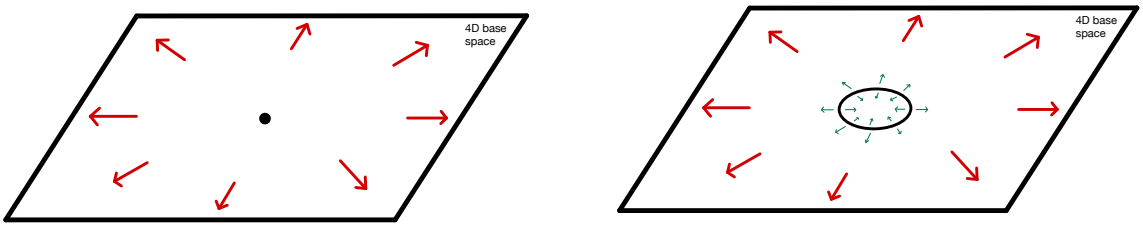

Figure 1.6 – Schematic picture of a singular brane bound-state (left) and its supertube transition (right). Asymptotically, the two configurations source the same fields. But locally, the fields sourced by the supertube are less singular than its singular counterpart.

sourced in the vicinity of the branes will be less singular that those sourced by the brane system localized at a point on the base space, although both configurations source the same fields asymptotically. Let us also note that the supertube has locally twice as many supercharges as the original configuration, although both configuration preserve the same number of supersymmetries globally. See Fig. 1.6. The supertube transition phenomenon is analog to what happens in electromagnetism: An electric charge, q, defined at a point in (3 spatial dimensions) sources an electric potential scaling as $A(r) \sim \frac{q}{r}$ at the vicinity of the point; whereas the same electric charge smeared on a ring sources an electric potential which behaves like $A(r) \sim q \log(r)$ in the vicinity of the ring.

Crucially, the less the fields singular are, the less they are likely to source a macroscopic horizon – and any horizon at all – in the $g_s N \gg 1$ regime. Sometimes, a simple supertube transition is not enough to get rid of horizons – the resulting geometry may have a horizon of zero area – and one needs to perform a "double supertube transition" [49], which corresponds to giving a thickness to the ring of Fig. 1.6.

Superstrata

Schematically, superstrata [50–53] are microstate geometries whose construction consists in applying the supertube transition to the D1-D5-P black-hole solution. Start with a D1-D5 brane configuration and perform the supertube transition in a closed profile in the $\mathbb{R}^4$ base space. See Fig. 1.7.

Because of their tension, the branes have the tendency to shrink the profile in the base space to zero size. To make the system stable, one has to add an angular momentum along the profile; the amount of angular momentum needed depends on the size of the profile.

But how does one get the momentum of the D1-D5-P system? In the original proposal for the superstrata [49,54], the momentum is supposed to be carried by the transverse motion of the D1-D5 supertube in the base space. The transverse motion constitutes the *shape modes*, in the sense that, in a snapshot of the configuration at a given time, the supertube changes its shape on the base space as one moves along y. As these modes move at the speed of light along y, they carry a momentum.

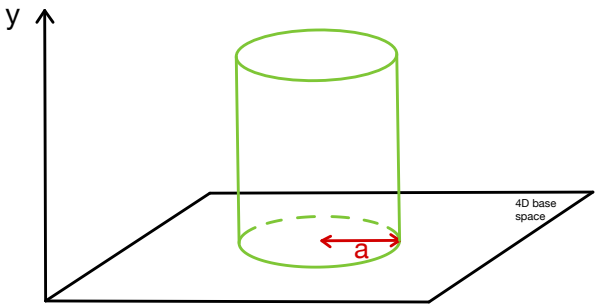

Figure 1.7 – Schematic picture of D1-D5 supertube of a circular shape in the base space. As one includes the direction of the y circle, the supertube locus corresponds to a cylinder. For the black hole, the brane system lies instead on a straight line along y.

The superstrata that have been *constructed in supergravity* [51, 52] correspond to a simpler version of the more general superstrata proposed in [49, 54]. First, one imposes a circular shape for the supertube in the base space for all y: it is a straight and rigid cylinder, like in Fig. 1.7. This time, in order to get the momentum, one adds, on top of the D1-D5 supertube, density modes of D1-D5 branes extended orthogonally to y (and along T^4). It correspond to having an increment of D1-D5 density at some locations, and a decrease of the D1-D5 density at some other locations. Because all these density modes are moving at the speed of light along the y circle, they induce collectively a macroscopic momentum charge, Q_P, in the supergravity solution.

The constructed superstrata have the same asymptotic charges and asymptotic geometry as that of the black hole. As such, in the language of microstate geometries, different density modes of constructed superstrata (or shape modes, for the generalised superstrata) give rise to different black-hole microstates.

1.4.2 Some challenges of the Microstate Geometries programme

The number of microstates accounted by Supergravity

A first challenge for the Microstate Geometries programme is to answer the following question:

> *What fraction of the black-hole entropy can microstate geometries describe? Do they form a basis of the black-hole Hilbert space?* (1.4.1)

It has been shown in [55, 56] that the constructed superstrata account for an entropy scaling like

$$S_{\text{superstrata}} \sim 2\pi\sqrt{N_1 N_5} N_P^{1/4}\,, \tag{1.4.2}$$

which is parametrically less than that of their corresponding BMPV black hole (1.2.7). Of course, this does not mean that one could never find more microstate geometries than the number associated to the entropy (1.4.2). But it is not clear whether the microstate geometries actually need to account for the entirety of the black-hole entropy to be relevant for black-hole physics, as

microstate geometries could capture many of the physics characterizing fuzzballs although they do not have the stringy degrees of freedom.

One could see, in the discrepancy between (1.4.2) and (1.2.7), an indication that the metric is an effective description of collective modes of black-hole microstates, and that most of individual microstates do not admit a metric. Within this hypothesis, one could hardly make sense of the Fuzzball hypothesis, as if there is no metric, one cannot define the absence or presence of a horizon. However, recent developments suggest that "horizonless" in the sense of the metric could be generalized to a notion which does not involve the metric [57].

Besides, a theorem in quantum mechanics shows that in a finite-dimensional Hilbert space, one can find an overcomplete basis of coherent states in the Hilbert space [58]. In quantum mechanics, the coherent states minimize Heisenberg's uncertainty principle and follow closely classical trajectories. For black-hole physics, coherent black-hole microstates could be the microstates corresponding to the superposition of coherent supergravitons, and that admit subsequently a metric description.

Furthermore, what would happen when a macroscopic infalling observer interacts with the black hole? Would the black hole's wavefunction collapse into that of a coherent state? If yes, the question whether the observer encounters a smooth horizon or something else does make sense.

Thus, perhaps the real question about supergravity is the following. *Consider all the possible coherent states of the black hole which admit a metric: Do they account for the black-hole entropy? Do they have a finite curvature, so that they can be captured by supergravity?* For the 2-charge black hole, for which the number of microstates match the number of Lunin-Mathur geometries [59–62] one can construct, the most typical states have a curvature that is arbitrarily high, making them out of range of supergravity description. Nevertheless, the two-charge black hole has its horizon and singularity at the same location. Therefore it is not clear whether the high-curvature of the microstates comes from the singularity or from the horizon. A question the Microstate Geometries programme tries to address concerns the three-charge black holes, whose horizon and singularity do not lie at the same point: *Do the horizonless states admitting a metric account for the three-charge black-hole entropy, and do they have a low enough curvature to be described by supergravity?*

Before going further, let us note that the above formula (1.4.2) counts the number of superstrata that have been constructed in [51, 52]. The *originally designed superstrata*, corresponding to the shape modes along a general supertube profile in the $g_s N \ll 1$ regime, have an entropy scaling like [54]

$$S_{\text{shape superstrata}} \sim 2\pi\sqrt{N_1 N_5 N_P}\,, \tag{1.4.3}$$

which matches the Bekenstein-Hawking entropy (1.2.7). However, their gravitational backreaction have not been constructed, as their base space metric would not be simply flat, but almost hyper-Kähler, which introduces a technical difficulty.

Typicality and quantum fluctuations

An important constraint about the basis of the Hilbert space made of fuzzballs or microstate geometries concerns the typicality of a general quantum state made out of this basis [63]. Sta-

tistically, a random quantum state should have much similarities with respect to the statistical average, *i.e.* the black-hole solution.

Consider a Hermitian operator, A, acting on a finite-dimensional Hilbert space of dimension e^S. The average value of A, $\langle A\rangle$, is given by the trace of its product with the density matrix of the microcanonical ensemble, ρ_E:

$$\langle A\rangle = \mathrm{tr}(\rho_E A)\,. \tag{1.4.4}$$

Then, if one embeds the probability distribution, $d\mu_\Psi$, on the set of pure states, one can compute the average deviation of pure states, $|\Psi\rangle$, around the average value, $\langle A\rangle$:

$$\int d\mu_\Psi \left(\langle\Psi|A|\Psi\rangle - \langle A\rangle\right)^2 . \tag{1.4.5}$$

If one *assumes* $d\mu_\Psi$ to be the Haar measure, one can show that [63]

$$\int d\mu_\Psi \left(\langle\Psi|A|\Psi\rangle - \langle A\rangle\right)^2 = \mathcal{O}\left(e^{-S}\right)\,. \tag{1.4.6}$$

The relation (1.4.6) means that the average displacement of an operator on a pure state with respect to its value on the maximally mixed state is exponentially suppressed.

The vectors in the basis $(|f_1\rangle, \ldots, |f_{e^S}\rangle)$ of the Hilbert space can be more atypical, but they are expected to satisfy [63]

$$\left|\langle f_i|A|f_i\rangle - \langle A\rangle\right| = \mathcal{O}\left(\frac{1}{\sqrt{S}}\right)\,. \tag{1.4.7}$$

However, for the case of fuzzballs, it is not clear which are the correct Hermitian operators, A, on which one can effectively apply the relations (1.4.6) and (1.4.7). Indeed, how can one take A to be the metric components one Planck length above the horizon, $g_{\mu\nu}(r_h + l_P)$, and then compare the value of A for a black hole and a fuzzball, if Fuzzballs do not have a horizon? Should one rather define this point in both geometries by sending light rays from the asymptotic infinity, in which case one needs to send the light rays with a high precision to be able to define the point just above the horizon?

Another challenge for the Microstate Geometries programme pertains to the quantum fluctuations of such supergravity solutions [64]. Indeed, the solution space of all microstate geometries of a given black hole should be quantized, as the solutions are described by supergravity. It means that one particular supergravity solution cannot be defined precisely in a phase-space location, but rather as a "cell" or a "droplet" occupying a volume of h^{2m}, where h is Planck's constant and $2m$ is the dimension of the phase space. However, if two points of the same cell in the phase space correspond to two geometries that are macroscopically different one another, then it means that quantum fluctuations are large for any geometry defined in that cell; therefore, the supergravity description breaks down.

As a consequence, if one happens to find a basis of horizonless solutions from supergravity, not only should the solutions be typical enough from relation (1.4.7), but they also should not have too large quantum fluctuations.

Finally, within the Microstate Geometries programme, one still has to make sense of a quantum superposition of geometries. One may then define the averaging over geometries and answer to the question:

How does the horizon emerges from averaging over the microstructure defining the fuzzball? (1.4.8)

Stability of microstate geometries

Large families of microstate geometries have been constructed up to now, and one may one day construct e^S of them. However, could these geometries be in some sense unstable, and that the horizon-scale microstructure that replaces the horizon evolves into a standard horizon?

Of course, the answer to this question could differ depending on supersymmetric and non-supersymmetric configurations. Let us, for the following, focus on the supersymmetric case. For supersymmetric configurations, the solutions are stationary. However, one can model the instability in the following way. One of the main properties of constructed microstate geometries is their deep throat and large redshift the bottom to the top of the throat. As such, a small amount of energy as seen from the asympotics will become large at the bottom of the throat due to blueshift, and this energy could perturb the structure replacing the horizon, and force the solution to move in moduli space. This raises two questions:

1. Take p_0 and p_1 two points in moduli space, corresponding to two microstate geometries (or more generally, two solutions of string theory). Is there a definition of a distance on moduli space that characterises the possibility of moving adiabatically from p_0 to p_1 by adding a finite amount of energy to p_0 and within a finite time? (A finite distance linking p_0 and p_1 would mean that it is possible, while an infinite distance means that it is not possible.)
2. What actually happens when one perturbs the microstate geometry with that energy? Does this energy dissolves into the numerous degrees of freedom lying at the bottom of the throat, or is there a mechanism that drives the solution to move in one particular direction in moduli space? In the latter scenario, could the solution move towards the black-hole solution and reach it?

General properties of capped geometries

Known microstate geometries look like black holes except in the horizon region where they cap-off smoothly. The presence of a smooth cap introduces physics that could differ from that of a classical black hole.

What are the properties of microstate geometries that are similar, or different, from those of a classical black hole? In particular, do they display gravitational echoes? Do they induce tidal forces? How long does it take for an infalling particle to scramble into the microstate geometry? Do microstate geometries display properties of quantum chaos?

Finally, can one observe signatures of a horizonless structure? If fuzzballs and classical black holes differ in some properties, can one experimentally distinguish them?

1.4.3 Contributions of this manuscript

In Chapter 2 and 3, we investigate the notion of distance on the space of solutions of a class of microstate geometries – the bubbling solutions. On the one hand, the moduli space of microstate geometries is thought as a classical phase space upon which *geometric quantization* gives the number of quantum microstates of the black hole. On the other hand, the moduli space of Calabi-Yau compactifications is a space of effective field theories whose domain of validity can be delimited by Swampland notions.

Following [16], we investigate the connection between these two viewpoints, in the region of the moduli space where *multi-centered solutions* degenerate into the black hole – the *scaling limit*. We show, from the Kähler structure of the solution's phase space and using *quiver quantum mechanics*, that although the metric component in moduli space blows up near the scaling limit, the distance to the scaling limit is surprisingly *finite*.

Furthermore, following [17], we confirm these results by computing a DeWitt distance applied to the scaling limit. However, from another DeWitt distance which is used in the context of the Swampland programme, the distance of the scaling limit is *infinite*. This infinite distance seems natural from the Swampland perspective, as in the scaling limit, an infinite tower of Kaluza-Klein modes become massless. We comment on the possible physical implications of this mismatch.

In Chapter 4, we study *gravitational multipole moments* which are a class of observables that can distinguish microstate geometries with black holes from general relativity. Following [18], we analyse a family of non-supersymmetric extremal black holes and their horizonless microstate geometries in four dimensions, which provide interesting prototypes to study deviations from Kerr solutions caused by new horizon-scale physics. We then invent a method to analytically compute gravitational multipoles of a new family of four-charge non-supersymmetric rotating black holes and of their microstate geometries. We further show that these black holes we constructed from the *STU supergravity* model can have the same mass, charges and spin as an almost-neutral Kerr-Newman black hole, but with a very different tower of gravitational multipoles. Therefore, this work sheds light on possible observables that can be detected in the near-future by the detector eLISA.

In Chapter 5, we compute the tidal effects on a string following infalling null geodesics in a family of black hole microstate geometries — the superstata. Indeed, a notable difference between holographic correlators in a black hole background and those in a microstate geometry is that the latter display gravitational echoes due to the presence of the smooth cap in place of the horizon. However, as shown in earlier literature, stringy corrections to these correlators can be large, as *tidal forces* excite the massive modes of a massless string falling into the geometry from infinity, prohibiting the probe to return back to infinity.

An intriguing question is to understand what is the holographic dual of these tidal forces; the first step for solving this puzzle is to characterize their effects on the string. The results in earlier literature suggest there are no tidal forces along the toroidal directions. However, following [19], we show that this was an artefact of a particular geodesic. On a more generic geodesic, we prove, using *Penrose limits*, that the string feels tidal stresses along *all* possible directions. Furthermore, we show that the tidal effects alternate between compression and stretching, whereas in earlier

literature the effects were either one or the other. This is important data that informs the picture of *tidal scrambling* in the CFT.

In Chapter 6, we follow [20] and bring to light, by using *string duality generating techniques*, *new degrees of freedom* that prevent a macroscopic horizon to form in the limit where superstrata seem to degenerate into black holes. To do so, we construct solutions with zero horizon area that have the same charges as a three-charge F1-NS5-P Type-IIA black hole and preserve the black hole's spherical symmetry. The solutions have degrees of freedom which correspond to local brane density modes along the common F1-NS55 circle, and are momentum carriers that have no extension in the non-compact spatial directions. We argue that these solutions should be interpreted as the long-throat limit of superstrata. The existence of these geometries thus indicates that a finite-size horizon does not appear even in the singular corners of the moduli space of three-charge microstate geometries.

Chapter 2

Black holes and the Swampland: the Deep Throat Revelations

2.1 Introduction

The fact that black holes are statistical objects with temperature and entropy raises two key issues. First, how to describe the microstates accounting for the statistical entropy? Second, how does the black hole restore the information that falls in it? String Theory's historical answer to the first question is to describe the microstates at low string coupling, where all the possible open strings that stretch between brane bound states have an entropy that matches the statistical entropy of the black hole. As the string coupling constant is tuned to larger values to a regime where gravity is dominant, the branes expand in size, so one could expect that the microstates differ from the black hole at horizon-scale.

The Fuzzball paradigm [7, 8] proposes that black hole microstates do possess a horizon-size structure that differs from the classical black hole. Within this approach, it is expected that the black hole evaporation is similar to the burning of a star or a piece of coal [12], differing from Hawking's calculation which leads to the Information Paradox. Within the Fuzzball paradigm, the Microstate Geometries programme [13,14] endeavours to describe these black hole microstates within the Supergravity approximation of String Theory by smooth horizonless solutions. If one succeeds in finding a large number — hopefully e^S — of them, then one has answered to the question "What do black hole microstates look like?".

In many classes of microstate geometries, the infinitely-long throat of an extremal black hole is replaced by a cap at the end of a long, but finite throat [43, 50, 51] (See Fig. 2.1). The procedure to construct a large number of Supergravity microstates is the following: Take a black hole with given charges and angular momenta. Supergravity admits a large number of solutions with finite throat length, with charges and angular momenta equal to those of the black hole. In the moduli space (of a particular superselection sector, if any),[1] each of these solutions admits

[1] In some models of microstate geometries, as in Multi-centered bubbling models, there are families of solutions labeled by the fluxes Γ_i wrapping the bubbles (see Section 2.2). Inside each of these families, or *superselection sectors* [65], there are still real parameters left to characterize the solutions, defining a moduli space. There are restrictions on the bubble fluxes (and on the superselection sectors) to admit a

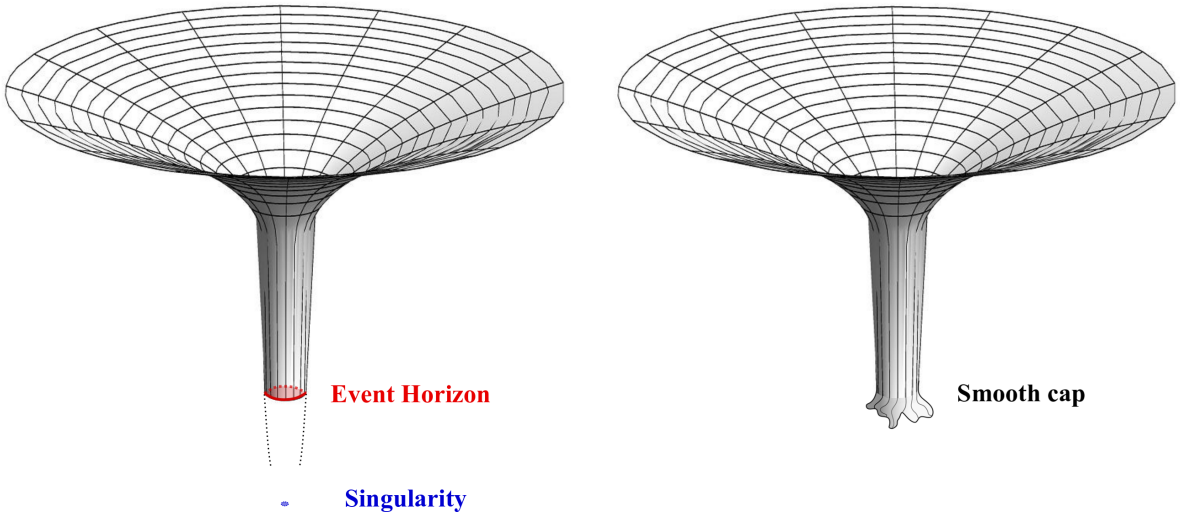

Figure 2.1 – Schematic picture of a classical black hole (left) and a microstate geometry (right). From the asymptotic observer's point of view, instead of the event horizon lying at the bottom of a throat of infinite length, a microstate geometry would replace it with a smooth cap lying at the bottom of a throat of finite length. In the scaling limit, its throat length increases to infinity while the cap's geometry stays constant. The figures are from [15].

a limit — called the *scaling limit* — where, from the perspective of an observer at infinity, they become more and more similar to the black hole; in particular, their throat length increases to infinity in the scaling limit, while the size of the cap remains fixed.[2]

In the moduli space of solutions, the scaling limit point plays a particular role, for the following reasons:
(1) The scaling limit lies at the boundary of moduli space where the throat length increases to infinity.
(2) As we approach the scaling limit, global symmetries of the black hole, which obeys the no-hair theorem, are restored. For instance, microstate geometries do not generically possess the SO(3)-rotational symmetry of the black hole.
(3) Everywhere in moduli space, energy excitations at the bottom of the throat of deep microstates are gapped. Their gap matches that of their dual CFT states [43, 68]. However, in the scaling limit, the mass gaps of these modes decrease to zero, because of the increasing redshift due to the lengthening of the throat.

Taking the limit to a boundary point of moduli space is reminiscent of the Swampland Distance Conjecture [69], that we are reformulating hereinbelow. Consider an effective field theory consistent with quantum gravity, with an arcwise-connected moduli space — a point in

scaling limit; but here, we consider one superselection sector which does.

[2]Infinitely-long throats arise in extremal black holes, but not in non-extremal ones, so this procedure to construct microstate geometries *a priori* applies only for extremal black holes. Although in this paper we will only consider a class of extremal BPS black holes and their microstate geometries, scaling solutions can arise in similar non-BPS extremal black holes as well [66, 67, 18].

the moduli space fixes the expectation value of the scalar fields of the EFT. The Swampland Distance Conjecture states that:
(1) The moduli space is not bounded in terms of its geodesic distance d. In other words, given p_0 a point in the bulk of the moduli space, there exists a family of arcwise-connected points $\{p\}$ going from p_0 to an infinite geodesic distance with respect to p_0.
(2) Global symmetries are restored at infinite distance in moduli space. [70]
(3) Given the point p_0 and the path of points $\{p\}$ defined in (1), there exists $\alpha > 0$ and there exists an infinite tower of states with an associated mass scale $M(p)$ such that

$$M(p) \underset{d(p_0,p)\to\infty}{\sim} M(p_0)\, e^{-\alpha d(p_0,p)}\,. \tag{2.1.1}$$

Originally, the distance in moduli space was defined according to the kinetic terms of the scalar fields in the EFT in the following sense: Consider a d-dimensional EFT whose action in the d-dimensional Einstein frame is written as

$$S = \int d^d x\sqrt{-g}\left[\frac{R}{2} - g_{ij}\left(\phi^i\right)\partial\phi^i\partial\phi^j + ...\right]\,. \tag{2.1.2}$$

Then g_{ij} defines a metric on the moduli space of effective field theories. Following [71], it has been proposed to generalise the Swampland Distance Conjecture — about moduli spaces of scalar fields — to a space of metrics. A notion of distance can be defined on a transverse-traceless metric $g_{\mu\nu}$ of a spacetime M of volume $V_M = \int_M \sqrt{g}$ [72]

$$\Delta_{\text{generalized}} = c\int_{\tau_i}^{\tau_f}\left(\frac{1}{V_M}\int_M \sqrt{g}\,\mathrm{tr}\left[\left(g^{-1}\frac{\partial g}{\partial\tau}\right)^2\right]\right)^{\frac{1}{2}}\mathrm{d}\tau\,. \tag{2.1.3}$$

This distance boils down to the moduli space of the scalar fields in the case of Calabi-Yau compactifications on 4-dimensional Minkowski space [73].

Thanks to this notion of distance between two metrics, it was argued in [71] that the vanishing limit of the negative cosmological constant, Λ, in an AdS vacuum in String Theory leads to an infinite tower of light states — for instance the tower of Kaluza-Klein modes of some decompactifying parts from the internal manifold. Using the distance (3.1.7), the authors of [74] computed distances on the space of black holes metrics and related the infinite black-hole-entropy limits to both massless Kaluza-Klein modes of an internal Calabi-Yau manifold and possibly Goldstone modes of BMS-like transformations on the black hole horizon.

To extend the Swampland Distance Conjecture for metrics to the scaling limit of microstate geometries, we would like to show that the infinite tower of gapped modes on top of any microstate geometry collapses, and the masses of all these modes decrease exponentially. In this paper, we study a class of *bubbling microstate geometries*, that descend in 4 dimensions to *multicentered solutions* [46, 44]. In the scaling limit, different microstate geometries approach the BMPV black hole [42]. These microstate geometries possess an $\mathrm{AdS}_2 \times \mathrm{S}^3$ throat. We will show that, in the scaling limit, the mass the Kaluza-Klein modes of the S^3 measured by an observer at spacial infinity decrease exponentially with respect to the length of the throat. At the bottom of this throat lie also non-trivial two-cycles; the mass of the M2 branes wrapping these two-cycles

decrease exponentially in the same fashion in the scaling limit. By reading off the expression inside the exponential, one can infer the distance in moduli space $\Delta_{\text{exponential}}$ that would be in agreement with the extension of the Swampland Distance Conjecture; one thus expects this distance to be proportional to the length of the AdS_2 throat, which is becoming *infinite* in the scaling limit. As a result, our study quite possibly extends the Swampland Distance Conjecture in a rather unusual way.

In addition, we will also compare this distance with another notion of distance in the moduli space of solutions, whose computation is independent of Swampland notions. Out of a Lagrangian theory characterizing a set of fields ϕ^A, the symplectic form, Ω, of the theory can be defined, from the Crnković-Witten-Zuckerman formalism, as an integral over a Cauchy surface Σ [75, 76]

$$\Omega = \int d\Sigma_l \; \delta \left(\frac{\partial L}{\partial(\partial_l \phi^A)} \right) \wedge \delta\phi^A \,. \tag{2.1.4}$$

If Ω is closed and non-degenerate, the $2m$-dimensional solution-space manifold is reinterpreted as the *phase space*, whose symplectic volume (in units of h^m) gives the number of microscopic ground states. When the phase-space manifold is furthermore endowed with an integrable complex structure, J, and if $\Omega(\cdot, J\cdot)$ is a Riemannian metric, the manifold is Kähler and one can define a distance, Δ_{phase}, on the moduli space of solutions using the Kähler metric $\Omega(\cdot, J\cdot)$. Luckily, the solution space of *three-centered multicenter solutions* one constructs as Microstate geometries is a Kähler manifold [64]; so we will measure the distance to the scaling limit with respect to this Kähler metric.

Surprisingly, we find that with respect the "canonical" Δ_{phase} that would be in agreement with computations in [64], the scaling limit lies at *finite* distance in moduli space, in tension with the distance $\Delta_{\text{exponential}}$. However, the computation of Δ_{phase} is performed at weak string coupling regime using quiver quantum mechanics, and one can wonder whether this computation is still reliable in the regime where Supergravity dominates. However, in [64], the authors argue that the reduced symplectic form does not vary with the string coupling constant thanks to a non-renormalization theorem, and further conclude that Supergravity is breaking down because of large quantum fluctuations in scaling geometries, and hence could not be a good description of these geometries. From the weak-coupling regime, they also infer that the scaling limit, which was perfectly in reach within Supergravity, is actually prohibited if one accounts for quantum effects, which prevent the quantum wave functions to populate the region of classical moduli space close to the scaling limit. Thus, if the correct normalization of distance on moduli space is given by $\Delta_{\text{exponential}}$ and not by Δ_{phase}, then the breakdown of Supergravity due to quantum effects prescribed in [64] would be softened.

The organisation of the paper is the following. In Section 2.2, we review smooth multi-centered bubbling solutions in five dimensions (and their M-theory uplift) of [43]. In Section 2.3, we first compute how the throat lengths of bubbling solutions behave in the scaling limit. We then find an exponential decrease of the S^3 Kaluza-Klein mass tower, consistent with a naive extension of the Swampland Distance Hypothesis to this system. In Section 2.4, we study the moduli space of three-centre bubbling solutions, independently of the Swampland programme. Using the results of [64], we determine the metric on moduli space of solutions coming from

the symplectic form. We show that with this distance, Δ_{phase}, the scaling limit lies at finite distance in moduli space and that all the moduli space is bounded. In section 2.5, we discuss the tension between the two distances on moduli space and share some insight about the ability of Supergravity to describe black hole microstates with arbitrarily deep throats.

2.2 Multicenter bubbling solutions

2.2.1 Multicenter bubbling solutions in 5 and 11 dimensions

Upon compactifying maximal eleven-dimensional Supergravity on Calabi-Yau threefold, the resulting five-dimensional $\mathcal{N} = 2$ supergravity coupled to n_V vector multiplets with $n_V \leq 2$ contains the following bosonic fields:

- a gravitational field, g,
- $n_V + 1$ U(1) vector gauge fields, A^I_μ, whose field strengths are denoted $F^I = d_5 A^I$,
- $n_V + 1$ scalars, X^I.

This theory is described by the action

$$(16\pi G_5)\, S_5 = \int d^5x\, \sqrt{-g}\, R - Q_{IJ} \int \left(F^I \wedge \star_5 F^J - d_5 X^I \wedge \star_5 d_5 X^J\right) + \frac{C_{IJK}}{6} \int A^I \wedge F^J \wedge F^K\,, \tag{2.2.1}$$

where C_{IJK} are the structure constants satisfying the fixed-volume constraint

$$\frac{1}{6}\, C_{IJK}\, X^I X^J X^K \,=\, 1 \qquad \Longrightarrow \qquad X_I \,=\, \frac{1}{6}\, C_{IJK}\, X^J X^K\,, \tag{2.2.2}$$

and the couplings Q_{IJ} depend on the scalars via

$$Q_{IJ} \,=\, \frac{9}{2}\, X_I X_J - \frac{1}{2}\, C_{IJK} X^K\,. \tag{2.2.3}$$

The action admits the following Einstein-Maxwell-scalar equations of motion

$$\begin{aligned} R_{\mu\nu} \,+\, Q_{IJ} \left(\partial_\mu X^I \partial_\nu X^J \,+\, F^I_{\mu\rho}\, F^{J\rho}_\nu \,-\, \frac{1}{6}\, g_{\mu\nu}\, F^I_{\rho\sigma}\, F^{J\rho\sigma}\right) \,&=\, 0\,, \\ d_5 \left(Q_{IJ} \,\star_5\, F^J\right) \,+\, \frac{1}{4}\, C_{IJK}\, F^J \wedge F^K \,&=\, 0\,, \\ -d_5 \star_5 d_5 X_I \,+\, \left(C_{IJK} X_L X^K - \frac{1}{6} C_{ILJ}\right) \left(F^L \wedge \star_5 F^J - dX^L \wedge \star_5 dX^J\right) \,&=\, 0\,. \end{aligned} \tag{2.2.4}$$

The most general supersymmetric solution to $\mathcal{N} = 2$ five-dimensional Supergravity coupled to n_V extra gauge fields with structure constant C_{IJK}, admitting a time-like Killing vector ∂_t are characterized by $n_V + 1$ electric warp factors Z_I, $n_V + 1$ magnetic self-dual two-forms Θ^I, an angular momentum one-form ω, and a space-like hyper-Kähler manifold $\mathcal{B}$. The metric and the field strengths are stationary, and are split in the following way [77, 78]:

$$\begin{aligned} ds_5^2 \,&=\, -\left(\frac{1}{6} C_{IJK}\, Z_I Z_J Z_K\right)^{-\frac{2}{3}} (dt + \omega)^2 \,+\, \left(\frac{1}{6} C_{IJK}\, Z_I Z_J Z_K\right)^{\frac{1}{3}} ds\,(\mathcal{B})^2\,, \\ F^I \,&=\, d_4 A^I \,=\, d_4 \left(Z_I^{-1}\,(dt + \omega)\right) \,+\, \Theta^I\,. \end{aligned} \tag{2.2.5}$$

In terms of these new data, the Einstein-Maxwell-scalar equations of motion (B.1.11) are rewritten as the so-called BPS equations

$$\star_4 \Theta^I \;=\; \Theta^I\,, \quad \text{with } d_4\Theta^I \;=\; 0\,, \tag{2.2.6}$$

$$\nabla_4{}^2 V \equiv \star_4 d_4 \star_4 d_4\, Z_I \;=\; \frac{1}{2} C_{IJK}\, \star_4 \left(\Theta^J \wedge \Theta^K\right)\,, \tag{2.2.7}$$

$$d_4\omega \;+\; \star_4 d_4 \omega \;=\; Z_I\, \Theta^I\,. \tag{2.2.8}$$

The first set of $n_V + 1$ equations (2.2.6) ($I = 1, \ldots, n_V + 1$) determine the magnetic two-forms. The second set of $n_V + 1$ equations (2.2.7) determine the electric warp factors, sourced by the magnetic fields. The fact that magnetic fluxes source a net electric charge is made possible thanks to the Cherns-Simons term in the five-dimensional Supergravity action (B.1.9); this is essential in the construction of smooth solitonic solutions in Supergravity. The last equation (2.2.8) tells that the angular momentum ω is sourced by electric and magnetic fields, recalling the Poynting vector in electromagnetism.

We now consider $\mathcal{B}$ to be a four-dimensional Gibbons-Hawking space. The Gibbons-Hawking space is made of multiple centers of Kaluza-Klein monopoles. The Gibbons-Hawking space possesses non-trivial two-cycles called bubbles, defined by the shrinking of the coordinate ψ fibered along any line running between a pair of Gibbons-Hawking points in $\mathbb{R}^3$. The spatial part of the metric in (2.2.5) is thus an S^1 fibered along $\mathbb{R}^3$; it is determined by a harmonic function V in $\mathbb{R}^3$ ($\nabla_3{}^2 V \equiv \star_3 d_3 \star_3 d_3 V \;=\; 0$) and a one-form A (with $\nabla_3 A \equiv \star_3 d_3 A = d_3 V$):

$$ds\,(\mathcal{B})^2 \;=\; V^{-1}\,(d\psi + A)^2 \;+\; V\,\left[\, d\rho^2 + \rho^2\,\left(d\vartheta^2 + \sin^2\vartheta\, d\phi^2\right)\right]\,. \tag{2.2.9}$$

The potential V is sourced by a set of n Gibbons-Hawking centres labeled by j, of charge q_j:

$$V(\vec{\rho}) \;=\; h_\infty \;+\; \sum_{j=1}^{n} \frac{q_j}{\rho_j}\,, \qquad A \;=\; \sum_{j=1}^{n} q_j\, \cos\vartheta_j\, d\phi_j\,, \tag{2.2.10}$$

where $(\rho_j, \vartheta_j, \phi_j)$ are the shifted spherical coordinates around the j^{th} center. The potential V is a harmonic function on $\mathbb{R}^3$. The Gibbons-Hawking space pinches off smoothly around each center j: the geometry is a flat $\mathbb{R}^4$ modded by $\mathbb{Z}_{|q_j|}$ along ψ, where $q_j \in \mathbb{Z}$. Besides, $\mathbb{R}^4$ is asymptotically modded by $\mathbb{Z}_{\sum |q_j|}$, so it is convenient to subsequently impose $\sum_j |q_j| = 1$ to have an asymptotic $\mathbb{R}^4$.

We will consider solutions that are independent of ψ. With this assumption, the other solution data — Z_I, Θ^i and ω — are all given in terms of harmonic functions on $\mathbb{R}^3$.

The $n_V + 1$ self-dual magnetic two-forms Θ^I are of the form

$$\Theta^I \;=\; \partial_a \left(V^{-1}\, K^I\right) \Omega^a\,, \tag{2.2.11}$$

where $(\Omega^1, \Omega^2, \Omega^3)$ is a basis of self-dual (in 4 dimensions) two-forms and K^I are harmonic functions on $\mathbb{R}^3$ of the form

$$K^I \;=\; k^I_\infty \;+\; \sum_{j=1}^{n} \frac{k^I_j}{\rho_j}\,. \tag{2.2.12}$$

The number $k_i^I - k_j^i$ is the magnetic flux on the two-cycle between centres i and j.

The $n_V + 1$ warp factors Z_I are

$$Z_I \;=\; L_I \;+\; \frac{C_{IJK}}{2}\frac{K^J K^K}{V} \tag{2.2.13}$$

where L_I is a harmonic function on $\mathbb{R}^3$ is

$$L_I \;=\; l^I_\infty \;+\; \sum_{j=1}^{n} \frac{l^I_j}{\rho_j}\,. \tag{2.2.14}$$

From the 5-dimensional Supergravity perspective, l^I_j is the electric charge of L_I at the j^{th} center.

Finally, the angular-momentum one-form can be decomposed along the U(1) ψ-fiber:

$$\omega = \left(M \;+\; \frac{K^I L_I}{2\,V} \;+\; \frac{C_{IJK}}{6}\frac{K^I K^J K^K}{V^2}\right)(d\psi + A) \;+\; \varpi \equiv \mu\,(d\psi + A) \;+\; \varpi\,, \tag{2.2.15}$$

where ϖ is a one-form on $\mathbb{R}^3$ and M — the harmonic conjugate of ω in (2.2.8) — is a harmonic function on $\mathbb{R}^3$ of the form

$$M \;=\; m_\infty \;+\; \sum_{j=1}^{n} \frac{m_j}{\rho_j}\,. \tag{2.2.16}$$

To put it in a nutshell, the multicenter bubbling solutions are characterized by the harmonic functions $\Gamma = (V, K^1, \ldots, K^{n_v+1}; L_1, \ldots, L_{n_v+1}, M)$ on $\mathbb{R}^3$. Schematically, we can write

$$\Gamma = \Gamma_\infty + \sum_{j=1}^{n} \frac{\Gamma_j}{\rho_j}\,. \tag{2.2.17}$$

One can define a symplectic product on $\mathbb{R}^{2n_V+4}$: for $A = (A^0, A^1, \ldots, A^{n_v+1}; A_1, \ldots, A_{n_v+1}, A_0)$ and $B = (B^0, B^1, \ldots, B^{n_v+1}; B_1, \ldots, B_{n_v+1}, B_0)$,

$$\langle A, B\rangle \;\equiv\; A^0 B_0 - A_0 B^0 + A^I B_I - A_I B^I\,. \tag{2.2.18}$$

The absence of Dirac-Misner strings in the multicenter bubbling solutions then leads to conditions on the relative positions of the Gibbons-Hawking centres, the so-called *bubble equations*, or *Denef integrability equations* [46, 41]:

$$\sum_{j=1}^{n} \frac{\langle \Gamma_i, \Gamma_j\rangle}{\rho_{ij}} \;=\; \langle \Gamma_\infty, \Gamma_i\rangle\,, \qquad \text{for } i \;=\; 1, \ldots n\,. \tag{2.2.19}$$

2.2.2 The STU model

The requirement that the five-dimensional geometry be asymptotically flat $\mathbb{R}^{1,4}$ constrains the asymptotic values of the harmonic functions h_∞, l_∞ and k_∞ such that

$$V = \sum_{j=1}^{n} \frac{q_j}{\rho_j}\,, \qquad L_I = 1 + \sum_{j=1}^{n} \frac{l^I_j}{\rho_j}\,, \qquad K^I = \sum_{j=1}^{n} \frac{k^I_j}{\rho_j}\,, \qquad M = m_\infty \;+\; \sum_{j=1}^{n} \frac{m_j}{\rho_j}\,. \tag{2.2.20}$$

Besides, requiring the resulting geometry to be smooth in five-dimensions amounts to constraining the values of the electric and momentum charges in terms of the magnetic and Kaluza-Klein monopole charges [40, 79]:

$$l_j^I \;=\; -\frac{1}{2} C_{IJK} \frac{k_j^J k_j^K}{q_j}\,, \qquad m_j \;=\; \frac{1}{12} C_{IJK} \frac{k_j^I k_j^J k_j^K}{q_j^2}\,. \tag{2.2.21}$$

These conditions allow each centre to preserve 16 supercharges; the overall solution, made of several centres, preserves 4 supercharges as the BMPV black hole [42]. It can be shown that this solution is equivalent to multiple stacks of D3-branes at angles in a T-dual frame [79].

The $\mathcal{N}=2$ five-dimensional Supergravity coupled to $n_V = 2$ extra vector fields has a metric and field strength (2.2.5) that simplify to three-charge solutions:

$$\begin{aligned} ds_5^2 \;=\; & -\left(Z_1 Z_2 Z_3\right)^{-\frac{2}{3}} \left(dt + \mu\left(d\psi + A\right) + \varpi\right)^2 \;+\; V^{-1}\left(Z_1 Z_2 Z_3\right)^{\frac{1}{3}} \left(d\psi + A\right)^2 \\ & +\; V\,\left(Z_1 Z_2 Z_3\right)^{\frac{1}{3}} \left[d\rho^2 + \rho^2 \left(d\vartheta^2 + \sin^2\vartheta\, d\phi^2 \right) \right], \\ F^I \;=\; & d_3 \left(Z_I^{-1} \left(dt + \omega \right) \right) \;+\; \Theta^I\,. \end{aligned} \tag{2.2.22}$$

This class of horizonless solutions have the same asymptotic geometry as the 4-supercharge five-dimensional rotating BMPV black holes [42], which have a macroscopic horizon and are described by the harmonic functions

$$V \;=\; \frac{1}{\rho}\,, \qquad L_I \;=\; 1 + \frac{Q_I}{\rho}\,, \qquad K^I \;=\; 0\,, \qquad M \;=\; \frac{J_L}{\rho}\,. \tag{2.2.23}$$

Indeed, asympototically, these bubbling solutions behave like a BMPV black hole with charges Q_I, and left angular momentum J_L:

$$\begin{aligned} Q_I \;&=\; \sum_{j=1}^{n} l_j^I \;+\; C_{IJK} \sum_{(i,j)=1}^{n} k_i^J k_j^K\,, \\ J_L \;&=\; \frac{1}{2}\sum_{j=1}^{n} m_j \;+\; \frac{1}{2}\sum_{(i,j)=1}^{n} l_i^I k_j^I \;+\; \frac{C_{IJK}}{6} \sum_{(i,j,k)=1}^{n} k_i^I k_j^J k_k^K\,. \end{aligned} \tag{2.2.24}$$

In addition, the bubbling solutions have a right angular momentum J_R:

$$j \equiv J_R \;=\; \frac{1}{2}\left| \sum_{i<j} \langle \Gamma_i, \Gamma_j \rangle\, \hat{\rho}_{ij} \right| \;=\; \frac{1}{2}\left| \sum_{i} \langle \Gamma_\infty, \Gamma_i \rangle\, \vec{\rho}_i \right|, \qquad \text{with } \hat{\rho}_{ij} \;\equiv\; \frac{\vec{\rho}_i - \vec{\rho}_j}{|\vec{\rho}_i - \vec{\rho}_j|}\,. \tag{2.2.25}$$

Note that the left angular momentum J_L is the one on the ψ-fiber, whereas the right angular momentum J_R is understood as the angular momentum on $\mathbb{R}^3$. The BMPV black hole does not have any right angular momentum. Hence, as expected, by taking the scaling limit of multi-centered solutions, J_R vanishes.

The *scaling limit* is defined as the limit where the inter-centre distances ρ_{ij} (between centres i and j) shrinks uniformly to zero. The limit is parameterized by the *scaling parameter*, λ: $\rho_{ij} = \lambda d_{ij}$, with $\max d_{ij} \equiv d = \mathcal{O}(1)$.

Thus, given some charges Q_I and an angular momentum J_L for a BMPV black hole, there are various horizonless smooth bubbling solutions of n Gibbons-Hawking centres that have the same asymptotic charges as the BMPV black hole. Counting how many of these solutions there are decomposes into two steps. The first step is to count the number of possibilities for the charges of the GH centres $\Gamma_j = (q_j, k_j^I; l_j^I, m_j)$ such that their asyptotic charges (Q_I, J_L) matches the BMPV black hole's. Then, each charge configuration $(\Gamma_j)_{j=1,\dots,n}$ defines a superselection sector[3] that possesses a connected moduli space of solutions, whose quantization gives the number of states in that particular superselection sector. Now, right angular-momentum of the bubbling solutions, J_R, is generically different from 0 (the value for the BMPV black hole). So, if one wishes to count the number of states in a superselection sector that have J_R smaller than a threshold value ε, then one should apply the quantization procedure only in the region of moduli space where $J_R < \varepsilon$, which is in the vicinity of the scaling limit.

2.3 Kaluza-Klein modes at the scaling limit

The scaling limit is a point at the boundary of moduli space that plays a special role in the construction of microstate geometries. In order to understand the general shape of the vicinity of the scaling limit, there are two interesting questions. The first is whether the volume of the entire moduli space is finite. The second is whether the distance in moduli space between the scaling limit and any point in the bulk moduli space is finite or infinite. As distance on moduli space is a notion that arises in the Swampland context, we will try to tackle the second question through the lens of the Swampland programme.

2.3.1 The length of the AdS_2 throat in terms of the scaling parameter

It has been mentioned in the Introduction that in the scaling limit, the throat of microstate geometries deepens. We would like to estimate the length of the throat of a near-scaling solution presented in section 2.2.2, in terms of the scaling parameter λ. We will compute the length of the throat of bubbling solutions approaching the scaling limit, and compare its behaviour with respect to λ with the logarithmic divergence of the throat length of the BMPV black hole. The position of the centres in bubbling solutions is arbitrary (insofar as they satisfy the bubble equations), and different centre configurations will modify the throat length; however, we will show that this modification is set by the (coordinate) size of the region containing the centres.

For a BMPV black hole, the (radial) throat length is infinite, with the divergence being logarithmic. In other terms, let us fix a coordinate ρ_M not too far at infinity ($\rho_M < Q_I$); its distance to a near-horizon cut-off ρ_0 is

$$L^{\text{BMPV}}_{\text{throat}}(\rho_0, \rho_M) = \int_{\rho_0}^{\rho_M} V^{1/2} \left(Z_1 Z_2 Z_3\right)^{1/6} \mathrm{d}\rho \underset{\rho_0 \to 0}{=} \left(Q_1 Q_2 Q_3\right)^{1/6} \ln\left(\frac{\rho_M}{\rho_0}\right) + F(\rho_M)\,. \tag{2.3.1}$$

[3]The term *superselection sector* is here used in the sense that microstate geometries with different Γ_j fluxes — which are quantized — cannot be related from one to another by moving in the moduli space of solutions [65], except by quantum tunnelling.

The correction $F(\rho_M)$ is of order $\mathcal{O}\left(\frac{\rho_M}{Q_I}\right)$ and induced by the constant term in Z_I. At first order in ρ_M, it is equal to $\frac{\rho_M-\rho_0}{Q_{\text{har}}}$, where Q_{har} is the harmonic mean of (Q_1, Q_2, Q_3). This correction behaves like a constant as ρ_0 approaches 0.

Now, consider a family of smooth multi-center bubbling solution in 5D approaching the scaling limit. The Gibbons-Hawking centres are at a coordinate distance $\rho_{ij}(\lambda) = \lambda d_{ij}$ of each other, where $d \equiv \max d_{ij}$ is of order 1. We choose the origin of the coordinates such that all the GH centres are within a radius of $\rho = \lambda d$. We want to know how the throat length scales with the scaling parameter λ. The throat length shall be computed from the same $\rho_M < Q_I$ to a region at the bottom of the throat at coordinate $\rho_0(\lambda) > \lambda d$. We shall define for instance

$$\rho_0(\lambda) = 2 \max_{i,j} \rho_{ij}(\lambda) = 2\lambda d\,, \tag{2.3.2}$$

so that we are looking at the distance between the asymptotics and the blob of GH centres. The point is to keep some distance with respect to each individual GH centres. The length of the throat in question is

$$L_{\text{throat}}(\rho_0(\lambda), \rho_M) = \int_{\rho_0(\lambda)}^{\rho_M} V^{1/2} \left(Z_1 Z_2 Z_3\right)^{1/6} \mathrm{d}\rho\,. \tag{2.3.3}$$

As the scaling parameter λ is sent to zero, the metric of a bubbling solution approaches that of a BMPV black hole. The more we are away from the bottom of the throat, the better the BMPV black hole approximation to the bubbling solution is. More precisely, in the integration domain of the integral (2.3.3), $\rho_j = \rho + \mathcal{O}(\lambda d)$, and $\frac{1}{\rho_j} = \frac{1}{\rho}\left(1 + \mathcal{O}\left(\frac{\lambda d}{\rho}\right)\right)$; so the function $Z_I V$ approximates to

$$Z_I V = \frac{Q_I + \mathcal{O}(\lambda d \times \text{charges})}{\rho^2} + \frac{1}{\rho}\,. \tag{2.3.4}$$

The integrand of (2.3.3) is then

$$V^{1/2} \left(Z_1 Z_2 Z_3\right)^{1/6} = \frac{\left(Q_1 Q_2 Q_3\right)^{1/6}}{\rho} \left[1 + \mathcal{O}\left(\frac{\rho}{Q_I}\right) + \mathcal{O}\left(\frac{\lambda d}{\text{charges}}\right)\right]. \tag{2.3.5}$$

The first correction to the logarithm comes from the asymptotic behaviour dominated by the $1/\rho$ term in (2.3.4), and is exactly the same one as for the BMPV black hole. The second correction comes from the fact that the centres are arbitrarily distributed in a region of radius λd. Therefore, integrating the dominant term and its corrections leads to the following reorganization of terms [4]:

$$L_{\text{throat}}(\rho_0(\lambda), \rho_M) \underset{\lambda\to 0}{=} -\left(Q_1 Q_2 Q_3\right)^{1/6} \ln\left(\frac{2d\lambda}{\rho_M}\right) + F(\rho_M) + \mathcal{O}\left(\frac{\lambda d}{\text{charges}}\right) \ln\left(\frac{2d\lambda}{\rho_M}\right). \tag{2.3.6}$$

Although the positions of the Gibbons-Hawking centres are arbitrary, they lie in a small region inside $\rho < \lambda d$. So in the scaling limit, they give rise to the geometry of the BMPV black hole

[4] Note that we could have taken ρ_M arbitrarily big. The important point is that integrating the $\mathcal{O}\left(\frac{\rho}{Q_I}\right)$ term in (2.3.5) gives exactly the function $F(\rho_M)$ appearing in (2.3.1).

outside of the blob region ($\rho \geq 2\lambda d$), only up to small corrections. These are dominated by a $\lambda \ln(\lambda)$ term whose limit is zero. It was important to know that this correction's limit is zero, so that inverting equation (2.3.6) gives

$$\rho_0(\lambda) \underset{\lambda\to 0}{\sim} \rho_M \exp\left(-\frac{L_{\text{throat}}(\rho_0(\lambda),\rho_M) - F(\rho_M)}{(Q_1Q_2Q_3)^{1/6}}\right) . \tag{2.3.7}$$

2.3.2 The AdS_2 throat and Kaluza-Klein modes

In this section we compute the mass scale of the S^3 Kaluza-Klein towers. The five-dimensional metric (2.2.22) asymptotes to the $AdS_2 \times S^3$ metric in the throat region. Of course, near the Gibbons-Hawking centres, the geometry differs, but as long as we do not approach the GH centres too closely (for example $\rho \geq 10d\lambda$),

$$Z_I = \frac{Q_I}{\rho}\left(1 + \mathcal{O}(\rho)\right) , \qquad V = \frac{1}{\rho}\left(1 + \mathcal{O}(\rho)\right) , \tag{2.3.8}$$

so that we get the metric of an $AdS_2 \times S^3$ up to

$$\begin{aligned} ds_5^2 = &-\left[(Q_1Q_2Q_3)^{-\frac{2}{3}}\rho^2 + \mathcal{O}(\rho^3)\right](dt+\omega)^2 + \left[(Q_1Q_2Q_3)^{\frac{1}{3}}\frac{1}{\rho^2} + \mathcal{O}\left(\frac{1}{\rho}\right)\right]d\rho^2 \\ &+ \left[(Q_1Q_2Q_3)^{\frac{1}{3}} + \mathcal{O}(\rho)\right]\left[(d\psi + A)^2 + d\vartheta^2 + \sin^2\vartheta\, d\phi^2\right] . \end{aligned} \tag{2.3.9}$$

At the location where $\rho = \rho_0(\lambda)$, which, can be understood being roughly the "bottom of the throat", there is an infinite tower of Kaluza-Klein modes on the S^3, with the lightest mass measured at the bottom of the throat being

$$m_{KK}(\rho_0(\lambda)) \propto \frac{1}{R_{S^3}(\rho_0(\lambda))} \approx \frac{1}{(Q_1Q_2Q_3)^{\frac{1}{6}}} . \tag{2.3.10}$$

The mass of the n^{th} Kaluza-Klein mode measured at infinity gets redshifted to

$$M_n = n\, m_{KK}\sqrt{g_{tt}}|_{\rho=\rho_0(\lambda)} = n\, m_{KK}\,(Z_1Z_2Z_3)^{-1/3}\,|_{\rho=\rho_0(\lambda)} \approx \frac{n\,\rho_0(\lambda)}{(Q_1Q_2Q_3)^{1/2}} . \tag{2.3.11}$$

Injecting (2.3.7) into (2.3.11), we deduce that the tower of Kaluza-Klein states have masses that scale like

$$M_n(L_{\text{throat}}) \underset{\lambda\to 0}{\approx} \frac{n\,G(\rho_M)}{(Q_1Q_2Q_3)^{1/2}} \exp\left(-\frac{L_{\text{throat}}}{(Q_1Q_2Q_3)^{1/6}}\right) , \tag{2.3.12}$$

where $G(\rho_M) = \rho_M \exp\left(\frac{F(\rho_M)}{(Q_1Q_2Q_3)^{1/6}}\right)$ [5] . This decreasing exponential mass is consistent with the extension of the Swampland Distance Conjecture to this system that we discussed in the Introduction.

[5] The approximation sign $\approx$ in (2.3.12) is here for the factor $\frac{n\,G(\rho_M)}{(Q_1Q_2Q_3)^{1/2}}$ in front of the exponential, but the exponential is exact.

2.3.3 M2 branes at the bottom of the throat

More generally, any locus in the cap verifies the approximation $\rho_i \ll Q_I$, so although g_{tt} is not constant in the cap, its dependence with respect to the scaling parameter λ is the same everywhere in the cap, leading to the same redshift behavior

$$\sqrt{g_{tt}}|_{\rho_i=\lambda d_i} \underset{\lambda\to 0}{\sim} f(d_i)\,\lambda\,. \tag{2.3.13}$$

The proportionality factor, $f(d_i)$, depends on the location of the point in the cap and is set by the charges Γ_j.

As a result, M2-branes wrapping the two-cycle linking two Gibbons-Hawking centres will experience a redshift that globally scales like λ in the scaling limit, so using (2.3.7) and dropping the proportionnality constant gives

$$M_{\text{M2}} \underset{\lambda\to 0}{\sim} \exp\left(-\frac{L_{\text{throat}}}{(Q_1Q_2Q_3)^{1/6}}\right)\,. \tag{2.3.14}$$

We meet again the same exponential mass decrease for the tower of M2 branes.

As we go into the scaling limit and the throat becomes longer and longer, the M2 branes become also exponentially light.

Our system can be used to extend the Swampland Distance hypothesis. In our example, we move in the moduli space of metrics. In the scaling limit, the asymptotic geometry is unchanged. Besides, the size of the cap remains constant, as well as the inter-center physical proper distances [80], up to order $\mathcal{O}(\lambda)$: the geometry of the cap remains also fixed. In the scaling limit, the only modulus we are moving is the throat length which grows to infinity.

Let p_0 a point in moduli space (a reference point), characterising a solution that possesses a throat region; and $\{p(\lambda)\}_{\lambda\in(0,\lambda_0]}$ the set of points in moduli space approaching the scaling limit ($\lambda \to 0$) from $p(\lambda_0) = p_0$. By reading off the argument inside the exponential, one possible conclusion is that the distance in moduli space between p_0 and $p(\lambda)$ should be proportional to the length of $p(\lambda)$'s throat, $L_{\text{throat}}(\lambda)$:

$$\alpha\,\Delta_{\text{exponential}}(p_0, p(\lambda)) \underset{\lambda\to 0}{\sim} \frac{L_{\text{throat}}(\rho_0(\lambda), \rho_M)}{(Q_1Q_2Q_3)^{1/6}}\,, \tag{2.3.15}$$

where α corresponds to the mass decay rate of the Swampland Distance Conjecture in (3.1.9). The distance to the scaling limit would then be *infinite*.

Note that, instead of having n BPS Gibbons-Hawking centres coming closer to reach the scaling limit, the limit of n coincident BPS black holes in $\mathcal{N} = 1$ Supergravity merging together lies also at *infinite* distance in moduli space [81]. The computation leading to (2.3.12) does not require the horizonless regularity conditions (3.2.4) at each centre, and Gibbons-Hawking centres with a horizon going to the scaling limit are actually merging black holes. Our results thus agree with the infinite distance in moduli space in [81]. However, it is not clear that those two computations should give the same result. Indeed, the bubble equations (3.2.5) constrains the relative position of the "Denef black holes" (the Gibbons-Hawking centres with a horizon) from one another to be dependent of the charges Γ_i; whereas there is no such a constraint on

the relative position of the "Michelson-Strominger black holes" of [81].

Interestingly, $(Q_1Q_2Q_3)^{1/6}$ is approximately the radius of the 3-sphere in the regime $\rho_0(\lambda) < \rho < Q_I$. Indeed, the radius of the 3-sphere is $(Q_1Q_2Q_3)^{1/6}$ up to corrections of order $\mathcal{O}\left(\frac{\rho}{Q_I}\right)$ near $\rho \sim Q_I$, and corrections of order the magnitude of the charges Γ_j in the vicinity of $\rho \sim \rho_0(\lambda)$; so the throat looks very much like a cylinder with an S^3 base. Let us define the aspect ratio $\mathcal{R}$ of the throat to be the throat length divided by the radius of the S^3 base. Then

$$\alpha\, \Delta_{\text{exponential}}(p_0, p(\lambda)) \underset{\lambda\to 0}{\sim} \frac{L_{\text{throat}}(\rho_0(\lambda), \rho_M)}{R_{S^3}} = \mathcal{R}(\lambda)\,. \tag{2.3.16}$$

Note that reading off the argument of the decreasing exponential gives only the distance in moduli space in the vicinity of the scaling limit, and only in the direction towards the scaling limit; we do not have any piece of information about how the distance behaves near p_0.

2.4 Distance on the Phase space of Multi-centered bubbling solutions

The dimensional reduction of the smooth five-dimensional Supergravity solutions of Sections 2.2 and 2.3 along the ψ-fiber leads to the four-dimensional multi-centered solutions [44]. Describing these centres at equilibrium separations from each other (3.2.5) from Supergravity at $g_sN \gg 1$ is related to the quiver description of wrapped D-branes at $g_sN \ll 1$ [82]. As mentioned in the Introduction, one can compute the symplectic form from the quiver description, and, when possible, use the compatible complex structure to define a distance on moduli space, Δ_{phase}.

In this section, we wish to check whether the distance Δ_{phase} coincides with the distance obtained by reading off the exponential decrease.

2.4.1 Symplectic form from Quiver Quantum Mechanics

Given L, the Lagrangian governing the dynamics of n-centered bubbling solutions of four-dimensional $\mathcal{N} = 2$ Supergravity, coupled to n_V gauge fields, and given ϕ^A a basis of the fields appearing in the Lagrangian, the symplectic form of the Supergravity-solution space is defined by

$$\Omega \equiv \int d\Sigma_l\ \delta\left(\frac{\partial L}{\partial(\partial_l \phi^A)}\right) \wedge \delta\phi^A\,, \tag{2.4.1}$$

where Σ is a Cauchy surface (in the 4-dimensional spacetime). We consider $\tilde{\Omega}$ the restriction of the symplectic form Ω to the space of multicentered solutions (which verify the bubble equations). This consists of changing and restricting the variable fields ϕ^A, such that the new fields ϕ'^I define the $2n-2$-dimensional configuration of the n GH centres.

The symplectic form of BPS solutions in Supergravity is difficult to compute for multi-centre solutions through the Supergravity action. Nevertheless, in [64], the authors computed the symplectic form in the open string description, valid when the centres do not backreact

($g_s N \ll 1$). Thanks to a non-renormalization theorem in a similar spirit as [82], this symplectic form is independent of g_s and equal to the symplectic form of BPS Supergravity solutions.

Indeed, the authors of [64, 82, 46] argue that the open string dual of n GH centers in Supergravity is described by supersymmetric vacua of a (0+1)-dimensional quiver gauge theory, whose Coulomb branch consists — after integrating out the massive bifundamentals — of n abelian vector multiplets. Each of the vector multiplets comprises three scalars (x^1, x^2, x^3) which characterize the positions of the D6 branes in $\mathbb{R}^3$, one auxiliary field, D, and one gauge field, A, which corresponds to the spatial components of the 4D gauge field $\mathcal{A}$ in Supergravity. The effective action of the vector multiplets in the Coulomb branch is determined by the Lagrangian

$$L_{\text{quiver}} = \sum_{p=1}^{n}(-U_p D_p + A_p \cdot \dot{x}_p) + \text{ fermions } + \text{ higher-order terms}, \tag{2.4.2}$$

where U_p is found to be

$$U_p = \langle \Gamma_p, H_p(x_p) \rangle \equiv \left\langle \Gamma_p \, , \, \theta + \sum_{q \neq p} \frac{\Gamma_q}{|x_p - x_q|} \right\rangle . \tag{2.4.3}$$

The symplectic form can be extracted from L_{quiver}.

Applying (2.4.1) to L_{quiver}, the authors of [64] obtain the symplectic form to be of the form $\sum_p \delta x_p \wedge \delta A_p$. The restriction to BPS solutions corresponds, in the open string language, to restricting the solution space to $\bigcap_p \{U_p = 0\}$. In terms of the Supergravity data, the restricted symplectic form becomes

$$\tilde{\Omega} = \frac{1}{2} \sum_p \delta x_p^i \wedge \langle \Gamma_p, \delta \mathcal{A}_d^i(x_p) \rangle \, . \tag{2.4.4}$$

After calculations detailed in [64], the infinitesimal variations of the field $\delta \mathcal{A}_d^i(x_p)$ in (2.4.4) can be replaced by infinitesimal variations of the locations of the GH centres $\delta \mathbf{x}_p$, such that

$$\tilde{\Omega} = \frac{1}{4} \sum_{p \neq q} \langle \Gamma_p, \Gamma_q \rangle \frac{\epsilon_{ijk} (\delta(x_p - x_q)^i \wedge \delta(x_p - x_q)^j) \, (x_p - x_q)^k}{|\mathbf{x}_p - \mathbf{x}_q|^3} \, . \tag{2.4.5}$$

Because the GH centres satisfy the bubble equations (3.2.5), acting on the positions $\mathbf{x}_p$ of a solution with SO(3) rotations gives another configuration satisfying the bubble equations. Thus, if we impose the variations of the positions of the GH centres to be an infinitesimal rotation along the $\mathbf{n}$-axis as $\delta x_p^i = \epsilon^{iab} n^a x_p^b$, and call X_n the vector field corresponding to the rotation, then the reduced symplectic form satisfies

$$\tilde{\Omega}(X_n, \cdot) = n^i \delta J^i \, , \tag{2.4.6}$$

where J^i are the components of the angular momentum vector

$$J^i = \frac{1}{4} \sum_{p \neq q} \langle \Gamma_p, \Gamma_q \rangle \frac{x_p^i - x_q^i}{|\mathbf{x}_p - \mathbf{x}_q|} \, . \tag{2.4.7}$$

Using equation (2.4.6), it is possible to deduce the whole reduced symplectic form for two and three GH centres. Furthermore, the reduced symplectic form (2.4.5) is closed, so the $(2n-2)$-dimensional solution space can be viewed as a phase space.

2.4.2 The moduli space of three-centre solutions

We now specialize in a solution with three Gibbons-Hawking centres. In this superselection sector, the moduli space of solutions, which is also the phase space, has $2n-2=4$ dimensions. Here, we have already set the centre of mass of the three GH points to be at the origin of $\mathbb{R}^3$. The total angular momentum vector J of the three-centre system (2.4.7) is described by its norm, j, and its direction — parameterized by the (θ,ϕ) angles in S^2. Now, rotating the triangle formed by the GH centres around the axis of J does not modify the angular momentum vector, so the fourth real variable that we call σ characterizes this U(1) rotational symmetry.

In a nutshell, (j,θ,ϕ,σ) are the coordinates on the four-dimensional phase space. Once the charges on each GH centre are fixed, the intersection products $\langle h,\Gamma_p\rangle$ and $\langle\Gamma_p,\Gamma_q\rangle$ are also fixed. Given the length of two sides of the triangle of the GH centres, the third one is determined by the bubble equations (3.2.5). In other terms, for a given size of the triangle, its shape is determined. And what controls the size of triangle in these coordinates is the angular momentum j through

$$j=\frac{1}{2}\sqrt{-\sum_{p<q}\langle h,\Gamma_p\rangle\langle h,\Gamma_q\rangle\,\rho_{pq}^2}\,, \tag{2.4.8}$$

where p and q label the centres. The angles (θ,ϕ,σ) then parameterize how the triangle orients itself in $\mathbb{R}^3$. They do not change the nature of the bubbling solution, but they do contribute to the phase space of solutions.

Using (2.4.6), the symplectic form reduces to [64]

$$\tilde{\Omega}=-\mathrm{d}(j\cos\theta)\wedge\mathrm{d}\phi-\mathrm{d}j\wedge\mathrm{d}\sigma\ . \tag{2.4.9}$$

We can then define $x\equiv j$ and $y\equiv j\cos\theta$, so that

$$\tilde{\Omega}=-\mathrm{d}x\wedge\mathrm{d}\sigma-\mathrm{d}y\wedge\mathrm{d}\phi\ . \tag{2.4.10}$$

Note that $(x,y;\sigma,\theta)$ are the symplectic (or action-angle) coordinates, since in these coordinates, the symplectic form $\tilde{\Omega}$ is flat.

On the one hand, the "action" coordinates x and y satisfy the following inequalities

$$x-j_-\geq 0,\quad j_+-x\geq 0,\quad x-y\geq 0,\quad x+y\geq 0. \tag{2.4.11}$$

So on the (x,y)-plane, the solution space is a convex polytope. In particular, when $j_-=0$, this is a triangle, as shown in figure 2.2. On the other hand, the "angle" coordinates define a two-torus fibration over the polytope. On each facet of the polytope, one of the angles σ or ϕ becomes degenerate, that is to say the cycle they parameterize shrinks to zero size. Indeed, on the $x-y=0$ and $x+y=0$ facets, ϕ becomes degenerate, whereas on the $x-j_-=0$ and $j_+-x=0$ facets, σ becomes degenerate.

We consider the instance $j_-=0$ where scaling solutions are admitted. The polytope of the (x,y) moduli space is defined by 3 inequalities defining a triangle:

$$l_1(x,y)=-x+j_+\geq 0\qquad l_2(x,y)=x-y\geq 0\qquad l_3(x,y)=x+y\geq 0\,. \tag{2.4.12}$$

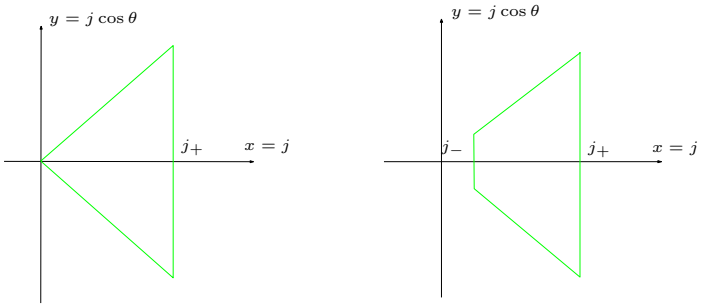

Figure 2.2 – The moduli space on the (x, y)-plane is a polytope, deliminated by the facets (they are edges too) of the polytope. The picture on the left depicts the moduli space when $j_- = 0$ while the one on the right applies when $j_- > 0$. We only consider the former instance. The scaling limit lies at point $(0, 0)$. The figures are from [64].

The scaling limit lies at $(0, 0)$ in the (x, y)-plane. The scaling limit loci lie at $(0, 0, \sigma, \phi)$. As both ϕ and σ become degenerate at the scaling point $(0, 0)$, this shows the scaling limit boils down to one point, at the boundary of moduli space.

The phase space is a convex toric manifold endowed with a closed symplectic form, and the vertices lie on integer coordinates (so our polytope is a 2-dimensional Delzant polytope [6]). Consequently, the symplectic form is compatible with an integrable complex structure, so that our phase space is a Kähler manifold [83]. Thus, we can use the following result for Kähler toric manifolds to determine the Kähler metric:

With the set of p inequalities characterizing the (two-dimensional) polytope P of the Kähler toric manifold,

$$l_i(\mathbf{x}) = c_i^x x + c_i^y y - \lambda_i \geq 0\,, \tag{2.4.13}$$

one can define the "canonical potential" of the polytope P

$$g_P(\mathbf{x}) = \frac{1}{2}\sum_{r=1}^{p} l_r(\mathbf{x}) \log l_r(\mathbf{x}) \tag{2.4.14}$$

whose Hessian $G = \left(\frac{\partial^2 g_P}{\partial x_i \partial x_j}\right)_{i,j}$ in the "action" coordinates determines the complex Kähler structure in the action-angle coordinates [83, 84]

$$J = \left(\begin{array}{c|c} 0 & -G^{-1} \\ \hline G & 0 \end{array}\right)\,. \tag{2.4.15}$$

[6] Further details on Kähler toric manifolds and definition of Delzant polytopes can be found in Appendix B of [64]

Thus the Riemannian Kähler metric in the action-angle coordinates is

$$\tilde{\Omega}(\cdot, J\cdot) = G_{ij}\mathrm{d}x^i \otimes \mathrm{d}x^j + (G^{-1})_{ij}\mathrm{d}\theta^i \otimes \mathrm{d}\theta^j = \left(\begin{array}{c|c} G & 0 \\ \hline 0 & G^{-1} \end{array}\right) . \tag{2.4.16}$$

Consequently, we apply this result and deduce that the moduli space metric in the symplectic coordinates is of the form (2.4.16) with

$$G = \frac{1}{x^2 - y^2}\begin{pmatrix} \frac{2xj_+ - x^2 - y^2}{2(j_+ - x)} & -y \\ -y & x \end{pmatrix} \quad , \quad G^{-1} = \frac{1}{2j_+ - x}\begin{pmatrix} 2x(j_+ - x) & 2y(j_+ - x) \\ 2y(j_+ - x) & 2xj_+ - x^2 - y^2 \end{pmatrix} . \tag{2.4.17}$$

We immediatly see that the G part of the Riemannian metric blows up on all the facets of the triangle. Thus, the metric is defined only in the interior of the triangle. In this regard, the scaling limit is not part of the bulk moduli space, but in its boundary.

Actually, the symplectic form on the Kähler toric manifold does not define a unique "potential" determining J. In fact, J can be defined by any potential g of the form

$$g = g_P + h\,, \tag{2.4.18}$$

where h is a smooth function on the whole polytope P satisfying the requirements that [83]:

(1) the Hessian G of g is positive definite on the interior P° of P, and

(2) the determinant of G is of the form

$$\det(G) = \gamma(\mathbf{x})\left(\prod_{r=1}^{p} l_r(\mathbf{x})\right)^{-1} , \tag{2.4.19}$$

with γ being a smooth and strictly positive function on the *whole* P.

The Hessian $G = \left(\frac{\partial^2 g}{\partial x_i \partial x_j}\right)_{i,j}$ defines the compatible toric complex structure J and Riemannian Kähler metric $\tilde{\Omega}(\cdot, J\cdot)$ the same way as in using (2.4.15) and (2.4.16).

Nevertheless, we will continue our computations with the metric defined by the "canonical potential" g_P, as did [64].

2.4.3 The distance to the scaling limit

The volume of the moduli space of the bosonic sector of BPS, classical configurations of Supergravity (which is our phase space) naively counts, in units of the Planck constant h^{n-1} (where n is the number of GH centres), the number of quantum states in a particular superselection sector. Indeed,

$$\mathcal{V}_{\text{phase}} = \hbar^2 \int \mathrm{d}x\,\mathrm{d}y\,\mathrm{d}\sigma\,\mathrm{d}\phi\,\sqrt{\det(GG^{-1})} = h^2 {j_+}^2 \tag{2.4.20}$$

in the instance where $j_- = 0$. When $j_- \neq 0$, the number of states is ${j_+}^2 - {j_-}^2$. This naive counting, which does not include the fermionic degrees of freedom, matches nevertheless with the result in [64]. From the symplectic-form derivation, the volume of the entire moduli space is finite.

Imposing that the volume of the entire moduli space is finite has a consequence on the shape of the vicinity of scaling limit. Indeed, if the length to the scaling limit was infinite, then the area of its orthogonal directions should shrink at a rate such that the volume remains finite. Then, for a parametrically small angular momentum, j, in the classical regime, the density of quantum states at that given phase-space hypersurface (defining a given throat length) would be parametrically small. Each superselection sector's vicinity to the scaling limit would have the shape of a spike of infinite-length and finite volume.

Now we wish to assess whether the geodesic distance in solution space between the scaling limit and any point in the bulk moduli space is infinite. The symplectic coordinates of the solution space are bounded, and the metric is not singular in its bulk, so any two points in the bulk solution space are at finite distance of each other. The only place where the distance could be infinite is at the facets of the polytope.

The coordinate values of (σ, ϕ) are chosen in $[0, 2\pi]$ and their metric is bounded by $2j_+$ from above. We will therefore only consider the metric from the (x, y) coordinates.

Consider the straight path between the scaling limit $\overrightarrow{0} = (0, 0)$ and the point $\overrightarrow{r_0} = (x_0, y_0) = r_0(\cos\alpha, \sin\alpha)$, with $\alpha \in [-\pi/4, \pi/4]$. The distance of this path is given by

$$\Delta_{\text{phase}}(\overrightarrow{0}, \overrightarrow{r_0}) = \int_0^{r_0} \sqrt{G_{ab} \frac{\mathrm{d}x^a}{\mathrm{d}r} \frac{\mathrm{d}x^b}{\mathrm{d}r}} \mathrm{d}r \,. \tag{2.4.21}$$

In the vicinity of the scaling point, although the metric blows up ($G_{ab} \frac{\mathrm{d}x^a}{\mathrm{d}r} \frac{\mathrm{d}x^b}{\mathrm{d}r} \underset{r\to 0}{\sim} \frac{\cos\alpha}{r}$), to compute the distance we integrate its square root:

$$\Delta_{\text{phase}}(\overrightarrow{0}, \overrightarrow{r_0}) \underset{r_0\to 0}{\sim} 2\sqrt{\cos\alpha}\,\sqrt{r_0} = 2\sqrt{x_0} \,. \tag{2.4.22}$$

Then the distance to the scaling limit $\Delta_{\text{phase}}(\overrightarrow{0}, \overrightarrow{r_0})$ is *finite*; therefore the geodesic distance in moduli space is finite too. This contradicts the naive extension of the Swampland Distance Conjecture.

With similar reasoning, we can show that although the metric is blowing up on the facets of polytope in the (x, y)-plane, the entire moduli space is bounded. The details are in the Appendix.

We wish now to relate the distance on moduli space with the masses S^3 Kaluza-Klein modes. Recall that the angular momentum j is proportional to the scaling parameter λ:

$$j = \frac{1}{2}\sqrt{-\sum_{a<b} \langle h, \Gamma_a\rangle \langle h, \Gamma_b\rangle \, \rho_{ab}(\lambda)^2} \,, \tag{2.4.23}$$

where $\rho_{ab}(\lambda) = \lambda d_{ab}$ is the coordinate distance between centres a and b. We can therefore express the masses of the Kaluza-Klein modes (2.3.11) in terms of the angular momentum j:

$$M_n(j) = \kappa n j + \mathcal{O}(j^2) \,, \tag{2.4.24}$$

where κ is a positive constant

$$\frac{1}{\kappa} \approx \frac{1}{4d} \left(Q_1 Q_2 Q_3\right)^{1/2} \sqrt{-\sum_{a<b} \langle h, \Gamma_a\rangle \langle h, \Gamma_b\rangle \, d_{ab}^2} \,. \tag{2.4.25}$$

As we have seen in equation (2.4.22), the distance in moduli space from any point p at finite angular momentum j to the scaling limit $j = 0$ is finite. We deduce that as j approaches 0, the mass of the Kaluza-Klein tower depends quadratically on this distance:

$$M_n(j) \underset{j\to 0}{\sim} \frac{\kappa n}{4}\Delta_{\text{phase}}(0,j)^2 \ . \tag{2.4.26}$$

This quadratic dependence deviates from the exponential dependence advocated by the Swampland Distance Conjecture.[7] This indicates that the distance of the moduli space seen as a phase space computed using the non-renormalization theorem and the canonical potential — according to [64] — differs from the distance one should use in order to extend the Swampland Distance Conjecture.

2.5 Discussion

In this paper, we have focused our attention on the scaling limit of a class of microstate geometries — the bubbling solutions — in the moduli space of solutions. This limit plays a particular role, as microstates geometries approach the black hole solution from the asymptotic observer's perspective. As one moves towards the scaling limit, bubbling solutions develop a throat whose depth is increasing to infinity. Besides, the deepening of the throat makes the redshift from the cap to the spatial asymptotics stronger and stronger, so the energy of all excitations lying at the bottom of the throat decrease to zero.

This decrease of energy excitations at the bottom of the throat is independent of the type of excitation we consider, as the redshift affecting them, set by $\sqrt{g_{tt}}$, is the same. In Section 2.3, we have proved that the redshift decreases the energy excitations by a factor of $\exp\left(-\frac{L_{\text{throat}}}{(Q_1Q_2Q_3)^{1/6}}\right)$. Thus, one may argue that our model is a new instance of the Swampland Distance Conjecture for metrics. If it turns out to be true, one can extract, from the mass decay, a notion of distance in moduli space, $\Delta_{\text{exponential}}\left(p(\lambda_0), p(\lambda)\right)$, from a reference solution $p(\lambda_0)$ to a solution $p(\lambda)$ approaching the scaling limit ($\lambda \to 0$).

As discussed in Section 2.3.3, the Michelson-Strominger derivation of the distance in moduli space [81] shows that the merging of n BPS black holes happens as well at an *infinite* moduli space distance from the bulk, and seems to support the $\Delta_{\text{exponential}}$ distance. However, it is not clear that these two distances — one involving black holes with unconstrained positions, and the other involving charged Gibbons-Hawking centres/black holes whose positions satisfy the Denef integrability equations — should agree.

A second notion of distance, Δ_{phase}, can be derived from the Kähler metric of the phase space of three-centre solutions. This distance is *a priori* computed in the weak coupling regime. The first question is whether one can extrapolate this distance up to strong string coupling regime. The non-renormalization theorem of [64] shows that the reduced symplectic form, $\tilde{\Omega}$, (2.4.4) remains the same in the Supergravity regime up to a normalization factor. Nevertheless, the

[7] Since the distance to the scaling limit is finite here, we are measuring distances from the moving point $p(j)$ to the scaling limit $p(0)$; while in Section 2.3, as the distance to the scaling limit was infinite, we were considering distances from the moving point $p(j)$ to a reference point $p(j_0)$ at finite angular momentum.

potential g_P (2.4.14) used to compute the integrable structure J is not unique (2.4.18) — and is so in *all* regimes of the string coupling. As a result, in order to assert that the complex structure, J, and the metric of the moduli space are invariant under the tuning of the string coupling, one must show that the effects of h in (2.4.18) on the metric on moduli space are dominated by those of the canonical potential, g_P.

We have shown that there exists a tension between the "canonical" distance according to the phase-space computation, Δ_{phase}, whose distance to the scaling limit is finite, and $\Delta_{\text{exponential}}$. Now, there is only one correct normalization of the distance on the moduli space of bubbling solutions at strong string coupling: the one from the variations of the effective Supergravity action. Thus, we have the following possibilities:

(1) Neither Δ_{phase} nor $\Delta_{\text{exponential}}$ give the correct normalization.

(2) Only the canonical Δ_{phase} gives the correct distance on moduli space, even in the strong string coupling regime. If the Swampland Distance Hypothesis for metrics is correct, then it will not apply to our metrics.

(3) The Swampland Distance Hypothesis applies to our solutions, and $\Delta_{\text{exponential}}$ gives the correct normalization of the distance to the scaling limit. The use of canonical Δ_{phase} is not reliable in the strong coupling regime.

If possibility (2) is correct, then our computation gives an explicit example of a metric on moduli space which blows up at all points on the boundary of moduli space, but where all of the boundary points lie at finite distance in moduli space. In particular, the scaling limit of bubbling solutions — at which global symmetries of the Black hole are restored — is within *finite*-distance reach from any other point in the moduli space. Besides, the mass decay of the tower of Kaluza-Klein modes does not behave like a decreasing exponential with respect to the moduli space distance Δ_{phase} between $p(\lambda_0)$ and $p(\lambda)$.

Although there is an infinite tower of states whose mass is decaying to zero, the decay is due to an universal redshift in a fixed-warp region of space-time, and thus does not introduce any singularities.[8] Besides, the three-sphere at the bottom of the throat on which the Kaluza-Klein modes live is macroscopic and is part and parcel of the five-dimensional Supergravity solution. Therefore, the example we provide here differs from the usual Swampland picture, in which going at a corner in moduli space implies the appearance of singularities (for instance the shrinking of Calabi-Yau cycles in [85]), which involve the breakdown of the effective field theory.

As a result, the Swampland conjectures would not forbid the scaling limit to be accessible from the bulk moduli space. However, in possibility (2), as argued in [64], quantum mechanics, by virtue of the uncertainty principle, will imply the breakdown of Supergravity at the scaling limit.

If possibility (3) is correct, then one cannot extend the "canonical" Δ_{phase} to the strong coupling regime, because the integrable complex structure, J, is not invariant under the shift of g_s, or because one has to take into account the effect of the additional potential h at weak coupling in the first place. However, the authors of [64] computed J in the open string picture with the canonical potential g_P, and used it at strong coupling regime. In particular, the probability

[8] Actually, this argument does not depend on assuming possibility (2).

distribution $e^{-\mathcal{K}}$ of quantum wave functions in the phase space of bubbling solution they derive depends on the Kähler potential $\mathcal{K}$, whose value will shift if one considers the potential h in addition of the canonical potential g_P.

Therefore, if the canonical Δ_{phase} somehow gives the wrong normalization of distance, some of the conclusions in [64] could be revisited. The relative coordinate positions of the centers $\overrightarrow{\rho_{ij}}$ define solutions in Supergravity. In particular, near the scaling limit, the coordinate positions $\overrightarrow{\rho_{ij}}$ need to be arbitrarily precise. However, because of the form of the symplectic form (2.4.5) computed from the open string sector, these coordinates do not commute; hence, it is not possible to localize the positions $\overrightarrow{\rho_{ij}}$ with arbitrarily good precision in *coordinate space*. In the closed string sector, the fully back-reacted solution does not require its Gibbons-Hawking centres to be localized with arbitrarily good precision in the geometry in terms of *proper distance*, as the cap keeps its shape in the scaling limit. However, if one follows the logic of [64], the uncertainty about positions in coordinate space at weak string coupling is transported unto the phase space of three-centered solutions in Supergravity: one cannot localize any classical Supergravity bubbling solution with arbitrary high precision in phase space. Instead, each classical Supergravity bubbling solution is defined with some inherent quantum uncertainty and must be coarse-grained with a "droplet" of solutions around it in a volume h^m in the phase space. How far in the phase space one should apply the coarse-graining depends on the metric/distance in moduli space around that particular classical Supergravity solution p_1.

On the one hand, when the components of the moduli-space metric have small values, as one schematically moves away from p_1 within the coarse-graining droplet region of p_1, one can reach solutions that are very different from p_1. In particular, according to the *canonical* distance on moduli space that [64] used — where the metric behaves like $1/J_R$ in the vicinity of the scaling limit — the scaling limit lies at *finite* distance to any other point in the moduli space, so the coarse-graining of a solution p_1 close to the scaling limit point contains solutions $\{p\}$ which possess throats that have very different macroscopic physical lengths. Therefore, Heisenberg's uncertainty principle prevents classical solutions from Supergravity to be a good description of black hole microstates.

On the other hand, when the components of the moduli-space metric are large around the solution p_1, the solutions $\{p\}$ reached within a distance $\sim \sqrt{h}$ look much more like p_1. In particular, with a metric that, in the vicinity of the scaling limit, scales like $1/{J_R}^2$ [9] as advocated by the Swampland Distance Hypothesis, the distance in moduli space to the scaling limit is *infinite*. Wandering around p_1 within a distance $\sqrt{h}$ along the angular-momentum coordinate J_R (or equivalently the scaling-parameter coordinate λ) cannot give solutions $\{p\}$ whose physical throat length is arbitrarily long. Instead, with $\Delta_{\text{exponential}}$, one deduces from (2.3.16) that the variation of the length of the throat in the set of solutions $\{p\}$ will be of order

$$\Delta L_{\text{throat}} = \alpha\, R_{S^3}\,. \tag{2.5.1}$$

Whether quantum fluctuations in p_1's coarse-graining droplet are negligible or too large depends on the value of the mass decay rate α of (2.3.16). If $\alpha \ll 1$, the geometries described by Supergravity are reliable and well-defined. If α is of order one or bigger however — as in the

[9] This gives the logarithmic dependence of the distance on λ in (2.3.6)

context of Calabi-Yau compactifications [86–88] —, quantum fluctuations of the throat length of each bubbling solution have macroscopic size, so describing those arbitrarily deep geometries with Supergravity is still not reliable. Nonetheless, in both instances, the breakdown (should it happen) of Supergravity here is milder than the one from the canonical phase space distance of [64].

In a nutshell, regardless of the value of α, coarse-graining droplets defined using $\Delta_{\text{exponential}}$ contain a much smaller range of solutions than those using the canonical Δ_{phase}. While with the canonical Δ_{phase} as the correct normalization of distance on the moduli space, the coarse-graining droplet of a deep-throat bubbling solution could contain the scaling limit point; the droplet derived from the $\Delta_{\text{exponential}}$ normalization only contains solutions with similar throat lengths. Therefore, with $\Delta_{\text{exponential}}$, the breakdown of Supergravity at the scaling limit is softened.

If extending the Swampland Distance Hypothesis to our model is possible, then we have drawn a parallel between (i) travelling within Planckian field range in field space to avoid the breakdown of the EFT in the context of the Swampland Distance Hypothesis and (ii) travelling a distance of $\sqrt{h}$ around a classical solution in phase space within the region of its quantum fluctuations. While the Swampland Distance Hypothesis only considers field ranges that are isotropic in moduli space, the fundamental quantity on the phase space side is the coarse-grained volume h^m, and the symplectic form defines an anisotropic "droplet" around a classical solution. In our example, the Swampland Distance Hypothesis could be interpreted as a consequence of the symplectic form establishing Heisenberg's uncertainty principle. Whether or not this interpretation is legitimate is a question to explore.

As for Black Hole physics, both possibilities (2) and (3) entail at least *some* breakdown of Supergravity as the description of arbitrarily-deep-throat bubbling solutions. As one approaches the scaling limit from a bubbling solution, the resulting geometry enters into a new phase, whose precise description may require other tools, for instance perturbative String Theory — that one uses in the microstate solutions of [89–91, 31, 92]. However, the extent of the breakdown, depending on which one of possibility (2) or (3) is correct, is very different.

With possibility (2), the bubbling solution acquires a critical maximal throat length after which supergravity completely breaks down. Thus, the new phase can possess a throat that is not arbitrarily deep, like in the instances of [93–96] and [90, 91, 31, 92].

With possibility (3), when the Supergravity description of a geometry with a very long throat (of length L_{throat}) becomes unreliable, one has to scramble the initial Supergravity solution with solutions whose throat length is between $L_{\text{throat}} - \alpha\, R_{S^3}$ and $L_{\text{throat}} + \alpha\, R_{S^3}$. Therefore, the new phase should still possess a throat which can be tuned to be arbitrarily deep. Thus, any complete description of bubbling solutions up to the scaling limit should still capture the presence of a cap and an arbitrarily deep throat. Finding such a description beyond Supergravity of those geometries would then be an interesting direction for the future.

Chapter 3

An Alliance in the Tripartite Conflict over Moduli Space

3.1 Introduction

The moduli space of solutions of a given theory describes a set of solutions parameterized by continuous parameters. For our intuition, it is practical to define a distance on the moduli space so that similar solutions are close one to another in the space of solutions. There are, in the literature, three ways to define distances on moduli spaces which come from a priori different formulas and viewpoints.

1. The phase-space distance. A first way to think about moduli space is to start with a semi-classical theory; one can define a classical phase space upon which geometric quantization [97–99] gives the number of quantum states in a given region of the phase space. For instance, this is the point of view one can take in order to count the number of quantum black-hole microstates that a given set of supergravity solutions (parameterized by continuous parameters) account for [100, 101, 64, 56]. In detail, given a Lagrangian theory characterizing a set of fields, ϕ^A, one defines the symplectic form of the theory, Ω, from the Crnković-Witten-Zuckerman formalism [75, 76]:

$$\Omega = \int d\Sigma_l \; \delta\left(\frac{\partial L}{\partial(\partial_l \phi^A)}\right) \wedge \delta\phi^A \,, \tag{3.1.1}$$

where the integral is performed over a Cauchy surface Σ in space-time. The fundamental quantity in phase space is given by the symplectic form, Ω, and there is not necessarily a notion of distance on it. Nevertheless, the symplectic structure of the manifold is sometimes compatible with an almost complex structure, J; then one can define a Kähler metric out of Ω and J:

$$G_{\text{phase}} = \Omega(\cdot, J\cdot) \,. \tag{3.1.2}$$

Given a path, γ, linking two points p_1 and p_2 on moduli space, one can define the distance along the path, γ, between the two solutions:

$$\Delta_{\text{phase}}(p_1, p_2) = \int_\gamma \sqrt{G_{ab} \frac{\partial x^a}{\partial \tau} \frac{\partial x^b}{\partial \tau}} \mathrm{d}\tau \,. \tag{3.1.3}$$

2. The low-velocity distance. In the context of a solution describing multiple static, extremal Reissner-Nordström black holes, one can define a distance on the moduli space parameterized by the distance between the black holes [102, 103]. Because each black hole sources electric and gravitational forces that cancel out one another, the overall system is stable, and any configuration of those black holes described by their coordinate in space, $\vec{x_j}$, solves the equations of motion. One can allow the black holes to move with small velocities $\vec{v_j} \equiv \frac{\mathrm{d}\vec{x_j}}{\mathrm{d}t}$, and find the expansion of the action up to order $\mathcal{O}(v^2)$. Then, one rewrites this effective action so that it involves the velocities, $\vec{v_i}$, as an overall factor of the Lagrangian [81, 104–106]:

$$S_{\text{eff},\,\mathcal{O}(v^2)} = \int dt (v_i)^a (v_j)^b (G^{ij})_{ab}\,, \tag{3.1.4}$$

from which we deduce the metric of the $(d\,n)$-dimensional (where d is the dimension of the physical space and n is the number of black holes) configuration space of the positions $\vec{x_j}$:

$$ds^2_{\text{low}-\text{v.}} = (G^{ij})_{ab}\,\mathrm{d}x_i{}^a\,\mathrm{d}x_j{}^b\,. \tag{3.1.5}$$

Then the moduli space is a submanifold embedded in this configuration space, as it satisfies additional constraints, such as the conservation of the angular momentum of the whole system of black holes.

This notion of distance can be extended to other configurations of supersymmetric objects that satisfy a no-force condition. A geodesic in this moduli space represents the trajectories of the individual components of the dynamical system in physical space-time [102].

3. The DeWitt distances. Another possibility to define a metric on the moduli space of metrics has been formulated by DeWitt [72]. The original DeWitt distance applies to the moduli space of induced metrics on Cauchy slices, but one can generalise it to moduli space of (Riemannian) metrics on the entire spacetime manifold. There are two possible generalisations:
3a. *The DeWitt distance without the volume factor.* Given a metric $g_{\mu\nu}$ of a spacetime $\mathcal{M}$, the distance on a path, γ, parameterized by τ and on which the metric variations are transverse-traceless, can be defined as [107]

$$\Delta_{\text{DeWitt 1}} = c \int_{\tau_i}^{\tau_f} \left(\int_{\mathcal{M}} \sqrt{g}\,\mathrm{tr}\left[\left(g^{-1} \frac{\partial g}{\partial \tau} \right)^2 \right] \right)^{\frac{1}{2}} \mathrm{d}\tau\,, \tag{3.1.6}$$

where c is a constant of order 1, depending on the dimension of $\mathcal{M}$.
3b. *The DeWitt distance with the volume factor.* Let $V_{\mathcal{M}} = \int_{\mathcal{M}} \sqrt{g}$ be the volume of $\mathcal{M}$. Another distance on the same path γ can be defined as

$$\Delta_{\text{DeWitt 2}} = c \int_{\tau_i}^{\tau_f} \left(\frac{1}{V_{\mathcal{M}}} \int_{\mathcal{M}} \sqrt{g}\,\mathrm{tr}\left[\left(g^{-1} \frac{\partial g}{\partial \tau} \right)^2 \right] \right)^{\frac{1}{2}} \mathrm{d}\tau\,, \tag{3.1.7}$$

where c is a constant of order 1, depending on the dimension of $\mathcal{M}$. This distance has been used in the context of the Swampland programme, in order to formulate the Generalized Distance Conjecture [71]. The distance (3.1.7) boils down to the moduli space distance of the scalar fields in the case of Calabi-Yau compactifications on 4-dimensional Minkowski space [73], thus making the link with the original Swampland distance conjecture [69].

The "Swampland" perspective on moduli space is that given a set of scalar fields of a d-dimensional effective field theory, ϕ^i, their kinetic terms, G_{ij}, that appear in the action written in the d-dimensional Einstein frame

$$S = \int \mathrm{d}^d x \sqrt{-g} \left[\frac{R}{2} - G_{ij}\left(\phi^i\right) \partial\phi^i \partial\phi^j + ... \right] , \tag{3.1.8}$$

defines a metric on moduli space of the ϕ^i's. The geodesic distance on moduli space, Δ, is then used to delimit the domain of validity of the space of effective field theories (EFT's) [86, 108]. Indeed, as one moves away from a point, p_0, in the bulk moduli space, there should exist an infinite tower of states with an associated mass scale, $M(p)$, such that

$$M(p) \sim M(p_0)\, e^{-\alpha \Delta(p_0,p)} , \tag{3.1.9}$$

with α a constant of order 1 in Planck units. Thus, the effective field theory defined by p breaks down if one moves a few Planck units away from the original effective theory, p_0. In [71], the fact that the kinetic terms define a metric on moduli space was extended to the kinetic terms and the moduli space of all dynamical fields, and was linked to the DeWitt distances (3.1.6,3.1.7).

The previous three/four definitions come from different viewpoints, and are used in different contexts. Indeed, the moduli space of flux vacua is a space of effective field theories, whereas the moduli space of multiple extremal black holes or of black hole microstates is a space of solutions within the same EFT. However, from the string theory perspective, all these moduli spaces are subsectors of a solution space of the same UV-complete theory. An obvious question is whether these three different notions of moduli space measure the same distance.

In this letter, we compare these three different notions on a specific space of metrics: the so-called five-dimensional *bubbling geometries*, or equivalently, the four-dimensional *multi-centered solutions*.

Bubbling geometries [40,41,14] are smooth, supersymmetric solutions of five-dimensional, ungauged, $\mathcal{N} = 2$ supergravity, coupled to vector multiplets. They have the same asymptotics and asymptotic charges as the three-charge, five-dimensional, supersymmetric black hole (the BMPV black hole [42]). Unlike the extremal black hole whose horizon lies at the bottom of an infinitely-long AdS_2 throat, the bubbling solutions have a smooth cap at the bottom of a long, but finite AdS_2 throat. As such, they are sometimes considered as coherent superpositions of the black hole microstates [43, 13]. Much like their corresponding black hole, the bubbling geometries can also be constructed with $\mathbb{R}^{1,3} \times S^1$ asymptotics; reduced to four dimensions, they correspond to a class of *multi-centered solutions* [44–46], which still have the same asymptotics and asymptotic charges as the four-dimensional black hole, but are singular from a 4D perspective.

One can think the multi-centered solutions as coming from splitting the black hole's asymptotic charges (Q_1, Q_2, Q_3) into local charges at different locations in space, denoted *centres*. The centres are located at the coordinates $\lambda\, \vec{d}_j$ in $\mathbb{R}^3$, with j enumerating the centres and λ a positive parameter. If one wishes the metric to be smooth in five dimensions, then the relative positions of the centres are constrained.

From the classical point of view, there is no obstruction to send the parameter λ to 0, so that the coordinates of the centres approach the origin of $\mathbb{R}^3$ while approximately keeping their

collective shape [43]. This limit in the moduli space of bubbling geometries is called the *scaling limit*. In this limit, in gravity, the length of the bubbling geometry's throat increases towards infinity, while the geometry of the cap remains fixed. This limit constitutes a well-defined path in moduli space. So, given a solution in the bulk moduli space, $p(\lambda_0)$, it is possible to compute its distance to a solution approaching the scaling limit, $p(\lambda)$, with $\lambda \to 0$. In this letter, we compare the distance to the scaling limit from $p(\lambda_0)$ according to the three definitions of distance on moduli space mentioned above. In particular, the new computation we do in this letter is the one using the formula with the DeWitt distances (3.1.6) and (3.1.7).

Before computing the distance to the scaling limit in the moduli space of bubbling geometries, let us recall a good illustrative example where the second DeWitt distance (3.1.7) is used in the context of the Swampland: Take a family of $\mathrm{AdS}_p \times \mathrm{S}^q$, where the radius of AdS space fixes the size of the sphere [71]. The limit in moduli space where the value of the cosmological constant vanishes lies at infinite distance from the bulk moduli space. Besides, while going to that limit, an infinite tower of Kaluza-Klein (KK) modes of the sphere becomes exponentially massless, in accordance with the Swampland distance conjecture.

Now, take a family of warped geometries that are asymptotically $\mathrm{AdS}_p \times X$, where X is a compact manifold. To compute the exact mass of the KK modes of X, one needs to take a scalar deformation of the metric, solve the wave equations, and the quantized energies measured at spatial infinity give the masses of the KK tower [68].

For our bubbling geometries with a long $\mathrm{AdS}_2 \times \mathrm{S}^3$ throat, any energy excitation at the bottom of the throat is redshifted when one measures it at spatial infinity. In the scaling limit, the redshift becomes stronger and stronger, so the energy measured at spatial infinity gets more and more suppressed. Moreover, this decay is exponential with respect to the throat length, L_{throat} [16]:

$$M(L_{\text{throat}}) \underset{\lambda \to 0}{\sim} \exp\left(-\frac{L_{\text{throat}}}{(Q_1 Q_2 Q_3)^{1/6}}\right) . \tag{3.1.10}$$

Knowing the Swampland distance conjecture (3.1.9), it appeared natural to propose that the distance to the scaling limit in moduli space is given by the argument of the decreasing exponential, up to some constant factor of order 1 [16]:

$$\Delta_{\text{exponential}}(\lambda_0, \lambda) = \frac{|L_{\text{throat}}(\lambda) - L_{\text{throat}}(\lambda_0)|}{(Q_1 Q_2 Q_3)^{1/6}} . \tag{3.1.11}$$

Thus, with $\Delta_{\text{exponential}}$, the distance to the scaling limit would be infinite, as the throat length increases to infinity to match that of the extremal black hole.

However, this notion of moduli space distance can only be used if one could show that every tower of massless states emerges at infinite distance: namely, that the converse of the Swampland distance conjecture applies in this limit.

But it was also shown from [16] that the distance to the scaling limit according to the phase-space definition (3.1.3) would give a *finite* distance. This distance was derived at weak string coupling from quiver quantum mechanics, and, according to [64], can be extrapolated to strong coupling thanks to a non-renormalization theorem [82, 64]. In the scaling limit, the relevant metric component on moduli space, $G_{\lambda\lambda}$, blows up like $1/\lambda$, so the phase-space distance behaves

like

$$\Delta_{\text{phase}}(\lambda_0,\lambda)=\int_{\lambda}^{\lambda_0}d\lambda'\,\sqrt{G_{\lambda\lambda}}\propto\sqrt{\lambda_0}-\sqrt{\lambda}\approx\sqrt{\lambda_0} \tag{3.1.12}$$

in the vicinity of the scaling limit.

The phase-space distance indicates that an infinite tower of massless modes can emerge at finite distance in moduli space. However, the phase-space distance is not the one used to formulate the Generalized Distance Conjecture [71]. Therefore, in this letter, we compute the distance to the scaling limit according to the DeWitt distances.

In Section 3.2, we review some properties of bubbling geometries. In Section 3.3, we show that the first DeWitt distance (without the volume factor) for the scaling limit matches the phase-space distance (3.1.12), while the second DeWitt distance (with the volume factor) matches the "exponential" distance (3.1.11). In Section 3.4, we confront these two distances with a distance computed in the literature [102, 106, 109] using the low-velocity distance.

3.2 Bubbling geometries

The metric of the bubbling geometries is of the form

$$\begin{aligned}ds_5^2=&-(Z_M)^{-2}\,(dt+\omega)^2+\frac{Z_M}{V}\,(d\psi+A)^2\\&+VZ_M\left[d\rho^2+\rho^2\left(d\theta^2+\sin^2\theta\,d\phi^2\right)\right],\end{aligned} \tag{3.2.1}$$

where the warp factor $Z_M\equiv(Z_1Z_2Z_3)^{1/3}$ is the geometric mean of the functions (Z_1,Z_2,Z_3) which encode the three asymptotic charges of the black hole.

While the black hole has warp factors Z_I sourced by a charge Q_I at the origin of the four-dimensional space and which is of the form

$$Z_I=1+\frac{Q_I}{\rho}\,, \tag{3.2.2}$$

the multi-centered solution are determined by eight harmonic functions on the base $\mathbb{R}^3$, $(V,K^I;L_I,M)\equiv\mathbf{H}$, that depend on the location of their poles, in the following generic form:

$$H=h_\infty+\sum_{j=1}^{n}\frac{h_j}{|\vec{\rho}-\lambda\,\vec{d}_j|}\,. \tag{3.2.3}$$

The integer n denotes the number of centres. The coefficient h_∞ is the asymptotic value of the harmonic function H; collectively, the h_∞ are chosen to be $\mathbf{h}_\infty\equiv(v_\infty,l^I_\infty;k^I_\infty,m_\infty)=(1,1,1,1;0,0,0,m_\infty)$ for $\mathbb{R}^{1,3}\times S^1$ asymptotics. The coefficient h_j is the charge associated to the centre j; collectively, the $\mathbf{h}_j\equiv(v_j,l^I_j;k^I_j,m_j)$ satisfy

$$l^I_j\;=\;-\frac{|\varepsilon_{IJK}|}{2}\frac{k^J_jk^K_j}{q_j}\,,\qquad m_j\;=\;\frac{|\varepsilon_{IJK}|}{12}\frac{k^I_jk^J_jk^K_j}{q_j^2}\,, \tag{3.2.4}$$

with ε_{IJK} being the Levi-Civita symbol. The equations (3.2.4) guarantee the smoothness of the bubbling geometries in five dimensions. Besides, the absence of Dirac-Misner strings (which give of closed time-like curves) in bubbling geometries leads to constraints on the relative positions of the centres, $\rho_{ij} \equiv |\lambda\,\vec{d}_j - \lambda\,\vec{d}_i|$, the so-called *bubble equations*, or *Denef equations* [46, 41]:

$$\sum_{j=1}^{n} \frac{\langle \mathbf{h}_i, \mathbf{h}_j \rangle}{\rho_{ij}} \;=\; \langle \mathbf{h}_\infty, \mathbf{h}_i \rangle\,, \qquad \text{for } i \;=\; 1, \dots n\,. \tag{3.2.5}$$

Here, the symplectic product, $\langle \cdot, \cdot \rangle$, for $\mathbf{A} = (A^0, A^I; A_I, A_0)$ and $\mathbf{B} = (B^0, B^I; B_I, B_0)$ is defined as $\langle \mathbf{A}, \mathbf{B} \rangle \equiv A^0 B_0 - A_0 B^0 + A^I B_I - A_I B^I$.

The metric of the bubbling geometries (3.2.1) comprises warp factors (and angular momentum) whose building blocks are the harmonic functions $(V, K^I; L_I, M)$:

$$Z_I \;=\; L_I \;+\; \frac{|\varepsilon_{IJK}|}{2}\frac{K^J K^K}{V}\,. \tag{3.2.6}$$

Asymptotically, the different local charges $\mathbf{h}_j \equiv (v_j, l_j^I; k_j^I, m_j)$ put on the centres develop into the black hole's asymptotic charges, (Q_1, Q_2, Q_3), in the following fashion:

$$Q_I \;=\; \sum_{j=1}^{n} l_j^I \;+\; |\varepsilon_{IJK}| \sum_{(i,j)=1}^{n} k_i^J k_j^K\,. \tag{3.2.7}$$

3.3 The DeWitt distances between deep-throat geometries

a. The metric and its inverse in the throat region. As the cap and the asymptotics are fixed in the scaling limit, we only need to compare the distance between solutions with throats of different lengths, using the DeWitt distance (3.1.6).[1]

The throat region we are interested in is defined to be delimited by $\rho \in [\rho_0(\lambda), \rho_M]$. See Fig. 3.1. The upper-bound, ρ_M, is chosen so that the top of our region of interest is inside the AdS_2 throat: $\rho_M \ll Q_I$. The lower-bound, $\rho_0(\lambda)$, is chosen to be not too close from the centres, say $\rho_0(\lambda) = 2\lambda \max |\vec{d}_j|$. Then in the throat region, the metric is well-approximated by

$$ds_5^2 = -\frac{\rho^2}{Q_M^2}(dt + \omega)^2 + \frac{Q_M}{\rho^2} d\rho^2 + Q_M d\Omega_3^2\,, \tag{3.3.1}$$

where $Q_M \equiv (Q_1 Q_2 Q_3)^{1/3}$ and

$$d\Omega_3^2 = (d\psi + A)^2 + d\theta^2 + \sin^2\theta\, d\phi^2\,, \qquad A \equiv \cos\theta d\phi\,. \tag{3.3.2}$$

In the basis $\mathcal{B} \equiv (dt + \omega, d\rho, d\psi + A, d\theta, \sin\theta\, d\phi)$, the inverse metric is written in diagonal form:

$$g^{-1} = \text{diag}\left[\frac{(Q_M)^2}{\rho^2}, \frac{\rho^2}{Q_M}, \frac{1}{Q_M}, \frac{1}{Q_M}, \frac{1}{Q_M}\right]. \tag{3.3.3}$$

[1] The geometry in the cap and in the asymptotic flat region does not depend on the scaling parameter, λ, so the $\frac{\partial g}{\partial \lambda}$ term in (3.1.6) vanishes in these regions.

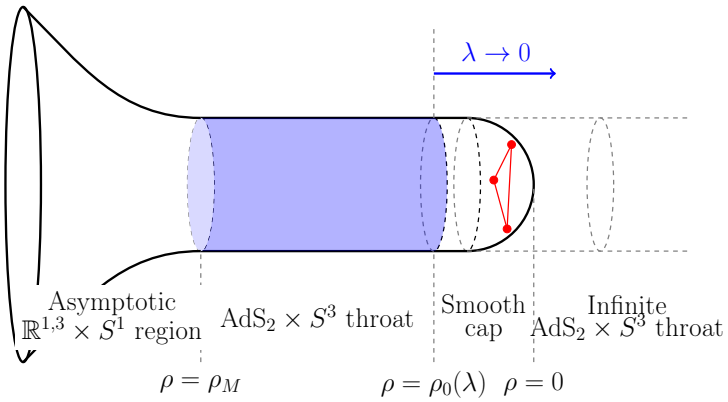

Figure 3.1 – A schematic depiction of the bubbling geometries. The centres at coordinate $\lambda\,\vec{d}_j$, depicted in red, lie in the cap region. In the scaling limit ($\lambda \to 0$), the geometry of the cap and of the asymptotic region remains fixed, while the throat region delimited by $\rho \in [\rho_0(\lambda), \rho_M]$ and shaded in blue, becomes longer and longer.

b. The derivatives in the throat region. Recall that

$$\frac{\partial|\vec{\rho} - \lambda\,\vec{d}_j|}{\partial\lambda} = -\frac{(\vec{\rho} - \lambda\,\vec{d}_j)\cdot\vec{d}_j}{|\vec{\rho} - \lambda\,\vec{d}_j|}\,. \tag{3.3.4}$$

Then, given a harmonic function H of the form (3.2.2), the derivative of H with respect to the scaling parameter λ is given by

$$\frac{\partial H}{\partial\lambda} = \sum_{j=1}^{n} h_j \frac{\left(\vec{\rho} - \lambda\,\vec{d}_j\right)\cdot\vec{d}_j}{|\vec{\rho} - \lambda\,\vec{d}_j|^3}\,. \tag{3.3.5}$$

In the throat region, as $\rho \gg \lambda$,

$$\frac{\partial H}{\partial\lambda} \sim \frac{\vec{\rho}}{\rho^3}\cdot\left(\sum_{j=1}^{n} h_j\vec{d}_j\right) = \mathcal{O}\left(1/\rho^2\right)\,. \tag{3.3.6}$$

Thus, the derivative with respect to λ of any harmonic function is an $\mathcal{O}\left(1/\rho^2\right)$-function in the throat region.

Using (3.3.6) and that the harmonic functions are of order $\mathcal{O}(1/\rho)$ in the throat region, we successively deduce, from formula (3.2.6) and $Z_M \equiv (Z_1 Z_2 Z_3)^{1/3}$, that

$$\frac{\partial Z_I}{\partial\lambda} = \mathcal{O}\left(1/\rho^2\right)\,, \qquad \frac{\partial Z_M}{\partial\lambda} = \mathcal{O}\left(1/\rho^2\right)\,. \tag{3.3.7}$$

Written in the basis $\mathcal{B}$, the derivative of the metric (3.2.1) with respect to λ gives in the throat region

$$\frac{\partial g}{\partial\lambda} = \mathrm{diag}\left[\mathcal{O}(\rho), \mathcal{O}(1/\rho^3), \mathcal{O}(1/\rho), \mathcal{O}(1/\rho), \mathcal{O}(1/\rho)\right]\,. \tag{3.3.8}$$

c. The distance to the scaling limit. Combining (3.3.3) and (3.3.8) gives that in the basis $\mathcal{B}$,

$$\frac{\partial g}{\partial \lambda} g^{-1} = \text{diag}\left[\mathcal{O}(1/\rho), \mathcal{O}(1/\rho), \mathcal{O}(1/\rho), \mathcal{O}(1/\rho), \mathcal{O}(1/\rho)\right] , \tag{3.3.9}$$

so that

$$\text{tr}\left[\left(\frac{\partial g}{\partial \lambda} g^{-1}\right)^2\right] = \mathcal{O}(1/\rho^2) . \tag{3.3.10}$$

Therefore, the metric component on moduli space behaves like

$$\int_{\mathcal{M}} \sqrt{g}\, \text{tr}\left[\left(g^{-1}\frac{\partial g}{\partial \tau}\right)^2\right] \propto \int_{\rho_0(\lambda)}^{\rho_M} d\rho\, \frac{1}{\rho^2} \propto \frac{1}{\lambda} . \tag{3.3.11}$$

In the scaling limit, the metric component on moduli space along λ blows up like $1/\lambda$, but this gives a DeWitt distance (3.1.6) (between a point $p(\lambda_0)$ in bulk moduli space and a point $p(\lambda)$ closer to the scaling limit)

$$\Delta_{\text{DeWitt}\,1}(\lambda_0, \lambda) \propto c \int_{\lambda}^{\lambda_0} d\lambda' \, \frac{1}{\sqrt{\lambda'}} \propto \sqrt{\lambda_0} - \sqrt{\lambda} , \tag{3.3.12}$$

which is *finite. This dependence in the scaling parameter, λ, matches exactly that of the phase-space distance (3.1.12)!*

Note that if we wanted $\Delta_{\text{DeWitt}\,1}$ to match the infinite distance of $\Delta_{\text{exponential}} \sim |L_{\text{throat},i} - L_{\text{throat},f}|$, we would have needed

$$\Delta_{\text{DeWitt}\,1,\,\text{false}} \propto -\ln\left(\frac{\lambda_i}{\lambda_f}\right) , \tag{3.3.13}$$

that is to say

$$\text{tr}\left[\left(\frac{\partial g}{\partial \lambda} g^{-1}\right)^2\right] \propto \frac{1}{\rho^3} . \tag{3.3.14}$$

This last behaviour is too singular and impossible given (3.3.10), whose most singular power in ρ near $\rho = 0$ is *at most* $1/\rho^2$.

d. The distance with the volume factor. The volume of the asymptotic $\mathbb{R}^{1,3} \times S^1$ region is infinite, so in the chosen coordinates, the DeWitt distance with the volume factor (3.1.7) between any two bubbling geometries is 0.

In fact, the distance (3.1.7) is not invariant under diffeomorphisms of the spacetime metric, and, as explained in [74], one should choose a frame which satisfies the condition of a vanishing Lie derivative. For metrics parameterized by a single dimensionfull scale, the distance (3.1.7) computed in such a frame gives a logarithmic divergence [74]. Thus, for a bubbling geometry approaching the scaling limit and only parameterized by the scaling parameter λ, the distance to the scaling limit diverges logarithmically:

$$\Delta_{\text{DeWitt}\,2} \propto -\ln\left(\frac{\lambda_i}{\lambda_f}\right) . \tag{3.3.15}$$

This behaviour in λ matches that of the exponential distance (3.1.11).

3.4 The conflict over moduli space

In this letter, we have compared the distance in moduli space between two bubbling geometries of different throat lengths, using the two DeWitt distances. Our computation in Section 3.3 shows an agreement between the distance to the scaling limit according to the phase-space distance (3.1.3) computed in [16] and to the DeWitt distance *without the volume factor* (3.1.6). Both formulas, (3.1.12) and (3.1.6), give a finite result for this distance. On the other hand, the distance to the scaling limit according to the DeWitt distance *with the volume factor* (3.1.7) is infinite and matches with that of the exponential distance (3.1.11).

One of the motivations to take (3.1.7) to be the generalised Swampland distance is that it gives the exponential mass decrease (3.1.9) with respect to the moduli space distance [74]. But the distance (3.1.6) is also a well-defined distance that can be used in the context of the Swampland. The two DeWitt distances (3.1.6) and (3.1.7) do not agree, and measure different physical notions – if they correspond to any physical notions at all. Could the lew-velocity distance match one of the two DeWitt distances?

At first sight, both the results (3.3.12) and (3.3.15) appear to be in tension with an earlier works in the literature [109, 82], which use the low-velocity distance (3.1.5) of [102].

Our computation in Section 3.3 leading to (3.3.12) did not involve the use of the smoothness conditions (3.2.4) nor the bubble equations (3.2.5). Indeed, we applied the DeWitt distance to AdS_2 throat regions of different lengths. As the throat is far from the centres, it is insensitive to the physics at the bottom of the throat. For instance, the throat is insensitive to the details of the charges $\mathbf{h}_j$ at the centres, as long as they give the right black-hole asymptotic charges (3.2.7).

As such, one can take $k^I_j = 0$ for all j and I, so that the black-hole charge Q_I is only given by the l^I_j's:

$$Q_I = \sum_{j=1}^{n} l^I_j \,, \qquad Z_I = L_I \,, \tag{3.4.1}$$

and one would still find the same finite result for the distance to the scaling limit (3.3.12). In addition to the condition $K^I = 0$, let us take the simple example of a two-center solution and further impose

$$V = L_1 = L_2 = L_3 \,. \tag{3.4.2}$$

From the four-dimensional point of view, equation (3.4.2) means that the centres of the multi-centered solutions become extremal Reissner-Nordström black holes at the same coordinate location. However, this is exactly the system considered in [109] and previously in [102] (see also [106]). In [109], it was computed that the low-velocity metric in moduli space is

$$ds^2 = \frac{1}{2} \frac{(l_1)^3 l_2 + l_1 (l_2)^3}{(\rho_{12})^3} \, (\mathrm{d}\rho_{12})^2 \,, \tag{3.4.3}$$

where ρ_{12} denotes the distance between centre 1 and 2, and l_1, l_2 are the respective electric charges at centre 1 and 2. (The results match the same $1/\rho^3$ dependence found in [82].) Therefore, the

distance to the scaling limit is given by

$$\Delta_{\text{low-v.}}(\lambda_0, \lambda) \propto \int_{\lambda}^{\lambda_0} d\lambda \frac{1}{\lambda^{3/2}} \propto \frac{1}{\lambda^{1/2}} - \frac{1}{{\lambda_0}^{1/2}} \,. \tag{3.4.4}$$

The distance to the scaling limit is infinite, and blows up like $\frac{1}{\lambda^{1/2}}$. This is, at first sight, in contradiction not only with the distance to the scaling limit according to the phase-space distance (3.1.12) and to the first DeWitt distance (3.3.12), but also with the second DeWitt distance (3.3.15).

However, there is a subtlety here:[2] the low-velocity distance measures the moduli-space distance on a higher dimensional moduli space. For instance, the dimension of three-centered solutions before applying the bubble equations (3.2.5) is 6, while after imposing them the dimension becomes 4. The low-velocity distance measures distances on the 6-dimensional moduli space, while the phase-space distance and the two DeWitt distances measure the distance on the 4-dimensional moduli space. This is why the low-velocity distance does not necessarily contradict both the DeWitt distances.

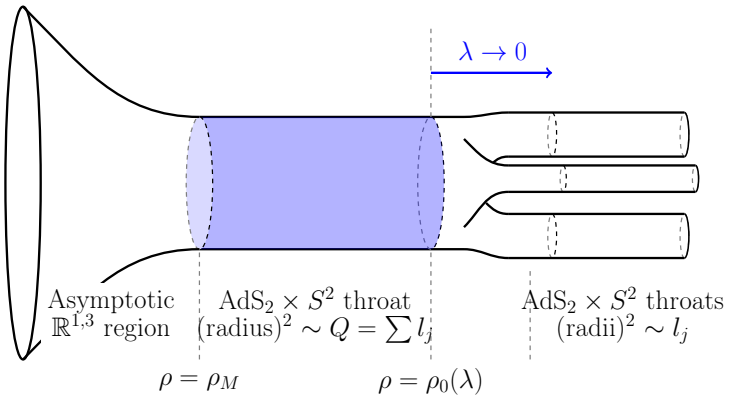

Figure 3.2 – Geometry of multiple near-coincident extremal black holes. The main AdS_2 throat, shaded in blue, divides itself into multiple infinite AdS_2 throats corresponding to the individual black holes. In the scaling limit ($\lambda \to 0$), only the length of the main throat increases.

But regardless of the above subtlety, the physical picture of the scaling limit of multiple extremal black holes is quite similar to that of the smooth cap being pushed deeper by the AdS_2 throat. For near-coincident extremal black holes, after the asymptotically flat region, there is a main AdS_2 throat region corresponding to the sum of all the black hole charges, $Q = \sum_{j=1}^{n} l_j$. See Fig. 3.2. This main throat region eventually divides itself into multiple AdS_2 throat regions, corresponding to the different local charges, l_j, of the individual extremal black holes [109]. In the scaling limit, the geometry of the bottom of the throat remains fixed, and only the main AdS_2 throat of the bigger black hole becomes longer and longer [81, 109]. Thus, the main AdS_2 throat is insensitive to whether lies at its bottom a smooth cap or a set of black holes: this is why the computations in Section 3.3 leading to (3.3.12) will give the same result for a deepening

[2] I would like to thank Micha Berkooz for pointing out this subtlety.

AdS_2 throat with black holes at its bottom.

In this letter, we compared the phase-space distance and the two DeWitt distances, on a moduli space of geometries developing longer and longer AdS_2 throats. In the specific example of path on moduli space we took, the phase-space distance and the DeWitt distance *without the volume factor* agree, while the DeWitt distance *with the volume factor* disagrees with them:

- According to the phase-space distance and the DeWitt distance *without the volume factor*, the locus in moduli space where the lengths of these throats become infinite – *i.e.* the *scaling limit* locus – lies at *finite distance* in moduli space. Indeed, for both of these distances, the metric component on moduli space along the scaling parameter, λ, blows up as $1/\lambda$ in the vicinity of the scaling limit ($\lambda \to 0$), so the distance to the scaling limit is finite.

  In the scaling limit, an infinite tower of KK modes becomes massless due to the increasing redshift from the cap to the asymptotics. According to the phase-space distance and the DeWitt distance *without the volume factor*, this infinite tower of massless states emerges at finite distance in moduli space. If the DeWitt distance *without the volume factor* is the relevant distance to use in the context of the Swampland, these results constitute a counter-example to the converse of the Generalized Distance Conjecture.
- However, according to the DeWitt distance *with the volume factor*, the distance in moduli space to the scaling limit locus is *infinite*, and scales like $\log \lambda$. This $\log \lambda$ behaviour would lead to a tower of KK states whose mass decrease matches the exponential decrease of the usual Swampland picture, should the converse of the Generalized Distance Conjecture apply in the scaling limit of deep-throat geometries.

According to the low-velocity distance, the distance in moduli space to the scaling limit locus is *infinite*, and scales like $1/\lambda^{1/2}$. However, the low-velocity distance computed here concerns a *higher-dimensional moduli space of solutions* on which one has not yet imposed the bubbles equations. Finding out which are the fields that need to be integrated out in order to get the lower-dimensional moduli space will indicate the behaviour of the low-velocity distance to the scaling limit for bubbling geometries. This last result should match one of the two DeWitt distances, and thus shedding light on the physical interpretation of the matched distance. We hope to report on this in the future.

Chapter 4

Gravitational Footprints of Black Holes and their Microstate Geometries

4.1 Introduction

The observation of gravitational waves by the LIGO collaboration [110] from colliding black holes has lead to a paradigm shift in how we think about black holes: they are physical objects that can be observed and studied in nature. Furthermore, gravitational-wave interferometers [111] and telescope arrays [112] have began to measure effects that are sensitive to possible new physics at the scale of the horizon, and this sensitivity is only bound to increase with the advent of space-based gravitational-wave interferometers [113] and third-generation ground-based ones [114].

On the other hand, black holes have served as the primary theoretical lab for exploring quantum gravity. Their theoretical studies have led to many interesting puzzles and paradoxes which have offered important windows into quantum gravity; chief among them are the origin of the microstates that make up the Bekenstein-Hawking entropy, and the unitary problem of black hole evaporation. The study of microstates is an inherently top-down question as it requires an understanding of the microscopic degrees of freedom of quantum gravity. In contrast, the unitary problem can be studied from a bottom-up perspective by exploring consistency of quantum mechanics near black hole environments. An important lesson from the latter is that black-hole evaporation is compatible with the standard rules of quantum mechanics only when there is new structure at the scale of the black horizon [9]. This is also articulated more recently in the firewall paradox [38].

One of the crowning successes of string theory is reproducing the Bekenstein-Hawking entropy for a wide classes of supersymmetric black holes from stringy microscopic states [28]. A fundamental question that follows is: What are the gravitational properties of such microstates? While generically it is hard to characterize their quantum mechanical properties, there can exist wide classes of microstates that are sufficiently coherent to admit classical descriptions as smooth horizonless geometries [13, 51]. These states are called microstate geometries. These geometries are indistinguishable from their corresponding black hole up to the region of the would-be horizon, where the spacetime ends in a smooth horizonless cap that contains non-trivial topological cycles wrapped by fluxes.

The key lesson from the top-down studies of microstate geometries and as well as the bottom-up analysis is: *black holes as observed in nature may correspond to ultra compact objects made up of new phases of matter from quantum gravity.* In the fast emerging field of gravitational-wave astronomy and astrophysics, an important goal will be to characterize the possible deviations from astrophysical Kerr black holes in general relativity (GR) coming from the new black hole microstructure in string theory.

An important class of observables that can distinguish microstate geometries with horizon-size structure from classical GR black holes is the tower of gravitational multipole moments. These observables are already astrophysically interesting and will become more so in the era of gravitational-wave astronomy. In this paper, we aim to characterize gravitational multipole moments of microstate geometries that correspond to a class of four-dimensional non-supersymmetric spinning extremal black holes, dubbed almost-BPS [115, 67, 66, 116, 117]. There are several benefits in studying the almost-BPS black holes and their microstates:

First, almost-BPS black holes and their microstate geometries are constructed from supergravity by subtly breaking supersymmetry while maintaining the general linear structure that allows for solvability [115, 67]. This has several benefits as compared to their widely studied supersymmetric[1] cousins. Indeed, the supersymmetric four-dimensional black holes in string theory are non-rotating, extremal and carry large charges;[2] these features undermine their phenomenological interest. In contrast, almost-BPS black holes can have angular momentum, small charge-to-mass ratios,[3] and can therefore have the same conserved charges as astrophysical black holes. In this regard, it is phenomenologically relevant to study the multipole structure of these black holes and compare it to the multipole structure of Kerr black holes. This initial analysis will provide the baseline to study deviations of multipoles caused by horizon-scale microstructure in the almost-BPS microstate geometries when compared to the almost-BPS black holes and to the Kerr black holes.

Another benefit of studying almost-BPS solutions is to contrast them with the phenomenological modeling of Exotic Compact Objects (ECOs) [123, 124, 122]. These are bottom-up objects that force structure at horizon scale and thereby violate black hole no-hair theorems and the Buchdahl bound [125]. Their description require exotic matter with no UV physics. Almost-BPS solutions on the other hand can be understood directly in string theory.

The multipole structure of almost-BPS black holes and their microstate geometries is very rich. This is owed to the non-trivial four-dimensional angular momentum that is absent in the non-spinning supersymmetric black holes. We show that the multipoles of almost-BPS black holes have a similar functional dependence on the mass-to-spin ratio as the multipoles of Kerr(-Newman) black holes. Moreover, unlike the latter, almost-BPS multipoles also have an interesting dependence on the charge-to-mass ratio. Furthermore, the generic almost-BPS black holes have all non-zero multipoles, including the odd-parity multipoles which vanish in Kerr; the presence

[1] For recent study of gravitational multipoles for supersymmetric microstate geometries see [118–121]. For a more general discussion of observables of supersymmeric microstate geometries see [122].

[2] These charges emerge from string theory and can be associated to dark Maxwell fields.

[3] Even if almost-BPS black holes are extremal, their four-dimensional charges can be made arbitrarily small compared to their mass by turning on non-trivial scalar fields that modify the effective electromagnetic coupling in four dimensions. We discuss this in detail in section 4.3.3.

of these multipoles indicates a breaking of equatorial symmetry ($\theta \leftrightarrow \pi - \theta$) which could have interesting observable consequences. This is a significant deviation from Kerr black holes.

Multipoles of almost-BPS microstate geometries have a highly non-trivial dependence on the internal degrees of freedom of the geometry. These deviate from the multipoles of the almost-BPS black hole at the same scale as the size of the microstructure in the near horizon region.[4] We show that the deviations are rather "random" as they depend on the geometry of the topologically non-trivial bubbles that give the horizon-scale structure, and they can be either positive or negative; this is in contrast with the analysis of [119], where the multipoles of certain microstate geometries were found to be larger than the multipoles of their corresponding black holes. In a broader scope, our constructions and studies in this paper allow us to understand the physics of potential microstructure of the Kerr black hole much better than what one could hope from naively extrapolating the supersymmetric microstate results as was previously done in [118–121].

The structure of the paper is as follows. In the next subsection we summarize our main results. In section 4.2, we review non-supersymmetric four-dimensional solutions obtained by the almost-BPS ansatz and some generalities about the derivation of multipole moments. In section 4.3, we construct non-supersymmetric rotating almost-BPS black holes that look almost neutral and we compare their physics to that of Kerr-like GR black holes. In section 4.4, we construct a family of multicenter microstate geometries and discuss their physics and their multipole structure with respect to the almost-BPS black holes they correspond to. In particular, we compare and contrast properties of the almost-BPS microstate multipoles with previous work and conjectures on (supersymmetric) microstate geometry multipoles. Finally, we conclude in section 4.5 with a brief overview of possible future directions.

4.1.1 Summary of our results

Using the almost-BPS ansatz in $\mathcal{N} = 2$ four-dimensional supergravity, we construct four-charge non-supersymmetric rotating black holes and smooth horizonless microstate geometries thereof. We describe the new (astro)physics brought about by the horizon-scale structure compared to the classical black holes of general relativity. The expected modifications can be separated in two categories:

- Deviations between the physics of almost-BPS black holes and the physics of Kerr black holes.
- Deviations that arise from the presence of a smooth horizonless microstructure replacing the horizon of almost-BPS black holes.

The physics of almost-BPS black holes

Our discussion starts with non-supersymmetric four-charge extremal black holes constructed from the almost-BPS ansatz. We highlight the role of a dimensionless parameter, h, that allows to dial the ratio between the four-dimensional mass and charges. Therefore, our string-theory

[4] Extremal black holes have a throat of infinite length, that an infalling observer can traverse in finite proper time, so the"size" of the microstructure above the horizon is subtle to define [126].

black holes can have the same mass, charges and spin as an almost-neutral Kerr-Newman black hole.

We first discuss the geometrical differences between the near-horizon regions of these two solutions. Being extremal, rotating almost-BPS black holes have no ergosphere and the area of their horizon and their cosmic censorship bounds scale differently with the charges compared to Kerr black holes. Second, the multipoles of almost-BPS black holes have a similar dependence on the mass/spin ratio compared to Kerr black holes. However, they also depend non-trivially on the mass/charge ratio (determined by the parameter h) unlike Kerr(-Newman) solutions. Moreover, all multipoles of the rotating almost-BPS black hole are non-zero, irrespective of their parity.

We highlight the important similarities and differences that exist between the multipole moments of generic almost-BPS black holes in string theory and those of Kerr black holes.

For $h = 1$, the almost-BPS black hole is the *purest spinning black hole*: all its multipoles except the mass and angular momentum vanish. This is unique among rotating gravitational solutions (for example Kerr has infinite towers of non-zero multipole moments).

The physics of almost-BPS microstate geometries

In the second part of the paper, we discuss the physics of almost-BPS microstate geometries (near their black hole limit) and compare it to the physics of their corresponding almost-BPS black holes.

- The multipole moments of microstate geometries are equal to the multipoles of the black hole they correspond to with deviations proportional to the "size" of the microstructure above the would-be black-hole horizon. More concretely,

$$\text{Mult}\,(\text{Microstate}) \;=\; \text{Mult}\,(\text{BH})\;\left(1 \,+\, \mathcal{O}\left(\delta_{\text{micro}}\right)\right)\,, \tag{4.1.1}$$

  where $\delta_{\text{micro}} \ll 1$ is the scale of the solution which characterizes how "close" in moduli space the microstate geometry is to the black hole [64, 16]. When $\delta_{\text{micro}} \to 0$, the microstate geometry becomes identical to the black hole.
- When δ_{micro} is finite, the microstate-dependent contribution proportional to $\mathcal{O}\left(\delta_{\text{micro}}\right)$ can modify the classical-black-hole result. In particular, in [121, 119] an analysis of certain families of microstate geometries suggested that microstate geometries have bigger multipoles than the black hole with the same charges, implying that perhaps the black hole is an extremum in the phase space of solutions for certain observables.[5] We have constructed a number of almost-BPS microstate geometries that show explicitly that the black hole is not an extremum in solution phase space, at least not as far as multipoles are concerned. For the geometries we construct, the multipoles deviate from their expected average black hole values by $\mathcal{O}\left(\delta_{\text{micro}}\right)$ terms that behave as small microstate-dependent "noise-type" contributions and that can be either positive or negative.

[5] This conjecture came from comparing supersymmetric non-scaling microstate geometries to Kerr black holes. As mentioned at the beginning of the summary section, a careful analysis should be done in two steps: (i) comparing scaling microstate geometries to their corresponding black hole in string theory, and then (ii) comparing this black hole to the astrophysical Kerr black hole with the same conserved charges (or at least the same mass and angular momentum).

4.2 The class of solutions and multipole moments

In this section, we review the construction of non-supersymmetric almost-BPS four-dimensional solutions and give a few generalities about the computation of gravitational multipole moments.

4.2.1 Almost-BPS solutions

We work with non-supersymmetric solutions of string theory that are asymptotic to four-dimensional Minkowski space times a six-dimensional CY manifold. More specifically, our solutions fit within the so-called *almost-BPS* ansatz, in which one can construct multi-center non-supersymmetric black holes as well as horizonless microstate geometries [115, 67, 66, 116, 117]. Despite breaking supersymmetry, the equations governing the solutions in this ansatz can be solved using a linear algorithm. This linear structure comes because of an underlying nilpotent algebra [127], and is present in several other ansatze governing non-supersymmetric solutions [128, 129].

In general the almost-BPS ansatz can be used obtain solutions to any $U(1)^n$ five-dimensional supergravity, but in this paper we will focus on the STU solutions that arise from a compactification of M-theory on $T^6 \times S^1$ [130–132]. The solutions have a Taub-NUT base space, and have an additional isometry, which allows us to compactify them to four dimensions. We describe in detail the four-dimensional STU Lagrangian in appendix B.1, starting from the string theory realization of these solutions. This Lagrangian contains, besides the *four-dimensional metric*, *four vector gauge fields* (hence generic solutions have four electric and four magnetic charges) and *three complex scalar fields* that are all non-trivially coupled.

The metric of an almost-BPS solution is described by eight scalar functions $(V, K^1, K^2, K^3, Z_1, Z_2, Z_3, \mu)$, together with an angular momentum one-form ϖ:

$$ds_4^2 = -\mathcal{I}_4{}^{-\frac{1}{2}} \, (dt + \varpi)^2 \, + \, \mathcal{I}_4{}^{\frac{1}{2}} \, ds_3^2 \, , \qquad \mathcal{I}_4 \, \equiv \, Z_1 Z_2 Z_3 V - \mu^2 V^2 \, , \tag{4.2.1}$$

where ds_3^2 is the metric of a flat three-dimensional base that we parameterize by the spherical coordinates

$$ds_3^2 \, = \, d\rho^2 \, + \, \rho^2 \left(d\theta^2 + \sin^2\theta \, d\phi^2 \right) \, . \tag{4.2.2}$$

The gauge fields and scalars also have a specific form (which depends on all of the functions $(V, K^1, K^2, K^3, Z_1, Z_2, Z_3, \mu)$), which we give in appendix B.1.3.

These almost-BPS solutions have *ten conserved quantities*: four electric charges q_Λ ($\Lambda = 0, \cdots, 3$) and four magnetic charges p^Λ in addition to a four-dimensional mass M and an angular momentum J. We work in units where Newton's constant in four dimensions is $G_4 = 1$. Thus, asymptotically we always have:

$$\mathcal{I}_4 \, \sim \, 1 \, + \, \frac{4M}{\rho} \, , \qquad \mathcal{I}_4^{-\frac{1}{2}} \, \varpi\big|_{d\phi} \sim \, \frac{2J}{\rho} \, \sin^2\theta \, , \tag{4.2.3}$$

The almost-BPS ansatz contains a non-BPS extremal four-charge black hole (the "almost-BPS black hole"), as well as horizonless solutions that are smooth in string theory[6] and allow

[6] In four dimensions, the centers of these solutions correspond to D6 branes and D4 branes with Abelian worldvolume flux, hence are singular. However, the metric near each of these centers becomes completely smooth and non-singular when uplifted to a six-dimensional duality frame.

scaling limits where they can approach the black hole geometry arbitrarily well [66]. Thus, we can think about these solutions as "almost-BPS microstate geometries". Crucially, the equations of motion for these microstate geometries have an "almost-linear" structure (see (B.1.26)), which allows one to generate multi-center configurations. In appendix B.3, we review the method to solve these equations for solutions where all the centers are collinear [67].

4.2.2 Gravitational multipole moments

One important physical property that we will study in detail for almost-BPS solutions is the structure of their gravitational multipoles. For asymptotically-flat four-dimensional solutions, these can most easily be read off by using the ACMC-coordinate[7] formalism developed by Thorne [133], which we briefly review here. All of the almost-BPS solutions constructed thus far are stationary and axisymmetric, so we will only discuss ACMC spacetimes satisfying these symmetries.

We will follow [120] by first writing the metric in AC coordinates: these are asymptotically Cartesian coordinates that are not necessarily mass-centered. This means that the mass dipole moment, $\tilde{M}_1$, does not necessarily vanish (as it must in ACMC coordinates). One can then obtain ACMC coordinates from any AC coordinate system by a simple shift of origin.

In such AC coordinates[8], the asymptotic expansion of the metric is:

$$g_{tt} = -1 + \frac{2M}{\rho} + \sum_{\ell\geq 1}^{\infty} \frac{2}{\rho^{\ell+1}} \left(\tilde{M}_\ell P_\ell + \sum_{\ell'<\ell} c^{(tt)}_{\ell\ell'} P_{\ell'} \right), \tag{4.2.4}$$

$$g_{t\phi} = -2\rho \sin^2\theta \left[\sum_{\ell\geq 1}^{\infty} \frac{1}{\rho^{\ell+1}} \left(\frac{\tilde{S}_\ell}{\ell} P'_\ell + \sum_{\ell'<\ell} c^{(t\phi)}_{\ell\ell'} P'_{\ell'} \right) \right], \tag{4.2.5}$$

$$g_{\rho\rho} = 1 + \sum_{\ell\geq 0}^{\infty} \frac{1}{\rho^{\ell+1}} \sum_{\ell'\leq\ell} c^{(\rho\rho)}_{\ell\ell'} P_{\ell'}, \qquad g_{\theta\theta} = \rho^2 \left[1 + \sum_{\ell\geq 0}^{\infty} \frac{1}{\rho^{\ell+1}} \sum_{\ell'\leq\ell} c^{(\theta\theta)}_{\ell\ell'} P_{\ell'} \right], \tag{4.2.6}$$

$$g_{\phi\phi} = \rho^2 \sin^2\theta \left[1 + \sum_{\ell\geq 0}^{\infty} \frac{1}{\rho^{\ell+1}} \sum_{\ell'\leq\ell} c^{(\phi\phi)}_{\ell\ell'} P_{\ell'} \right], \qquad g_{\rho\theta} = (-\rho\sin\theta) \left[\sum_{\ell\geq 0}^{\infty} \frac{1}{\rho^{\ell+1}} \sum_{\ell'\leq\ell} c^{(\rho\theta)}_{\ell\ell'} P'_{\ell'} \right],$$

The argument of the Legendre polynomials P_ℓ (and their derivatives) appearing above is always $\cos\theta$. The terms that contain $c^{(ij)}_{\ell\ell'}$ correspond to non-physical "harmonics", and depend on the particular AC(MC)-N coordinates used. Even though these coefficients $c^{(ij)}_{\ell\ell'}$ are unphysical, it is a condition of ACMC coordinates that only $c^{(ij)}_{\ell\ell'}$ appear with $\ell' < \ell$.[9]

[7] Asymptotically-Cartesian and Mass-Centered

[8] Note that here we are only discussing ACMC-∞ coordinates, from which all of the multipoles M_ℓ, S_ℓ can be read off. More generically, one can also have ACMC-N (or AC-N) coordinate systems from which we can only read off the multipoles to order $N+1$. Fortunately, for almost-BPS solutions the coordinates we find are AC-∞.

[9] For example, the $g_{\rho\rho}$ component of the Kerr metric in Boyer-Lindquist coordinates does not satisfy this condition, since there is a $g_{\rho\rho}$ component already at order ρ^{-2} [133, 120].

As mentioned above, AC coordinates are also ACMC if and only if the mass dipole vanishes, $\tilde{M}_1 = 0$. The gravitational multipoles M_ℓ, S_ℓ are then simply the $\tilde{M}_\ell, \tilde{S}_\ell$ quantities appearing above. However, if our AC coordinate system has $\tilde{M}_1 \neq 0$, it is easy to obtain ACMC coordinates by a simple shift of the origin along the z-axis by $z_0 = -\tilde{M}_1/\tilde{M}_0$. We can then express the true multipoles M_ℓ, S_ℓ in terms of the $\tilde{M}_\ell, \tilde{S}_\ell$ for any AC coordinate system [120]:

$$M_\ell = \sum_{k=0}^{\ell} \binom{\ell}{k} \tilde{M}_k \left(-\frac{\tilde{M}_1}{\tilde{M}_0}\right)^{\ell-k}, \qquad S_\ell = \sum_{k=0}^{\ell} \binom{\ell}{k} \tilde{S}_k \left(-\frac{\tilde{M}_1}{\tilde{M}_0}\right)^{\ell-k} \tag{4.2.7}$$

The coordinate-independent multipoles then consist of the mass multipoles M_ℓ (of which the mass is $M_0 = M$) and the current (or angular momentum) multipoles S_ℓ (of which the angular momentum is $S_1 = J$).

4.3 Almost-BPS extremal black hole

In this section, we review the stationary and axisymmetric almost-BPS black hole constructed in [66]. We shall add to the solutions of [66] non-trivial asymptotic values for the eight scalar functions (V, K^I, Z_I, μ). These asymptotic values, parameterized by h, will add interesting physical decorations to the black hole solution as they can be used to dial the ratio between the mass and the charges in four dimensions. We will further compute the multipole moments of this black hole, and compare them to those of Kerr-Newman black holes.

4.3.1 The solution

We consider a specific family of almost-BPS black holes that has the form (4.2.1), with:

$$V = h + \frac{Q_0}{\rho}, \qquad Z_I = \frac{1}{h} + \frac{Q_I}{\rho}, \qquad K^I = 0, \qquad \mu V = m_\infty + \alpha \frac{\cos\theta}{\rho^2}, \qquad \varpi = -\alpha \frac{\sin^2\theta}{\rho} d\phi. \tag{4.3.1}$$

Note that in order to have a physical solution, one needs $\mathcal{I}_4 > 0$ in (4.2.1). A necessary condition is that h and Q_Λ have the same sign, which we will assume to be positive.
These solutions are asymptotically flat when $\mathcal{I}_4 \to 1$ in (4.2.1). This requires

$$h^{-2} - m_\infty^2 = 1 \qquad \Longleftrightarrow \qquad m_\infty = \pm \frac{\sqrt{1-h^2}}{h}. \tag{4.3.2}$$

We can define the warp factor

$$\begin{aligned} \Delta &\equiv \rho^2 \sqrt{V Z_1 Z_2 Z_3 - \mu^2 V^2} \\ &= \sqrt{(Q_0 + h\,\rho)\left(Q_1 + \frac{\rho}{h}\right)\left(Q_2 + \frac{\rho}{h}\right)\left(Q_3 + \frac{\rho}{h}\right) - (m_\infty \rho^2 + \alpha\cos\theta)^2}\,, \end{aligned} \tag{4.3.3}$$

and then express the four-dimensional metric as:

$$ds_4^2 = -\frac{\rho^2}{\Delta}\left(dt - \alpha\frac{\sin^2\theta}{\rho}\,d\phi\right)^2 + \Delta\left[\frac{d\rho^2}{\rho^2} + d\theta^2 + \sin^2\theta\, d\phi^2\right], \tag{4.3.4}$$

The spherical coordinates we use are isotropic coordinates for the black hole, where the horizon is at $\rho = 0$; the timelike Killing vector ∂_t vanishes at this locus. As mentioned above, this solution is supported by three non-trivial complex scalars and four gauge fields, which are given in detail in appendix B.2.

4.3.2 Properties

The mass and angular momentum of this solution can be read off from (4.2.3) and are:

$$M = \frac{Q_0 + h^2(Q_1 + Q_2 + Q_3)}{4\,h^3}\,, \qquad J = -\frac{\alpha}{2}\,. \tag{4.3.5}$$

Moreover, the electromagnetic charges p^Λ, q_Λ sourcing the solutions are given by (see appendix B.2):

$$(p^0, p^1, p^2, p^3; q_0, q_1, q_2, q_3) = (Q_0, 0, 0, 0; 0, Q_1, Q_2, Q_3)\,. \tag{4.3.6}$$

The black hole thus has one magnetic charge and three electric charges. To consider this black hole as an astrophysically relevant one, these charges should not be thought of as standard model charges; rather, they should be viewed as "hidden" or dark charges, and their corresponding gauge fields considered as dark photons. Interestingly, the bounds on such dark charges (especially if they only interact gravitationally with standard model fields) from gravitational wave observations [134] or black hole imaging [135, 136] are still very weak — in particular, black holes with large (even near-extremal) dark charges have not necessarily been ruled out yet.

The event horizon is located at $\rho = 0$, and has the topology of an S^2. The horizon area is

$$A_H = 4\pi\sqrt{Q_0 Q_1 Q_2 Q_3 - \alpha^2}\,. \tag{4.3.7}$$

which is the same as the area of the horizon of a supersymmetric extremal D6-D2-D2-D2-D0 black hole in four dimensions. This comes from the fact that the near-horizon geometry of the almost-BPS black hole is identical to the near-horizon geometry of its BPS cousin when uplifted to five dimensions.

The metric (4.3.4) is already given in AC coordinates (as introduced in section 4.2.2). We can then easily read off the coefficients $\tilde{M}_\ell$ and $\tilde{S}_\ell$:

$$\widetilde{M}_0 = M\,, \qquad \widetilde{M}_1 = -\frac{1}{2}\,m_\infty\,\alpha\,, \qquad \widetilde{M}_\ell\big|_{\ell\geq 2} = 0\,, \tag{4.3.8}$$

$$\widetilde{S}_0 = 0\,, \qquad \widetilde{S}_1 = J\,, \qquad \widetilde{S}_\ell\big|_{\ell\geq 2} = 0\,. \tag{4.3.9}$$

Upon using (4.3.2) to express everything in terms of h, the multipoles (4.2.7) become:

$$M_\ell = (\mp 1)^\ell\,(1-\ell)\,M\left(\frac{1-h^2}{h^2}\right)^{\frac{\ell}{2}}\left(\frac{J}{M}\right)^\ell\,, \qquad S_\ell = (\mp 1)^{\ell-1}\,\ell\,J\left(\frac{1-h^2}{h^2}\right)^{\frac{\ell-1}{2}}\left(\frac{J}{M}\right)^{\ell-1}\,, \tag{4.3.10}$$

where the expressions are valid for every $\ell \geq 0$ and where ∓ 1 corresponds to the choice of branches for m_∞ in (4.3.2).[10] Note that for $h = 1$, when the mass is determined by the sum of the charges (4.3.5), all multipoles (except M_0 and S_1) vanish, despite the presence of a finite angular momentum. This makes this solution unique among all spinning gravitational solutions and, as we explained in the Introduction, we can think about it as the *purest spinning black hole*.

[10] More precisely, $(\mp 1)^\ell$ is $(-1)^\ell$ if $m_\infty = \frac{\sqrt{1-h^2}}{h}$ and $(+1)^\ell$ if $m_\infty = -\frac{\sqrt{1-h^2}}{h}$.

4.3.3 Comparing with Kerr black holes

One can see that almost-BPS black holes have a common point with the electrically and magnetically charged Kerr-Newman solution when $Q_0 = Q_1 = Q_2 = Q_3$. Taking in addition $\alpha = m_\infty = 0$ (implying $h = 1$) gives precisely the extremal Reissner-Nordstrom metric in isotropic coordinates. However, more generic almost-BPS black holes have significant differences that might affect their gravitational footprints compared to black holes in general relativity. In this section we compare the almost-BPS black holes to Kerr and Kerr-Newman black holes in order to further assess their phenomenological viability.

Cosmic censorship and ergosphere

A Kerr-Newman black hole of mass M, angular momentum J and carrying any number of charges $\mathcal{Q}_I$ has an allowed regime of parameters dictated by the cosmic censorship bound:

$$M^2 - \sum_I \mathcal{Q}_I - \frac{J^2}{M^2} \geq 0\,. \tag{4.3.11}$$

This is very different from the cosmic censorship bound of the almost-BPS black hole, which is given by demanding that (4.3.7) remains real and can be expressed in terms of the angular momentum J and conserved charges p^0, q_i in (4.3.6) as:

$$p^0 q_1 q_2 q_3 - 4J^2 > 0\,. \tag{4.3.12}$$

Note that the mass M does not appear explicitly in this formula.

Moreover, a Kerr-Newman black hole generically has an ergosphere, where the asymptotically timelike Killing vector ∂_t becomes spacelike. The almost-BPS black hole does *not* have an ergosphere, despite having a non-zero angular momentum. It would be interesting to understand how this could give rise to potential dynamical differences between Kerr(-Newman) and almost-BPS black holes, for example for photon orbits or gravitational-wave emission.

Multipole moments

We calculated the multipoles of the almost-BPS black hole in (4.3.10). We can compare these to the multipoles of a Kerr(-Newman) black hole, of which the non-zero multipoles can be written as:

$$\text{Kerr:}\quad M_{2\ell}^{\text{Kerr}} = (-1)^\ell M \left(\frac{J}{M}\right)^{2\ell}, \quad S_{2\ell+1}^{\text{Kerr}} = (-1)^\ell J \left(\frac{J}{M}\right)^{2\ell}, \quad M_{2\ell+1}^{\text{Kerr}} = S_{2\ell}^{\text{Kerr}} = 0\,. \tag{4.3.13}$$

Note that the gravitational multipoles of Kerr and (charged) Kerr-Newman are the same, and thus (perhaps surprisingly) they are independent of the black hole charges [137]. For an almost-BPS and Kerr-Newman black hole of equal mass M and angular momentum J, we can compare the even-mass and odd-current multipole moments:

$$\frac{M_{2\ell}}{M_{2\ell}^{\text{Kerr}}} = (-1)^{\ell+1}(2\ell-1)\left(\frac{1-h^2}{h^2}\right)^\ell, \qquad \frac{S_{2\ell+1}}{S_{2\ell+1}^{\text{Kerr}}} = (-1)^\ell(2\ell+1)\left(\frac{1-h^2}{h^2}\right)^\ell. \tag{4.3.14}$$

We see that the multipoles differ significantly because of the overall sign difference and the presence of h. As we will discuss below, h is related to the ratio of mass and charges of the black hole. For example, in the small h limit, $0 < h \ll 1$, the mass M over charge Q (where Q stands for any of the p^Λ, q_Λ charges) ratio scales as $M/Q \sim 1/h^3$ (see (4.3.16)), so that (4.3.14) scales as:

$$0 < h \ll 1 : \qquad \frac{M_{2\ell}}{M_{2\ell}^{\text{Kerr}}} \sim (-1)^{\ell+1} (2\ell - 1) \left(\frac{M}{Q}\right)^{\frac{2\ell}{3}} . \tag{4.3.15}$$

Hence, unlike Kerr-Newman black holes, the almost-BPS multipoles have a non-trivial dependence on the charges of the solution, that comes through the dependence on h.

In the opposite regime, $h = 1$, we see from (4.3.10) that all of the almost-BPS multipoles vanish with the exception of the mass $M_0 = M$ and of angular momentum $S_1 = J$. It is worth pointing out that this is an unique physical system — to our knowledge, no other known (super)gravity solution can have a non-zero angular momentum $S_1 \neq 0$ without *any* other multipole turned on. Hence, we can think about the $h = 1$ black hole as the *purest* spinning black hole.

We can tune h in (4.3.14) to set the mass quadrupole moments equal, $M_2 = M_2^{\text{Kerr}}$; this sets $h^{-1} = \sqrt{2}$. Of course, then the higher-order multipoles will differ by larger and larger factors as we increase ℓ. We note that while current and near-future observations (will) constrain the quadrupole moment rather well (constraining M_2/M^3 within 10^{-4}), it is unlikely that for example eLISA will be able to constrain many higher multipole moments to a similar degree [138–141].[11]

Finally, we also note that the odd mass multipoles $M_{2\ell+1}$ and even current multipoles $S_{2\ell}$ of the almost-BPS black hole do not vanish, in contrast to the Kerr(-Newman) black hole. These multipoles are odd-parity: they correspond to terms in the metric that break the equatorial symmetry ($\theta \leftrightarrow \pi - \theta$) and thus can give rise to interesting new equatorially asymmetric phenomena [142–145]. Heuristically, the presence of these odd-parity multipoles are a consequence of the curious fact that the *center of mass of the black hole* is not the same location as the *center* of the black hole. The coordinates used in (4.3.4) are centered around the location of the black hole horizon at $\rho = 0$. However, as discussed above, these coordinates are AC and not ACMC (since the mass dipole $\tilde{M}_1 \neq 0$ in these coordinates). Rather, the ACMC coordinates where the dipole vanishes are related to these coordinates by a shift of the origin by a distance proportional to $\tilde{M}_1/\tilde{M}_0$ (see (4.2.7)).

The physics of the h parameter

From the discussions above, it is clear that the parameter h, which can be freely chosen in the almost-BPS solution (4.3.1) between $0 < h \leq 1$, has a great influence on the physical properties of the almost-BPS black hole. First of all, it sets the ratio between the mass (4.3.5) and the conserved charges (4.3.6):

$$\frac{M}{(p^\Lambda, q_\Lambda)} = \underset{h\ll 1}{\mathcal{O}}\left(\frac{1}{h^3}\right) , \qquad \text{and} \qquad \frac{M}{4} \underset{h=1}{=} \sum_\Lambda (p_\Lambda + q^\Lambda) . \tag{4.3.16}$$

[11] Although note that in most if not all such modeling, it is assumed that the odd parity multipoles M_{2n+1}, S_{2n} vanish, so it is unclear to what extent observations will be able to distinguish spacetimes where these are non-zero.

Taking h small introduces a large discrepancy between the four-dimensional mass and the charges, $M \gg (p^\Lambda, q_\Lambda)$. Consequently, our solutions can describe black holes with very small charges and large mass. However, even it these charges are small, our black holes are still extremal.

Similarly, one can compute the ratio of the mass squared over the area of the event-horizon (4.3.7), assuming that the angular momentum parameter $\alpha \sim \mathcal{O}(h^0)$:

$$\frac{M^2}{A_H} = \underset{h\sim 0}{\mathcal{O}}\left(\frac{1}{h^6}\right) \qquad \text{and} \qquad \frac{M^2}{A_H} = \underset{h=1}{\mathcal{O}}(1)\,. \tag{4.3.17}$$

Therefore, h also changes the relative size of the horizon with respect to the mass; as the mass becomes much larger than the charges, $M \gg (p^\Lambda, q_\Lambda)$, the horizon area also becomes relatively small, $A_H \ll M^2$ (note that the Schwarzschild black hole has $A_H^{\rm S} = 16\pi M^2$.)

From a four-dimensional perspective, h corresponds to non-trivial profiles for the three scalar fields of the solutions (B.2.3). Because the STU Lagrangian (B.1.16) has non-trivial couplings between scalar and gauge fields, these profiles change the effective electromagnetic couplings, increasing the effect of the charges on the deformation of the spacetime. More precisely, taking h small increases the impact of a small charge on the geometry.

This parameter h can have great implications in new black hole astrophysics. In this paper, we have mostly focussed on its effect on the multipole structure of the almost-BPS black holes and how it differs from that of Kerr black holes. It would be interesting to study further processes, such as gravitational wave emission, tidal Love numbers, or scattering, to understand further the implications of this parameter.

Because the almost-BPS and BPS black holes have a similar structure, one can wonder what the effect would be of such a scalar profile on a four-dimensional supersymmetric black hole. It appears that a similar parameter h for the BPS solutions can be used to freely dial the ratio between the four-dimensional mass and charge ratio and construct an effective neutral solution. However, the magnetic charge (Q_0) needs to be turned off for the BPS solutions when $h \neq 1$, so the area of the horizon will vanish and the BPS black hole corresponds to a microscopic black hole (which, although microscopic, would have potentially a large mass and small charges).

4.4 Smooth microstate geometries

The almost-BPS black hole is only one member of the very large family of almost-BPS solutions [115, 67, 66, 116, 117]. This family of solutions is controlled by a specific ansatz (see (4.2.1), (B.1.14), and (B.1.15)), and the equations of motion have a nested linear structure (see (B.1.26)), similar to that of BPS solutions. This allows the construction of almost-BPS multicenter solutions [67], which include multicenter black holes and black rings, as well as solutions that are smooth, horizonless microstate geometries. In this section, we will review their construction heuristically (relegating most of the technical details to the appendices) and discuss some of their basic properties.

4.4.1 Construction

In this section, we construct horizonless almost-BPS microstate geometries. First, we review the principles behind this construction and then we give the specific details of the family of microstate geometries that we consider in this paper.

Heuristics: blowing up topological cycles

The microstate geometries we are interested in are solutions that match the almost-BPS black hole up to the region close to the would-be horizon. In this region, the multicenter configuration has a non-trivial, horizonless structure. In four dimensions, those solutions are singular at all the almost-BPS centers. When embedded in higher dimensions, these singularities have a very specific form, and become smooth regions of spacetime in different duality frames.

The construction of such solutions can be rather technical. However, the main philosophy is simple to depict (see Fig.4.1). By embedding the four-dimensional STU Lagrangian in higher dimensions, some of the four-dimensional scalars and gauge fields become geometric, corresponding to metric components along the extra dimensions. In particular, certain singularities of the four-dimensional solution have scalars and gauge fields that diverge in such a way that the uplift of the solution to higher dimensions is smooth, and the singularity corresponds to an "end of spacetime". The best example of this is the D6 brane compactified on a six-torus, which appears singular from a four-dimensional perspective, but is smooth when uplifted to M-theory.

As depicted in Fig.4.1, having several end-of-spacetime loci gives a *bubbling topology* induced by the behavior of the extra dimensions. These bubbles are kept from collapsing by being wrapped by electromagnetic fluxes, which generate the same asymptotic charges as the four-dimensional black hole, but without a horizon.

In a sense, the microstate geometry *blows up* or *resolves* the black-hole singularity, dissolving the horizon into smooth topological cycles wrapped by fluxes in higher dimensions. A crucial point with microstate geometries is that they allow a *scaling limit*, where the centers can come arbitrarily close to each other [44, 43, 80] from the point of view of the $\mathbb{R}^3$ base of the solution, $|\vec{\rho}_i - \vec{\rho}_j| \sim \lambda \ll (M, Q, J)$, which makes the solution resemble the black hole more and more, but still allows it to end in a smooth horizonless cap [43].

In the almost-BPS Ansatz, the main ingredients that are used as smooth end-to-spacetime loci are *supertube centers* and *Taub-NUT centers*. A *Taub-NUT center*, located at the position $\vec{\rho}_0$, sources only V and μV (4.2.1) such as

$$V = \ldots + \frac{Q_0^{(0)}}{|\rho - \vec{\rho}_0|} + \ldots , \qquad \mu V = \ldots + \frac{m^{(0)}}{|\rho - \vec{\rho}_0|} + \ldots . \tag{4.4.1}$$

This will end up sourcing a magnetic charge p^0 (through the equations of motion, see (B.1.26)). The i^{th} center is a *supertube center of species "I"*, with $I = 1, 2, 3$, located at a position $\vec{\rho}_i$. It

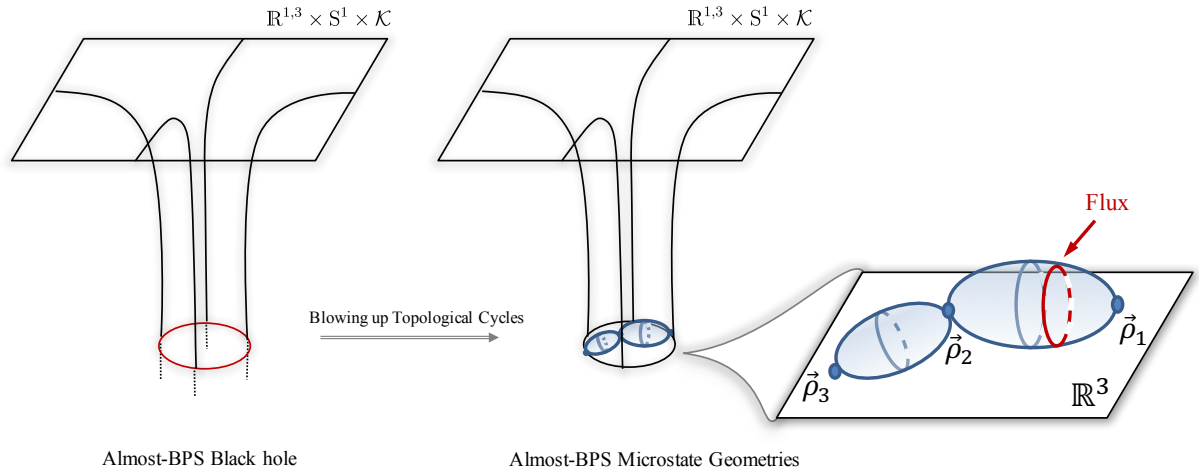

Figure 4.1 – Schematic description of the time-slices of an almost-BPS black hole and their corresponding multicenter smooth solutions. The horizon is resolved by blowing up topological cycles wrapped by fluxes in higher dimensions, where $\mathcal{K}$ denotes these extra compact dimensions.

has a source in K^I, two sources in Z_J and Z_K with $I \neq J \neq K$, and one source in μV [146]:[12]

$$K^I = ..+\frac{k^{(i)}}{|\rho-\vec{\rho}_i|}+.., \quad Z_J = ..+\frac{Q_J^{(i)}}{|\rho-\vec{\rho}_i|}+.., \qquad Z_K = ..+\frac{Q_K^{(i)}}{|\rho-\vec{\rho}_i|}+.., \quad \mu V = ..+\frac{m^{(i)}}{|\rho-\vec{\rho}_i|}+.. \tag{4.4.2}$$

This will source a magnetic charge p^I and two electric charges q_J, q_K. Therefore, by combining Taub-NUT centers and supertube centers of at least two species, we will be able to construct solutions that have the same charges as the almost-BPS black hole.

When embedded in five dimensions, the metric near a Taub-NUT center is that of smooth $\mathbb{R}^{4,1}$. For each of the species of supertube centers, one can dualize to a six-dimensional supergravity where they are smooth [146] providing that their charges satisfy:[13]

$$m^{(1)} = \frac{Q_J^{(1)} Q_K^{(1)}}{2k^{(1)}}. \tag{4.4.3}$$

[12] These supergravity sources were shown in [146] to correspond to the backreaction of the supertubes constructed using the DBI action [47, 48].

[13] At first sight, it may appear that we cannot have a unique duality frame where a solution with multiple species of supertubes is smooth at each supertube. However, one can perform a "generalized spectral flow" duality [147], that transforms each type of supertube into a smooth center [148]. These transformations give a new solution that does not belong to the almost-BPS ansatz [148, 116], but from a four-dimensional perspective they leave the metric invariant and simply reshuffle the scalars and the vectors [116]. Hence, for simplicity, we will continue working with almost-BPS supertubes and Taub-NUT centers.

Two supertubes in Taub-NUT

We now construct a specific family of horizonless, multicenter geometries that have the same charges, mass and angular momentum as the almost-BPS black hole. In addition, the family of solutions we want to construct consists of *scaling solutions*, which means we can make the distance between the centers arbitrarily small in the $\mathbb{R}^3$ base, so that the multi-center solution matches the single-center black hole arbitrarily well.

As discussed above, the supertube and Taub-NUT centers of the solution look singular in four dimensions, but the origin of these singularities is understood: they are 16-supercharge fluxed D4 or fluxed D6 branes that make perfect sense in string theory, and moreover can be uplifted to smooth solutions in higher dimensions.

The technical details of the construction can be found in appendix B.3. We will consider multicentered configurations with centers on the z-axis, so that the resulting solution is axisymmetric. We use the smallest number of ingredients that allow us to construct a horizonless solution with the same charges as the almost-BPS black hole: one Taub-NUT center and two supertube centers:

- The Taub-NUT center is at the origin of our spherical coordinates in the $\mathbb{R}^3$ base of the solution. It has charge Q_0 in V and a momentum parameter $m^{(0)}$ in μV.
- The first supertube center is of species 2, and is on the z-axis at position $z = a_2$. It carries a magnetic charge parameter $k^{(2)}$ in K^2, two electric charges $Q_1^{(2)}$ and $Q_3^{(2)}$ in the harmonic functions appearing in Z_1 and Z_3, respectively, and a momentum parameter $m^{(2)}$ in the harmonic part of μV.
- The second supertube center is of species 3, and is located at $z = a_3$. It has a magnetic charge parameter $k^{(3)}$ in K^3, two electric charges $Q_1^{(3)}$ and $Q_2^{(3)}$ in the harmonic functions appearing in Z_1 and Z_2, respectively, and a momentum parameter $m^{(3)}$ in the harmonic part of μV.

The regularity of the supertubes requires, from (4.4.3)

$$m^{(2)} \,=\, \frac{Q_1^{(2)} Q_3^{(2)}}{2k^{(2)}}\,, \qquad m^{(3)} \,=\, \frac{Q_1^{(3)} Q_2^{(3)}}{2k^{(3)}}\,. \tag{4.4.4}$$

For simplicity we consider $a_3 > a_2 > 0$. We introduce the local spherical coordinates around the I^{th} center, (ρ_I, θ_I, ϕ),

$$\rho_I \,\equiv\, \sqrt{\rho^2 + a_I^2 - 2\rho a_I \cos\theta}, \qquad \cos\theta_I \equiv \frac{\rho\cos\theta - a_I}{\rho_I}.$$

The interested reader can find details on the resolutions of the equations of motion in appendix B.3, and the gauge fields and scalars of the three-center solutions in appendix B.3.1. The metric is still given by (4.2.1):

$$ds_4^2 = -\mathcal{I}_4{}^{-\frac{1}{2}}\,(dt+\varpi)^2 \,+\, \mathcal{I}_4{}^{\frac{1}{2}}\,\left[d\rho^2 \,+\, \rho^2\left(d\theta^2 + \sin^2\theta\, d\phi^2\right)\right]\,, \qquad \mathcal{I}_4 \,\equiv\, Z_1 Z_2 Z_3 V - \mu^2 V^2\,, \tag{4.4.5}$$

where now the functions (V, Z_I, μ) and the rotation one-form ϖ are given by:

$$V \,=\, h \,+\, \frac{Q_0}{\rho}\,, \qquad Z_1 \,=\, \frac{1}{h} \,+\, \frac{Q_1^{(2)}}{\rho_2} \,+\, \frac{Q_1^{(3)}}{\rho_3} \,+\, \left(h + \frac{Q_0\,\rho}{a_2\,a_3}\right)\frac{k^{(2)}\,k^{(3)}}{\rho_2\,\rho_3}\,,$$

$$
\begin{aligned}
Z_2 = \frac{1}{h} + \frac{Q_2^{(3)}}{\rho_3}\,, \quad Z_3 &= \frac{1}{h} + \frac{Q_3^{(2)}}{\rho_2}\,,\\
\mu\, V &= m_\infty + \frac{m^{(0)}}{\rho} + \frac{m^{(2)}}{\rho_2} + \frac{m^{(3)}}{\rho_3} + \left(\frac{k^{(2)}}{2h\rho_2} + \frac{k^{(3)}}{2h\rho_3}\right) V + \frac{h}{2\,\rho_2\rho_3}\left(k^{(2)}Q_2^{(3)} + k^{(3)}Q_3^{(2)}\right)\\
&\quad - \frac{Q_0\,\cos\theta}{(a_3-a_2)\,\rho_2\rho_3}\left(k^{(2)}Q_2^{(3)} - k^{(3)}Q_3^{(2)}\right) + \frac{Q_0\,(\rho^2+a_2a_3)}{2(a_3-a_2)\,\rho\rho_2\rho_3}\left(\frac{k^{(2)}}{a_2}Q_2^{(3)} - \frac{k^{(3)}}{a_3}Q_3^{(2)}\right)\,,\\
\varpi &= -\sum_{I=2,3}\frac{k^{(I)}}{2}\left[\cos\theta_I + Q_0\frac{\rho - a_I\cos\theta}{h\,a_I\rho_I}\right]d\phi + \varpi_0\,d\phi + \left(m^{(0)}\cos\theta + m^{(2)}\cos\theta_2 + m^{(3)}\cos\theta_3\right)d\phi\\
&\quad + \sum_{J\neq I}\frac{Q_I^{(J)}k^{(I)}}{2(a_J-a_I)\rho_I\rho_J}\Big[h(\rho^2 + a_Ia_J - (a_I+a_J)\rho\cos\theta)\\
&\qquad\qquad - Q_0\frac{\rho(a_J + a_I\cos 2\theta) - (\rho^2 + a_Ia_J)\cos\theta}{a_I}\Big]d\phi\,.
\end{aligned}
\tag{4.4.6}
$$

There are regularity conditions (see (B.3.19)) that the geometry must satisfy, as well as the condition to be asymptotic to flat four-dimensional spacetime; together, these give 5 algebraic conditions. Three directly fix ϖ_0, m_∞ and $m^{(0)}$; the other are called *bubble equations* and are non-linear relations that constrain the distances between the centers:

$$
\begin{aligned}
m_\infty^2 &= \pm\frac{1-h^2}{h^2}\,,\\
\varpi_0 &= \frac{k^{(2)}}{2}\left(\frac{h\,Q_2^{(3)}}{a_3-a_2} - \frac{Q_0}{ha_2}\right) - \frac{k^{(3)}}{2}\left(\frac{h\,Q_3^{(2)}}{a_3-a_2} + \frac{Q_0}{ha_3}\right)\,,\\
\frac{m^{(0)}}{Q^{(0)}} &= -\frac{k^{(2)}}{2ha_2}\left(\frac{h\,Q_2^{(3)}}{a_3-a_2} + 1\right) + \frac{k^{(3)}}{2ha_3}\left(\frac{h\,Q_3^{(2)}}{a_3-a_2} - 1\right)\,,\\
m^{(2)} = \frac{Q_1^{(2)}Q_3^{(2)}}{2k^{(2)}} &= -\frac{1}{2(a_3-a_2)}\left(k^{(3)}Q_3^{(2)}\left(h + \frac{Q_0}{a_3}\right) - k^{(2)}Q_2^{(3)}\left(h + \frac{Q_0}{a_2}\right)\right) + \frac{k^{(2)}}{2h}\left(h + \frac{Q_0}{a_2}\right)\,,\\
m^{(3)} = \frac{Q_1^{(3)}Q_2^{(3)}}{2k^{(3)}} &= \frac{1}{2(a_3-a_2)}\left(k^{(3)}Q_3^{(2)}\left(h + \frac{Q_0}{a_3}\right) - k^{(2)}Q_2^{(3)}\left(h + \frac{Q_0}{a_2}\right)\right) + \frac{k^{(3)}}{2h}\left(h + \frac{Q_0}{a_3}\right)\,.
\end{aligned}
\tag{4.4.7}
$$

We can also calculate the integer magnetic charges of the supertube centers, by integrating the corresponding gauge field around the centers [67, 117]. These magnetic charges, $\kappa^{(I)}$, are:

$$
\kappa^{(I)} \equiv \left(h + \frac{Q_0}{a_I}\right)k^{(I)}\,. \tag{4.4.8}
$$

The solutions are guaranteed to be physical when the warp factors, Z_I, and the quartic invariant, $\mathcal{I}_4$, satisfy everywhere the inequalities [40, 79]:

$$
Z_I\,V \geq 0\,, \qquad \mathcal{I}_4 \equiv Z_1Z_2Z_3\,V - \mu^2V^2 \geq |\varpi|^2\,. \tag{4.4.9}
$$

By expanding this expression near each pole one can obtain inequalities constraining the supertube charges. The easiest way to satisfy these is to take all electric charges, $Q_I^{(J)}$, to be positive, and have one magnetic charge to be negative.[14]

4.4.2 Properties

The almost-BPS multicenter solutions constructed above have a rather complicated and unintuitive form. It is therefore important to point out their key physical properties:

First of all, note that the system is only constrained by the two bubble equations (4.4.7), so that the phase space of solutions is very large. An important subclass of solutions, called *scaling solutions*, are the ones in which the intercenter distances can be made arbitrarily small; we will mainly be interested in such scaling solutions.

When we approach this *scaling limit* and bring the centers close to each other, we can call λ the overall size of the cluster of centers in the $\mathbb{R}^3$ base space, so that each center position satisfies $a_I = \mathcal{O}(\lambda)$. Far away from the centers, $\rho \gg \lambda$, the main functions (4.4.6) determining the metric match the functions that enter in the almost-BPS black hole solution with the same charges, up to $\mathcal{O}(\lambda)$ corrections. In other words, the solutions are virtually indistinguishable from the black hole at these scales. In the IR, when $\rho = \mathcal{O}(\lambda)$, the structure of the multicenter configuration starts to be visible and distinguishable from the black hole horizon. We will quantify these statements further by comparing the conserved quantities and the multipole moments of the solutions to the black hole results.

Conserved quantities

We compute the ADM mass, the angular momentum and the four electric and magnetic charges of the solution. We can again obtain the mass and angular momentum via (4.2.3):

$$\begin{aligned} M &= \frac{1}{4h^3}\left[Q_0 + h^2\left(Q_1^{(2)} + Q_1^{(3)} + Q_2^{(3)} + Q_3^{(2)} + Q_0\,\frac{k^{(2)}k^{(3)}}{a_2 a_3} \mp 2\sqrt{1-h^2}\,\left(k^{(2)}+k^{(3)}\right)\right)\right], \\ J &= \frac{Q_0}{4h}\left(\frac{2\,h\,k^{(3)}\,Q_3^{(2)}}{a_3} + k^{(2)} + k^{(3)}\right) + \frac{h}{4}\left(k^{(3)}Q_3^{(2)} - k^{(2)}Q_2^{(3)}\right), \end{aligned} \tag{4.4.10}$$

where the "$\mp$" depends on which choice of branch have been chosen for m_∞ in (4.4.7). Note that these expressions are obtained "on shell", after enforcing the bubble equations (4.4.7). The four magnetic and electric charges are given by (see (B.1.25)):

$$\begin{aligned} (p^0, p^1, p^2, p^3) &= \left(Q_0\,,\,0\,,\,-h\,k^{(2)}\,,\,-h\,k^{(3)}\right) \\ (q_0, q_1, q_2, q_3) &= \left(\frac{k^{(2)}+k^{(3)}}{h}\,,\,Q_1^{(2)} + Q_1^{(3)} + Q_0\frac{k^{(2)}k^{(3)}}{a_2 a_3}\,,\,Q_2^{(3)}\,,\,Q_3^{(2)}\right) \end{aligned} \tag{4.4.11}$$

Note that there are more charges turned on compared to the almost-BPS black hole solution of (4.3.6). This is because of the presence of the magnetic dipole charges, $k^{(2)}$ and $k^{(3)}$, which are

[14] By reshuffling the bubble equations above, one can see that at least one charge needs to be negative.

crucial elements that allow the spacetime to be smooth around the centers in higher dimensions. However, although they must be non-vanishing, we can freely take them small compared to the main charges: $k_i \ll Q_0, Q_k^{(j)}$. In this limit, the D0 charge can be ignored as well, and we have

$$\begin{aligned}
&(p^0, p^1, p^2, p^3; q_0, q_1, q_2, q_3) \sim (Q_0, 0, 0, 0; 0, Q_1^{(2)} + Q_1^{(3)} + Q_0 \frac{k^{(2)} k^{(3)}}{a_2 a_3}, Q_2^{(3)}, Q_3^{(2)}) \,, \\
&M \sim \frac{1}{4h^3} \left[Q_0 + h^2 \left(Q_1^{(2)} + Q_1^{(3)} + Q_2^{(3)} + Q_3^{(2)} + Q_0 \frac{k^{(2)} k^{(3)}}{a_2 a_3} \right) \right] \,, \\
&J \sim \frac{h}{4} \left(k^{(3)} Q_3^{(2)} - k^{(2)} Q_2^{(3)} \right) + Q_0 \frac{k^{(3)}\, Q_3^{(2)}}{2 a_3} \,,
\end{aligned} \tag{4.4.12}$$

so that the microstate geometry has the same conserved charges as the black hole.

Multipole moments

In appendix B.4, we derive the multipole moments of generic multicenter solutions in Taub-NUT. In this section, we apply these formulas to our specific three-center solutions.

Note that the coordinates used in the almost-BPS ansatz (4.2.1) are automatically AC coordinates as defined in section 4.2.2. Therefore, one can read off the coefficients $\tilde{M}_\ell, \tilde{S}_\ell$ from simply expanding the metric in powers of $1/\rho$, and obtain the true multipoles using (4.2.7):

$$M_\ell = \sum_{k=0}^{\ell} \binom{\ell}{k} \tilde{M}_k \left(-\frac{\tilde{M}_1}{\tilde{M}_0} \right)^{\ell-k} , \qquad S_\ell = \sum_{k=1}^{\ell} \binom{\ell}{k} \tilde{S}_k \left(-\frac{\tilde{M}_1}{\tilde{M}_0} \right)^{\ell-k} . \tag{4.4.13}$$

For our specific three-center solution, the relevant AC-coordinate frame coefficients, $\tilde{M}_\ell$, are then given by (B.4.23):

$$\begin{aligned}
4\tilde{M}_\ell \,=\, & \left(\frac{Q_0}{h^3} - 2 m_\infty m^{(0)} \right) {a_0}^\ell + \sum_{\substack{I=2 \\ J,K=1}}^{3} \frac{|\varepsilon_{IJK}|}{2h} \left(Q_J^{(I)} + Q_K^{(I)} - h\, m_\infty \left(k^{(I)} + \frac{Q_J^{(I)} Q_K^{(I)}}{k^{(I)}} \right) \right) {a_I}^\ell \\
& + \sum_{I,J=2}^{3} \frac{Q_0\, |\epsilon_{IJ}|}{h} \left[\frac{k^{(I)} k^{(J)}}{2 a_I a_J} q_\ell^{(2)}(a_I, a_J) - h m_\infty \frac{k^{(J)} Q_J^{(I)}}{a_I - a_J} \left(\frac{q_\ell^{(2)}(a_I, a_J)}{a_J} - \frac{2\ell}{2\ell - 1} q_{\ell-1}^{(2)}(a_I, a_J) \right) \right]
\end{aligned} \tag{4.4.14}$$

where ϵ_{IJ} and ϵ_{IJK} are the Levi-Civita tensors of dimension two and three respectively and we have defined $a_0 = 0$ as the coordinate of the Taub-NUT center, with also ${a_0}^\ell \equiv \delta_{\ell 0}$. We define the polynomial

$$q_\ell^{(2)}(a_I, a_J) \equiv \binom{2\ell}{\ell}^{-1} \sum_{p+q=\ell} \binom{2p}{p} \binom{2q}{q} {a_I}^p {a_J}^q \,. \tag{4.4.15}$$

The coefficients $\tilde{S}_\ell$, are given by (B.4.33)

$$\begin{aligned} 4\tilde{S}_\ell \,=\, &-2m^{(0)}\,{a_0}^\ell + \sum_{\substack{I=2\\J,K=1}}^{3} \frac{|\varepsilon_{IJK}|}{2}\left(k^{(I)} - \frac{Q_J^{(I)}Q_K^{(I)}}{k^{(I)}}\right){a_I}^\ell \\ &- \sum_{I,J=2}^{3} Q_0\,|\epsilon_{IJ}|\frac{k^{(J)}Q_J^{(I)}}{a_I - a_J}\left(\frac{q_\ell^{(2)}(a_I,a_J)}{a_J} - \frac{2\ell}{2\ell-1}q_{\ell-1}^{(2)}(a_I,a_J)\right). \end{aligned} \tag{4.4.16}$$

It is of particular interest to consider the scaling limit of (4.4.14)-(4.4.16), or more generally of (B.4.23)-(B.4.33), when $a_I = \mathcal{O}(\lambda)$ and $\lambda \to 0$. Using the regularity conditions (4.4.7) (or (B.3.19)), one can see that the AC coefficients behave as (for $h \neq 1$):

$$\begin{aligned} &\tilde{M}_0 = M^{\rm BH}\,(1+\mu_0\lambda) + \mathcal{O}(\lambda^2), \\ &\tilde{M}_1 = \tilde{M}_1^{\rm BH}\,(1+\mu_1\lambda) + \mathcal{O}(\lambda^2), \qquad\qquad \tilde{S}_1 = J^{\rm BH}\,(1+\sigma_1\lambda) + \mathcal{O}(\lambda^2), \\ &\tilde{M}_\ell = \tilde{M}_1^{\rm BH}\,\frac{(\tilde{M}_1^{\rm BH})^{\ell-1}}{(M^{\rm BH})^{\ell-1}}\,\mu_\ell\,\lambda^{\ell-1} + \mathcal{O}(\lambda^\ell), \quad \tilde{S}_\ell = J^{\rm BH}\frac{(\tilde{M}_1^{\rm BH})^{\ell-1}}{(M^{\rm BH})^{\ell-1}}\sigma_\ell\lambda^{\ell-1} + \mathcal{O}(\lambda^\ell), \end{aligned} \tag{4.4.17}$$

where $M^{\rm BH}, \tilde{M}_1^{\rm BH}, S_1^{\rm BH} = J^{\rm BH}$ are the non-vanishing AC coefficients for the almost-BPS black hole with the same charges in (4.3.8) and (4.3.9), and μ_ℓ, σ_ℓ are microstate-dependent dimensionless numbers. The ACMC multipole moments then behave as:

$$M_0 = M^{\rm BH}\,(1+\mu_0\lambda) + \mathcal{O}(\lambda^2), \tag{4.4.18}$$

$$S_1 = J^{\rm BH}\,(1+\sigma_1\lambda) + \mathcal{O}(\lambda^2), \tag{4.4.19}$$

$$M_\ell = M_\ell^{\rm BH}\left(1 + \left[(1-\ell)\mu_0 + \ell\left(\mu_1 - \frac{1}{2}\mu_2\right)\right]\lambda\right) + \mathcal{O}(\lambda^2), \tag{4.4.20}$$

$$S_\ell = S_\ell^{\rm BH}\left(1 + \left[(1-\ell)\mu_0 + \sigma_1 + (\ell-1)\left(\mu_1 - \frac{1}{2}\sigma_2\right)\right]\lambda\right) + \mathcal{O}(\lambda^2), \tag{4.4.21}$$

where the black hole ACMC multipoles $M_\ell^{\rm BH}$, $S_\ell^{\rm BH}$ were given in (4.3.10). Note that (4.4.17)-(4.4.21) are only valid for $h \neq 1$; when instead $h = 1$ and thus $m_\infty = 0$, it is easy to show that $\tilde{M}_\ell \sim \mathcal{O}(\lambda^\ell)$ and $\tilde{S}_\ell \sim \mathcal{O}(\lambda^{\ell-1})$ so that also $M_\ell \sim \mathcal{O}(\lambda^\ell)$ (for $\ell \neq 1$) and $S_\ell \sim \mathcal{O}(\lambda^{\ell-1})$ (for $\ell \geq 1$) — interestingly, this is similar but not exactly the same as the scaling with λ that one has for multipoles of scaling supersymmetric microstate geometries [118, 120], which is $(M_\ell^{\rm SUSY}, S_\ell^{\rm SUSY}) \sim \mathcal{O}(\lambda^\ell)$.

We can summarize the behavior of the multipole moments of scaling almost-BPS microstate geometries in an (intuitive) conjecture:

All multipoles of scaling microstate geometries match the values of the black hole they correspond to, up to small deviations proportional to the scale for which the microstructure starts to be manifest and resolve the horizon into smooth topologies.

Clearly, smooth horizonless solutions can mimic classical black hole characteristics with a very high accuracy. As λ gets vanishingly small, this implies that the microstructure of the microstate geometry can become virtually indetectable, at least as far as the multipole moments are concerned.

Moreover, nothing dictates a priori the value of μ_ℓ and σ_ℓ as they depend on the internal degrees of freedom of the family of solutions. As we illustrate later, they can either be positive or negative. In particular, as we show explicitly in section 4.4.4, this leads to counterexamples to conjectures based on the analysis of [121], where it was suggested that multipole moments of smooth horizonless geometries will be larger than those of the corresponding black hole.

4.4.3 Explicit examples

We give several examples of three-center almost-BPS microstate geometries, whose general form is given in (4.4.6). We also give the parameters of the almost-BPS black hole with the same charges.

Finding explicit parameters that give rise to physical three-center solutions in the family constructed above is relatively easy. Our family initially contains 16 parameters. After imposing the supertube regularity (4.4.4) and the regularity conditions (4.4.7), we end up with 9 free parameters. The physicality condition (4.4.9) gives a bound on the parameters; it is sufficient to assume that all charges are positive except one magnetic dipole charge, that we will assume to be $\kappa^{(2)}$. Moreover, we aim to construct scaling solutions for which the centers can be tuned to come arbitrarily close to each other.

A simple example

The first solution we consider is given by the following charges:[15]

$$-4\,\kappa^{(2)} \,=\, 4\,\kappa^{(3)} \,=\, 2\,Q_0 \,=\, \frac{4}{3}\,Q_1^{(2)} \,=\, Q_1^{(3)} \,=\, \frac{4}{3}\,Q_3^{(2)} \,=\, 20000\,, \qquad Q_2^{(3)} \,=\, 15001\,, \qquad h \,=\, 0.01\,, \tag{4.4.22}$$

The bubble equations (4.4.7) fix the distance between the centers

$$a_2 \simeq 0.21\,, \qquad a_3 \simeq 0.28\,, \tag{4.4.23}$$

which gives, from (4.4.8)

$$k^{(2)} \simeq -0.11\,, \qquad k^{(3)} \simeq 0.14\,, \tag{4.4.24}$$

The mass and angular momentum of the solution (4.4.10) are

$$M \,\simeq\, 2.5\times 10^9\,, \qquad J \,=\, -3.7\times 10^7\,, \tag{4.4.25}$$

and the eight charges (4.4.11) are

$$\begin{aligned}(p^0,p^1,p^2,p^3) \,&\simeq (10000\,,\,0\,,\,0.0011\,,\,-0.0014)\\ (q_0,q_1,q_2,q_3) \,&\simeq (3.5\,,\,32500\,,\,15001\,,\,15000)\end{aligned} \tag{4.4.26}$$

The scaling point can be obtained by shifting $Q_3^{(2)} \to 15000$ which gives $a_2, a_3 \to 0$.

The solutions match very closely the non-BPS extremal black hole detailed in section 4.3.1 with a mass and an angular momentum given by (4.4.25), and one magnetic charge $Q_0 = p^0$ and three electric charges $Q_I = q_I$. As detailed in section 4.3.3, the ratio between the mass and charges is of order $h^{-3} = 10^6$.

[15] Recall that the effective dipole charges κ_I are given by (4.4.8).

A one-parameter family

We can easily expand the above example to a one-parameter family of microstate geometries, where we allow h to vary while we keep the other charges in (4.4.22) fixed. For example, when $h \ll 1$, the intercenter distances are then approximately:

$$a_2 \simeq 21\, h\,, \qquad a_3 \simeq 28\, h\,, \tag{4.4.27}$$

The mass, angular momentum and eight charges of the solutions are, at leading order in h:

$$\begin{aligned} M \;&\simeq\; \frac{2500}{h^3}\,, \qquad J \;\simeq\; -3.7\times 10^7\,, \\ (p^0,p^1,p^2,p^3) \;&\simeq\; (10000\,,\,0\,,\,0\,,\,0) \\ (q_0,q_1,q_2,q_3) \;&\simeq\; (3.5\,,\,32500\,,\,15001\,,\,15000) \end{aligned} \tag{4.4.28}$$

Interestingly, h does not change the topology of the IR geometry since it acts as a scaling factor. As expected and discussed above, by fine-tuning h to be small, one can construct solutions that look almost neutral from a four-dimensional perspective.

4.4.4 Aspects of microstate multipoles

In this section, we discuss some aspects of the gravitational multipoles for the almost-BPS solutions. For the black holes, the multipole formulas were derived in section 4.3.3, whereas the microstate geometry multipoles can be found in section 4.4.2. We will focus in this section on discussing multipoles (and certain ratios) as studied in [119, 121] for families of supersymmetric black holes. In appendix B.4.4, we also show that the multipole *ratio* analysis of [118, 120] for supersymmetric black holes and their multicentered microstate geometries can also be extended straightforwardly to the multipole ratios of almost-BPS black holes and their microstate geometries described here. It would be interesting to expand this analysis (in the spirit of [120] for supersymmetric black holes); we leave this for future work.

It will be convenient to define the following dimensionless, positive quantities:[16]

$$\mathcal{M}_\ell := \left|\frac{M_\ell M_0^{\ell-1}}{S_1^\ell}\right|, \qquad\qquad \mathcal{S}_\ell := \left|\frac{S_\ell M_0^{\ell-1}}{S_1^\ell}\right|, \tag{4.4.29}$$

In [119, 121] these multipole ratios were computed for supersymmetric multi-center microstates, and compared to those of the non-supersymmetric Kerr(-Newman) black holes of the same mass and angular momentum. Note that for any Kerr(-Newman) black hole, $\mathcal{M}_{2n} = \mathcal{S}_{2n+1} = 1$ and $\mathcal{M}_{2n+1} = \mathcal{S}_{2n} = 0$. The analysis of the families of supersymmetric microstate geometries in [119, 121], had certain striking universalities, which suggests the following conjectures regarding the universal behavior of multipoles of microstate geometries:

- **C.i**: Generically $\mathcal{M}_2 > 1$. In other words, the (absolute value of) the quadrupole moment M_2 of microstate geometries is generically *larger* than that of Kerr with the same mass and angular momentum. Similar statements are valid for higher-order multipole moments that are non-zero for Kerr-Newman (in particular, $\mathcal{S}_3 > 1$ is mentioned explicitly) [119, 121].

[16] These were denoted by $\mathfrak{M}_\ell$ and $\mathfrak{S}_\ell$ in [121].

- **C.ii**: Both $\mathcal{M}_\ell$ and $\mathcal{S}_\ell$ (for any ℓ) are *always* monotonically increasing functions of the intercenter distance λ for scaling solutions [121]. In particular, a corollary is that $(\partial_\lambda \mathcal{M}_\ell(\lambda))_{\lambda=0} > 0$ and similar for $\mathcal{S}_\ell$.

While these conjectures are based on extrapolations of suggestive features of supersymmetric microstate geometries, here we will show that they are contradicted explicitly by the physics of the more realistic non-supersymmetric microstate geometries we built.

To illustrate this, we take a family of microstate geometries (as constructed in section 4.4.1) with charge parameters:[17]

$$\begin{aligned} m_\infty &= (-1)^n \frac{\sqrt{1-h^2}}{h}, & \kappa^{(2)} &= -7000, & \kappa^{(3)} &= 5000, \\ Q_0 &= 7000, & Q_1^{(2)} &= 6000x, & Q_3^{(2)} &= 6000, \\ a_0 &= 0, & a_2 &= \lambda, & a_3 &= 2\lambda. \end{aligned} \tag{4.4.30}$$

The parameters $Q_1^{(3)}, Q_2^{(3)}$ are then determined by the bubble equations (4.4.7). Thus, this family of solutions depends on the choice of branch for m_∞ through n (where $n = 1, 2$) and has three free parameters, given by h, x, and the distance λ between centers. The mass, angular momentum, and electromagnetic charges of this family is given by:

$$\begin{aligned} M &\simeq \frac{250}{7h^3}\left(49 + h^2 \frac{115 + 36x(13x-3)}{6x-5}\right) + \mathcal{O}(\lambda)\,, \quad J \simeq -15\times 10^6 + \mathcal{O}(\lambda) \\ (p^0, p^1, p^2, p^3) &\simeq (7000\,,\, 0\,,\, 0\,,\, 0) + \mathcal{O}(\lambda) \\ (q_0, q_1, q_2, q_3) &\simeq \left(0\,,\, \frac{1000\,(36x^2+25)}{6x-5}\,,\, \frac{36000x}{7} - \frac{30000}{7}\,,\, 6000\right) + \mathcal{O}(\lambda) \end{aligned} \tag{4.4.31}$$

When the centers merge at $\lambda = 0$, the solution corresponds to the almost-BPS black hole with the conserved charges above. We will show that by varying the parameters h and x in this family of microstates, one can easily invalidate both conjecture C.i and C.ii.

For the almost-BPS black hole, $\mathcal{M}_\ell/\mathcal{M}_\ell^{\rm Kerr}$ was calculated in (4.3.14). We can already see from this expression that the value of, say, $\mathcal{M}_\ell$ for the almost-BPS black hole can be made smaller or larger than the corresponding Kerr(-Newman) value (for a black hole of equal mass and angular momentum), by adjusting the value of h. For the microstates (whose $\lambda \to 0$ limit corresponds to an almost-BPS black hole), this is then obviously also true; see Fig. 4.2. This shows that conjecture C.i is not generically true for almost-BPS microstates and more generically for non-supersymmetric microstate geometries.

In Fig. 4.3, we plotted $\mathcal{M}_2$ and $\mathcal{S}_3$ (normalized by the $\lambda = 0$ black hole value) for $h = 433/500$, $n = 1$, and various values of x; we can clearly see that $\mathcal{M}_2$ and $\mathcal{S}_3$ are *not* always a monotonically increasing function of λ; in particular, these are counterexamples to conjecture C.ii.

Note that the plots in figures 4.2 and 4.3 show the behaviour of the multipole ratios for a range of center separation λ near the scaling point $\lambda = 0$; these plots can be extended for larger

[17] We wish to thank J. F. Morales for pointing out the unphysicality of the microstate geometry family we had in an earlier version of this paper.

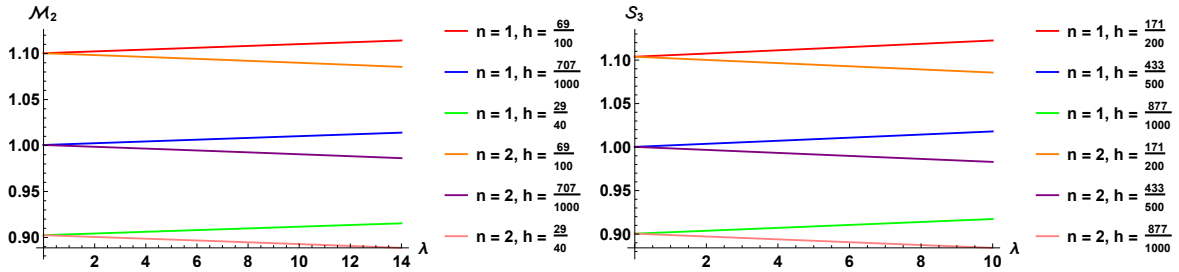

(a) $\dfrac{\mathcal{M}_2}{\mathcal{M}_2^{\text{Kerr}}}$ (b) $\dfrac{\mathcal{S}_3}{\mathcal{S}_3^{\text{Kerr}}}$

Figure 4.2 – Plots of $\mathcal{M}_2/\mathcal{M}_2^{\text{Kerr}}$ and $\mathcal{S}_3/\mathcal{S}_3^{\text{Kerr}}$ (where the corresponding Kerr(-Newman) black hole is chosen to have the same mass and angular momentum as the microstate) as a function of λ for $x = 1$ and the different values of h and n indicated by the legend.

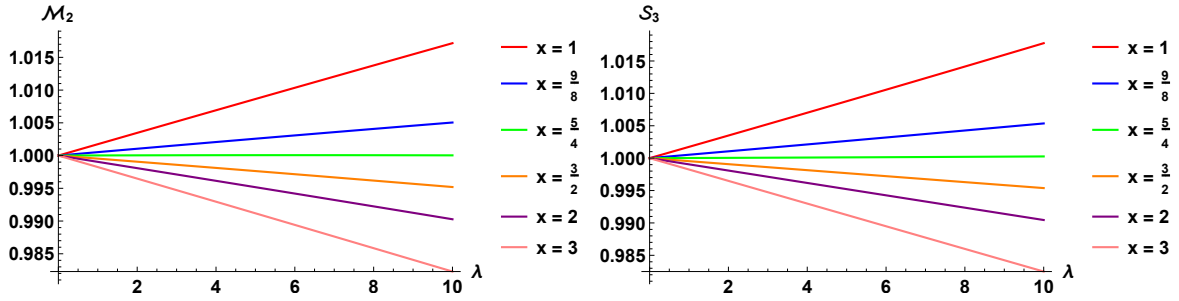

(a) $\dfrac{\mathcal{M}_2(\lambda)}{\mathcal{M}_2(\lambda=0)}$ (b) $\dfrac{\mathcal{S}_3(\lambda)}{\mathcal{S}_3(\lambda=0)}$

Figure 4.3 – Plots of $\mathcal{M}_2$ and $\mathcal{S}_3$ (normalized with respect to their $\lambda = 0$ black hole values) as a function of λ for $h = 433/500$, $n = 1$, and x taking on various values indicated by the legend.

values of λ, although this generally does not show any additional interesting physical phenomena. The maximum possible value of λ depends also on the details of the microstate. We illustrate the two main possibilities in figure 4.4 and 4.5. In figure 4.4, we show a choice of parameters for which there is a maximum possible λ value at which the mass diverges; a consequence is that considering a microstate with such a λ which is close to this point will no longer have a mass comparable to that of the corresponding $\lambda = 0$ black hole. In figure 4.5, we show a choice of parameters where there is no maximum for λ: the intercenter distance can be chosen arbitrarily large without introducing any pathologies; the mass and multipoles all have relatively simple behaviour as λ gets larger.[18]

One of the main hopes coming from the conjectures of [119] was that microstate geometries might be observationally distinguishable from astrophysical (Kerr) black holes by their multipole

[18]Note that there can be spurious values of λ at which certain multipoles happen to vanish. (For example, in fig. 4.5, we have $M_2 = 0$ at $\lambda \approx 421.68$.) These values of "accidental symmetry" are an artifact of the microstate geometry having a low number of centers; see also appendix C of [120].

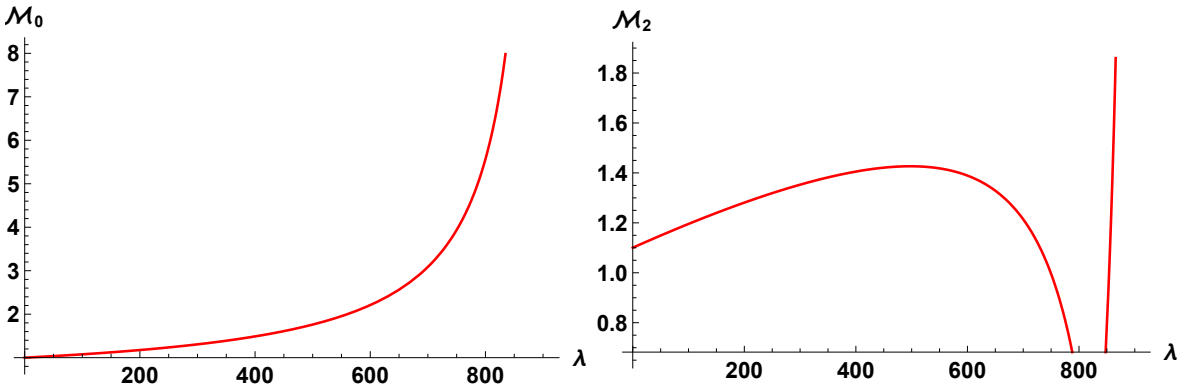

(a) $\dfrac{M(\lambda)}{M(\lambda=0)}$ (b) $\dfrac{\mathcal{M}_2}{\mathcal{M}_2^{\rm Kerr}}$

Figure 4.4 – For $n=1, h=69/100, x=1$, we plot the normalized mass $M(\lambda)/M(\lambda=0)$ and $\mathcal{M}_2/\mathcal{M}_2^{\rm Kerr}$ for the complete allowed range of λ. Note that when λ gets near the maximal allowed value, it no longer makes any sense to compare the microstate geometry to the $\lambda=0$ limit as the mass is drastically different.

moments; in particular, (most of) the microstate geometries considered in [119] had quadrupole moments larger than those of the corresponding Kerr black hole with equal mass and angular momentum, which in turn led to conjecture C.i. The analysis in [119, 121] and the conjectures C.i and C.ii seemed to imply that the black hole solution is somehow an *extremum* on the space of solutions. However, we show here that there exist microstate geometries for which this is not true.

In particular, we show that the multipole moments of the almost-BPS black hole and its microstate geometries can be larger or smaller than those of Kerr for equal mass and angular momentum. Nevertheless, we want to emphasize that the multipole moments are generically *different* from those of the Kerr black hole, so that they remain a good distinguishing criteria and can be observationally relevant.

4.5 Conclusions

In this paper, we have argued for using the almost-BPS class of black holes and microstate geometries as phenomenological models of black holes. These solutions have two advantages over the more commonly-used supersymmetric microstate geometries: First, our solutions are not supersymmetric and in particular can have a large mass over charge ratio. Second, and most importantly, the almost-BPS solutions can have arbitrarily large rotation, in stark contrast to the supersymmetric geometries which have small and limited angular momentum (which moreover must vanish in the scaling limit).

There has already been a considerable body of work studying supersymmetric microstate geometries as phenomenological models [122]. While these geometries already give rise to interesting observable phenomena, it is important to start considering string theory geometries that

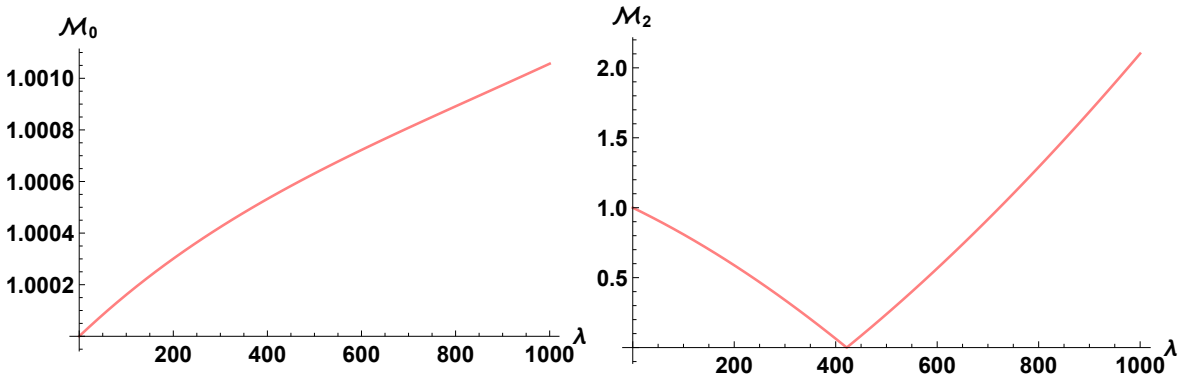

(a) $\dfrac{M(\lambda)}{M(\lambda=0)}$ (b) $\dfrac{\mathcal{M}_2(\lambda)}{\mathcal{M}_2(\lambda=0)}$

Figure 4.5 – For $n=1, h=433/500, x=3$, we plot the normalized mass $M(\lambda)/M(\lambda=0)$ and $\mathcal{M}_2(\lambda)/\mathcal{M}_2(\lambda=0)$. There is no maximum value for λ in this case. (Note that there is an "accidental symmetry" at $\lambda \approx 421.68$ at which the quadrupole M_2 happens to vanish for this microstate geometry.)

are more realistic and can be made to resemble actual astrophysical black holes more closely. The almost-BPS class of black holes and their microstates thus present a prime target for phenomenological study.

We initiated the phenomenological study of almost-BPS geometries here by describing their multipoles (and multipole ratios) in some detail. As we have mentioned in section 4.3.3, the particular family of almost-BPS black holes we have considered can be tuned (by choosing the parameter h) such that the quadrupole moment matches that of a Kerr black hole (with equal mass and angular momentum); the deviations of the almost-BPS black hole from Kerr then only show up at higher multipole moments — such deviations at higher multipole orders will be harder (but not impossible) to detect at future experiments.

In addition, the almost-BPS black holes break equatorial symmetry $\theta \leftrightarrow \pi - \theta$ by having non-zero parity-odd multipoles (M_{2n+1} and S_{2n}). Equatorial symmetry breaking of black holes has been largely unexplored phenomenologically; it would be interesting to understand if this can lead to clear observational signatures [149].

Recent studies of supersymmetric microstate geometries include the analysis of their shadows and images [150] (relevant for EHT observations), and scalar field echoes on these geometries [151] (relevant for the ringdown phase in mergers). These studies showed the intricate and subtle behavior that allows the supersymmetric microstate geometries to behave very similarly to a black hole, but nevertheless allowing for certain observable signatures when far from the scaling point. Expanding these studies to include almost-BPS black holes and their microstates would show how moving away from supersymmetry and adding rotation will alter these mechanisms, and is an important next step to understand possible observable signatures of string theoretic black hole models.

Chapter 5

Toroidal Tidal Effects in Microstate Geometries

5.1 Introduction

The AdS/CFT duality [152] is one of the major tools to study the black hole information paradox [5]. The correspondence supports unitary black hole evolution and provides a dual description of black hole microstates within a non-gravitational theory. For example, a known family of three-charge horizonless geometries with a cap at the bottom of a long throat is dual to CFT states which, at the orbifold point, are constructed by acting with momentum-generating operators on Ramond-Ramond ground states obtained from length-one component strings [51, 52]. Although such CFT states account only for a parametrically small fraction of the entropy [55,56] of extremal black holes [28], they may offer insights about generic microstates of the corresponding black holes within the bulk theory [59, 7–9]. Furthermore, away from the free orbifold point, the lowest possible mass gap in the strongly-coupled CFT matches that of energy excitations in such geometries [68].[1]

A well studied example is the extremal D1-D5-P black hole, with a known match between the Bekenstein-Hawking entropy and the number of appropriate microscopic brane configurations [28]. In the D1-D5 system, a large class of capped geometries that have a well-understood CFT description are superstrata [50–52, 153–155, 53, 156, 157], which have the same charges and asymptotic structure as the black hole [42], but instead of having a horizon and an infinitely long throat, they cap off smoothly at the end of a long, but finite, $AdS_2 \times S^1_y$ throat (see figure 5.1). They are part of the microstate geometries programme which constructs smooth horizonless solutions within supergravity that represent black hole microstates.

Non-trivial structure at the bottom of the throat implies physics that deviates from that of a classical black hole, ranging from tidal effects [158–160] to gravitational multipole moments [118–121, 18]. If capped geometries correspond to typical states of black holes, their inherent horizonless nature could lead to phenomena observable by future detectors [122], for example in

[1] However, it is currently unclear how this small mass gap arises by deforming the CFT away from the free orbifold point.

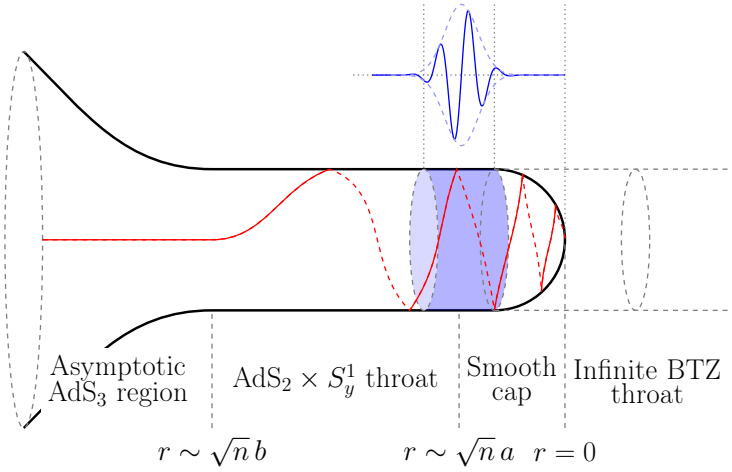

Figure 5.1 – A schematic depiction of the $(1, 0, n)$ superstrata in the $r - y$ directions. The red curve depicts a trajectory of an infalling and spiralling null geodesic along which a string probe is travelling. The details of the microstructure are most prominent at the bottom of the throat (shaded in blue), where the tidal forces are greatest. The curve in blue above the geometry illustrates the alternation between tidal stretching and compressing the string experiences as it approaches the cap region.

gravitational echoes [126], as a massless probe falling into a horizonless geometry reaches the cap but is able to return to infinity [161, 162].

Gravitational echoes are weakened if one considers a stringy probe. Namely, tidal forces are able to excite massive string modes, causing the probe to get trapped in the cap region [163]. In that paper, a massless string was sent along a null geodesic into an asymptotically $\text{AdS}_3 \times S^3 \times T^4$ superstratum geometry. It was found that the string gets tidally excited only along the S^1_y direction of AdS_3 and the S^3, while there are no tidal forces acting along the toroidal directions. This observation is in tension with insights coming from the dual CFT. There, excitations along the sphere can be described by fermionic degrees of freedom and excitations along the torus can be described by bosonic degrees of freedom [164]. Hence, if an infalling string gets tidally excited only along the S^3, the dual excitations are only fermionic in nature. However, the initial probe propagating within the superstrata geometry has a precise CFT dual. Indeed, using deformations of the CFT, one can compute transitions from this state to bosonic and fermionic excitations. These transitions thus appear to be CFT signatures of tidal excitations of probes in the bulk [165, 166]. As a guiding principle, this suggests that a probe moving within the superstrata geometries should experience tidal excitations not only along the S^3, as shown in [163], but also along the T^4 directions, thus motivating the investigation of this paper.

We consider a null geodesic in the so-called $(1, 0, n)$ superstratum [50–52]. We choose the geodesic to be in the $\theta = \pi/2$ hypersurface of S^3. Even though we also choose it to be directed radially in the asymptotic region, due to the momenta and angular momenta of the underlying geometry, the geodesic develops a spiral motion along S^1_y and S^3 as it approaches the smooth cap (see figure 5.1).

The physical setup we have in mind is that of a massless string propagating along the chosen

null geodesic. To account for the interaction between the superstratum and the string probe, one needs to solve the string equations of motion. However, to study the tidal effects felt by a string as it moves along the geodesic, one can use the Penrose limit [167] to capture local quadratic environment around a null geodesic. After taking the limit, the metric can be written in the Brinkmann form and the equations of motion for the k-th string oscillator mode in the light-cone gauge can be written as

$$\partial_\tau^2 w^i + k^2\, w^i + \left(\alpha' E\right)^2 \mathcal{A}_{ij}(\tau)\, w^j + ik\,\alpha' E\, B_{ij}(\tau)\, w^j = 0\,, \tag{5.1.1}$$

where w^i denote directions orthogonal to the geodesic, τ is the world-sheet temporal coordinate and E denotes energy. The matrix $\mathcal{A}_{ij}$ encodes tidal forces acting on the string. In the above equation, it acts as a time dependent mass matrix, most importantly, if it is too negative, the system becomes unstable and massive string modes get excited. In the above B is the NS 2-form gauge potential, which will not be considered here.

Our results support the intuition from the CFT picture – as a string propagates towards the cap, it encounters tidal stresses along all spatial directions, with the tidal forces in the toroidal directions being of the same order as those in the S^1_y and S^3 directions. In addition, we show that the tidal effects display an oscillatory behaviour: a string alternately experiences compression and stretching. We analyse how these oscillations depend on the various parameters of the superstrata. We also discuss the interpretation of tidal forces within the dual CFT. There one can construct a simple state corresponding to a graviton moving within the superstrata geometry. By turning on an interaction of the theory one can then compute transitions of the initial probe into multiple excitations which carry polarizations along transverse directions such as the S^3 and the T^4. These amplitudes exhibit a growth in time which is suggestive of tidal effects from the perspective of the CFT.

In Section 5.2, we review the geometry of $(1, 0, n)$ superstrata and analyse the structure of infalling null geodesics. In Section 5.3, by using the Penrose limit around a null geodesic at $\theta = \pi/2$, we determine and analyse the tidal effects along the chosen trajectory. In Section 5.4, we discuss the implications of these tidal effects in the CFT picture. We finish with a conclusion and outlook on future work in Section 5.5.

5.2 Microstate geometry in the string frame

In this section we describe a family of capped and horizonless geometries, called $(1, 0, n)$ superstrata which have the same charges as the D1-D5-P black hole. Since our aim is to describe how a massless string interacts with the background as it falls towards the cap region, we consider the ten-dimensional metric in the string frame. We analyse a particular set of null geodesics and rewrite the metric in a form that is useful in the study of tidal forces along these geodesics.

5.2.1 Background geometry

Consider the line element of $(1,0,n)$ superstrata in the string frame [50–52]

$$ds_{10}^2 = \Pi \left(\frac{1}{\Lambda}\, ds_6^2 \;+\; \sqrt{\frac{Q_1}{Q_5}}\, ds_{T^4}^2 \right) , \tag{5.2.1}$$

where ds_6^2 is the six dimensional metric in the Einstein frame and $ds_{T^4}^2 = \delta_{ab}\, dz^a\, dz^b$ denotes the metric on the four-torus T^4, which we take to be flat. Typically the size of the latter is taken to be much smaller than the size of the six-dimensional part of spacetime and thus T^4 is often considered as an internal manifold [62]. We focus on the near-horizon limit of the geometry in which ds_6^2 is asymptotically $\mathrm{AdS}_3 \times S^3$

$$ds_6^2 = \; \sqrt{Q_1 Q_5} \left(ds_{\mathrm{AdS}_3}^2 + ds_{S^3}^2 \right) , \tag{5.2.2}$$

with $ds_{\mathrm{AdS}_3}^2$ and $ds_{S^3}^2$ denoting the asymptotically AdS_3 and S^3 parts of the spacetime respectively. For the $(1,0,n)$ superstrata these can be written as

$$ds_{\mathrm{AdS}_3}^2 = \; \Lambda \left[\frac{dr^2}{r^2+a^2} + \frac{2\, r^2 (r^2+a^2)}{R_y^2\, a^4}\, dv^2 - \frac{1}{2\, R_y^2\, A^4 G} \left(du + dv + \frac{2A^2 r^2}{a^2}\, dv \right)^2 \right] , \tag{5.2.3a}$$

$$\begin{aligned} ds_{S^3}^2 = \; & \Lambda\, d\theta^2 + \frac{\sin^2\theta}{\Lambda} \left(d\varphi_1 - \frac{1}{\sqrt{2}\, R_y A^2} \left(du + dv \right) \right)^2 \\ & + \frac{G\, \cos^2\theta}{\Lambda} \left(d\varphi_2 + \frac{1}{\sqrt{2}\, R_y\, a^2 A^2\, G} \left(a^2 (du - dv) - b^2 F\, dv \right) \right)^2 , \end{aligned} \tag{5.2.3b}$$

where we have used

$$u \;=\; \tfrac{1}{\sqrt{2}} (t - y) , \qquad v \;=\; \tfrac{1}{\sqrt{2}} (t + y) , \tag{5.2.4}$$

with t being the usual time coordinate and y denoting the compact direction of AdS_3 with radius R_y and is thus periodically identified as $y \;\sim\; y \;+\; 2\pi R_y$.

The detailed microscopic structure of the six dimensional geometry is encoded in what we call bump functions

$$F \;\equiv\; 1 - \frac{r^{2n}}{(r^2+a^2)^n} , \qquad \Gamma \;\equiv\; \sqrt{1 - \frac{b^2}{(2a^2+b^2)}\, \frac{r^{2n}}{(r^2+a^2)^n}} , \tag{5.2.5a}$$

$$G \;\equiv\; 1 - \frac{a^2\, b^2}{2a^2+b^2}\, \frac{r^{2n}}{(r^2+a^2)^{n+1}} , \qquad \Lambda \;\equiv\; \sqrt{1 - \frac{a^2\, b^2}{(2a^2+b^2)}\, \frac{r^{2n}}{(r^2+a^2)^{n+1}}\, \sin^2\theta} . \tag{5.2.5b}$$

However, the ten-dimensional metric in the string frame (5.2.1) involves an additional bump function appearing as an overall conformal factor

$$\Pi \equiv \sqrt{1 + \frac{a^2\, b^2}{(2a^2+b^2)}\, \frac{r^{2n}}{(r^2+a^2)^{n+1}}\, \sin^2\theta\, \cos\left(\frac{2\sqrt{2} n v}{R_y} + 2\varphi_1 \right)} . \tag{5.2.6}$$

As we will show in the next sections, this function contains all information about tidal excitations in the internal directions.

Finally, the geometry (5.2.1) contains several parameters that characterize its properties. The asymptotic radii of AdS_3 and S^3 are determined by Q_1 and Q_5, which denote the supergravity charges of the D1 and D5 branes in this system (see for example [8]). Furthermore, the angular momenta and the momentum are determined by the real-valued parameters a and b and an integer n as [52]

$$J_L \;=\; J_R \;=\; \frac{R_y}{2}\,a^2\,, \qquad Q_P \;=\; \tfrac{1}{2}\,n\,b^2\,. \tag{5.2.7}$$

However, not all parameters are independent as one has to impose

$$Q_1 Q_5 \;=\; a^2\,R_y^2\,A^2\,, \qquad A \;\equiv\; \sqrt{1+\frac{b^2}{2a^2}}\,, \tag{5.2.8}$$

to ensure that the geometry is smooth everywhere [52].

Crucially, a, b, and n determine the onset of the throat and cap regions in the geometry (see figure 5.1) [51, 163]. Focusing on the AdS_3 part of the metric, asymptotically ($r \gg \sqrt{n}\,b$) the spacetime is approximately that of the extremal BTZ black hole and is thus locally AdS_3. At $r \sim \sqrt{n}\,b$ the geometry transitions into a $AdS_2 \times S^1_y$ throat, just like in the BTZ black hole. However, unlike in the case of the black hole, the throat region in the superstratum is long, but finite and ends around $r \sim \sqrt{n}\,a$. The bottom of the throat is the region that contains most of the microstructure – the bump functions have maxima/minima and consequently the superstratum significantly differs from an ordinary black hole. In fact, for the latter the throat is infinitely long, while for the superstratum the length of the throat is governed by the ratio b/a, which we usually take to be large in order to approximate the behaviour of black holes. Finally, in the region $r \lesssim \sqrt{n}\,a$, (5.2.3a) smoothly caps off.

5.2.2 Spiral infall along null geodesics

Our aim is to calculate the tidal forces felt by a massless string as it falls through the throat region towards the cap. As such we are interested in null geodesics of (5.2.1), which are fully integrable [168]. For the metric in the string frame (5.2.1) there are six Killing vector fields $K^{(2)} \equiv (\partial/\partial\varphi_2)$, $K^{(4)} \equiv (\partial/\partial u)$ and $K^{(a)} = (\partial/\partial z^a)$, and two conformal Killing vector fields $\tilde{K}^{(1)} \equiv (\partial/\partial\varphi_1)$ and $\tilde{K}^{(3)} \equiv (\partial/\partial v)$, all of which can be used to form eight scalars which are conserved along *null* geodesics

$$L_1 \equiv \tilde{K}^{(1)}_M \frac{dx^M}{d\lambda}\,, \quad L_2 \equiv K^{(2)}_M \frac{dx^M}{d\lambda}\,, \quad P \equiv \tilde{K}^{(3)}_M \frac{dx^M}{d\lambda}\,, \quad \hat{E} \equiv K^{(4)}_M \frac{dx^M}{d\lambda}\,, \quad P_a \equiv T^{(a)}_M \frac{dx^M}{d\lambda}\,, \tag{5.2.9}$$

where λ denotes the affine parameter along a null geodesic in the string frame. In addition, one can find a conformal Killing tensor [168]

$$\Xi \;=\; Q_1 Q_5\,\Pi^2 \left(\frac{d\theta}{d\lambda}\right)^2 + \frac{L_1^2}{\sin^2\theta} + \frac{L_2^2}{\cos^2\theta}\,, \tag{5.2.10}$$

which can be shown to be conserved along null geodesics. Combining all these quantities with the null condition

$$g_{MN}\frac{dx^M}{d\lambda}\frac{dx^N}{d\lambda} \;=\; 0\,, \tag{5.2.11}$$

allows us to fully parametrise null geodesics in $(1,0,n)$ superstrata.

In what follows we focus on the set of geodesics with

$$L_1 \;=\; L_2 \;=\; 0\,, \qquad P \;=\; \hat{E}\,, \qquad P_a \;=\; 0\,, \qquad \Xi \;=\; 0\,. \tag{5.2.12}$$

Due to the highly non-trivial structure of the metric (5.2.3), this choice does not mean that the motion is purely along the radial direction. In fact one can use (5.2.9), (5.2.10) and (5.2.11) to find

$$\frac{du}{d\lambda} \;=\; -\frac{R_y\,A\,\left(a^2+b^2F\right)}{a\,(a^2+r^2)\,\Pi}\,\hat{E}\,, \qquad \frac{dv}{d\lambda} \;=\; -\frac{a\,R_y\,A}{(a^2+r^2)\,\Pi}\,\hat{E}\,, \qquad \frac{dr}{d\lambda} \;=\; -\frac{\sqrt{2}A\Gamma}{\Pi}\,\hat{E}\,, \tag{5.2.13a}$$

$$\frac{d\theta}{d\lambda} \;=\; 0\,, \qquad \frac{d\varphi_1}{d\lambda} \;=\; -\frac{\sqrt{2}\,a\,A\,\Gamma^2}{(a^2+r^2)\,\Pi}\,\hat{E}\,, \qquad \frac{d\varphi_2}{d\lambda} \;=\; 0\,, \qquad \frac{dz^a}{d\lambda} \;=\; 0\,, \tag{5.2.13b}$$

which shows that even if the geodesic is directed radially in the asymptotic region of spacetime, as it traverses the throat, the momentum and angular momentum of the geometry cause the trajectory to rotate into other spatial directions – a massless particle travelling along such a geodesic towards the cap in a helical trajectory (see figure 5.1).

We now perform a change of coordinates so that one of the coordinates is the affine parameter along the null geodesics with charges (5.2.12). We choose to replace the radial coordinate r with λ, which induces

$$v \;=\; v(\lambda) + \frac{\tilde{t}+\tilde{y}}{\sqrt{2}}\,, \qquad u \;=\; u(\lambda) + \frac{\tilde{t}-\tilde{y}}{\sqrt{2}}\,, \qquad r \;=\; r(\lambda)\,, \tag{5.2.14a}$$

$$\theta \;=\; \frac{\pi}{2} - \tilde{\theta}\,, \qquad \varphi_1 \;=\; \varphi_1(\lambda) + \tilde{\varphi}_1\,, \qquad \varphi_2 \;=\; \tilde{\varphi}_2\,, \qquad z^a \;=\; \tilde{z}^a\,, \tag{5.2.14b}$$

where the variables with a tilde correspond to independent coordinates labelling different null geodesics.[2] Inserting (5.2.14) into (5.2.1) and using (5.2.13) yields

$$\begin{aligned} ds_{10}^2 \;=\; & d\lambda\,d\tilde{t} + \Pi\left\{\sqrt{Q_1Q_5}\left[-\frac{\left(a^2+r^2\right)}{a^2R_y^2A^4\,\Gamma^2}\,d\tilde{t}^2 + \frac{r^2\Gamma^2}{a^2R_y^2G}\left(d\tilde{y}+\frac{b^2F}{2a^2A^2\Gamma^2}d\tilde{t}\right)^2 + d\tilde{\theta}^2\right.\right. \\ & \left.\left. + \frac{\cos^2\tilde{\theta}}{\Lambda^2}\left(d\tilde{\varphi}_1 - \frac{d\tilde{t}}{A^2R_y}\right)^2 + \frac{G\sin^2\tilde{\theta}}{\Lambda^2}\left(d\tilde{\varphi}_2 - \frac{\Gamma^2}{R_yG}\left(\frac{b^2F}{2a^2A^2\Gamma^2}d\tilde{t} + d\tilde{y}\right)\right)^2\right] + \sqrt{\frac{Q_1}{Q_5}}\,ds_{T^4}^2\right\}, \end{aligned} \tag{5.2.15}$$

where it should be understood that all bump functions are amended according to (5.2.14) and furthermore, to avoid clutter we suppress the explicit dependence on the affine parameter, thus all coordinates without a tilde should be understood as being implicit functions λ according to

[2] The choice to shift in θ by $\pi/2$ is for future convenience.

(5.2.13). Note that we have also chosen $\hat{E} = \frac{1}{2\sqrt{2}}$ to set the coefficient of $d\lambda\, d\tilde{t}$ to 1. So far, this is just a rewriting of the initial metric using a set of null geodesics, however this form is convenient when considering the Penrose limit to focus on the neighbourhood of a particular null geodesic, which in turn allows us to extract the tidal forces felt by a string as it moves along the chosen null trajectory.

5.3 Tidal forces

In this section we focus on a particular null geodesic in the $(1,0,n)$ superstratum and use the Penrose limit to analyse its neighbourhood. Rewriting the resulting metric in the Brinkmann form allows us to extract information about the tidal forces felt by an object travelling along the chosen geodesic. We find that there exist non-vanishing tidal forces along the T^4 directions, stemming from the overall conformal factor appearing in the string frame metric.

5.3.1 Penrose limit

Let us now consider a null geodesic with (5.2.12) at $\theta = \pi/2$ or more equivalently $\tilde{\theta} = 0$, and $\tilde{y} = \tilde{\varphi}_1 = \tilde{\varphi}_2 = 0$. To extract the behaviour of (5.2.15) in the neighbourhood of this geodesic, we use the Penrose limit [167] which amounts to rescaling[3]

$$\lambda \;\to\; \lambda\,, \qquad \tilde{t} \;\to\; \Omega^2\,\tilde{t}\,, \qquad \left(\tilde{y}\,,\tilde{\varphi}_1\,,\tilde{\theta}\right) \;\to\; \Omega\left(\tilde{y}\,,\tilde{\varphi}_1\,,\tilde{\theta}\right), \qquad \tilde{\varphi}_2 \;\to\; \tilde{\varphi}_2\,, \tag{5.3.1}$$

followed by taking $\Omega \to 0$ and retaining only the terms in the metric which scale as Ω^2. Applying the above scaling to (5.2.15) yields

$$ds_{10}^2 \;=\; d\lambda\, d\tilde{t} + \Pi_0\sqrt{Q_1 Q_5}\left(\frac{r^2\Gamma^2}{a^2 R_y^2 G}d\tilde{y}^2 + \frac{1}{G}d\tilde{\varphi_1}^2 + d\tilde{\theta}^2 + \tilde{\theta}^2 d\tilde{\varphi}_2^2\right) + \Pi_0\sqrt{\frac{Q_1}{Q_5}}\,\delta_{ab}\,d\tilde{z}^a d\tilde{z}^b, \tag{5.3.2}$$

where we defined

$$\Pi_0 \;\equiv\; \sqrt{1 + \frac{a^2 b^2}{2a^2+b^2}\,\frac{r^{2n}}{(a^2+r^2)^{n+1}}\,\cos\left(\frac{2\sqrt{2}nv}{R_y} + 2\varphi_1\right)}\,, \tag{5.3.3}$$

which is the leading behaviour of (5.2.6) in the Penrose limit ($\Pi \to \Pi_0 + \mathcal{O}(\Omega)$). It is important to recall that after the change of coordinates (5.2.14) r, v, and φ_1 appearing in Π_0 (as well as other bump functions appearing in (5.3.2)) are all implicitly functions of λ. Nonetheless, using (5.2.13), one can express Π_0 as a function of r and we depict its behaviour for some values of b and n in figure 5.2. By relabelling the eight coordinates transverse to $\tilde{t}$ and λ

[3]Note that at $\tilde{\theta} = 0$, the $\tilde{\varphi}_2$ circle pinches off, hence the latter must not be rescaled in the Penrose limit as the relevant focusing is already contained within the scaling of $\tilde{\theta}$.

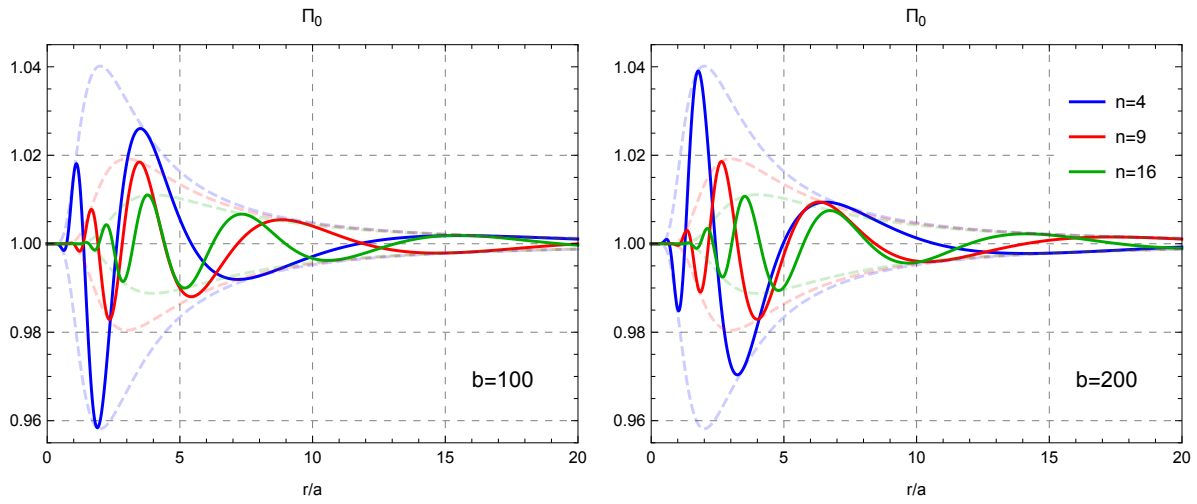

Figure 5.2 – Plots of Π_0 as a function of r. Plots on the left correspond to $\tilde{b} \equiv b/\sqrt{2}a = 100$, while $\tilde{b} = 200$ on the right. In each case we plot the curves for three different values of $n = 4, 9, 16$. The dashed curves represent the envelopes of oscillations.

as $\tilde{x}^i = (\tilde{y}, \tilde{\varphi}_1, \tilde{\theta}\cos\tilde{\varphi}_2, \tilde{\theta}\sin\tilde{\varphi}_2, \tilde{z}^1, \tilde{z}^2, \tilde{z}^3, \tilde{z}^4)$, where in particular we introduced a set of polar coordinates $\tilde{x}^3 \equiv \tilde{\theta}\cos\tilde{\varphi}_2$ and $\tilde{x}^4 \equiv \tilde{\theta}\sin\tilde{\varphi}_2$, then we can rewrite (5.3.2) in a diagonal form

$$ds^2_{10} \;\equiv\; d\lambda\, d\tilde{t} + \sum_{i,j=1}^{8} a_i^2(\lambda)\,\delta_{ij}\, d\tilde{x}^i d\tilde{x}^j\,, \tag{5.3.4}$$

where all diagonal entries are functions of λ only.[4] For the analysis of the tidal forces acting on a string, it is convenient to rewrite the metric in the Penrose limit in the Brinkmann form [167][5]

$$ds^2_{10} \;=\; 2dx^+\, dx^- - \left(\sum_{i,j=1}^{8} \mathcal{A}_{ij}(x^-)\, w^i\, w^j\right)(dx^-)^2 + \sum_{i,j=1}^{8} \delta_{ij}\, dw^i dw^j\,. \tag{5.3.5}$$

Since (5.3.4) is diagonal, the change of coordinates that yields the desired form of the metric is

$$\lambda \;=\; 2x^-\,, \qquad \tilde{t} \;=\; x^+ + \frac{1}{2}\sum_{i,j=1}^{8} \frac{a_i'(x^-)}{a_i(x^-)}\,\delta_{ij}\, w^i\, w^j\,, \qquad \tilde{x}^i \;=\; \frac{w^i}{a_i(x^-)}\,, \tag{5.3.6}$$

from which it follows that the matrix $\mathcal{A}_{ij}$ is also diagonal

$$\mathcal{A}_{ij}(x^-) \;=\; -\frac{1}{a_i(x^-)}\frac{d^2 a_i(x^-)}{d(x^-)^2}\delta_{ij}\,. \tag{5.3.7}$$

In our case the explicit expressions of the mass matrix elements are given by

$$\mathcal{A}_{11} \;=\; -\sqrt{\frac{G}{r^2\,\Gamma^2\,\Pi_0}}\,\frac{d^2}{d(x^-)^2}\sqrt{\frac{r^2\,\Gamma^2\,\Pi_0}{G}}\,, \qquad \mathcal{A}_{22} \;=\; -\sqrt{\frac{G}{\Pi_0}}\,\frac{d^2}{d(x^-)^2}\sqrt{\frac{\Pi_0}{G}}\,, \tag{5.3.8}$$

[4] Albeit implicitly through r, v, and φ_1.

[5] Our sign convention for the matrix $\mathcal{A}_{ij}$ follows [163], which is opposite of what is used in [167].

which correspond to the directions along y and φ_1 respectively, while the remaining six entries are equal and given by[6]

$$\mathcal{A}_{55} \;=\; -\frac{1}{\sqrt{\Pi_0}}\,\frac{d^2}{d(x^-)^2}\sqrt{\Pi_0}\,. \tag{5.3.9}$$

These are the elements of the effective mass matrix appearing in the equations of motion (5.1.1) and thus contain the information about the tidal forces felt by the string as it travels along the null geodesic. We notice that no direction is flat – the string feels tidal forces in all spatial directions, including those of the T^4. Furthermore, since the Penrose limit probes only the immediate neighbourhood of a null geodesic, it is insensitive to the overall size of the manifold. As a consequence, the mass matrix elements related to the toroidal directions are of the same order as those of the three sphere, despite the warp factor of T^4 typically being parametrically smaller compared to the warp factors of S^3.

5.3.2 Tidal effects along the geodesic

Tidal stresses along the toroidal directions

Explicit expressions for $\mathcal{A}_{ij}$ are not very illuminating thus we do not show them here, however, we present plots of $\mathcal{A}_{11}$, $\mathcal{A}_{22}$, and $\mathcal{A}_{55}$ for some values of the parameters b and n (see figure 5.3). We emphasize that the curves are rescaled by $\tilde{b}^2 \equiv (b/\sqrt{2}a)^2$ and given in units of a^2, which is consistent with results in [158]. Thus when $\tilde{b}$ is taken to be large in order to approximate the infinite throat of a black hole, the tidal forces become large as well. One can observe that the effective mass terms in all directions are of the same order of magnitude. Most importantly this implies that *tidal stresses along the toroidal directions felt by the infalling string are not negligible compared to other spatial direction.*

We also observe that all mass matrix elements $\mathcal{A}_{ii}$ are oscillating. This is a direct consequence of the spiral motion along the throat and the string frame metric having an overall conformal factor of Π which oscillates as the string moves in the y and φ_1 directions (see figure 5.2). The tidal effects $\mathcal{A}_{11}$ on the string in the y-direction are always positive (see also figure 5.4) – along this direction the string is always compressed and stabilised. In the remaining directions tidal effects oscillate between positive and negative values – the string feels an alternation of compression and stretching. When mass matrix elements are negative and large enough massive string modes can get get excited [163]. In particular, it follows that due to these oscillations, the null geodesic eventually passes through a region in which $\mathcal{A}_{55}$ is negative. Therefore, according to (5.1.1), *it is possible for the infalling string to lose its kinetic energy by exciting string modes along the T^4 directions.* This has important consequences in context of the AdS/CFT duality as excitations along the toroidal directions are identified with bosonic fields in the dual CFT. We explore this connection further in the next section.

In figure 5.4 we depict the envelopes of the oscillations of the $\mathcal{A}_{ii}$ functions for $b \gg a$. The shape of the envelope is determined by the radial direction, r, whereas the oscillations come

[6]For concreteness we schematically denote with $\mathcal{A}_{55}$ all $\mathcal{A}_{kk}$ entries, where $k = 3, 4, \ldots 8$ which includes the θ and φ_2 directions. It should be understood that the results presented are valid for any other $\mathcal{A}_{kk}$.

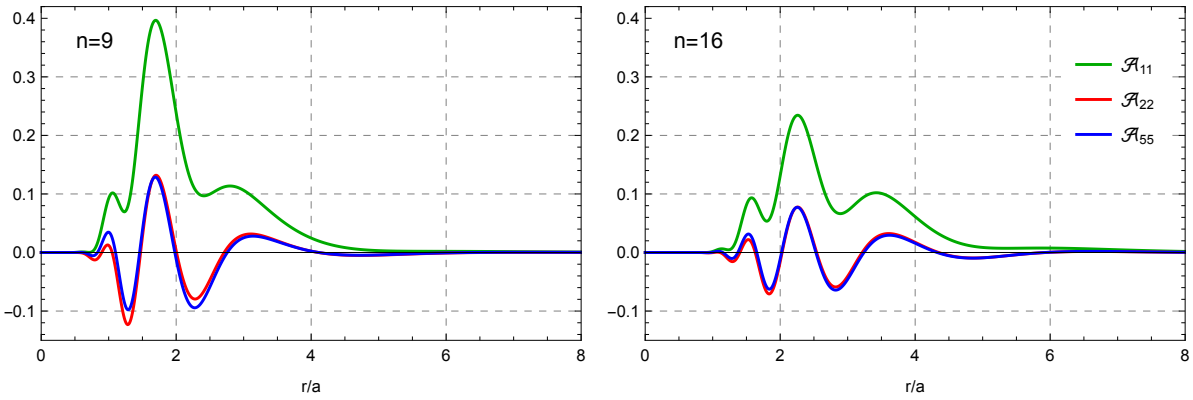

Figure 5.3 – Plots of $\mathcal{A}_{11}$, $\mathcal{A}_{22}$ and $\mathcal{A}_{55}$ with $\tilde{b} \equiv b/\sqrt{2}a = 100$ and $n = 9$ (left) and $n = 16$ (right). The curves are rescaled by $\tilde{b}^2$ and given in units of a^2. We observe oscillatory behaviour in all three mass matrix elements. While $\mathcal{A}_{11}$ is always positive, $\mathcal{A}_{22}$ and $\mathcal{A}_{55}$ are negative in some regions. The tidal forces along the toroidal directions are not negligible compared to other directions.

from its motion along y and φ_1. As already mentioned, one observes that despite its oscillatory behaviour $\mathcal{A}_{11}$ is always positive, while $\mathcal{A}_{22}$ and $\mathcal{A}_{55}$ can be both positive and negative. The envelopes, and thus the tidal effects, are extremal around $r \sim \sqrt{n}\, a$, which is the bottom of the throat where the microstructure of the superstratum is located.

Again, the envelopes in figure 5.4 are rescaled by $\tilde{b}^2 \equiv (b/\sqrt{2}a)^2$ and given in units of a^2, meaning that at large $\tilde{b}$ the amplitudes of oscillations in $\mathcal{A}_{ii}$ scale as $\tilde{b}^2$. One can explain this by noting that as $\tilde{b}$ grows, the length of the throat increases. In the scaling limit,[7] $\tilde{b} \equiv b/\sqrt{2}a \to \infty$, and the throat deepens to infinity while the geometry of the cap remains fixed [80, 16]. A particle dropped from spatial infinity with fixed energy E encounters the mircrostructure at the bottom of the throat with higher kinetic energy and thus its interaction with the tidal forces are greater.

The discrete shift-symmetry of the throat length

As $\tilde{b}$ increases, the amplitudes of the tidal forces increase and in addition the crests of the oscillations within the envelopes shift as well – see figure 5.5. One notices that after the usual rescaling of the envelope by $\tilde{b}^2$, the mass matrices are identical for two different and carefully tuned throat lengths, $\tilde{b}_0$ and $\tilde{b}_1$. In fact, one can show that this pattern continues for an infinite number of throat lengths $\tilde{b}_n$. The origin of this behaviour is the v and φ_1 dependent cosine function in Π_0. For specific values of the throat length $\tilde{b}_n$ the argument of that cosine function differs exactly by an integer multiple of 2π for all values of λ (or r). For large $\tilde{b}$ this means that at specific values $\tilde{b}_n$ the corresponding mass matrix elements $\mathcal{A}_{ii}$ are identical up to an overall scaling factor of $\tilde{b}^2$.

[7] More precisely, one has to take $a \to 0$, while keeping b is fixed. But rescaling r with a to get to the bottom of the throat, is as if one is sending $b \to \infty$.

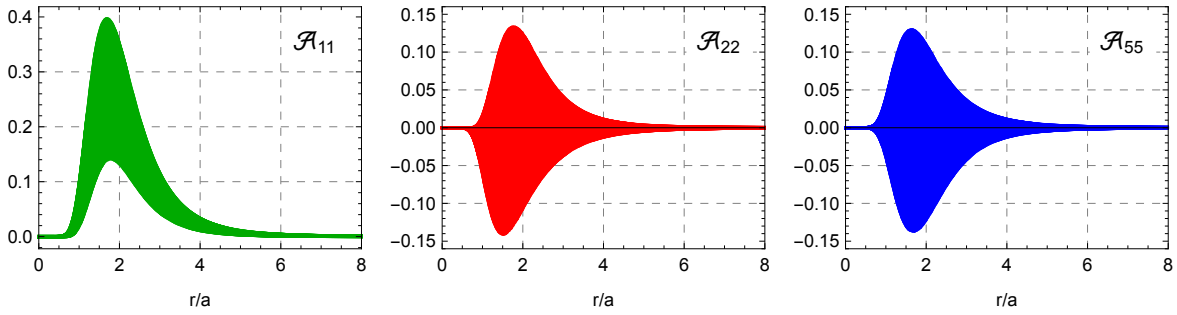

Figure 5.4 – Plots of envelopes of $\mathcal{A}_{11}$ (left), $\mathcal{A}_{22}$ (middle) and $\mathcal{A}_{55}$ (right), at $n = 9$. The curves are rescaled by $\tilde{b}^2 \equiv (b/\sqrt{2}a)^2$ and given in units of a^2. In true scale $\mathcal{A}_{ii}$ become large as $\tilde{b}$ is increased to obtain a long throat.

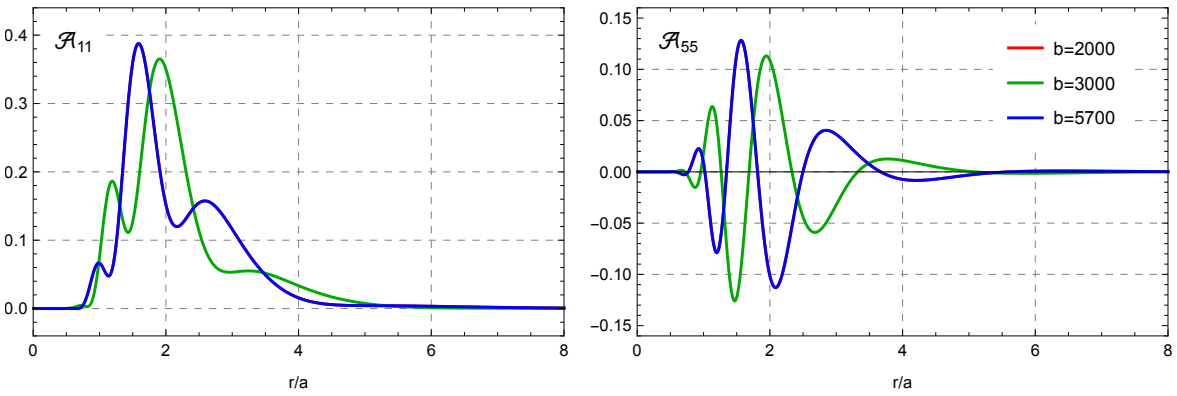

Figure 5.5 – Graphs of $\mathcal{A}_{11}$ and $\mathcal{A}_{55}$ for $n = 9$ and $\tilde{b} = 2000$, 3000 and 5700. The curves are rescaled by $\tilde{b}^2 \equiv (b/\sqrt{2}a)^2$ and given in units of a^2. For generic values of $\tilde{b}$ the graphs differ, but for specific values of $\tilde{b}$, such as $\tilde{b}_0 = 2000$ and $\tilde{b}_1 = 5700$, the plots are identical – in the above plots, the two curves are actually coinciding.

As $\tilde{b} \to \infty$, the family of trajectories of null geodesics in the φ_1 direction, $\{\varphi_1(\tilde{b}; r)\}_{\tilde{b}}$, converges uniformly to a continuous function. On the contrary, the family of trajectories in the v direction, $\{v(\tilde{b}; r)\}_{\tilde{b}}$, converges pointwise to a limit function which is not integrable and therefore the trajectory $v(r)$ (and thus $y(r)$) varies with $\tilde{b}$. Consequently, when $\tilde{b} \gg 1$, increasing the throat length modifies the trajectory in the v-direction, while leaving the stabilized trajectory in φ_1 unchanged. Furthermore, it follows that the oscillations in all $\mathcal{A}_{ii}$, induced by the argument in the cosine function in (5.2.6), are mainly due to the motion along the y-circle. The change in position in φ_1 does not exceed π. This also explains why at large $\tilde{b}$, the number of oscillations scales with n.

Physically, due to a $\mathbb{Z}_{2n}$-symmetry of the superstrata along $\sqrt{2}v$ in the string frame, the specific values of $\tilde{b}_n$ correspond to throat lengths such that differences in trajectories along y between two geodesics is an integer multiple of $-\frac{2\pi R_y}{2n}$. This precisely induces a phase shift that

is an integer multiple of 2π at all r in the argument of the cosine function of Π_0.

5.4 CFT perspective on tidal effects

The presence of tidal excitations along T^4 can be motivated by considering the dual D1-D5 CFT. It consists of a bound state of D1 and D5 branes wrapping compact dimensions of the theory, namely the S^1_y and T^4. More specifically, the D1 branes wrap S^1_y and the D5 branes wrap $S^1_y \times T^4$. The theory is then described by 'component' strings composed of the wrapped D-branes which live on the common direction, S^1_y, denoted as the y circle. There is a well defined map between the superstrata geometries and states within the D1-D5 system (see [169] and references therein). The degrees of freedom correspond to open string excitations which can be either bosonic or fermionic. Bosonic excitations, which we schematically write as α_{-n}, are polarized along the torus and fermionic excitations, which we schematically write as d_{-r}, are polarized along the torus and the 3-sphere. These bosonic and fermionic degrees of freedom can be combined into composite operators such as L_{-n}, J_{-n}, G_{-r} (we have suppressed the charge indices for brevity). The L_{-n}'s are Virasoro operators and are written in terms of the energy momentum tensor of the theory. The J_{-n}'s are current operators which are written in terms of composite fermionic degrees of freedom. Finally the G_{-r}'s are supercharge operators which are written as composites of fermionic and bosonic operators. They exchange fermionic degrees of freedom for bosonic degrees of freedom and vice versa.[8]

One can write down the CFT dual of an infalling probe propagating within the superstrata geometry considered in this paper. In order to understand tidal excitations of the probe, which is a dynamical process, we must turn on an interaction in the CFT which is schematically given by the following action

$$S \;=\; S_0 + \lambda \int d^2 w D(w, \bar{w})\,, \tag{5.4.1}$$

where S_0 is the action of the free theory. For more work on the deformed CFT see [170–174]. The parameter λ is the coupling of the interaction and w corresponds to the CFT coordinates which describe the location of the operator $D(w, \bar{w})$. This operator consists of two operators which we write schematically as $D = G\sigma$. G is a supercharge operator described previously and σ is a twist operator. The twist operator joins and splits component strings wrapping the y circle. The twisting-untwisting process applied to component strings in the vacuum generate excitations in the final state.

To study a probe falling into the superstrata geometry one considers an initial excitation combined with a CFT state which is dual to the superstrata geometry. The CFT dual of the superstrata geometry considered in this paper consists of a left moving momentum wave generated by [50, 52]

$$|\text{background geometry}\rangle \;\sim\; \Big((L_{-1} - J^3_{-1})^n |00\rangle_1\Big)^{N_{00}} \Big(|++\rangle_1\Big)^{N_{++}}\,. \tag{5.4.2}$$

[8] For more details, see for example [164].

The $|00\rangle_1$ strands correspond to singly wound vacua which contain no net angular momentum along S^3 with $N_{00} \propto b^2$. The $|++\rangle_1$ strands correspond to singly wound vacua which contain angular momenta along S^3 with $N_{++} \propto a^2$. The CFT dual of the string probe moving within the superstrata geometry can be schematically given by

$$|\text{single graviton probe}\rangle \sim \left((L_{-1} - J^3_{-1})^n |00\rangle_1\right)^{N_{00}} \alpha_{-n}\bar{\alpha}_{-n}\left(|++\rangle_1\right)^{N_{++}}, \tag{5.4.3}$$

where the unbarred notation represents a left mover and the barred notation represents a right mover. Note that these excitations correspond to deformations of the metric components in the T^4 directions [175]. A radial infall with no initial motion along y, implies from the CFT perspective, that the left and right movers have the same energy. There is no net momentum along the y circle.

In order to investigate tidal effects within the CFT, we need a mechanism which takes an initial probe and generates further excitations which grow as a function of time, a process reminiscent of tidal effects experienced by a string in the bulk. In the CFT this effect is produced by acting with a pair of operators, DD on the initial state, (5.4.3) for example. The first operator D twists two smaller component strings in the initial state into a larger component string, and then the second one untwists the larger copy back into two smaller component strings in the final state. By applying two D's, one can compute the transition amplitude for the initial excitation, one left and right moving boson for example, (5.4.3), to split into multiple excitations in the final state. Examples of such amplitudes are given by

$$\langle\text{multiple boson state}|DD|\text{single graviton probe}\rangle\,, \tag{5.4.4a}$$

$$\langle\text{multiple fermion state}|DD|\text{single graviton probe}\rangle\,, \tag{5.4.4b}$$

where for example

$$|\text{multiple boson state}\rangle \sim \alpha_{-p}\bar{\alpha}_{-p}\alpha_{-q}\bar{\alpha}_{-q}\alpha_{-r}\bar{\alpha}_{-r}|\text{background geometry}\rangle \tag{5.4.5}$$

corresponds to a final state containing bosonic excitations, and similarly

$$|\text{multiple fermion state}\rangle \sim \alpha_{-p}\bar{\alpha}_{-p}d_{-q}\bar{d}_{-q}d_{-r}\bar{d}_{-r}|\text{background geometry}\rangle \tag{5.4.6}$$

which is a final state containing both bosonic and fermionic excitations. The bosonic mode is required to obtain a non-zero amplitude. To compute such processes, two D operators are preferred because their combined action ensures that the initial and final twist sectors are the same. This provides the best attempt at maintaining a fixed background to cleanly study processes which happen on top of it. Furthermore, we expect such transitions to occur because the twist operator dynamically changes the size of the vacuum. Borrowing intuition from quantum fields in curved space, we know that dynamically changing the vacuum creates particles. The logic here is similar. In addition, the theory is supersymmetric. Therefore, given an initial state, the operation of D can produce both bosonic and fermionic excitations.

Recent work [165, 166] suggests that this amplitude should grow in time. This growth indicates the transfer of energy from a single bosonic mode to multiple modes in the final state which share the initial energy amongst themselves. This includes both bosonic and fermionic

excitations. The initial mode contains a large momentum in the supergravity picture. This can be pictured as an L_{-1}, which functions as a boost generator in AdS, acting many times on an α_{-1} (similarly for the right-moving sector). The multimode final state, however, roughly corresponds in the bulk to a graviton which has lost some of its linear momentum in favour of generating a rest mass, a sign of stringy behaviour. This is suggestive, in the supergravity description, of a string being tidally excited along transverse directions, including the sphere [163].

Because of the supercharge operator, we expect that transition amplitudes involving the splitting of an initial bosonic excitation into only bosonic excitations in the final state should also grow with time, similar to the amplitude containing fermionic excitations. The bosonic excitations correspond to polarizations along T^4. Therefore the CFT process is suggestive of a probe moving within the superstratum geometry and becoming tidally excited along the T^4 directions. This is precisely what is suggested by the results of this paper. Tidal effects within the CFT are currently being investigated [165, 166].

5.5 Summary and outlook

We analysed the the tidal forces along an infalling and spiralling null geodesic in the $\theta = \pi/2$ hypersurface of the $(1, 0, n)$ superstata. Using the Penrose limit, we found that there exist tidal forces along all spatial directions orthogonal to the direction of the null geodesic. This includes tidal forces along the internal T^4 directions which scale with the length of the throat and are of the same order of magnitude as tidal effects in other, non-internal, directions. The elements of the mass matrix $\mathcal{A}_{ii}$ are oscillatory, with the amplitude of oscillation determined by the motion in the radial direction while the oscillatory behaviour coming from motion along y and φ_1 directions.

A massless string travelling along such a null geodesic alternately experiences compression and stretching. The presence of stretching regions in the toroidal directions allows for the possibility of string excitations along the T^4. In the dual CFT, such excitations correspond to bosonic degrees of freedom and we discussed the field theory manifestation of tidal forces and their properties. To conclude, our work supports the hypothesis that the CFT dual of tidal effects on any graviton probe consists in transition amplitudes between different excitations which exhibit a growth behaviour. The growth in the amplitude for a single-graviton excitation to transition into a final state comprising of multiple bosonic excitations suggests that the initial graviton loses energy, by tidal effects. The bosonic to fermionic amplitudes suggest that the graviton probe loses energy due to tidal excitations along the S^3, while the bosonic to bosonic amplitudes concern the energy loss along the T^4.

Our analysis suggests a new way in which a string can get trapped inside a capped geometry – as it spirals down the throat it encounters tidal forces which transform part of its kinetic energy into internal excitations along the T^4 directions. The superstratum background can thus be thought of as a viscous fluid in which the string gets captured.

The results presented here are in line with the findings of [163], where tidal excitations were found to excite an infalling string only along the S^3 and S^1_y directions. This is a consequence of analysing geodesics that lie entirely inside the $\theta = 0$ hypersurface. The overall conformal factor in the metric, Π, is then subleading in the Penrose limit ($\Pi \sim 1 + \mathcal{O}(\Omega^2)$) and thus tidal forces

along the T^4 are subleading compared to those in the S^3 and S^1_y directions. However, because Π is not subleading for any other infalling null geodesic, we believe that the takeaway from our analysis applies generically – tidal forces along T^4 are important. This would suggest that all of the ten dimensions are important when considering the scrambling of strings into capped geometries.

There are still many questions that need to be answered. First, throughout the paper, we have ignored the contribution from the B-field. This is because in (5.1.1) it merely mixes different directions, and furthermore, in the $(1, 0, n)$ superstrata the B-field has no legs along the T^4 directions, hence it should not spoil the results of our analysis. It is also interesting to observe that the tidal effects are identical between (some) directions in S^3 and those of T^4, despite possible difference in sizes. It would be interesting to see whether subleading effects in the Penrose limit can observe the overall size of individual spatial directions. Finally, we have shown that tidal forces along toroidal directions exist and can excite the string, but the exact fate of the string is yet to be determined. We hope to answer some of these questions in the future.

Chapter 6

Resolving Black-Hole Microstructure with New Momentum Carriers

6.1 Introduction

One of the remarkable achievements of string theory is that it can provide a microscopic description of black-hole entropy. It was found that, at vanishing string coupling, different string/brane configurations could reproduce the Bekenstein-Hawking entropy of the corresponding black hole [27, 28]. The black-hole geometry, and its horizon, then emerge as the string coupling, and hence Newton's constant, G_N, becomes finite. Indeed, the horizon grows with G_N [176–178], but because gravity generically compresses matter, it was believed that all the perturbative string states would collapse behind a horizon. Thus the perturbative microstates, whose counting gives the black-hole entropy, would not be visible once gravity takes effect.

Insights from brane physics show that this picture is too naïve. The tension of D-branes and NS-branes decreases as the coupling increases, and so adding momentum excitations causes them to spread in directions transverse to their world-volume. Indeed, it was noted in [34] that three-charge brane configurations carrying momentum would grow with G_N at the same rate as the black-hole horizon. It was then found that three-charge horizonless geometries supported by topological fluxes have the same behavior [40, 79, 179]. Thus was born the Microstate Geometry (MG) Programme in which one constructs *smooth, horizonless geometries* that approximate the classical black-hole solution everywhere except at the horizon scale, where MG's end in a smooth, horizonless cap.

Microstate Geometries are part of a larger framework, known as the *Fuzzball Programme*. The defining ideal of this programme is that individual black-hole microstates, generically referred to as fuzzballs, must be horizonless because horizons imply entropy and give rise to information loss [180, 38]. Fuzzballs have the same mass, charge and angular momentum as a given black hole and can be arbitrarily quantum and arbitrarily strongly curved. They describe pure states of the black hole and, if a holographic description is available, are dual to pure states of the CFT that can be used to account for the black-hole entropy. Microstate Geometries fit in this paradigm as the string-theory fuzzballs that are sufficiently coherent as to become well approximated by smooth solutions of supergravity.

There also exist fuzzballs that are not smooth supergravity solutions but can be described using other well-defined limits of string theory. Indeed, this led to the definition of a *Microstate Solution*, [39], which is a horizonless solution of supergravity, or a horizonless, physical limit of a supergravity solution, that has the same mass, charge and angular momentum as a given black hole. Microstate solutions are allowed to have singularities that either correspond to brane sources, or can be patch-wise dualized into a smooth solution. In this paper we will refine this classification further to distinguish microstate solutions corresponding to pure states from *Degenerate Microstate Solutions*, which correspond to a limited family of microstates.

It is important to emphasize that Fuzzballs are all, by definition, horizonless, regardless of whether they can be described within supergravity. In this paradigm, horizons arise only as a consequence of averaging over microstates and are thus necessarily related to ensembles of such states. This is what leads to the entropy-area relation. But if pure states correspond to horizonless microstates, then a solution with a horizon should not describe the physics of *any* pure state of the system and should not be holographically related to any pure state of the dual CFT.[1]

The purpose of this paper is to make some steps towards the resolution of what appears to be a counterexample to the Fuzzball paradigm: the possibility that some pure CFT states are dual to a supergravity solution with a horizon. The putative counterexample comes from a singular limit of a class of Microstate Geometries known as *superstrata.*

Superstrata are horizonless solutions that have the same charges as a D1-D5-P supersymmetric black hole. They are, perhaps, the most analyzed and well-studied of all MG's [50,51,181,52, 159,153,161,154–156,53,162,160,182,163,157,183,19,184,185], and the holographic dictionary for these geometries is now well-established [186,62,187–191,169,192]. The corresponding black holes have an infinitely-long AdS_2 throat, but in superstrata, this throat is capped off at a large but finite depth, which is inversely proportional to a parameter, a, that controls the angular momentum, and the spatial extent of the configuration. The momentum charge of a superstratum is carried by flux excitations whose Fourier amplitudes give an additional set of parameters, b_n. The problematic limit, and putative counterexample, arises as one takes $a \to 0$.

These parameters have a well-understood interpretation in the dual D1-D5 CFT [190]. The CFT states dual to superstrata are constructed starting from RR-ground states that are usually described as having $(+,+)$ strands and $(0,0)$ strands.[2] The former carry angular momentum but no momentum, and their number is proportional to a^2. The $(0,0)$ strands have vanishing angular momentum but, in the superstratum, carry momentum excitations with a quantum number, n. The number of such excited strands is proportional to b_n^2 and the total momentum charge is given by:

$$Q_P \sim \sum_{n=1}^{\infty} n\, b_n^2 \,. \tag{6.1.1}$$

Requiring the superstrata to be smooth and free of closed time-like curves imposes a constraint

[1] This has only been shown so far for (0+1)-dimensional CFT's dual to asymptotically-AdS_2 spacetimes [68].

[2] For explanation of this notation, see, for example, [164,50].

of the schematic form:

$$\frac{Q_1 Q_5}{R_y^2} \;=\; a^2 \;+\; \frac{1}{2}\sum_{n=1}^{\infty} b_n^2\,, \tag{6.1.2}$$

where Q_1 and Q_5 are the supergravity D1 and D5-brane charges and R_y is the asymptotic radius of the common D1-D5 direction. The important point is that adding more momentum-carrying modes (by increasing the b_n's) makes a smaller, so the AdS_2 throat becomes longer, capping off at higher and higher red-shifts. In the $a \to 0$ limit, the cap moves to infinite redshift and the superstratum solution appears to become identical to the classical extremal D1-D5-P black hole.

From the perspective of the dictionary to the dual CFT, this limit appears well-defined and corresponds to a pure state with only $(0,0)$ strands. Thus it appears that as one moves in the space of CFT states dual to superstrata, one encounters some pure states whose bulk dual has a horizon. This violates the basic principle of the Fuzzball/MG programme: Pure states should not be dual to a configuration that has a horizon.

As we discuss in Section 6.2, the appearance of a horizon is explained by noting that in the D1-D5-P frame, the standard superstratum construction not only restricts the momentum-carrying excitations, but also involves a smearing operation. This smearing preserves the details of the microstructure only when $a \neq 0$, while in the $a \to 0$ limit it averages over distinct momentum-carrying configurations and this gives rise to a solution with a horizon. If one avoids this smearing, and takes into account the degrees of freedom this smearing erases, the geometry remains horizonless even as $a \to 0$.

In this paper we show how this can be achieved by constructing a new class of three-charge solutions with vanishing horizon area that go beyond the standard superstratum construction by incorporating additional momentum-carrying excitations. We do this by working in the Type IIA F1-NS5-P duality frame, and the new momentum carriers that can resolve the microstructure are D0-brane and D4-brane charge densities that vary along the common F1-NS5 direction. These excitations have the important property that, unlike all other microstate geometries, they carry momentum *without* expanding the branes in directions transverse to their world-volume. Hence, one can think of them as giving rise to a longitudinally polarized momentum wave on branes that remain localized at a single point in the transverse directions, and do not break the rotational $SO(4)$ symmetry of the black-hole solution.

Since duality transformations preserve degrees of freedom while encoding them in different ways, our Type IIA F1-NS5-P supergravity solutions must have counterparts in the D1-D5-P frame. However, to get from one frame to the other, one must perform a T-duality along the common F1-NS5 direction, and the solutions we construct depend explicitly on this direction. As a result, our Type IIA supergravity solutions become configurations involving a coherent set of higher Kaluza-Klein modes, and thus cannot be described as D1-D5-P solutions in Type IIB supergravity.[3]

The main result of this paper is the solution given in equation (6.3.12): It represents a family of three-charge F1-NS5-P solutions with D0 and D4 densities and no macroscopic horizon.

[3]It is also interesting to note that the exact same phenomenon happens when one tries to dualize D1-D5-P superstrata that depend on the common D1-D5 direction to the IIA F1-NS5-P duality frame we consider: the smooth geometries are dualized into microstate solutions that contain excited towers of KK modes and are not describable in supergravity.

Globally, this solution preserves the four supercharges of the corresponding three-charge black hole. However, if we zoom in at a fixed location along the F1 and NS5-branes, we find that the configuration *locally* preserves eight supercharges. In this limit, the local D0 and D4 densities are approximately constant and the solution preserves eight Killing spinors, four of which are identical to those of the F1-NS5-P black hole. Hence, near the brane sources the solution behaves locally like a two-charge system with a vanishing horizon area.

It is important to emphasize that the solution presented here is a singular brane configuration with vanishing horizon area, and its role as a fuzzball needs clarification. As originally conceived, a *Microstate Solution* is a horizonless, but singular, brane configuration that corresponds to a black-hole microstate that can be fully resolved in string theory. We need to broaden this idea to include *Degenerate Microstate Solutions*. Such an object is defined to be a singular supergravity solution with the following properties:

- It must have vanishing horizon area.
- The source must correspond to a well-defined family of branes.
- The microstructure of the brane source can be revealed, and counted, through standard string theory methods.
- There must be geometric deformations, or transitions, that can resolve the solution into microstate solutions or microstate geometries.

One of the features of microstate solutions, and microstate geometries, is that if one zooms into their cores, the underlying geometric elements are "locally primitive," which means that they locally preserve 16 supercharges. Taken as a whole, the complete solution preserves only a subset of these supercharges. By contrast, the cores of degenerate microstate solutions will typically preserve only 8 supercharges. This is too much supersymmetry for the configuration to generate a horizon, and so the underlying structure can still be accessed and probed by string theory. However, the reduction from 16 supercharges to 8 supercharges reflects the fact that such solutions still correspond to a family of individual microstates, but this family is too small to generate a horizon in supergravity.

In the past, the configurations we are classifying as degenerate microstate solutions have sometimes been said to have "small" (string-scale) horizons because they represent stringy ensembles of states. We prefer the defining ideas of degenerate microstate solutions because they accentuate the accessibility of the microstructure to stringy analysis and geometric resolutions, while the cloaking of such things in horizons is, once again, just code for ensemble averaging of microstructure.

The archetype of a degenerate microstate solution is, of course, the pure D1-D5 solution, whose microstructure has been throughly understood in string theory [193, 60, 194]. As we will discuss, the degenerate microstate solutions that we will construct in this paper are, at their core, equivalent to D1-D5 degenerate microstate solutions. In subsequent work we plan to explore geometric transitions that will resolve these degenerate microstate solutions into microstate solutions and microstate geometries.

In Section 6.2 we describe the general features of the standard superstratum construction and how it neglects some degrees of freedom and necessarily results in smearing in the $a \to 0$ limit. We also discuss the supersymmetries preserved by the solution. In Section 6.3 we describe the construction of the eight-supercharge NS5 solution with D0-D4 charges that carry momentum

without transverse fluctuations. We then add coherent F1-string excitations to this system, and obtain the complete supergravity description. It is this microstate solution that provides the resolution of the $a \to 0$ limit: a solution with black-hole charges, vanishing horizon area, and SO(4) symmetry.

In Section 6.4 we analyze this new geometry and compare it to the three-charge black-hole solution. Section 6.5 contains a discussion of our results and an outline of possible future research. Some of the details of the construction that are omitted in Section 6.3 are presented in Appendix C.1. In Appendix C.2 we collect some of the conventions used throughout the paper.

6.2 Momentum carriers on superstrata

In five dimensions, a BPS black hole only has a finite-sized horizon if it has three charges and thus preserves four supercharges ($\frac{1}{8}$-BPS). The corresponding microstate geometries and microstate solutions must globally preserve the same supercharges, however their *cores* can have more supersymmetries *locally*. Indeed, their fundamental building blocks are locally *primitive* and have 16 supercharges [49], but have fewer supersymmetries when considered globally because their shapes and dipolar charge distributions break the supercharges down to the universal subset that is common to the entire configuration.

Since microstate geometries and microstate solutions are supported by sources that have locally more supersymmetries than the black hole, they do not have in general an event horizon. Indeed, the existence of superstrata was originally conjectured based on a double-bubbled geometric transition of the D1-D5 system [49]. Specifically, if one starts with a stack of D1-branes and adds a momentum wave, then the configuration is globally $\frac{1}{4}$-BPS but locally $\frac{1}{2}$-BPS. If one then combines a D1-brane with a profile carrying a momentum wave with a D5-brane with the same profile, the system is globally $\frac{1}{8}$-BPS but locally $\frac{1}{4}$-BPS. By adding angular momentum and a KKM dipole charge, one can make a geometric transition to a momentum carrying object that is globally $\frac{1}{8}$-BPS but locally $\frac{1}{2}$-BPS. The result is a superstratum [50].

To make a smooth geometry, the "special direction" of the KKM must coincide with the common D1-D5 direction, which we parameterize with the coordinate v.[4] However, the standard Kaluza-Klein Monopole (KKM) geometry must be v-independent,[5] and this conflicts with the addition of momentum excitations, which necessarily depend on v. Indeed, the v-circle pinches off at the KKM location, and so one cannot source v-dependent fluctuations on the KKM locus without creating a singularity.

This difficulty was resolved in [195] and is best understood by starting from the standard, maximally-spinning supertube [47,48]. One takes the D1-D5 system and adds a KKM dipole and angular momentum so that the supertube wraps a circle in an $\mathbb{R}^2$ of the $\mathbb{R}^4$ transverse space. The angle along this circle is denoted by ϕ, and the solution is independent of (ϕ, v). This describes

[4] To be more precise, the common D1-D5 direction is described by a periodic coordinate y, while v is a null coordinate: see equation (6.3.3). Supersymmetry requires the solution to be independent of the other null coordinate, u, and one can think of the latter as describing "time" while v denotes the "spatial" coordinate (see also [181] for a more careful discussion).

[5] One can obviate this difficulty by allowing higher Kaluza-Klein modes in the monopole, but this takes us outside of Type-IIB supergravity.

the maximally-spinning $\frac{1}{4}$-BPS supertube and it corresponds to a coherent superposition of RR ground states in the CFT consisting of only $(+,+)$ strands. One can now allow the density of D1- and D5-branes to vary *along the ϕ direction of the supertube*. In terms of the standard mode numbers inherent in superstrata, (k,m,n), this density fluctuation corresponds to a $(k,0,0)$ excitation. The result is still a $\frac{1}{4}$-BPS supertube, and it is still v-independent, but it is now a mixture of $(+,+)$ and $(0,0)$ strands (of length k). The numbers of such strands is determined by Fourier coefficients, a and $b_{k,m=0,n=0}$.

In superstrata one can think of the $(0,0)$ strands (or the ϕ-dependent density fluctuations in the $(k,0,0)$ solution) as the "medium" that carries the momentum, and the solutions where these modes are excited have generic values of (k,m,n). One necessarily has $k>0$ because the momentum is being carried by the density fluctuations around ϕ. As discussed in detail in [195], the v-dependent fluctuations are not, and cannot be, sourced on the original supertube locus: these fluctuations are delocalized in the fluxes and geometry of the topologically-non-trivial three-cycles of the D1-D5-KKM solution.

The $a\to 0$ limit of superstrata is motivated by the desire to construct solutions with vanishing angular momentum that resemble a black hole with arbitrary precision.[6] In view of the previous discussion it is now evident just how pathological this limit is for standard superstrata. Namely, by keeping the UV unchanged and taking $a\to 0$, one is collapsing both the supertube that defines the momentum carriers and the topological bubble that supports the momentum-carrying fluxes. The end result is to push the KKM locus and the center of the $\mathbb{R}^4$ base-space of the solution to a point, while keeping the momentum fixed. Since the KKM forces v-independence, the momentum charge only survives in this limit because the momentum carriers are smeared along the v-circle and as a result the geometry develops a horizon. Hence, the standard superstratum momentum carriers, which are v-dependent and have polarizations in the $\mathbb{R}^4$ directions are crushed to a point in the transverse space and smeared along the v-direction in the $a\to 0$ limit.

In the dual CFT picture, the $a\to 0$ limit of various superstratum solutions corresponds to various states that only have $(0,0)$ but no $(+,+)$ strands, and hence have no angular momentum. Hence, these pure states appear naively to be dual to a bulk solution with a horizon. Furthermore, the bulk information that distinguishes these pure states from one another appears to vanish in this limit. Thus in the limit of vanishing angular momentum, the superstratum holographic dictionary appears to break down. In order to solve this puzzle, and the apparent loss of information in the holographic dictionary, we need to consider all possible momentum carriers of the system, and, in particular, find the modes that carry momentum and have vanishing angular momentum in the space-time. The simplest duality frame in which one can build these modes is the Type IIA frame in which the three charges of the black hole correspond to F1 strings, NS5-branes and momentum.[7]

[6] As explained in [68], there are two such limits. In the first limit, one keeps finite the energy of asymptotic observers and the asymptotic structure of spacetime, and the AdS_2 throat becomes longer and longer and its cap becomes deeper and deeper, approaching the infinite throat of the supersymmetric black hole. In the second limit, one keeps finite the energy of an observer in the cap, and in this limit the cap remains fixed, while the asymptotic structure of the solution becomes AdS_2 times a compact space. This discussion is about the first limit.

[7] It is also possible to add such fluctuations in the D1-D5-P duality frame, but these correspond to fluctuations of brane and string densities that wrap partially the T^4 compact space, and hence break the

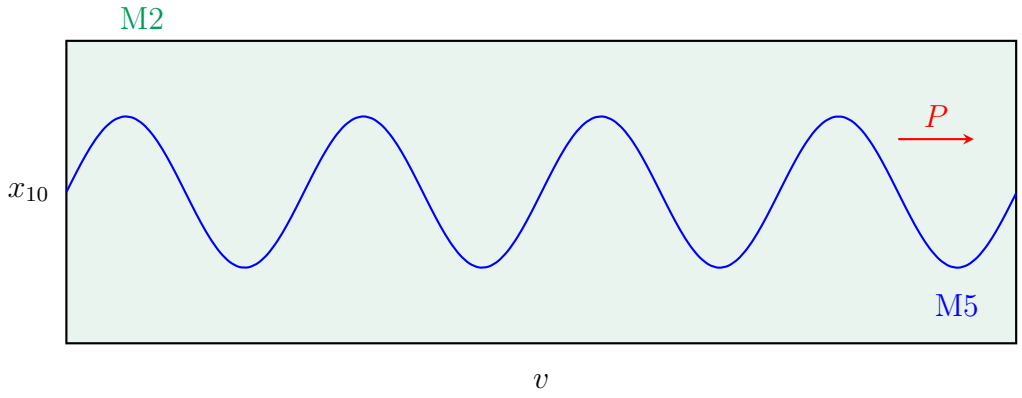

Figure 6.1 – Initial configuration in the M-theory frame: M2-branes (green) are wrapping the $S^1(v) \times S^1(x_{10})$ circles, while the M5-branes (blue) wrap the $S^1(v) \times T^4$ (T^4 is not pictured) and have a wave carrying a momentum, P, along v. The M5-branes with a momentum wave have a non-trivial profile in the $S^1(v) \times S^1(x_{10})$ plane, and hence have locally non-zero M5 charges parallel to the x_{10} direction, as well as non-trivial momentum along x_{10}. When one compactifies this M-theory solution to Type IIA along x_{10}, these charge components become D4 and D0 charge densities respectively.

One can relate this frame very easily to the normal IIB D1-D5-P frame by an S-duality to a Type IIB F1-NS5-P system, followed by a T-duality. In this duality frame, the NS5-brane can carry momentum along the common F1-NS5 direction by the excitation of the internal scalar field of the Type IIA NS5-brane. This corresponds in supergravity to turning on fluctuating Ramond-Ramond fields C_1 and C_3, that can be thought of as coming from D0- and D4-brane density fluctuations inside the NS5-brane. These density fluctuations can be chosen to integrate to zero, so that the total solution only has F1, NS5 and P charge. These momentum-carrying excitations have vanishing angular momentum in the transverse $\mathbb{R}^4$ space and are well-defined even in the $a \to 0$ limit.

The fact that adding D0-D4 dipole charges to the F1-NS5 system is natural is perhaps best understood by going to the M-theory frame. Consider Type IIA theory on $\mathbb{R}^{1,4} \times S^1(v) \times T^4$ and denote the M-theory circle by $S^1(x_{10})$. The F1-NS5 system lifts to a configuration of M5 and M2-branes, where the M5-branes wrap $T^4 \times S^1(v)$ and the M2-branes wrap $S^1(x_{10}) \times S^1(v)$. The D0-D4 densities carry momentum as a longitudinal wave along the common direction in the F1-NS5 system. In M-theory the NS5-D0-D4-P subsystem uplifts to a momentum-carrying wave on the M5-brane, whose transverse polarization is strictly in the M-theory direction. This M5-brane has 8 supersymmetries, but if one zooms near the profile at a specific location one finds an M5-brane with orthogonal momentum, which preservers 16 supercharges. When one reduces this configuration along the x_{10} direction to ten-dimensional Type IIA theory, the momentum and M5-charge polarized along the x_{10} become D0 and D4 charge densities.

This leads to the starting point of our analysis: Our aim is to construct three-charge Type

isotropy of the torus. The advantage of the IIA F1-NS5-P frame is that these modes preserve the T^4 isotropy.

IIA supergravity solutions with F1-NS5-P charges, where the momentum is carried by fluctuating D0-D4 density waves. In contrast to all the three-charge horizonless solutions constructed so far, our solutions are $SO(4)$ singlets under rotations on the $\mathbb{R}^4$ base space, exactly as the black hole. Furthermore, these solutions are $\frac{1}{8}$-BPS (4 supercharges) globally, but $\frac{1}{4}$-BPS (8 supercharges) locally, and hence have a vanishing horizon area. But as we explained earlier, the result of our analysis will be a new family of degenerate microstate solutions.

6.3 Construction of the new three-charge solution

Our construction starts from the well-known solution for the F1-P system in Type IIB supergravity in ten dimensions. We then use a series of S-dualities and T-dualities (whose details are presented in Appendix C.1) to arrive at the geometry corresponding to the two-charge NS5-P system with local D0-D4 charges. We then add a fundamental string charge to this system. We do this by applying an S-duality and then a T-duality to the initial frame which results in a system with D5 and P charges. In that duality frame one can add a D1 charge in a straightforward manner. After we add the D1 charge, reversing the last duality chain takes us to the solution we are seeking: One which carries F1-NS5-P charges, has SO(4) spherical symmetry and vanishing horizon area.

6.3.1 Generating an NS5-P solution with local D0-D4 charges

Starting point: the F1-P solution with a non-trivial T^4 profile

The solution in D spacetime dimensions sourced by a fundamental string carrying momentum lies entirely in the NS sector of the theory, and is given by [196, 197]:

$$ds^2 = -\frac{2}{H}\,dv\left[du - \frac{\dot{F}^2(v)}{2}\,(H-1)\,dv + \dot{F}_M(v)\,(H-1)\,dx^M\right] + \delta_{MN}dx^M\,dx^N\,, \tag{6.3.1a}$$

$$B = -\left(1-\frac{1}{H}\right)\left[du\wedge dv + \dot{F}_M(v)\,dv\wedge dx^M\right]\,, \qquad e^{2\phi} = \frac{1}{H}\,, \tag{6.3.1b}$$

with all other fields vanishing. The coordinates u and v define the light-cone directions along the world-sheet of the string. The remaining transverse directions are parameterized by Cartesian coordinates, x_M, with $M = 1,\dots D-2$. The shape of the string is given by profile functions, $F_M(v)$, with the dot denoting the derivative with respect to v. The string sources a warp factor which is a harmonic function, H, in the $D-2$ dimensional transverse space:

$$H \equiv 1 + \frac{Q}{|x_M - F_M(v)|^{D-4}}\,, \tag{6.3.2}$$

where Q is the supergravity charge associated to the fundamental string and is proportional to the ADM mass per unit length [197].

We take the space-time to be ten-dimensional with the topology $\mathbb{R}_t\times\mathbb{R}^4\times S^1(y)\times T^4$. We will refer to the $\mathbb{R}^4$ as the base space, and it will be parameterized by x_i, with $i = 1,2,3,4$, while

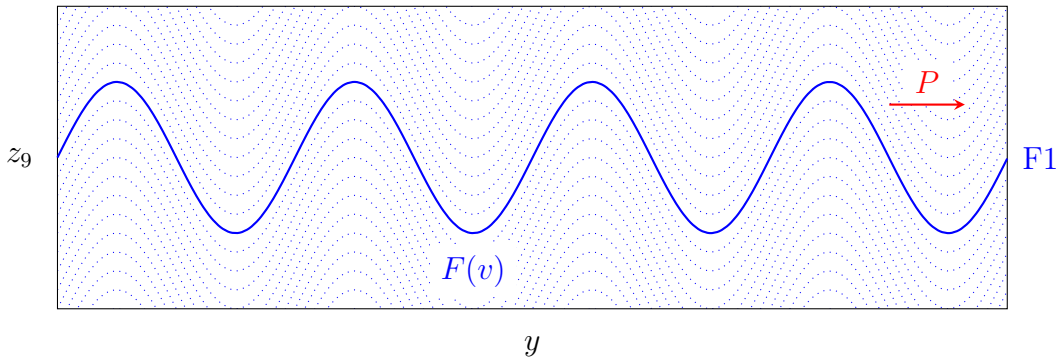

Figure 6.2 – The shape of the fundamental string in the $y - z_9$ plane at a fixed time t. The string is wrapping the y-circle while its profile in the z_9 direction is given by an arbitrary periodic function $F(v)$. The system has a global F1 charge and a global momentum charge, denoted by P. Finally, the profile is smeared on the $S(z_9)$ circle, the smearing process being here depicted with the dotted lines. The non-trivial profile results in local variations of the charges in the z_9 and y directions.

the T^4 will be parameterized by z_a with $a = 6, 7, 8, 9$. We take the radius of the circle $S^1(y)$ to be given by R_y, and the coordinate y is periodically identified with $y \sim y + 2\pi\, R_y$. The null coordinates appearing in (6.3.1) are related to the usual spacetime coordinates through:[8]

$$v = \frac{t+y}{\sqrt{2}}\,, \qquad u = \frac{t-y}{\sqrt{2}}\,. \tag{6.3.3}$$

We choose the momentum-carrying string to wrap the compact y direction and to be localized at the origin of $\mathbb{R}^4$. For simplicity, we take the string to oscillate along one of the directions of the torus, z_9. Since we are interested in a solution that is isotropic along the torus, we smear the string source along the full T^4. The corresponding profile function is

$$F_M(v) = \delta_{Ma}\, c_a + \delta_{M9}\, F(v)\,, \tag{6.3.4}$$

where $F(v)$ is an arbitrary periodic function of period $\sqrt{2}\pi R_y$ and we include constants c_a which are integrated over in the process of smearing. The solution after smearing on the torus (see also Figure 6.2) is

$$ds^2 = -\frac{2}{H_5}\, dv \left[du - \frac{\dot{F}^2(v)}{2}\,(H_5 - 1)\; dv + \dot{F}(v)\;(H_5 - 1)\; dz^9\right] + dx^i\, dx^i + dz^a\, dz^a\,, \tag{6.3.5a}$$

$$B = -\left(1 - \frac{1}{H_5}\right)\left[du \wedge dv + \dot{F}(v)\, dv \wedge dz^9\right]\,, \qquad e^{2\phi} = \frac{1}{H_5}\,, \tag{6.3.5b}$$

where the harmonic function (6.3.2) is now given by[9]

$$H_5(r) = 1 + \frac{Q_5}{r^2}\,, \qquad r^2 = x_i\, x_i\,. \tag{6.3.6}$$

[8] Note that compared to [196, 197], we have rescaled u and v by a factor of $\sqrt{2}$.

[9] The label is added to the harmonic function and to the charge for future convenience.

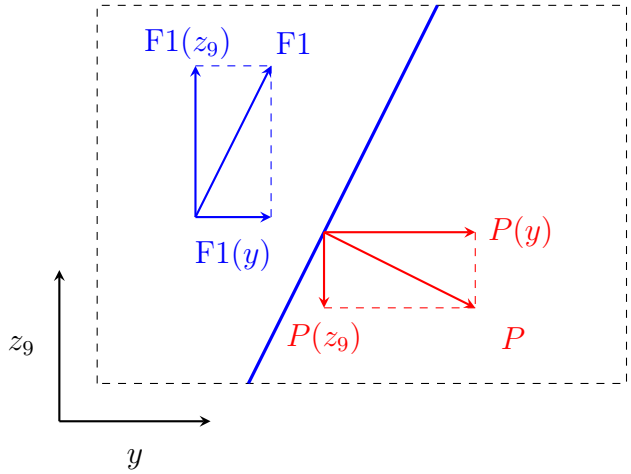

Figure 6.3 – Zoom in on a local piece of the fundamental string presented in Figure 6.2. We decompose the string charge F1 (directed along the string direction) and momentum P (directed transverse to the string) into components along the y and z_9 directions: They source the metric and B-field along these directions. Different charge components transform into different objects upon S and T-dualization.

The profile of the momentum-carrying wave, $F(v)$, is arbitrary in the $y-z_9$ plane, so the system has locally varying F1 and momentum charge densities, which generically source the metric and B-fields with components both along the y-direction and along the z_9-direction. We denote these configurations as F1(y), P(y), and F1(z_9), P(z_9), respectively (see figure 6.3). Since the string does not wind around the z_9 direction, the total value of the P(z_9) and F1(z_9) charges is zero. Only F1(y) and P(y) correspond to charges measured at infinity.

NS5-P solution with local D0-D4 charges

We now perform a series of S-dualities and T-dualities that take us to a solution with global NS5-P charges and local D0-D4 charges. We give here only the duality chain and the explicit expression for the final solution, leaving the solutions obtained at intermediate steps to Appendix C.1.

The duality chain starts from the type-IIB solution in Equation (6.3.5):

$$\begin{pmatrix} \text{F1}(y) \\ P(y) \\ \text{F1}(z_9) \\ P(z_9) \end{pmatrix}_{\text{IIB}} \overset{\text{S}}{\longleftrightarrow} \begin{pmatrix} \text{D1}(y) \\ P(y) \\ \text{D1}(z_9) \\ P(z_9) \end{pmatrix}_{\text{IIB}} \overset{\text{T}(z_9)}{\longleftrightarrow} \begin{pmatrix} \text{D2}(y, z_9) \\ P(y) \\ \text{D0} \\ \text{F1}(z_9) \end{pmatrix}_{\text{IIA}} \overset{\text{T}(z_8,z_7,z_6)}{\longleftrightarrow} \begin{pmatrix} \text{D5}(y, T^4) \\ P(y) \\ \text{D3}(z_6, z_7, z_8) \\ \text{F1}(z_9) \end{pmatrix}_{\text{IIB}}$$
$$\overset{\text{S}}{\longleftrightarrow} \begin{pmatrix} \text{NS5}(y, T^4) \\ P(y) \\ \text{D3}(z_8, z_7, z_6) \\ \text{D1}(z_9) \end{pmatrix}_{\text{IIB}} \overset{\text{T}(z_9)}{\longleftrightarrow} \begin{pmatrix} \text{NS5}(y, T^4) \\ P(y) \\ \text{D4}(T^4) \\ \text{D0} \end{pmatrix}_{\text{IIA}} . \tag{6.3.7}$$

The columns depict the objects appearing in each of the solutions, with the upper two entries denoting the charges that can be seen at infinity while the lower entries denote the local charges (which are the duals of the F1(z_9) and $P(z_9)$ local charges in the solution (6.3.5)). Above the double-headed arrows we write the duality that connects the two solutions, and show the direction along which we T-dualize. The subscripts of the parentheses denote the theory in which the solution exists.

At the end of the chain we obtain a solution corresponding to NS5-branes that wrap all five compact directions, momentum P along the y direction, as well as D4-branes wrapping the T^4 and D0-branes. Note that the solution has arbitrary and equal D0 and D4 charge densities, which can either integrate to finite values or to zero. Since we are trying to construct microstate geometries for the F1-NS5-P black hole, we choose an $F(v)$ profile that does not wind along the z_9 direction, and which gives a solution in which the total D0 and D4 charges vanish.

Following the rules of S-dualities and T-dualities (summarized in Appendix C.2, together with the democratic formalism [198] that we use to present the solution), we find that fields associated with the NS5-P solution with D0-D4 charges are given by

$$ds^2 = -2dv\left[du - \frac{\dot{F}(v)^2}{2}\left(1-\frac{1}{H_5}\right)dv\right] + H_5\, dx^i\, dx^i + dz^a\, dz^a\,, \tag{6.3.8a}$$

$$B_2 = \gamma\,, \qquad e^{2\phi} = H_5\,, \tag{6.3.8b}$$

$$C_1 = -\dot{F}(v)\left(1-\frac{1}{H_5}\right)dv\,, \tag{6.3.8c}$$

$$C_3 = -\dot{F}(v)\,\gamma\wedge dv\,, \tag{6.3.8d}$$

$$C_5 = -\dot{F}(v)\left(1-\frac{1}{H_5}\right)dv\wedge\widehat{\text{vol}}_4 = C_1\wedge\widehat{\text{vol}}_4\,, \tag{6.3.8e}$$

$$C_7 = -\dot{F}(v)\,\gamma\wedge dv\wedge\widehat{\text{vol}}_4 = C_3\wedge\widehat{\text{vol}}_4\,, \tag{6.3.8f}$$

where the two-form γ is defined by

$$d\gamma \equiv *_4 dH_5\,, \tag{6.3.9}$$

and $\widehat{\text{vol}}_4$ denotes the volume form of the torus. One should note that even though we started with a F1-P profile that was not isotropic along the T^4, through the chain of dualities (6.3.7) we arrive at (6.3.8) where the torus only appears through its volume form.

It is useful to note that our solution exhibits the expected features. The harmonic function H_5 appears in the solution in the way one expects for an NS5-brane: it multiplies the part of the metric that is transverse to the brane, it shows up in the expression for the dilaton (which diverges as one approaches the NS5-brane), and it determines the NS-NS two form which is sourced magnetically by the NS5-brane (see (6.3.9)). The solution also has non-vanishing momentum, which can be read off from the g_{vv} component of the metric. This momentum arises from the non-trivial profile function, $F(v)$, which also enters in the expression of the Ramond-Ramond gauge fields. Since the local contribution to the momentum of the solution is proportional to $\dot{F}(v)^2$, the total momentum is always positive for any non-constant profile function.

When $F(v)$ is a constant, the solution reduces to that of a stack of NS5-branes at the origin of $\mathbb{R}^4$. When the profile function is linear in v, the solution describes an NS5-brane with constant

D0, D4, and momentum charges. The D0-branes source C_1 electrically and C_7 magnetically, while the D4-branes source C_3 electrically and C_5 magnetically. These gauge fields have the structure $C_{p+4} = C_p \wedge \widehat{\text{vol}}_4$, which is a consequence of the fact that in our solution the D0 and D4 charges are locked and is related to the enhanced supersymmetry one observes when $\dot{F}(v)$ is constant.

It is interesting to observe that the solution with a non-trivial $F(v)$ profile can be written in a much simpler fashion by redefining $\tilde{v} \equiv F(v)$. Since $F(v)$ is periodic, and not monotonic, this re-definition is only locally well-defined, but it allows one to transform (6.3.8) into a solution in which all the fields and metric components except $g_{u\tilde{v}}$ are independent of the choice of profile. Hence, the only difference between the solution with a linear $F(v)$ profile and the v-dependent solution with an arbitrary profile comes from multiplying g_{uv} with an arbitrary function of v. The fact that this multiplication transforms a solution into another solution points to the possible existence of a simple method to add null waves on certain solutions, which we plan to further explore in future work.

6.3.2 Generating the F1-NS5-P solution with local D0-D4 charges

The solution (6.3.8) with a periodic $F(v)$ only has global NS5 and P charges and can be thought of as describing a microstate of the two-charge system. To add a third charge, we add a stack of fundamental strings on top of the NS5-P-D0-D4 solution. These strings will wrap the $S^1(y)$ circle along which the momentum is oriented, and will be smeared along the four-torus. To add this F1 charge we perform a duality chain on the solution in (6.3.8), we transform it to a certain class of D1-D5-P supersymmetric solutions [199], add an extra charge, and dualize back.

The most obvious way to dualize from the Type IIA F1-NS5-P frame to the D1-D5-P frame is to do a T-duality along the y direction, followed by an S-duality. However, this supergravity duality cannot be performed on (6.3.12), except upon smearing the profile $F(v)$, which results in a trivial solution with no v dependence. To preserve the non-trivial v-dependent information, one needs to T-dualize along another isometry direction.

We will use instead an isometry of the transverse space: Rewrite the flat metric on $\mathbb{R}^4$ in the Gibbons-Hawking form [200]

$$dx^i\, dx^i = \frac{1}{V}(d\psi + A)^2 + V\, ds_3^2\,, \tag{6.3.10}$$

where ψ is the Gibbons-Hawking fiber, ds_3^2 is the line-element of flat $\mathbb{R}^3$, V is a scalar function and A a one-form on this three-dimensional space, satisfying the relation $*_3 dA = dV$. Since the Gibbons-Hawking fiber is periodic, one can T-dualize along it without losing information about the local charges along the $S^1(y)$ circle, but at the cost of destroying the asymptotic structure of the solution. However, this does not cause any problems, since we only use this duality as a tool for introducing the F1 charge: The asymptotic behavior is restored after we dualize back to

the original frame. Hence the chain of dualities we consider is

$$\left(\begin{array}{c} \mathrm{NS5}(y,T^4) \\ P(y) \\ \mathrm{D4}(T^4) \\ \mathrm{D0} \\ \hline \mathrm{F1}(y) \end{array}\right)_{\mathrm{IIA}} \overset{\mathrm{T}(\psi)}{\longleftrightarrow} \left(\begin{array}{c} \mathrm{KKM}(y,T^4;\psi) \\ P(y) \\ \mathrm{D5}(T^4,\psi) \\ \mathrm{D1}(\psi) \\ \hline \mathrm{F1}(y) \end{array}\right)_{\mathrm{IIB}} \overset{\mathrm{S}}{\longleftrightarrow} \left(\begin{array}{c} \mathrm{KKM}(y,T^4;\psi) \\ P(y) \\ \mathrm{NS5}(T^4,\psi) \\ \mathrm{F1}(\psi) \\ \hline \mathrm{D1}(y) \end{array}\right)_{\mathrm{IIB}} , \tag{6.3.11}$$

where the $\mathrm{KKM}(y,T^4;\psi)$ denotes a KKM charge with special direction ψ that is distributed along the $S^1(y)$ circle and the torus. Note that the interpretations of these charges is heuristic, since the NS5-brane sits at a fixed point of the isometry of the T-duality along ψ, and the asymptotic structure is singular. Below the line we describe the duality chain for the fundamental string that we want to add to (6.3.8). In the final frame (which is often called the D1-D5 frame and is commonly used in the superstrata constructions) this corresponds to adding a D1-brane wrapped along the y circle. Since all the torus-independent supersymmetric solutions in this frame are perfectly understood [199], we know the precise way in which to add such a D1-brane to the dual of our initial two-charge configuration, and we present the details of the calculation in Appendix C.1.

After adding the D1-brane in the D1-D5 frame (6.3.11) and performing the duality transformations backwards (from right to left), we obtain the following solution describing an F1-NS5-P system with non-trivial D0-D4 density wave, localized at the origin of the flat $\mathbb{R}^4$ base (see also figure 6.4):

$$ds^2 = -\frac{2}{H_1} dv \left[du - \frac{\dot{F}(v)^2}{2} \left(1 - \frac{1}{H_5}\right) dv \right] + H_5\, dx^i\, dx^i + dz^a\, dz^a \,, \tag{6.3.12a}$$

$$B_2 = -\frac{1}{H_1}\, du \wedge dv + \gamma \,, \qquad e^{2\phi} = \frac{H_5}{H_1} \,, \tag{6.3.12b}$$

$$C_1 = -\dot{F}(v) \left(1 - \frac{1}{H_5}\right) dv \,, \tag{6.3.12c}$$

$$C_3 = -\dot{F}(v)\, \gamma \wedge dv \,, \tag{6.3.12d}$$

$$C_5 = -\dot{F}(v) \left(1 - \frac{1}{H_5}\right) dv \wedge \widehat{\mathrm{vol}}_4 = C_1 \wedge \widehat{\mathrm{vol}}_4 \,, \tag{6.3.12e}$$

$$C_7 = -\dot{F}(v)\, \gamma \wedge dv \wedge \widehat{\mathrm{vol}}_4 = C_3 \wedge \widehat{\mathrm{vol}}_4 \,, \tag{6.3.12f}$$

where we have introduced a new harmonic function associated with the F1 charge

$$H_1(r) = 1 + \frac{Q_1}{r^2} \,, \tag{6.3.13}$$

and the two-form γ is defined through (6.3.9). This solution is the main result of our construction. Note that this solution can be simplified locally in the same way as (6.3.8), by redefining the v coordinate as $\tilde{v} = F(v)$ and seeing that all the non-trivial fluctuations along the null direction can be absorbed into a fluctuation of $g_{u\tilde{v}}$.

In the next section we perform a detailed analysis of the this solution and compare it to the three-charge F1-NS5-P black-hole solution.

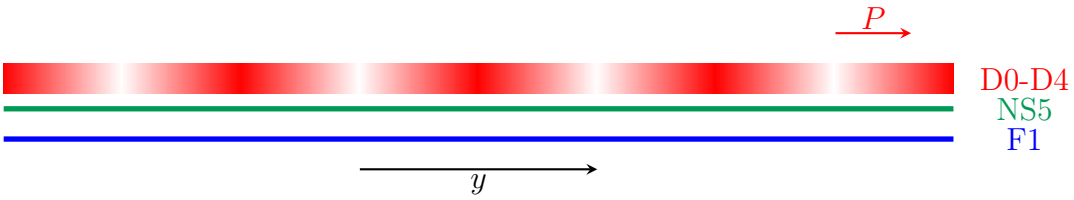

Figure 6.4 – A constant-time snapshot of the periodic y direction at the origin of $\mathbb{R}^4$. We have fundamental strings (F1, blue) and NS5-branes (green) wrapping the y circle with momentum-carrying D0-D4 charges densities (red density plot) living on the world-volume of the NS5-brane. The D0 and D4 charges have the same y (or v) dependence, given by the profile function $F(v)$, which is necessary for the configuration to be supersymmetric.

6.4 Analysis and comparison

In this section we compare the newly obtained three-charge solution (6.3.12) to the three-charge F1-NS5-P black-hole that has a finite-size horizon. We begin by reviewing this black hole, focusing on the behavior of the solution near the horizon. We then perform a similar analysis on the solution constructed above, and compare and contrast the results. We find that, while the two solutions asymptotically look alike, they differ drastically in the near-horizon region. In the black-hole solution the singular source appearing in the harmonic function associated with the momentum is responsible for stabilizing the y-circle thus giving rise to an event horizon with a finite area. This does not happen in the new solution (6.3.12), where the momentum is produced by the fluctuations of the local D0 and D4 charges, whose corresponding function remains finite at the location of the F1 and NS5-brane sources. As a consequence, the y-circle pinches off and the horizon area vanishes. The existence of our solution indicates that if one considers all the degrees of freedom of the system, an event horizon does not form even when the system has no transverse fluctuations.

6.4.1 The F1-NS5-P three-charge black hole

The F1-NS5-P three-charge black hole is obtained by superimposing a stack of NS5-branes (wrapping $S^1(y) \times T^4$) and a stack of F1-strings (wrapping $S^1(y)$), both of which are located at the origin of $\mathbb{R}^4$, and allowing for additional momentum charge in the y direction [201]. This yields the solution:[10]

$$ds^2 = -\frac{2}{H_1}\, dv \left(du + \frac{\mathcal{F}}{2}\, dv \right) + H_5\, dx^i\, dx^i + dz^a\, dz^a\,, \tag{6.4.1a}$$

$$B_2 = -\frac{1}{H_1}\, du \wedge dv + \gamma\,, \qquad e^{2\phi} = \frac{H_5}{H_1}\,, \tag{6.4.1b}$$

with all other fields vanishing.

The harmonic functions associated to the NS5-branes and F1-strings, H_5 and H_1, are given by the expressions (6.3.6) and (6.3.13). Furthermore, the magnetic component of B_2, which is

[10] Throughout section 6.4 we are working with string-frame metrics, unless explicitly stated otherwise.

sourced by the NS5-branes is given by the expression (6.3.9). The harmonic function associated to the momentum, $\mathcal{F}$, has a δ-function source at the origin of $\mathbb{R}^4$, whose strength is proportional to the momentum charge as measured at spatial infinity, Q_P:

$$\mathcal{F} = -\frac{2\,Q_P}{r^2}\,. \tag{6.4.2}$$

In the backreacted solution, there is an event horizon at $r = 0$. To calculate its area one needs to look at the size of the orthogonal dimensions as one approaches it. One can show that the radius of the $S^1(y)$ circle at an arbitrary value of r is

$$R_y(r) = \sqrt{\frac{Q_P + r^2}{Q_1 + r^2}}\,R_y\,, \tag{6.4.3}$$

where, as before, R_y denotes the value of this radius at infinity. We can see that the y-circle remains finite in size as we approach the horizon at $r = 0$. Combining this with the finite size of the S^3 of the $\mathbb{R}^4$, we find that (6.4.1) has a non-zero horizon area. This is a direct consequence of the stabilization of the $S^1(y)$ circle at the location of the horizon, caused by the balancing between the effect of the momentum, which exerts a centrifugal force towards a large radius, and the tension of the branes wrapping the circle, which try to shrink it. In the absence of momentum ($Q_P = 0$), one can see from (6.4.3) that the $S^1(y)$ circle wrapped by the NS5-branes and F1-strings pinches off as $r \to 0$ and thus the horizon area vanishes.

Finally, we note that the metric is actually smooth at the horizon, and it can be smoothly continued across it. As one would expect, the curvature invariants remain finite:

$$R = -20\frac{Q_1 - Q_5}{Q_1\,Q_5^2}\,r^2 + \mathcal{O}\left(r^3\right)\,, \tag{6.4.4a}$$

$$R_{\mu\nu}\,R^{\mu\nu} = \frac{24}{Q_5^2} + \mathcal{O}\left(r^2\right)\,, \tag{6.4.4b}$$

$$R_{\mu\nu\rho\sigma}\,R^{\mu\nu\rho\sigma} = \frac{24}{Q_5^2} + \mathcal{O}\left(r^2\right)\,. \tag{6.4.4c}$$

6.4.2 The new three-charge solution with local D0-D4 charges

We can write the metric of our new solution (6.3.12) as

$$ds^2 = -\frac{2}{H_1}dv\left[du - \frac{\dot{F}(v)^2}{2}\left(1 - \frac{1}{H_5}\right)dv\right] + H_5\,dx^i\,dx^i + dz^a\,dz^a\,, \tag{6.4.5a}$$

$$= \frac{1}{H_1}\left[-dt^2 + dy^2 + \frac{\dot{F}(v)^2}{2}\left(1 - \frac{1}{H_5}\right)(dt + dy)^2\right] + H_5\,dx^i\,dx^i + dz^a\,dz^a\,, \tag{6.4.5b}$$

where we used (6.3.3) to obtain the second line. If the harmonic functions H_1 and H_5 contain a constant, the geometry is asymptotically flat $\mathbb{R}^{4,1} \times S_y \times T^4$. The main difference with the black hole comes from the behavior of the g_{vv} component of the metric, which contains the information about the momentum of the system. In contrast to (6.4.1), this metric does not contain a freely

choosable harmonic function, $\mathcal{F}$, with an independent charge Q_P. Rather, the momentum is encoded in the profile $F(v)$ and the combination $(1 - H_5^{-1})$, which, as already mentioned, is finite everywhere in the base space. This is because the momentum is carried in a fundamentally different way compared to the black-hole solution. The finiteness of $(1-H_5^{-1})$ suggests an absence of a localized source for the momentum. This is in conflict with the naive "NS5 world-volume intuition," according to which the momentum is sourced by longitudinal fluctuations of the D0 and D4 densities inside the NS5-brane world-volume, and hence it should also be sourced at the location of the NS5-brane. Of course, the NS5 world-volume intuition ignores back-reaction, so it is not the appropriate intuition for the the full supergravity solution. But it is rather puzzling that other aspects of this world-volume intuition are described correctly in supergravity, while this particular aspect is not.

The asymptotics

Despite the absence of a singular source, one can calculate the value of the momentum along the y direction in this solution from the asymptotic expansion [202, 155]:

$$g_{vv} \approx \frac{1}{r^2}\left(2Q_P + \textit{oscillating terms}\right) + \mathcal{O}\left(r^{-3}\right) . \tag{6.4.6}$$

Thus we can read off

$$g_{vv} = \frac{\dot{F}(v)^2}{H_1}\left(1 - \frac{1}{H_5}\right) \approx \frac{Q_5\,\dot{F}(v)^2}{r^2} + \mathcal{O}\left(r^{-3}\right) , \tag{6.4.7}$$

from which we extract the non-oscillating part by averaging over the y-circle:

$$Q_P = \frac{Q_5}{2}\frac{1}{\sqrt{2}\pi R_y}\int_0^{\sqrt{2}\pi R_y} \dot{F}(v)^2\, dv\,. \tag{6.4.8}$$

Note that if the profile function admits a decomposition as a Fourier sum

$$F(v) = R_y\, a_0 + R_y \sum_{n=1}^{\infty}\left[\frac{a_n}{n}\cos\left(\frac{\sqrt{2}nv}{R_y}\right) + \frac{b_n}{n}\sin\left(\frac{\sqrt{2}nv}{R_y}\right)\right] , \tag{6.4.9}$$

then one can evaluate the integral in (6.4.8) and obtain

$$Q_P = \frac{Q_5}{2}\sum_{n=1}^{\infty}\left(a_n^2 + b_n^2\right) . \tag{6.4.10}$$

Thus, different solutions in the family we constructed (6.3.12), parameterized by different profile functions $F(v)$, have the same asymptotic momentum charge, Q_P, as the black hole (6.4.8). However, while the g_{vv} component of the black-hole solution only contains a harmonic function proportional to Q_P

$$g_{vv}^{\rm BH} = \frac{1}{H_1}\frac{2\,Q_P}{r^2}\,, \tag{6.4.11}$$

the metric of our solutions deviate from that of the black hole at higher order in the asymptotic expansion in r, because of the $(1 - H_5^{-1})$ term in g_{vv} (6.4.7):

$$g_{vv}(v) = \frac{\dot{F}(v)^2}{H_1}\left(\frac{Q_5}{r^2} - \frac{Q_5^2}{r^4} + \mathcal{O}\left(r^{-6}\right)\right) . \tag{6.4.12}$$

Averaging (6.4.12) over v suggests that the higher multipoles of our solutions may be different from those of the black hole:

$$\langle g_{vv}\rangle_v \equiv \frac{1}{\sqrt{2}\pi R_y}\int_0^{\sqrt{2}\pi R_y} g_{vv}(v)\, dv = \frac{1}{H_1}\left(\frac{2\,Q_P}{r^2} - \frac{2\,Q_5\,Q_P}{r^4} + \mathcal{O}\left(r^{-6}\right)\right) . \tag{6.4.13}$$

Hence, our solution deviates from the black-hole metric via $\frac{Q_5 Q_P}{r^4}$ and higher terms in g_{vv}, which indicates that the momentum wave of the microstructure in the backreacted solution develops a finite size. This will be further confirmed in Section 6.4.2.

The vanishing-area horizon

Much like in the two-charge F1-NS5 solution, one finds that g_{tt} goes to zero at $r = 0$, the location of the pole of the brane harmonic functions. Furthermore, the curvature invariants are finite at this point and are equal to those of the F1-NS5 two-charge solution[11] and those of the F1-NS5-P three-charge black hole (6.4.4). The crucial difference comes from behavior of the length of the y-circle near the brane sources, which we calculate using (6.4.5)

$$L_y = \sqrt{\frac{2}{H_1}}\int_0^{\sqrt{2}\pi R_y}\sqrt{1 + \frac{\dot{F}(v)^2}{2}\left(1 - \frac{1}{H_5}\right)}\, dv \approx r\sqrt{\frac{2}{Q_1}}\int_0^{\sqrt{2}\pi R_y}\sqrt{1 + \frac{\dot{F}(v)^2}{2}}\, dv\,, \tag{6.4.14}$$

where we have expanded around $r = 0$. Since the integrand is a strictly positive function, we find that near the origin the y-circle pinches off, despite the fact that the solution has a non-trivial momentum along that direction. One can show that, as $r \to 0$, all other dimensions are finite in size.[12] Therefore, (6.3.12) has a singularity that can be thought of as a zero-area horizon. This is the same type of singularity as in the F1-NS5 or D1-D5 two-charge solutions. Our new solution is thus very peculiar: For a non-trivial profile $F(v)$, we can see from (6.4.8) that it contains momentum along with F1 and NS5 charges, making it a three-charge solution. On the other hand, one can see from (6.4.14) that the y-circle shrinks at the origin, which gives rise to a singularity of the type present in two-charge solutions.

[11] One should remember that the near-brane limit of the two-charge solution is, locally, like Poincaré $AdS_3 \times S^3$, and so the curvature invariants are all well-behaved. What makes the solution singular is the fact that the S^1 pinches off in the $r \to 0$ limit, where g_{tt} also vanishes.

[12] One can show that the three-sphere which appears in the base space has an area of $\text{Area}(S^3) = 2\pi^2\left(r^2 H_5\right)^{\frac{3}{2}} \approx 2\pi^2 Q_5^{\frac{3}{2}}$, where we have expanded near $r = 0$. Furthermore, the volume of the T^4 is independent of r and is taken to be finite. Then the string-frame area of the would-be horizon is $A_H = L_y\,\text{Area}(S^3)\,\text{Vol}(T^4)$, which vanishes as one approaches the brane sources because of the pinching of the y-circle.

The near-horizon behavior - a first pass

There exist two ways to analyze the near-horizon behavior of the solution. One can, as we discuss in this subsection, focus on the region where

$$r^2 \ll Q_1, Q_5 \,. \tag{6.4.15}$$

By expanding (6.3.12) in small r, one can probe the solution in the vicinity of the brane sources. The expansion of the metric is, up to order $\mathcal{O}(r^2)$, given by:

$$ds^2 = \sqrt{\frac{Q_5}{Q_1}}\left[-\frac{2\,r^2}{\sqrt{Q_1\,Q_5}}\,dv\left(du - \frac{\dot{F}^2(v)}{2}dv\right) + \frac{\sqrt{Q_1\,Q_5}}{r^2}\,dr^2 + \sqrt{Q_1\,Q_5}\,d\Omega_3^2\right] + d\hat{s}_4^2\,, \tag{6.4.16}$$

which is locally $\mathrm{AdS}_3 \times S^3 \times T^4$, as can be seen more explicitly by introducing a new coordinate

$$w \equiv u - \int \frac{\dot{F}(v)^2}{2}\,dv\,, \qquad dw = du - \frac{\dot{F}(v)^2}{2}\,dv\,. \tag{6.4.17}$$

Thus, near the brane sources, the solution is locally simply empty AdS. The transformation (6.4.17) removes the metric component $g_{vv} \propto \dot{F}^2(v)\,r^2$, which is the only term in the near-horizon region sensitive to $\dot{F}^2(v)$. This metric component vanishes at $r \to 0$, but grows as r^2 with increasing radius. Therefore, it does not vanish at the boundary of AdS_3 ($r \to \infty$), but corresponds to a non-trivial deformation of the boundary metric.

The growing behavior of g_{vv} as one is increasing the radius implies that the momentum is not localized in the interior of the AdS region. Since the asymptotically-flat solution (6.3.12) contains non-vanishing momentum charge, the momentum wave must be located in the transition zone between the AdS_3 near-horizon region and the flat space region. This explains why our new solution has a momentum that can be measured at infinity (6.4.8), despite the absence of a no momentum-charge source at $r = 0$. Indeed, as can be seen from figure 6.5, which depicts the g_{vv} for arbitrary values of r, (6.4.16) captures only the leading near-horizon behavior but fails to capture the asymptotic fall-off. Furthermore, in the string frame the maximum of g_{vv} is located at $r^2 = \sqrt{Q_1\,Q_5}$, providing further evidence that the momentum wave is localized in the transition region between AdS_3 and flat space.

Finally, let us note that the metric (6.4.16) does not correspond to the results from the heuristic method of taking a near-horizon limit by "dropping the 1" in the harmonic functions. This method gives a metric which has an additional term:

$$ds^2 = \sqrt{\frac{Q_5}{Q_1}}\left[-\frac{2\,r^2}{\sqrt{Q_1\,Q_5}}\,dv\left(dw + \frac{\dot{F}^2(v)\,r^2}{2\,Q_5}dv\right) + \frac{\sqrt{Q_1\,Q_5}}{r^2}\,dr^2 + \sqrt{Q_1\,Q_5}\,d\Omega_3^2\right] + d\hat{s}_4^2\,, \tag{6.4.18}$$

where we have used the shifted coordinate (6.4.17). This metric corresponds holographically to a deformation of $\mathrm{AdS}_3 \times S^3 \times T^4$ with a non-normalizable mode corresponding to an irrelevant operator of the dual CFT. Furthermore, the metric is no longer locally AdS: the additional term in g_{vv} that scales as r^4 and diverges at the boundary of AdS cannot be reabsorbed by a coordinate transformation.

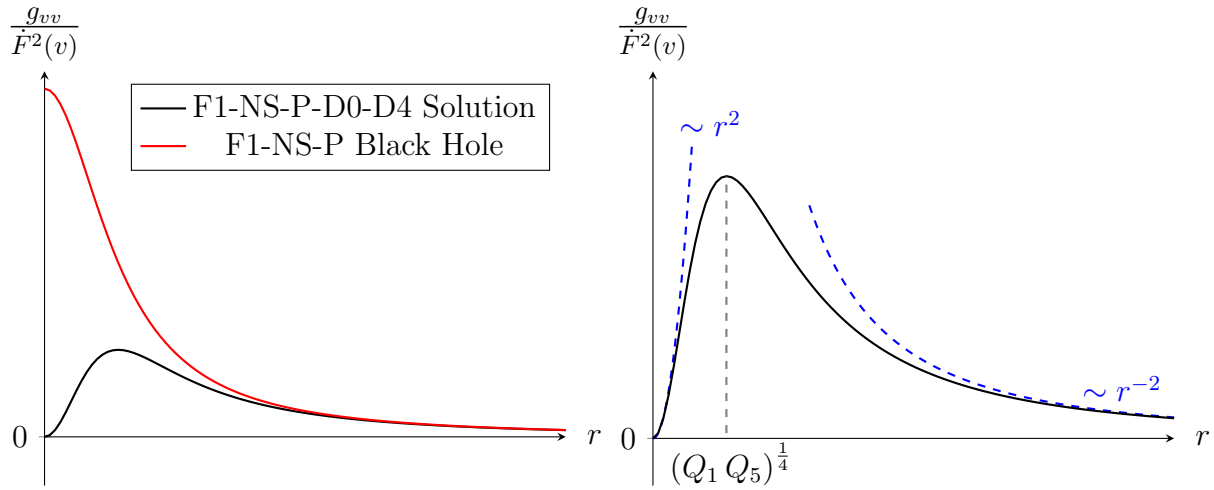

Figure 6.5 – The schematic behavior of the metric component g_{vv} as a function of the radial coordinate. On the left is the plot of the exact expression (modulo the $\dot{F}^2(v)$ function) for the new F1-NS5-P-D0-D4 solution (6.4.7) (black) and the F1-NS5-P black hole (red). The momentum charge of the latter is taken to be such that the asymptotic behavior of the two solutions match. In the bulk the two solutions differ significantly: At $r = 0$ the black hole has a finite value for g_{vv} which is related to the finite size of the horizon, while in the new solution this metric component vanishes and the $S^1(y)$ circle pinches off. On the right, we have a close-up of the solution with local D0-D4 charges, superposed with the asymptotic and near-brane behavior in blue. The momentum is localized away from the brane sources, with the maximum at $r^2 = \sqrt{Q_1\,Q_5}$.

This deformation of the metric is accompanied by a non-vanishing deformation of the RR gauge fields:

$$C_1 = \left(1 - \frac{r^2}{Q_5}\right) \dot{F}(v)\, dv\,, \qquad C_3 = -Q_5\, \dot{F}(v)\, \gamma' \wedge dv\,, \tag{6.4.19}$$

and all higher order forms can be obtained by using the self-duality conditions (C.2.3). In C_3 we have used the fact that when writing $\mathbb{R}^4$ in spherical coordinates, $d\gamma = *_4 dH_5 = 2Q_5\,\mathrm{vol}\left(S^3\right)$. Thus it is convenient to define a new, "bare", two-form γ' such that $d\gamma' \equiv 2\,\mathrm{vol}\left(S^3\right)$. It then naturally follows that C_3 remains unchanged in the near-horizon expansion, since it is independent of the radial coordinate. Finally, the NS-NS gauge field is the same as in the standard decoupling limit and the corresponding field strength supports the $\mathrm{AdS}_3 \times S^3$ structure.

The near-horizon behavior - a second pass

Another way of decoupling the near-horizon region from the asymptotically flat region and obtain a background that is holographically dual to the low-energy physics of a brane system is to take a double-scaling limit [152] involving α' and the transverse radial direction. To do this we need to first express the charges appearing in the supergravity solution, Q_1 and Q_5, in terms of the

moduli and the quantized numbers of F1 strings, N_1, and NS5-branes, N_5:

$$Q_1 = \frac{g_s^2\,\alpha'^3}{V_4}\,N_1\,, \qquad Q_5 = \alpha'\,N_5\,, \tag{6.4.20}$$

where g_s is the string coupling constant, α' is the Regge slope, and V_4 is the coordinate volume of the four-torus divided by $(2\pi)^4$. The double scaling limit is [152]

$$\alpha' \to 0\,, \qquad U \equiv \frac{r}{\alpha'} = \text{fixed}\,, \qquad v_4 \equiv \frac{V_4}{\alpha'^2} = \text{fixed}\,, \qquad g_6 \equiv \frac{g_s}{\sqrt{v_4}} = \text{fixed}\,, \tag{6.4.21}$$

and it yields the ten-dimensional string frame metric:

$$\frac{ds^2}{\alpha'} = N_5\left[-\frac{2\,U^2}{g_6^2\,N_1\,N_5}\,dv\left(du - \frac{\dot{F}^2(v)}{2}dv\right) + \frac{dU^2}{U^2}\,dU^2 + d\Omega_3^2\right] + dz^a\,dz^a\,. \tag{6.4.22}$$

This result is consistent with the near-brane expansion of the metric (6.4.16), provided one makes the substitutions $Q_1 \to g_6^2\,N_1$ and $Q_5 \to N_5$. Thus, as before, the metric in the decoupling limit corresponds to locally empty AdS, with a deformation that is non-trivial at the asymptotic boundary. Performing the same scaling on the gauge fields in the solution (6.3.12), one finds that the NS-NS two-form becomes such that the corresponding field strength is comprised of a part proportional to the volume form of AdS_3 and a part proportional to the volume form of S^3. On the other hand, the RR gauge fields C_p are such that all field strengths, F_{p+1}, vanish in this limit.

It is important to note that the double scaling limit (6.4.21) and the near-brane expansion considered in (6.4.16) lose all information about the harmonic function H_5 appearing in g_{vv} and about the nontrivial RR fields of the solution. It is interesting to try to construct a decoupling limit which does not erase this information. It is not hard to see that such a limit combines (6.4.21) with a scaling of the null coordinates defined in (6.4.17), while keeping fixed

$$d\tilde{v} \equiv \sqrt{\alpha'}dv = \text{fixed}\,, \qquad d\tilde{w} \equiv \frac{dw}{\sqrt{\alpha'}} = \text{fixed}\,. \tag{6.4.23}$$

This results in a metric[13]

$$\frac{ds^2}{\alpha'} = N_5\left[-\frac{2\,U^2}{g_6^2\,N_1\,N_5}\,d\tilde{v}\left(d\tilde{w} + \frac{\dot{F}^2(\tilde{v})\,U^2}{2\,N_5}d\tilde{v}\right) + \frac{dU^2}{U^2} + d\Omega_3^2\right] + dz^a\,dz^a\,, \tag{6.4.24}$$

corresponding to a non-trivial deformation of $\mathrm{AdS}_3 \times S^3 \times T^4$. We also find the non-trivial RR gauge fields

$$C_1 = -\frac{U^2}{N_5}\,\dot{F}(\tilde{v})\,d\tilde{v}\,, \qquad C_3 = -N_5\,\dot{F}(\tilde{v})\,\gamma' \wedge d\tilde{v}\,, \tag{6.4.25}$$

where in writing the latter expression we again used the two-form γ', as defined in (6.4.19). All higher-order forms can be obtained from these by using the democratic formalism. It is

[13]Note that despite the scaling (6.4.23) we keep $\dot{F}(v)$ fixed. This can be achieved by scaling $F(v)$ in a way which cancels out the scaling of v coming from the differentiation.

interesting to observe that despite the non-trivial scaling of the coordinates $\tilde{w}$ and $\tilde{v}$, the final result matches the one obtained by simply "dropping the 1" in the harmonic functions (6.4.18), if one appropriately identifies coordinates and moduli of the two solutions.

Finally, let us note that the same results can be obtained by another scaling limit which is more commonly used in the F1-NS5-P system [90, 91, 203]. Begin by defining dimensionless coordinates $\tilde{u} \equiv u/R_y$ and $\tilde{v} \equiv v/R_y$. Then one takes the AdS_3 decoupling limit[14] by scaling $g_s \to 0$ and $R_y \to \infty$, while keeping fixed the supergravity charges, Q_1 and Q_5, the coordinates $\tilde{u}$, $\tilde{v}$, and r/g_s, and the remaining string moduli. In practice, we can implement this limit by making the replacements [91]

$$r \to \epsilon\, r\,, \qquad R_y \to \frac{R_y}{\epsilon}\,, \tag{6.4.26}$$

followed by sending $\epsilon \to 0$.[15] One finds that the resulting metric is exactly equal to (6.4.16), obtained by the near-brane expansion of the full asymptotically flat geometry. If, on the other hand, one first performs the transformation (6.4.17), defines $\tilde{w} \equiv w/R_y$, and, in addition to (6.4.26), scales

$$\tilde{w} \to \epsilon\, \tilde{w}\,, \qquad \tilde{v} \to \frac{\tilde{v}}{\epsilon}\,, \tag{6.4.27}$$

then the $\epsilon \to 0$ limit yields the solution obtained by "dropping the 1" in the Harmonic functions (6.4.24).

6.4.3 Supersymmetries and singularities

Since our NS5-P-D0-D4 solution is a dual of the F1-P string, it must have eight supersymmetries, which are identical to the common supersymmetries preserved by NS5-branes and a momentum wave. Moreover, if one zooms in locally, the function, $F(v)$, becomes approximately linear in v, and the resulting solution has 16 supersymmetries. One can also confirm this by directly calculating the brane projectors, like in [49]. Alternatively, this can be seen by noting that such a linear solution comes from dualizing a tilted fundamental string boosted orthogonally, or equivalently, by uplifting to 11 dimensions, where the linear system becomes an M5-brane with orthogonal momentum, as depicted in Figure 6.1. Both such configurations preserve 16 supersymmetries.

It is natural to ask how the NS5-P-D0-D4 solution can preserve the same supersymmetries as the NS5-P system, despite the presence of D0 and D4 densities. This is achieved because the D0 and D4 densities have the same distribution on the $S^1(y)$-circle, which makes their joint contribution to the supersymmetry projector compatible with the Killing spinors preserved by NS5-branes and momentum. This phenomenon was observed in the construction of the

[14] For the F1-NS5-P system there exists an additional linear-dilaton region [33] which is obtained by taking only $g_s \to 0$ while keeping the ratio r/g_s fixed. As can be seen from (6.4.20), this limit focuses on the region of spacetime where $Q_1 \ll r^2 \ll Q_5$. We are interested in the scaling which accesses the region (6.4.15), which is achieved by the scaling described in the main text. We would like to thank David Turton and Soumangsu Chakraborty for helpful discussions on this point.

[15] Again we keep $\dot{F}(v)$ fixed in this scaling.

magnetube [204], and it is not hard to see that if one T-dualizes our solution twice along the D4-brane world-volume, one obtains an NS5-D2-D2-P brane configuration that uplifts to the M5-M2-M2-P magnetube of [204].

Upon adding F1-strings to the NS5-P-D0-D4 solution, the supersymmetry is reduced to half. Thus, the resulting solution has globally four supercharges, but if one zooms near the source (or considers a solution with a linear $F(v)$) the number of supercharges is enhanced to eight. This is consistent with the fact that the singularity in this solution is the same as that of a two-charge single-center solution.

6.5 Conclusion and discussion

The Fuzzball and Microstate Geometry Programmes exist precisely because string theory and supergravity have a rich variety of degrees of freedom that can be used to evade the formation of horizons. A recent, but illustrative example is the long-term trapping [205] near evanescent ergosurfaces which was believed to lead to Aichelburg-Sexl shockwaves and horizon formation. However, a more detailed analysis showed that this would actually result in scrambling into more and more typical modes of the solution [206]. Furthermore, the extremely long-term trapping needed to create singularities requires sub-stringy wavelengths for the modes [162]. In short, the stringy degrees of freedom are activated before horizons develop and one must explore the full range of supergravity and stringy phase space or one risks mimicking the limitations of General Relativity and concluding that horizons are inevitable.

In this work we examined another manifestation of this phenomenon: In the D1-D5 frame, a family of smooth, three-charge Microstate Geometries (the *superstrata* family) appears to develop a horizon in the limit of vanishing angular momentum ($a \to 0$). We have now given strong evidence that *the horizon only emerges because one has neglected degrees of freedom that are essential in the $a \to 0$ limit*. Indeed, we incorporated some of these degrees of freedom by introducing D0- and D4-brane densities in the Type IIA F1-NS5 frame and showed that these resulted in a solution that has a vanishing horizon area.

We have also understood that reason behind the failure of the naïve intuition according to which $a \to 0$ D1-D5-P superstrata appear to collapse into a black hole. The momentum of these superstrata is only carried by D1 and D5 dipole-charge distributions [195,50] that are compressed to zero size in the $a \to 0$ limit.[16] If one takes into account all possible momentum carriers, no such collapse happens.

Indeed, the D1-D5 configuration on which one builds the microstate geometries comes from dualizing an F1-string with momentum, and since the F1-string only carries momentum waves that are transversely polarized [193], this configuration has finite size. By contrast, we find that NS5-branes can carry momentum also through longitudinal fluctuations, via a non-trivial profile of world-volume fluxes corresponding to D0- and D4-brane densities. It is this fact that allows us to construct 3-charge zero-horizon-area solutions, despite the NS5-branes being localized at a single point in the $\mathbb{R}^4$ base space. Hence, our solutions are $SO(4)$ singlets under rotations on

[16] Furthermore, in bubbling solutions [40,79] the momentum charge comes from the non-trivial dipole fluxes, which also vanish when $a \to 0$.

the $\mathbb{R}^4$, exactly as the usual three-charge black hole solution.

An interesting observation, which only emerges from analyzing the full supergravity solution, is that the momentum "carried" by the D0 and D4 charge densities inside the NS5 world-volume is *not* localized near the NS5-brane source, but resides in the transition region between the near-horizon $\text{AdS}_3 \times S^3$ and the asymptotically flat region. As such, this momentum cannot prevent the $S^1(y)$ wrapped by the F1-strings and the NS5-branes from collapsing at the location of the brane sources, which in turn causes the horizon area to vanish.

As we remarked earlier, there is an important distinction between microstate solutions and degenerate microstate solutions. Both have vanishing horizon area, but the former represent pure states, whereas the latter encode a large number of microstates. The singularities of two-charge solutions, like the F1-NS5 singularity, or the D1-D5 singularity, and the singular core of our F1-NS5-P-D0-D4 solution are, in this sense, degenerate microstate solutions, and their cores represent ensembles of microstates that have neither the charges nor the degrees of freedom to create a macroscopic horizon.

Degenerate microstate solutions are also required to have microstructure that can be understood using string theory. Resolving the microstructure of the singular D1-D5 system was the focus of the original fuzzball program [193, 60]. More recently, our understanding of the microstructure of the F1-NS5 system has been greatly advanced using world-sheet methods [90, 91, 31, 207, 203].

Our work has enriched the "landscape" of superstrata by expanding the range of momentum carriers on the branes. As we have seen, the addition of the D0-D4 excitations reveals how the fuzzball paradigm works even in the singular corners [208, 16, 17] of the moduli space. This also suggests several interesting areas for further investigation: we expect that there are whole new classes of microstate geometries that come from the geometric transition of our degenerate microstate solutions. Another intriguing question is whether there are such transitions that only involve the T^4, and achieve this in a way that preserves the space-time $SO(4)$ invariance and the vanishing angular momentum.

It would also be interesting to see, in detail, how the solutions obtained in this paper emerge as a limit of smooth microstate geometries. In particular, one should be able to construct superstrata, with $a > 0$, that contain both "standard" momentum carriers and D0-D4 momentum carriers. In such a generalized superstratum with $a > 0$, the y-circle should pinch off smoothly, making a smooth cap at the bottom of a long BTZ-like throat. It would be interesting to construct this Type-IIA superstratum with F1-NS5-P charges, and to explore its $a \to 0$ limit and the relation of this limit to the solutions we construct in this paper.

In particular, if there exist Type IIA superstrata that limit to our solutions, there is then the question of what happens to the long BTZ throat. Do our solutions emerge in the center of a cap at the bottom of a long throat, or does the throat become much shallower? Indeed, this is directly related to the results presented in Section 6.4.2, where we showed that in the full supergravity solution, the momentum charge comes from modes localized in the junction between the near-horizon $\text{AdS}_3 \times S^3$ region and the asymptotic flat space. In a generalized superstratum, with D0-D4 momentum carriers and with $a > 0$, we would still expect that, like in the original superstrata, all the momentum waves should localize in a band that creates the transition between the horizonless cap and the long $\text{AdS}_2 \times S^1$ region of the BTZ throat. It

would be very interesting to see whether and how the location of the momentum waves shifts in the $a \to 0$ limit of the generalized superstratum.

Even though our solutions have the same spherical symmetry as a single-center black hole with the same charges, their asymptotic expansions are different. This happens because the momentum is carried by null waves located at the top of the $AdS_3 \times S^3$ throat, and hence there is no limit of our solutions where they approach those of the black-hole solution to arbitrary precision. This makes them different from the usual microstate geometries which have a "scaling" parameter controlling the depth of the throat, that can be tuned so that their metric and the gravitational multipoles approach those of the black hole [120,18]. Our new solutions do not have such a parameter and hence we expect them to have a metric whose asymptotics differs from that of the black-hole solution at higher orders in the radial distance. Furthermore, although the extra fields in our solutions fluctuate along a null coordinate, they all contribute to the metric with the same sign. Hence, even if one considers an ensemble of our new solutions with D0-D4 modes, these features will not average to zero, and the $1/r$-expansion will still differ from that of the black hole.

The location of the momentum also presents a puzzle in terms of the dual CFT picture. As discussed in the introduction, we expect that, in the $a \to 0$ limit, the state dual to the superstratum consists of momentum-carrying $(0,0)$ strands and no $(+,+)$ strands. However, in our solution taking the standard decoupling limit results in a locally $AdS_3 \times S^3 \times T^4$ spacetime, (6.4.22) with a deformation to the metric at the boundary of the spacetime. Furthermore, performing an alternative scaling, one can obtain an $AdS_3 \times S^3 \times T^4$ solution deformed with an non-normalizable momentum-carrying mode dual to an irrelevant deformation of the CFT. If, as mentioned above, in a generalized superstratum one were to find some microstructure at the center of a smooth cap, then there should exists an equivalent description in the dual CFT. Establishing the precise holographic dictionary for both the new microstate solution and potential generalized superstrata, is thus of great interest.

From a technical point of view, constructing generalized superstrata requires solving a new set of non-trivial BPS equations. From the perspective of six-dimensional supergravity, the ten-dimensional fields sourced by the D0 and D4 charge densities are encoded in a U(1) gauge field. Furthermore, the equations governing six-dimensional supersymmetric solutions with tensor and vector gauge fields were derived in [209]. It is important to remember that the construction of the original superstrata relied on the hidden linear structure of the BPS equations of six-dimensional supergravity with tensor fields, but no gauge fields [210, 50]. In a recent paper [211] it has been shown that such a linear structure persists when one adds U(1) gauge fields. This should alleviate some technical issues in the path of constructing smooth geometries in the F1-NS5-P frame.

Finally, in our analysis, we focused only on momentum-carrying modes that preserve the isometry of the T^4. It would be interesting to consider momentum-carrying waves coming from fluctuations of branes along some of the torus directions, and which break this isometry. These fluctuations give rise to U(1) vector fields even in the D1-D5-P duality frame. Furthermore, one can obtain examples of such solutions by performing a 9-11 flip on our solutions with D0-D4 density modes. Thus, the solutions we have constructed provide a simple way to access dynamics of compactification tori, while also preserving the isotropy of the T^4. We therefore expect the D0-D4 fluctuations to provide qualitatively similar results to analyzing more complicated excitations

on the T^4 of IIA or IIB supergravity [62, 212, 213].

Appendix A

Appendix for Chapter 2

A.1 Appendix: Boundedness of the moduli space of 3-centre solutions from the phase space distance

To show that the entire moduli space is bounded using the canonical Δ_{phase}, we will probe the asymptotic behaviour of the metric at all the different facets and vertices of the polytope: the vertex at $(0,0)$, (j_+, j_+) and $(j_+, -j_+)$, and the facets at $x = j_+$, $x - y = 0$ and $x + y = 0$.

The vertex at $(0,0)$ (the scaling limit). This instance has already been studied in the subsection 2.4.2.

The facets $x - y = 0$ and $x + y = 0$. Given $x_F \in (0, j_+)$, we approach any point $M_F(x_F, \pm x_F)$ on the facets by a straight horizontal line from a point $M_0(x_0, \pm x_F)$ in the bulk. On the path, at the point $M(x, \pm x_F)$,

$$G_{xx} \underset{M \to M_F}{\sim} \frac{j_+ x_F - x_F^2}{2(j_+ - x_F)x_F} \frac{1}{x - x_F} = \frac{1}{2(x - x_F)} \tag{A.1.1}$$

giving a square-root behaviour to the path distance

$$\Delta(M_F, M_0) \underset{M_0 \to M_F}{\sim} \sqrt{2(x_0 - x_F)}\,. \tag{A.1.2}$$

Therefore the distance in moduli space is finite.

Note that this computation does not take into account the scaling-limit point, as we used $x_F \neq 0$ in our equations.

The facet $x = j_+$. Given $y_F \in (-j_+, j_+)$, we approach any point $M_F(j_+, y_F)$ on the facet by a straight horizontal line from a point $M_0(x_0, y_F)$ in the bulk. On the path, at the point $M(x, y_F)$,

$$G_{xx} \underset{M \to M_F}{\sim} \frac{1}{2(j_+ - x)} \tag{A.1.3}$$

gives a square root behaviour to the path distance

$$\Delta(M_F, M_0) \underset{M_0 \to M_F}{\sim} \sqrt{2(j_+ - x)}\,. \tag{A.1.4}$$

Therefore the geodesic distance in moduli space is finite.

The vertex at (j_+, j_+). We approach this limit from the point M_0 of coordinates $(j_+ - r_0 \cos\alpha,\, j_+ - r_0 \sin\alpha)$, with $\alpha \in (\pi/4, \pi/2)$. Near the vertex, the metric behaves like

$$G_{ij} \frac{\mathrm{d}x^i}{\mathrm{d}r} \frac{\mathrm{d}x^j}{\mathrm{d}r} \underset{r \to 0}{\sim} \frac{\sin\alpha}{2r}\,, \tag{A.1.5}$$

so the path length is finite.

The vertex at $(j_+, -j_+)$. We approach this limit from the point M_0 of coordinates $(j_+ - r_0 \cos\alpha, -j_+ + r_0 \sin\alpha)$, with $\alpha \in (\pi/4, \pi/2)$. Near the vertex, the metric also behaves like

$$G_{ij} \frac{\mathrm{d}x^i}{\mathrm{d}r} \frac{\mathrm{d}x^j}{\mathrm{d}r} \underset{r \to 0}{\sim} \frac{\sin\alpha}{2r}\,, \tag{A.1.6}$$

so the path length is finite.

Appendix B

Appendix for Chapter 4

B.1 The almost-BPS ansatz in different dimensions

Our microstate geometries can be dualized to many duality frames, some of which are better suited for their description than others. In particular, in the duality frame in which the charges of the black hole correspond to D1 branes, D5 branes, momentum and KKM charge, some of the supertube centers that appear singular from a four- or five-dimensional perspective are smooth. These IIB solutions on T^4 can be trivially truncated to six-dimensional $\mathcal{N} = (1,0)$ supergravity coupled to one extra tensor multiplet, which then can be reduced to four-dimensional $\mathcal{N} = 2$ supergravity with three extra vector multiplets.

B.1.1 Six-dimensional frame

Six-dimensional $\mathcal{N} = (1,0)$ supergravity coupled to a tensor multiplet has the following bosonic fields coming from the graviton multiplet and the extra tensor multiplet [214–216, 209]:

- A gravitational field $g_{\mu\nu}$.
- 2 two-form gauge fields $B^I_{\mu\nu}$ and their field strengths $G^I = d_6 B^I$.
- 2 scalars v^I in the coset space $SO(1,1)/SO(1)$. It is convenient to group them into a constrained $SO(1,1)$ matrix:

$$\begin{gathered} \mathcal{S} = \begin{pmatrix} v_I \\ x_I \end{pmatrix}, \qquad I = 0,1\ , \\ v_I v^I = 1\,, \qquad v_I v_J - x_I x_J = \eta_{IJ}\,, \qquad v^I x_I = 0\,, \end{gathered} \tag{B.1.1}$$

  where the scalar indices, I or J, are raised by the $SO(1,1)$ Minkowski metric in light-cone coordinates with the mostly-minus signature,

$$\eta = \begin{pmatrix} 0 & 1 \\ 1 & 0 \end{pmatrix}. \tag{B.1.2}$$

The scalars are involved in the tensor dynamics through the metric

$$\mathcal{M}_{IJ} \,=\, \big(\eta\mathcal{S}^T\mathcal{S}\eta\big)_{IJ} \,=\, v_I v_J \,+\, x_I x_J \,=\, 2\, v_I v_J \,-\, \eta_{IJ}\,,$$

which dictates the twisted self-duality conditions of the tensors

$$\mathcal{M}_{IJ} G^J \,=\, \eta_{IJ} \star_6 G^J\,. \tag{B.1.3}$$

This implies that the tensor $v_I G^I$ is self-dual and belongs to the gravity multiplet whereas the tensor $x_I G^I$ is anti self-dual and belongs to the tensor multiplet. One can write down a "pseudo-action" [215, 209]

$$(16\pi G_6)\, S_6 \,=\, \int d^6x\,\sqrt{-g}\,\left(R \,-\, \eta_{IJ}\,\partial_\mu v^I \partial_\mu v^J \,-\, \frac{1}{3}\mathcal{M}_{IJ}\, G^I_{\mu\nu\rho} G^{J\,\mu\nu\rho}\right)\,, \tag{B.1.4}$$

The dynamics of the solutions of the action given in (B.1.4) is governed by the following Einstein-Maxwell-scalar equations [215, 209][1]

$$\begin{aligned} R_{\mu\nu} \,+\, \partial_\mu v^I \partial_\nu v_I \,-\, \mathcal{M}_{IJ}\, G^I_{\mu\alpha\beta} G_\nu^{J\alpha\beta} \,&=\, 0\,,\\ x_I^M\, d_6 \star_6 d_6 v^I \,+\, 4\, x_I^M v_J\, G^I \wedge \star_6 G^J \,&=\, 0\,,\\ d_6 G^I \,&=\, 0\,. \end{aligned} \tag{B.1.5}$$

We work with the floating-brane ansatz [148] that encompasses BPS and almost-BPS solutions. The axisymmetric solutions we consider have three spatial isometries and a flat three-dimensional base. The two isometries are parametrized by the coordinate y and the angle ψ, whereas the flat space is parameterized by the spherical coordinates (ρ, θ, ϕ):

$$\begin{aligned} v^1 \,&=\, \sqrt{\frac{Z_2}{2Z_1}}\,, \qquad G^1 \,=\, \frac{1}{\sqrt{2}}\left[\star_4 d_4 Z_2 \,-\, d_6\left(\sqrt{\frac{Z_2}{Z_1}}(dt+\omega)\wedge(dy+\beta)\right) \,+\, (dy+\beta)\wedge\Theta^1\right]\,,\\ v^2 \,&=\, \sqrt{\frac{Z_1}{2Z_2}}\,, \qquad G^2 \,=\, \frac{1}{\sqrt{2}}\left[\star_4 d_4 Z_1 \,-\, d_6\left(\sqrt{\frac{Z_1}{Z_2}}(dt+\omega)\wedge(dy+\beta)\right) \,+\, (dy+\beta)\wedge\Theta^2\right]\,,\\ ds_6^2 \,&=\, -\frac{1}{Z_3\sqrt{Z_1 Z_2}}\,(dt+\omega)^2 \,+\, \sqrt{Z_1 Z_2}\, ds_4(\mathcal{B})^2 \,+\, \frac{Z_3}{\sqrt{Z_1 Z_2}}(dy+\beta-Z_3^{-1}(dt+\omega))^2\,, \end{aligned} \tag{B.1.6}$$

where $ds_4(\mathcal{B})^2$ is a Gibbons-Hawking metric

$$ds_4(\mathcal{B})^2 \,=\, V^{-1}(d\psi - w^0)^2 \,+\, V\left(d\rho^2 + \rho^2(d\theta^2 + \sin^2\theta\, d\phi^2)\right)\,, \qquad \star_3 d_3 w^0 \,=\, \pm\, d_3 V \tag{B.1.7}$$

and we have defined

$$\omega \,=\, \mu(d\psi - w^0) \,+\, \varpi\,, \qquad \beta \,=\, K^3\,(d\psi - w^0) + w^3\,, \qquad \Theta_a \,=\, d_4\left(K^a\,(d\psi - w^0) + w^a\right)\,. \tag{B.1.8}$$

The "$\pm$" for the connection w^0 corresponds to different choice of orientation that leads to different types of solution. In our conventions the minus sign gives supersymmetric solutions while the plus sign gives almost-BPS solutions [115, 116].

[1] We used the self-duality condition to simplify the equations. This also reduces the usual Maxwell equations for the tensor fields to the Bianchi identity.

B.1.2 Five-dimensional frame

The STU model can be embedded in five-dimensional $\mathcal{N}=2$ supergravity coupled to two extra vector multiplets. It can be obtained from a KK reduction along y of the six-dimensional frame studied above [217] or more generically from the low-energy limit of M theory on T^6 [218].

Five-dimensional $\mathcal{N}=2$ supergravity coupled to 2 vector multiplets has the following bosonic-field content:

- One gravitational field $g_{\mu\nu}$.
- Three U(1) vector gauge fields A^I_μ and their field strengths $F^I = d_5 A^I$. One is coming from the graviton multiplet and is usually referred as the "graviphoton" and the others come from the extra vector multiplets.
- Three scalars X^I in the symmetric space $SO(1,1)\times(SO(1,2)/SO(2))$.

One can write down the five-dimensional action for the bosonic fields [219, 220]

$$(16\pi G_5)\, S_5 \;=\; \int d^5x\,\sqrt{-g}\,R \;-\; Q_{IJ}\int \left(F^I\wedge\star_5 F^J - d_5X^I\wedge\star_5 d_5X^J\right) \;+\; \frac{|\epsilon_{IJK}|}{6}\int A^I\wedge F^J\wedge F^K\,, \tag{B.1.9}$$

where ϵ_{IJK} is the antisymmetric Levi-Civita tensor and the coupling Q_{IJ} depends on the scalars via [219, 220]

$$Q_{IJ} \;=\; \frac{9}{2}\,X_IX_J - \frac{1}{2}\,|\epsilon_{IJK}|X^K\,. \tag{B.1.10}$$

The dynamics of solutions of the action given in (B.1.9) is governed by the following Einstein-Maxwell-scalar equations [77]

$$\begin{aligned} R_{\mu\nu} \;+\; Q_{IJ}\left(\partial_\mu X^I\partial_\nu X^J \;+\; F^I_{\mu\rho}\,F^{J\rho}_\nu \;-\; \frac{1}{6}\,g_{\mu\nu}\,F^I_{\rho\sigma}\,F^{J\rho\sigma}\right) \;&=\; 0\,,\\ d_5\left(Q_{IJ}\;\star_5 F^J\right) \;+\; \frac{1}{4}\,C_{IJK}\,F^J\wedge F^K \;&=\; 0\,,\\ -d_5\star_5\,d_5X_I \;+\; \left(C_{IJK}X_LX^K - \frac{1}{6}C_{ILJ}\right)\left(F^L\wedge\star_5F^J - dX^L\wedge\star_5 dX^J\right) \;&=\; 0\,. \end{aligned} \tag{B.1.11}$$

In the floating-brane ansatz [148], we have

$$\begin{aligned} X_I \;&=\; \frac{Z_I}{(Z_1Z_2Z_3)^{1/3}} \;=\; (X^I)^{-1}\,, \qquad F^I \;=\; d_5A^I \;=\; d_5\left(-\frac{dt+\varpi}{Z_I} + \left(K^I - \frac{\mu}{Z_I}\right)\left(d\psi - w^0\right) + w^I\right)\,,\\ ds_5^2 \;&=\; -\left(Z_1Z_2Z_3\right)^{-\frac{2}{3}}\left(dt + \mu\left(d\psi - w^0\right) + \varpi\right)^2 \;+\; \left(Z_1Z_2Z_3\right)^{\frac{1}{3}}\,ds(\mathcal{B})^2\,, \end{aligned} \tag{B.1.12}$$

where $ds(\mathcal{B})^2$ is the Gibbons-Hawking metric (B.1.7).

B.1.3 Four-dimensional frame and the STU model

The further reduction along the ψ isometry direction leads to four-dimensional $\mathcal{N}=2$ supergravity coupled to three vector multiplets. Now, there are four gauge fields, $\mathcal{A}^\Lambda$, for $\Lambda=\{0,I\}=\{0,1,2,3\}$,

with one belonging to the supergravity multiplet ($\mathcal{A}^0$ is induced by the metric fibration along ψ in five dimensions). The four-dimensional metric for the floating-brane ansatz takes the form

$$\begin{aligned} ds_4^2 &= -\mathcal{I}_4{}^{-\frac{1}{2}}\ (dt+\varpi)^2 \,+\, \mathcal{I}_4{}^{\frac{1}{2}}\, ds_3^2\,, \\ \mathcal{I}_4 &= Z_1 Z_2 Z_3 V - \mu^2 V^2\,. \end{aligned} \tag{B.1.13}$$

We have three complex scalars

$$z^I \,=\, K^I - \frac{\mu}{Z_I} \,-\, i\,\frac{\sqrt{\mathcal{I}_4}}{V Z_I}\,, \tag{B.1.14}$$

Then, the four gauge fields are

$$\mathcal{A}^0 \,=\, \frac{\mu V^2}{\mathcal{I}_4}\,(dt+\varpi) \,+\, w^0\,, \qquad \mathcal{A}^I \,=\, -\frac{V}{\mathcal{I}_4\, Z_I}\left(Z_1 Z_2 Z_3 - \mu V K^I Z_I\right)\,(dt+\varpi) \,+\, w^I\,. \tag{B.1.15}$$

More generally, the reduction to four dimensions leads to the four-dimensional STU model, for a Lagrangian of the form

$$\mathcal{L}_4 = \frac{1}{2}R - g_{IJ}\partial_\mu z^I \partial^\mu \bar{z}^J + \frac{1}{8}\mathcal{I}_{\Lambda\Sigma}F^\Lambda_{\mu\nu}F^{\Sigma\mu\nu} + \frac{1}{8}\mathcal{R}_{\Lambda\Sigma}F^\Lambda_{\mu\nu}\,(*_4 F)^{\Sigma\mu\nu} \tag{B.1.16}$$

with $(*_4 F)_{\mu\nu} = \frac{1}{2}\sqrt{-g}\epsilon_{\mu\nu\rho\sigma}F^{\rho\sigma}$ and $F^\Lambda = d\mathcal{A}^\Lambda$. Relabelling the scalar fields as $z^I = \{S = \sigma - is, T = \tau - it, U = v - iu\}$, the metric of the scalar σ -model g_{IJ} follows from the Kähler potential

$$\mathcal{K} = -\log(8stu) \tag{B.1.17}$$

the gauge kinetic couplings are

$$\mathcal{I} = -stu\begin{pmatrix} 1+\frac{\sigma^2}{s^2}+\frac{\tau^2}{t^2}+\frac{v^2}{u^2} & -\frac{\sigma}{s^2} & -\frac{\tau}{l^2} & -\frac{v}{u^2} \\ -\frac{\sigma}{s^2} & \frac{1}{s^2} & 0 & 0 \\ -\frac{\tau}{l^2} & 0 & \frac{1}{t^2} & 0 \\ -\frac{v}{u^2} & 0 & 0 & \frac{1}{u^2} \end{pmatrix} \tag{B.1.18}$$

and the axionic couplings are

$$\mathcal{R} = \begin{pmatrix} 2\sigma\tau v & -\tau v & -\sigma v & -\sigma\tau \\ -\tau v & 0 & v & \tau \\ -\sigma v & v & 0 & \sigma \\ -\sigma\tau & \tau & \sigma & 0 \end{pmatrix} \tag{B.1.19}$$

We are interested in computing electric and magnetic charges in four dimensions, which requires us to compute the electromagnetic dual of $\mathcal{A}^\Lambda$, $\mathcal{A}_\Lambda$. From the Lagrangian, we see that the dual field strength is not simply given by the Hodge star of F. Instead, we have

$$G_\Lambda \,=\, d\mathcal{A}_\Lambda \,=\, \mathcal{R}_{\Lambda\Sigma}\, F^\Sigma \,-\, \mathcal{I}_{\Lambda\Sigma}\, *_4\, F^\Sigma\,. \tag{B.1.20}$$

One can then rewrite the STU Lagrangian with the dual field and obtain a more usual Maxwell term, with a trivial electric coupling:

$$\mathcal{L}_4 = \frac{1}{2}R - g_{IJ}\partial_\mu z^I \partial^\mu \bar{z}^J + \frac{1}{8}F^\Lambda_{\mu\nu}\left(*_4 G_\Lambda\right)^{\mu\nu} \tag{B.1.21}$$

This non-trivial electromagnetic duality gives a non-standard charge lattice obtained from

$$\Gamma = -\frac{1}{4\pi}\int_{S^2_\infty}\mathcal{F} = \begin{pmatrix} q_0 \\ q_I \\ p^I \\ p^0 \end{pmatrix}, \tag{B.1.22}$$

where S^2_∞ is the asymptotic two-sphere parametrized by θ and ϕ and where

$$\mathcal{F}_{\mu\nu} = \begin{pmatrix} G_{\Lambda\mu\nu} \\ F^\Lambda_{\mu\nu} \end{pmatrix}. \tag{B.1.23}$$

Thus, we need to compute the value of $\mathcal{A}_\Lambda$ as well. We have

$$\mathcal{A}_\Lambda \,=\, \zeta_\Lambda(dt + \varpi) \,+\, v_\Lambda\,, \tag{B.1.24}$$

where the important parts encoding the electric charges, v_Λ, are present in the expressions of the tensors of the six-dimensional solution described above.

The magnetic charges p^Λ and the electric charges q_λ are obtained by integrating:

$$p^\Lambda \,=\, -\frac{1}{4\pi}\int_{S^2_\infty} d\mathcal{A}^\Lambda \,=\, -\frac{1}{4\pi}\int_{S^2_\infty} dw^\Lambda\,, \qquad q_\lambda \,=\, -\frac{1}{4\pi}\int_{S^2_\infty} d\mathcal{A}_\Lambda \,=\, -\frac{1}{4\pi}\int_{S^2_\infty} dv_\Lambda\,. \tag{B.1.25}$$

B.1.4 Equations of motion

The almost-BPS solutions are stationary solutions governed by the following reduced equations of motion

$$\begin{aligned}
&d\star_3 dZ_I \;=\; \frac{|\epsilon_{IJK}|}{2}\,V\,d\star_3 d(K^J K^K)\,, \qquad && d(\mu V) \,-\, \star_3 d\varpi \;=\; V Z_I\, dK^I\,,\\
&\star_3\, dw^0 \;=\; dV\,, && \star_3 dw^I \;=\; K^I\, dV - V\, dK^I,\\
&\star_3\, dv_0 \;=\; Z_I dK_I - K_I dZ_I \,+\, V d(K^1K^2K^3) - K^1K^2K^3\, dV\,,\\
&\star_3\, dv_I \;=\; dZ_I \,-\, \frac{|\epsilon_{IJK}|}{2}\left(V d(K^J K^K) - K^J K^K\, dV\right),
\end{aligned} \tag{B.1.26}$$

where ϵ_{IJK} is the three-dimensional Levi-Civita tensor and $\star_3$ is the Hodge star in the three-dimensional flat base. When considering more general $U(1)^N$ supergravities in five dimensions and the four-dimensional reductions thereof, $|\epsilon_{IJK}|$ is replaced by the corresponding symmetric tensor C_{IJK}.

By resolving these equations, one can extract the four-dimensional metric (B.1.13), the three scalars, z^I (B.1.14), the four gauge fields, $\mathcal{A}^\Lambda$ (B.1.15), and their duals $\mathcal{A}_\Lambda$ (B.1.24), using the fact that [116]

$$\begin{aligned}\zeta_0 &= \mathcal{I}_4{}^{-1}\left[Z_1Z_2Z_3-\mu V\left(VK^1K^2K^3+\sum_I Z_IK^I\right)+V\sum_{J<K}K^JK^KZ_JZ_K\right],\\ \zeta_I &= \mathcal{I}_4{}^{-1}\left[Z_I\left(\mu-\sum_{J\neq I}K^JZ_J\right)+\frac{|\epsilon_{IJK}|}{2}V\mu K^JK^K\right].\end{aligned} \tag{B.1.27}$$

B.2 Almost-BPS black hole: details

To complement the presentation of the metric of the almost-BPS black hole in the four-dimensional frame on section 4.3.1, we give the relevant expressions for the gauge fields and scalars. We have considered a single-center solution given by

$$V = h+\frac{Q_0}{\rho}, \qquad Z_I = \frac{1}{h}+\frac{Q_I}{\rho}, \qquad K^I = 0, \qquad \mu V = m_\infty+\alpha\frac{\cos\theta}{\rho^2}, \qquad \varpi = -\alpha\frac{\sin^2\theta}{\rho}d\phi. \tag{B.2.1}$$

The equations of motion (B.1.26) are solved by

$$\varpi = -\alpha\frac{\sin^2\theta}{\rho}d\phi, \quad w^0 = Q_0\cos\theta\,d\phi, \quad w^I = 0, \quad v_0 = 0, \quad v_I = Q_I\cos\theta\,d\phi. \tag{B.2.2}$$

Scalars

The three scalars are given by (B.1.14), which gives for the almost-BPS black hole:

$$z^I = -\frac{m_\infty\rho^2+\alpha\cos\theta}{(Q_0+h\rho)\left(Q_I+\frac{\rho}{h}\right)}-i\frac{\Delta}{(Q_0+h\rho)\left(Q_I+\frac{\rho}{h}\right)}, \tag{B.2.3}$$

where Δ has been defined in (4.3.3).

Gauge fields

The gauge fields are given by the generic equation (B.1.15), which for the black hole gives[2]

$$\begin{aligned}\mathcal{A}^0 &= Q_0\cos\theta\,d\phi+\frac{(m_\infty\rho^2+\alpha\cos\theta)(Q_0+h\rho)}{\Delta^2}\left(\rho\,dt-\alpha\sin^2\theta\,d\phi\right)-hm_\infty\,dt,\\ \mathcal{A}^I &= -\frac{Q_0+h\rho}{\Delta^2}\prod_{J\neq I}(Q_J+\frac{\rho}{h})\left(\rho\,dt-\alpha\sin^2\theta\,d\phi\right)+h^{-1}\,dt.\end{aligned} \tag{B.2.4}$$

[2]Note that we have gauged away the irrelevant asymptotics of the gauge fields by adding $-hm_\infty dt$ and $h^{-1}dt$ to $\mathcal{A}^0$ and $\mathcal{A}^I$ respectively.

Using (B.1.24), we can also derive the dual gauge fields, $\mathcal{A}_\Lambda$:

$$\begin{aligned}\mathcal{A}_0 &= \frac{\prod_I(Q_I+\frac{\rho}{h})}{\Delta^2}\left(\rho\,dt-\alpha\sin^2\theta\,d\phi\right)-h^{-3}\,dt\,,\\ \mathcal{A}_I &= Q_I\,\cos\theta\,d\phi+\frac{(m_\infty\,\rho^2+\alpha\,\cos\theta)(Q_I+\frac{\rho}{h})}{\Delta^2}\left(\rho\,dt-\alpha\sin^2\theta\,d\phi\right)-h^{-1}m_\infty\,dt\,.\end{aligned} \tag{B.2.5}$$

B.3 Axisymmetric almost-BPS multicenter solutions in Taub-NUT

In this section, we review the solutions derived in [67] for axisymmetric multi-center configurations in Taub-NUT where the centers are at positions a_j on the z axis of the $\mathbb{R}^3$ base, $j=1...n$. We consider the Taub-NUT harmonic function sourced at the center of the $\mathbb{R}^3$ spherical coordinates (ρ,θ,ϕ):

$$V\;=\;h+\frac{Q_0}{\rho}\,,\qquad w^0\;=\;Q_0\,\cos\theta\,d\phi\,.$$

We assume that the centers that source the vector fields are all distinct from the Taub-NUT center, $a_j\neq 0$. The shifted spherical coordinates around the j^{th} center, (ρ_j,θ_j,ϕ), are given by

$$\rho_j\;=\;\sqrt{\rho^2+a_j^2-2\rho\,a_j\,\cos\theta}\qquad\cos\theta_j\;=\;\frac{\rho\cos\theta-a_j}{\rho_j}\,. \tag{B.3.1}$$

We will sometimes use the index $j=0$ to denote the Taub-NUT center $(\rho_0,\theta_0)=(\rho,\theta)$ and $a_0=0$. We proceed step by step by solving first the magnetic field strengths before the warp factors and the angular momentum one-form. We end the discussion by deriving the regularity constraints.

- The anti-self dual magnetic two-forms Θ^I:

The two-form field strengths, Θ^I, are given by (B.1.8) with $\Theta^3 = d\beta$. We will assume for simplicity that the K^I are harmonic with no constant terms and no source at the Taub-NUT center

$$K^I = \sum_{j=1}^{n} \frac{k_I^{(j)}}{\rho_j} \,. \tag{B.3.2}$$

For axisymmetric center configurations, we have

$$*_3 dw^I = K^I dV - V dK^I \qquad \Rightarrow \qquad w^I = -\sum_{j=1}^{n} k_I^{(j)} \Big(h \cos\theta_j + Q_0 \, \frac{\rho - a_j \cos\theta}{\rho_j \, a_j} \Big) d\phi \,. \tag{B.3.3}$$

- The warp factors Z_I:

The warp factors, Z_I, are determined by the harmonic equations with quadratic sources (B.1.26). For axisymmetric centers in Taub-NUT, the generic solutions are

$$Z_I = L_I + \frac{|\epsilon_{IJK}|}{2} \sum_{j,k=1}^{n} \Big(h + \frac{Q_0 \, \rho}{a_j a_k} \Big) \frac{k_J^{(j)} k_K^{(k)}}{\rho_j \rho_k} \,. \tag{B.3.4}$$

The functions L_I are the electric harmonic functions one can freely add to the Z_I:

$$L_I = l_I^\infty + \frac{Q_I^{(0)}}{\rho} + \sum_{j=1}^{n} \frac{Q_I^{(j)}}{\rho_j} \,.$$

- The angular momentum one-form ω:

The last equation of the first line in (B.1.26) determines the two components, μ and ϖ, of the angular momentum one-form, ω. The source terms are

$$\begin{aligned} V Z_I d_3 K^I &= \sum_{j=1}^{n} l_I^\infty k_I^{(j)} \left(h \, s_j^{(1)} + Q_0 \, s_j^{(2)} \right) + \sum_{j=1}^{n} Q_I^{(j)} k_I^{(j)} \left(h \, s_j^{(3)} + Q_0 \, s_j^{(4)} \right) \\ &+ \sum_{i=0}^{n} \sum_{j=1, j\neq i}^{n} Q_I^{(i)} k_I^{(j)} \left(h \, s_{ij}^{(5)} + Q_0 \, s_{ij}^{(6)} \right) + \frac{|\epsilon_{IJK}|}{2} \sum_{i,j,k=1}^{n} k_I^{(i)} k_J^{(j)} k_K^{(k)} \left(h^2 \, s_{ijk}^{(7)} + Q_0^2 \, s_{ijk}^{(8)} + h Q_0 \, s_{ijk}^{(9)} \right) \,. \end{aligned} \tag{B.3.5}$$

where we have defined 9 generating functions, $s^{(\alpha)}$,

$$\begin{aligned} & s_j^{(1)} \equiv d_3 \left(\frac{1}{\rho_j} \right) , \qquad s_j^{(2)} \equiv \frac{1}{\rho} d_3 \left(\frac{1}{\rho_j} \right) , \qquad s_j^{(3)} \equiv \frac{1}{\rho_j} d_3 \left(\frac{1}{\rho_j} \right) , \qquad s_j^{(4)} \equiv \frac{1}{\rho \, \rho_j} d_3 \left(\frac{1}{\rho_j} \right) , \\ & s_{ij}^{(5)} \equiv \frac{1}{\rho_i} d_3 \left(\frac{1}{\rho_j} \right) , \qquad s_{ij}^{(6)} \equiv \frac{1}{\rho \, \rho_i} d_3 \left(\frac{1}{\rho_j} \right) , \qquad s_{ijk}^{(7)} \equiv \frac{1}{\rho_i \, \rho_j} d_3 \left(\frac{1}{\rho_k} \right) + \text{perm.} \,, \\ & s_{ijk}^{(8)} \equiv \frac{1}{a_i \, a_j \rho_i \, \rho_j} d_3 \left(\frac{1}{\rho_k} \right) + \text{perm.} \,, \qquad s_{ijk}^{(9)} \equiv \left(\frac{1}{\rho} + \frac{\rho}{a_i \, a_j} \right) \frac{1}{\rho_i \, \rho_j} d_3 \left(\frac{1}{\rho_k} \right) + \text{perm.} \,. \end{aligned} \tag{B.3.6}$$

We define the corresponding pairs of solutions $(f^{(\alpha)},\, t^{(\alpha)})$ that solve

$$d_3\, f^{(\alpha)} \,-\, \star_3 d_3\, t^{(\alpha)} \;=\; s^{(\alpha)}\,.$$

One can also freely add the pair of solution $(f^{(10)},\, t^{(10)})$ of the homogeneous equation

$$f^{(10)} \;=\; M\,, \qquad \star_3 d_3 t^{(10)} \;=\; d_3 M\,, \tag{B.3.7}$$

where M is a harmonic function that generically takes the form

$$M \;=\; m_\infty \,+\, \frac{m^{(0)}}{\rho} \,+\, \alpha\frac{\cos\theta}{\rho^2} \,+\, \sum_{j=1}^{n}\frac{m^{(j)}}{\rho_j} \,+\, \alpha_j\frac{\cos\theta_j}{\rho_j^2}\,, \tag{B.3.8}$$

which leads to

$$t^{(10)} \;=\; \varpi_0\, d\phi \,+\, m^{(0)}\cos\theta\, d\phi \,-\, \alpha\,\frac{\sin^2\theta}{\rho}\, d\phi \,+\, \sum_j\left(m^{(j)}\cos\theta_j - \alpha_j\,\frac{\rho^2\sin^2\theta_j}{\rho_j^3}\right) d\phi \tag{B.3.9}$$

Solving for each generating functions $s^{(\alpha)}$ gives

$$\begin{aligned}
&f_j^{(1)} \;=\; \frac{1}{2\,\rho_j}\,, \qquad t_j^{(1)} \;=\; -\frac{1}{2}\cos\theta_j\, d\phi\,, \qquad f_j^{(2)} \;=\; \frac{1}{2\,\rho\,\rho_j}\,, \qquad t_j^{(2)} \;=\; -\frac{1}{2}\,\frac{\rho - a_j\cos\theta}{a_j\,\rho_j}\, d\phi\,,\\
&f_j^{(3)} \;=\; \frac{1}{2\,{\rho_j}^2}\,, \qquad t_j^{(3)} \;=\; 0\,, \qquad f_j^{(4)} \;=\; \frac{\cos\theta}{2\,a_j\,{\rho_j}^2}\,, \qquad t_j^{(4)} \;=\; -\frac{\rho\,\sin^2\theta}{2\,a_j\,{\rho_j}^2}\, d\phi\,,\\
&f_{ij}^{(5)} \;=\; \frac{1}{2\,\rho_i\,\rho_j}\,, \qquad t_{ij}^{(5)} \;=\; \frac{\rho^2 + a_i a_j - (a_i + a_j)\rho\cos\theta}{2(a_i - a_j)\rho_i\rho_j}\, d\phi\,, \qquad f_{ijk}^{(7)} \;=\; \frac{1}{\rho_i\rho_j\rho_k}\,, \qquad t_{ijk}^{(7)} \;=\; 0\,,\\
&f_{ij}^{(6)} \;=\; \frac{\rho^2 + a_i a_j - 2a_j\rho\cos\theta}{2\,a_j\,(a_i - a_j)\rho\rho_i\rho_j}\,, \qquad t_{ij}^{(6)} \;=\; \frac{\rho\,(a_i + a_j\cos 2\theta) - \left(\rho^2 + a_i a_j\right)\cos\theta}{2a_j(a_j - a_i)\rho_i\rho_j}\, d\phi\,,\\
&f_{ijk}^{(8)} \;=\; \frac{\rho\,\cos\theta}{a_i a_j a_k\rho_i\rho_j\rho_k}\,, \qquad t_{ijk}^{(8)} \;=\; -\frac{\rho^2\sin^2\theta}{a_i a_j a_k\rho_i\rho_j\rho_k}\, d\phi\,,\\
&f_{ijk}^{(9)} \;=\; \frac{\rho^2\,(a_i + a_j + a_k) + a_i a_j a_k}{2a_i a_j a_k\,\rho\,\rho_i\rho_j\rho_k}\,,\\
&\qquad t_{ijk}^{(9)} \;=\; -\frac{\rho^3 \,+\, \rho\,(a_i a_j + a_i a_k + a_j a_k) - \left(\rho^2(a_i + a_j + a_k) + a_i a_j a_k\right)\,\cos\theta}{2a_i a_j a_k\,\rho_i\rho_j\rho_k}\, d\phi\,,
\end{aligned} \tag{B.3.10}$$

The complete expression for μ and ϖ is then

$$\begin{aligned}
\mu \;=\; &\sum_{j=1}^{n}\frac{l_I^\infty k_I^{(j)}}{2\rho_j} + \sum_{j=1}^{n}\frac{Q_I^{(j)}k_I^{(j)}}{2V\rho_j^2}\Big(h + \frac{Q_0\cos\theta}{a_j}\Big) + \sum_{i=0}^{n}\sum_{j=1,j\neq i}^{n}\frac{Q_I^{(i)}k_I^{(j)}}{2V\rho_i\rho_j}\Big(h + Q_0\frac{\rho^2 + a_i a_j - 2a_j\rho\cos\theta}{a_j(a_i - a_j)\,\rho}\Big)\\
&+ \sum_{i,j,k=1}^{n}\frac{k_1^{(i)}k_2^{(j)}k_3^{(k)}}{V\rho_i\rho_j\rho_k}\Big(h^2 + {Q_0}^2\,\frac{\rho\cos\theta}{a_i a_j a_k} + hQ_0\frac{\rho^2(a_i + a_j + a_k) + a_i a_j a_k}{2a_i a_j a_k\rho}\Big) + \frac{M}{V}\,,
\end{aligned} \tag{B.3.11}$$

$$\varpi \;=\; -\sum_{j=1}^{n}\frac{l_I^\infty k_I^{(j)}}{2}\Big(h\cos\theta_j + Q_0\frac{\rho - a_j\cos\theta}{a_j\rho_j}\Big)d\phi - \sum_{j=1}^{n}Q_I^{(j)}k_I^{(j)}\frac{Q_0\,\rho\sin^2\theta}{2a_j\rho_j^2}d\phi$$

$$+\sum_{i=0}^{n}\sum_{j=1,j\neq i}^{n}\frac{Q_I^{(i)}k_I^{(j)}}{2(a_i-a_j)\rho_i\rho_j}\Big(h(\rho^2+a_ia_j-(a_i+a_j)\rho\cos\theta) \tag{B.3.12}$$
$$-Q_0\frac{\rho(a_i+a_j\cos 2\theta)-(\rho^2+a_ia_j)\cos\theta}{a_j}\Big)d\phi$$
$$-\sum_{i,j,k=1}^{n}\frac{k_1^{(i)}k_2^{(j)}k_3^{(k)}}{a_ia_ja_k\rho_i\rho_j\rho_k}\Big({Q_0}^2\rho^2\sin^2\theta$$
$$+hQ_0\frac{\rho^3+\rho(a_ia_j+a_ia_k+a_ja_k)-(\rho^2(a_i+a_j+a_k)+a_ia_ja_k)\cos\theta}{2}\Big)d\phi$$
$$+\varpi_0\,d\phi+m^{(0)}\cos\theta\,d\phi-\alpha\frac{\sin^2\theta}{\rho}\,d\phi+\sum_{j=1}^{n}\left(m^{(j)}\cos\theta_j-\alpha_j\frac{\rho^2\sin^2\theta_j}{\rho_j^3}\right)d\phi\,.$$

- The electric one-forms v^Λ:

Since we are interested in the profile of the solutions in four dimensions, we need to derive the electromagnetic dual gauge fields A_Λ (B.1.24). For this purpose we need to integrate the equations for the one-forms v_Λ (B.1.26). We first decompose the source terms by defining some generating functions:

$$\begin{aligned}
\star_3 d_3 v_I &= Q_I^{(0)}\,\star_3\,d_3T^{(0)}+\sum_{j=1}^{n}Q_I^{(j)}\,\star_3\,d_3T_j^{(1)}+\frac{|\epsilon_{IJK}|}{2}\sum_{j,k=1}^{n}\frac{Q_0k_J^{(j)}k_K^{(k)}}{a_ja_k}\,\star_3\,d_3T_{jk}^{(3)}\,,\\
\star_3 d_3 v_0 &= l_I^\infty\sum_{j=1}^{n}k_I^{(j)}\,\star_3\,d_3T_j^{(1)}+Q_I^{(0)}\sum_{j=1}^{n}k_I^{(j)}\,\star_3\,d_3T_j^{(2)}+\sum_{j,k=1}^{n}Q_I^{(j)}k_I^{(k)}\,\star_3\,d_3T_{jk}^{(4)} \qquad \text{(B.3.13)}\\
&\quad+\frac{|\epsilon_{IJK}|}{6}\sum_{i,j,k=1}^{n}Q_0k_I^{(i)}k_J^{(j)}k_K^{(k)}\,\star_3\,d_3T_{ijk}^{(5)}\,,
\end{aligned}$$

where $T^{(0)}$, $T_j^{(1)}$, $T_j^{(2)}$, $T_{jk}^{(3)}$, $T_{jk}^{(4)}$ and $T_{ijk}^{(5)}$ satisfy

$$\begin{aligned}
\star_3 dT^{(0)} &= d\left(\frac{1}{\rho}\right), \qquad \star_3 dT_j^{(1)} = d\left(\frac{1}{\rho_j}\right), \qquad \star_3 dT_j^{(2)} = \frac{1}{\rho}d\left(\frac{1}{\rho_j}\right)-\frac{1}{\rho_j}d\left(\frac{1}{\rho}\right),\\
\star_3 dT_{jk}^{(3)} &= \left(1-\frac{a_ja_k}{\rho^2}\right)d\left(\frac{\rho}{\rho_j\rho_k}\right), \qquad \star_3 dT_{jk}^{(4)} = \frac{1}{\rho_j}d\left(\frac{1}{\rho_k}\right)-\frac{1}{\rho_k}d\left(\frac{1}{\rho_j}\right), \qquad \text{(B.3.14)}
\end{aligned}$$

$$\begin{aligned}
\star_3 dT_{ijk}^{(5)} &= \left(\frac{1}{a_ia_j}+\frac{1}{\rho^2}-\frac{1}{a_ia_k}-\frac{1}{a_ja_k}\right)\frac{\rho}{\rho_i\rho_j}d\left(\frac{1}{\rho_k}\right)\\
&\quad+\left(\frac{1}{a_ia_k}+\frac{1}{\rho^2}-\frac{1}{a_ia_j}-\frac{1}{a_ja_k}\right)\frac{\rho}{\rho_i\rho_k}d\left(\frac{1}{\rho_j}\right)\\
&\quad+\left(\frac{1}{a_ja_k}+\frac{1}{\rho^2}-\frac{1}{a_ia_j}-\frac{1}{a_ia_k}\right)\frac{\rho}{\rho_j\rho_k}d\left(\frac{1}{\rho_i}\right)\\
&\quad+\left(-\frac{1}{\rho^2}+\frac{1}{a_ia_j}+\frac{1}{a_ia_k}+\frac{1}{a_ja_k}\right)\frac{\rho^2}{\rho_i\rho_j\rho_k}d\left(\frac{1}{\rho}\right).
\end{aligned} \tag{B.3.15}$$

We find

$$
\begin{aligned}
T^{(0)} &= \cos\theta\, d\phi\,, \qquad T^{(1)}_j = \cos\theta_j\, d\phi\,, \qquad T^{(2)}_I = \frac{\rho - a_j\cos\theta}{a_j\,\rho_j}\, d\phi\,,\\
T^{(3)}_{jk} &= \frac{(\rho^2 + a_j a_k)\cos\theta - (a_j + a_k)\rho}{\rho_j\rho_k}\, d\phi\,, \qquad T^{(4)}_{jk} = \frac{\rho^2 + a_j a_k - (a_j + a_k)\rho\cos\theta}{(a_k - a_j)\,\rho_j\rho_k}\, d\phi\,,\\
T^{(5)}_{ijk} &= \frac{\rho^3 + \rho(a_i a_j + a_i a_k + a_j a_k) - \big(\rho^2(a_i + a_j + a_k) + a_i a_j a_k\big)\cos\theta}{a_i a_j a_k\,\rho_i\rho_j\rho_k}\, d\phi\,.
\end{aligned}
\tag{B.3.16}
$$

Thus, v_0 and v_I are given by

$$
\begin{aligned}
v_I &= Q^{(0)}_I\,\cos\theta\, d\phi + \sum_{j=1}^n Q^{(j)}_I\,\cos\theta_j\, d\phi + \frac{|\epsilon_{IJK}|}{2}\sum_{j,k=1}^n Q_0 k^{(j)}_J k^{(k)}_K\,\frac{(\rho^2 + a_j a_k)\cos\theta - (a_j + a_k)\rho}{a_j a_k\,\rho_j\rho_k}\, d\phi\,,\\
v_0 &= l^\infty_I \sum_{j=1}^n k^{(j)}_I\,\cos\theta_j\, d\phi + Q^{(0)}_I \sum_{j=1}^n k^{(j)}_I\,\frac{\rho - a_j\cos\theta}{a_j\,\rho_j}\, d\phi + \sum_{(j\neq k)=1}^n Q^{(j)}_I k^{(k)}_I\,\frac{\rho^2 + a_j a_k - (a_j + a_k)\rho\cos\theta}{(a_k - a_j)\,\rho_j\rho_k}\, d\phi\\
&\quad + \frac{|\epsilon_{IJK}|}{6}\sum_{i,j,k=1}^n Q_0 k^{(i)}_I k^{(j)}_J k^{(k)}_K\,\frac{\rho^3 + \rho(a_i a_j + a_i a_k + a_j a_k) - \big(\rho^2(a_i + a_j + a_k) + a_i a_j a_k\big)\cos\theta}{a_i a_j a_k\,\rho_i\rho_j\rho_k}\, d\phi\,.
\end{aligned}
\tag{B.3.17}
$$

- The regularity constraints:

The solutions constructed above are regular if:

- The one-form ϖ does not have Dirac-Misner string and must vanish on the z-axis.
- The absence of closed timelike curves requires the positivity of some metric components. It leads to

$$
Z_I\, V \geq 0\,, \qquad \mathcal{I}_4 \equiv Z_1 Z_2 Z_3\, V - \mu^2 V^2 \geq |\varpi|^2\,. \tag{B.3.18}
$$

The first condition implies $n+1$ algebraic equations. One can make these constraints explicit, for example, by solving them with respect to the $n+1$ variables ϖ_0, $m^{(0)}$ and $m^{(i)}$ for $i = 1, \ldots, n$. If one considers, for definiteness, a configuration in which all the poles a_i lie on one side of the Taub-NUT center ($0 < a_1 < \ldots < a_n$), then the regularity constraints are:

$$
\begin{aligned}
\varpi_0 &= Q_0 \sum_{j=1}^n \frac{l^\infty_I k^{(j)}_I}{2a_j} + h\sum_{i=0}^n \sum_{j=1,j\neq i}^n \frac{Q^{(i)}_I k^{(j)}_I}{2(a_j - a_i)} + hQ_0 \sum_{i,j,k=1}^n \frac{k^{(i)}_1 k^{(j)}_2 k^{(k)}_3}{2a_i a_j a_k}\,,\\
m^{(0)} &= -Q_0 \sum_{j=1}^n \frac{l^\infty_I k^{(j)}_I}{2a_j} - h\sum_{j=1}^n \frac{Q^{(0)}_I k^{(j)}_I}{2a_j} + Q_0 \sum_{i=0}^n \sum_{j=1,j\neq i}^n \frac{Q^{(i)}_I k^{(j)}_I}{2a_j(a_j - a_i)} - hQ_0 \sum_{i,j,k=1}^n \frac{k^{(i)}_1 k^{(j)}_2 k^{(k)}_3}{2a_i a_j a_k}\,,\\
m^{(i)} &= \frac{l^\infty_I k^{(i)}_I}{2}\Big(h + \frac{Q_0}{a_i}\Big) + \sum_{j=1}^n \frac{1}{2|a_i - a_j|}\Big[Q^{(j)}_I k^{(i)}_I\Big(h + \frac{Q_0}{a_i}\Big) - Q^{(i)}_I k^{(j)}_I\Big(h + \frac{Q_0}{a_j}\Big)\Big]\\
&\quad + \frac{hQ_0}{2}\Big[\frac{k^{(i)}_1 k^{(i)}_2 k^{(i)}_3}{a_i^3} + \frac{|\epsilon_{IJK}|}{2}\frac{k^{(i)}_I}{a_i}\sum_{j,k=1}^n \mathrm{sign}(a_j - a_i)\mathrm{sign}(a_k - a_i)\frac{k^{(j)}_J k^{(k)}_K}{a_j a_k}\Big] \quad (i \geq 1)\,.
\end{aligned}
\tag{B.3.19}
$$

Those equations are equivalent to the Denef equations or bubble equations [46, 82, 44] but for almost-BPS solutions. The requirement that the quartic invariant be everywhere positive does not translate in a set of algebraic conditions and must be verified for all (ρ, θ).

B.3.1 Three-center solution

For the family of three-center solutions used in the text in section 4.4.1, the one-forms (v_Λ, w^Λ) that encodes the charges of the gauge fields are given by:

$$\begin{aligned}
w^0 &= Q_0 \cos\theta \, d\phi, \qquad w^1 = 0\,, \\
w^2 &= -k^{(2)} \left(h\cos\theta_2 + Q_0 \frac{\rho - a_2\cos\theta}{\rho_2 a_2} \right) d\phi\,, \qquad w^3 = -k^{(3)} \left(h\cos\theta_3 + Q_0 \frac{\rho - a_3\cos\theta}{\rho_3 a_3} \right) d\phi\,, \\
v_0 &= \frac{k^{(2)}}{h}\cos\theta_2\, d\phi + \frac{k^{(3)}}{h}\cos\theta_3\, d\phi - \left(k^{(2)} Q_2^{(3)} - k^{(3)} Q_3^{(2)} \right) \frac{\rho^2 + a_2 a_3 - (a_2+a_3)\rho\cos\theta}{(a_3 - a_2)\,\rho_2\rho_3}\, d\phi\,, \\
v_1 &= Q_1^{(2)}\cos\theta_2\, d\phi + Q_1^{(3)}\cos\theta_3\, d\phi + Q_0 k^{(2)} k^{(3)} \frac{(\rho^2 + a_2 a_3)\cos\theta - (a_2+a_3)\rho}{a_2 a_3\,\rho_2\rho_3}\, d\phi\,, \\
v_2 &= Q_2^{(3)}\cos\theta_3\, d\phi\,, \qquad v_3 = Q_3^{(2)}\cos\theta_2\, d\phi\,.
\end{aligned} \tag{B.3.20}$$

B.4 Multipole moments of multicenter almost-BPS solutions in Taub-NUT

In this section, we will compute the multipole moments of axisymmetric multicenter almost-BPS solutions. Given the expression of the fields Z_I (B.3.4) and μ B.3.11), the procedure constructed in [120] to compute multipole moments of BPS multicenter solutions does not apply here, so in the following we generalize this procedure to almost-BPS multicenter solutions.

B.4.1 Algebra of multipole-decomposable functions

We expand every pole $1/\rho_i$ on the z-axis with the multipole expansion in Legendre polynomials P_l:

$$\frac{1}{\rho_i} = \frac{1}{\sqrt{\rho^2 + a_i^2 - 2ra_i\cos\theta}} = \sum_{l=0}^{\infty} {a_i}^l \frac{P_l(\cos\theta)}{\rho^{l+1}}\,. \tag{B.4.1}$$

Let F be a function such as

$$F = f_\infty + \sum_{l=0}^{\infty} \frac{1}{\rho^{l+1}} \left[P_l(\cos\theta) D_l(F) + (\text{lower harmonics than } P_l(\cos\theta)) \right]\,, \tag{B.4.2}$$

where the "lower harmonics" are comprised of products of Legendre polynomials $P_{l_1}\dots P_{l_m}$ with $\sum_j l_j < l$. In other terms, the polynomial degree of lower harmonic terms $P_{l_1}\dots P_{l_m}$ is at most X^{l-1}. We say that these functions "decompose into a multipole expansion", and will call the class of these functions to be "multipole-decomposable". For instance, a harmonic function G expands as

$$G = g^\infty + \sum_i \frac{g^{(i)}}{\rho_i} = g^\infty + \sum_i g^{(i)} \sum_{l=0}^{\infty} {a_i}^l \frac{P_l(\cos\theta)}{\rho^{l+1}}\,, \tag{B.4.3}$$

so H is multipole-decomposable and its multipole decomposition at order l is $D_l(H) = \sum_i g^{(i)} a_i^l$.

Applied on the vector space of multipole-decomposable functions, the multipole decomposition operator D_l satisfies linearity. When we multiply two multipole-decomposable functions together, at $O(\rho^{-(l+1)})$ we get:

$$(F_A F_B)_{\mathcal{O}(\rho^{-l-1})} = (f_A^\infty D_l(F_B) + f_B^\infty D_l(F_A)) \frac{P_l(\cos\theta)}{\rho^{l+1}} + \frac{\mathcal{LH}_l}{\rho^{l+1}}, \tag{B.4.4}$$

where $\mathcal{LH}_l$ denotes terms with lower harmonics than P_l (which are polynomials in $\cos\theta$ of degree less or equal to $l-1$). Thus, the vector space is an algebra and we read

$$D_l(F_A F_B) = f_A^\infty D_l(F_B) + f_B^\infty D_l(F_A)\,. \tag{B.4.5}$$

To extract the l-th multipole from a generic functional $f(F_1, \ldots, F_N)$ of multipole-decomposable functions F_A, the formula above generalizes to:

$$D_l\left[f(F_1, \ldots, F_N)\right] = \sum_{B=1}^{N} \partial_{f_B^\infty}\left[f(F_1, \ldots, F_N)_\infty\right] D_l(F_B)\,, \tag{B.4.6}$$

where we introduced the notation $f(F_1, \ldots, F_N)_\infty := \lim_{r\to\infty} f(F_1, \ldots, F_N)$ to denote the functional evaluated when the radius r is taken to infinity; this can be thought as a function of the moduli f_A^∞.

B.4.2 Mass multipoles

We want to compute the multipole moments of a class of almost-BPS bubbling multi-center solutions whose four-dimensional metric is:

$$ds^2 = -(\mathcal{Q}(F_I))^{-1/2}(dt+\omega)^2 + (\mathcal{Q}(F_I))^{1/2}\left(d\rho^2 + \rho^2 d\theta^2 + \rho^2 \sin^2\theta d\phi^2\right)\,, \tag{B.4.7}$$

where the warp factor of the four-dimensional solution $\mathcal{Q}(H)$ is given by the expression:

$$\mathcal{Q}(F_1, \ldots, F_N) = Z_1 Z_2 Z_3 V - (\mu V)^2. \tag{B.4.8}$$

In this class of almost-BPS solutions, only five moduli f^∞ are potentially turned on: l_1^∞, l_2^∞, l_3^∞, $h \equiv v^\infty$ and m_∞.[3] Therefore, we will use the following five multipole-decomposable functions

[3] By comparison, the class of BPS solutions in the same STU model will admit in addition the magnetic moduli k_1^∞, k_2^∞, k_3^∞.

$F_I = (Z_1, Z_2, Z_3, V, \mu V)$:

$$
\begin{aligned}
Z_I &= l_I^\infty + \frac{Q_I^{(0)}}{\rho} + \sum_{j=1}^{n} \frac{Q_I^{(j)}}{\rho_j} + \frac{|\epsilon_{IJK}|}{2} \sum_{j,k=1}^{n} \Big(h + \frac{Q_0\,\rho}{a_j a_k}\Big) \frac{k_J^{(j)} k_K^{(k)}}{\rho_j \rho_k}\,, \\
V &= h + \frac{Q_0}{\rho} \\
\mu V &= m_\infty + \frac{m^{(0)}}{\rho} + \sum_{j=1}^{n} \frac{m^{(j)}}{\rho_j} + \alpha \frac{\cos\theta}{\rho^2} + \sum_{j=1}^{n} \alpha_j \frac{\cos\theta_j}{\rho_j^2} \\
&\quad + \sum_j l_I^\infty k_I^{(j)} \left(h\, f_j^{(1)} + Q_0\, f_j^{(2)}\right) + \sum_j Q_I^{(j)} k_I^{(j)} \left(h\, f_j^{(3)} + Q_0\, f_j^{(4)}\right) \\
&\quad + \sum_{i=0}^{n} \sum_{j=1, j\neq i}^{n} Q_I^{(i)} k_I^{(j)} \left(h\, f_{ij}^{(5)} + Q_0\, f_{ij}^{(6)}\right) + \frac{C_{IJK}}{6} \sum_{i,j,k} k_I^{(i)} k_J^{(j)} k_K^{(k)} \left(h^2\, f_{ijk}^{(7)} + {Q_0}^2\, f_{ijk}^{(8)} + h Q_0\, f_{ijk}^{(9)}\right)
\end{aligned}
\tag{B.4.9}
$$

where the functions $f_i^{(m)}$, $f_{ij}^{(m)}$ and $f_{ijk}^{(m)}$ are given in appendix B.3 and are multipole-decomposable.

We wish to apply (B.4.6) with $f(Z_1, Z_2, Z_3, V, \mu V) = -\mathcal{Q}^{-\frac{1}{2}} = -\left(Z_1 Z_2 Z_3 V - (\mu V)^2\right)^{-\frac{1}{2}}$. As the quartic invariant at infinity equals

$$
\mathcal{Q}_\infty = l_1^\infty l_2^\infty l_3^\infty h - {m_\infty}^2\,, \tag{B.4.10}
$$

we deduce

$$
D_l\left[-\mathcal{Q}^{-\frac{1}{2}}\right] = \frac{1}{2} l_1^\infty l_2^\infty l_3^\infty D_l[V] + \frac{1}{2} h \left(l_1^\infty l_2^\infty D_l[Z_3] + l_2^\infty l_3^\infty D_l[Z_1] + l_3^\infty l_1^\infty D_l[Z_2]\right) - m_\infty D_l[\mu V]\,, \tag{B.4.11}
$$

where we have used that $\mathcal{Q}_\infty^{-\frac{3}{2}} = 1$ since we want to have an asymptotic flat space $\mathbb{R}^3$. Thus, it remains to compute $D_l[F_I]$; by linearity, we only need to compute $D_l[f_i^{(m)}]$, $D_l[f_{ij}^{(m)}]$ and $D_l[f_{ijk}^{(m)}]$.

By reading off the coefficient of the leading-degree monomial in $\cos\theta$, we deduce that $\frac{1}{\rho_i \rho_j}$ expands as

$$
\begin{aligned}
\frac{1}{\rho_i \rho_j} &= \sum_{l=1}^{\infty} \frac{1}{\rho^{l+1}} \sum_{p+q=l-1}^{p,q\geq 0} {a_i}^p {a_j}^q P_p P_q \\
&= \sum_{l=1}^{\infty} \frac{1}{\rho^{l+1}} \left[q_{l-1}^{(2)}(a_i, a_j) P_{l-1} + \mathcal{L}\mathcal{H}_{l-1}\right]\,,
\end{aligned}
\tag{B.4.12}
$$

where the bivariate polynomial $q_n^{(2)}$ is defined as

$$
q_n^{(2)}(a_i, a_j) \equiv \frac{1}{\binom{2n}{n}} \sum_{p+q=n} \binom{2p}{p} \binom{2q}{q} {a_i}^p {a_j}^q\,. \tag{B.4.13}
$$

Similarly, we define the multivariate polynomial $q_n^{(3)}$:

$$
q_n^{(3)}(a_i, a_j, a_k) \equiv \frac{1}{\binom{2n}{n}} \sum_{p+q+s=n} \binom{2p}{p} \binom{2q}{q} \binom{2s}{s} {a_i}^p {a_j}^q {a_k}^s\,. \tag{B.4.14}
$$

Note that

$$q_n^{(2)}(1,1) = \frac{4^n}{\binom{2n}{n}} \quad , \quad q_n^{(3)}(1,1,1) = 2n+1\,. \tag{B.4.15}$$

The following functions then expand as

$$\frac{\rho}{\rho_i\rho_j} = \sum_{l=0}^{\infty} \frac{1}{\rho^{l+1}} \left[q_l^{(2)}(a_i,a_j) P_l + \mathcal{LH}_l \right] \tag{B.4.16}$$

$$\frac{1}{\rho_i\rho_j\rho_k} = \sum_{l=2}^{\infty} \frac{1}{\rho^{l+1}} \left[q_{l-2}^{(3)}(a_i,a_j,a_k) P_{l-2} + \mathcal{LH}_{l-2} \right] \tag{B.4.17}$$

$$\frac{\rho}{\rho_i\rho_j\rho_k} = \sum_{l=1}^{\infty} \frac{1}{\rho^{l+1}} \left[q_{l-1}^{(3)}(a_i,a_j,a_k) P_{l-1} + \mathcal{LH}_{l-1} \right] \tag{B.4.18}$$

$$\frac{\rho^2}{\rho_i\rho_j\rho_k} = \sum_{l=0}^{\infty} \frac{1}{\rho^{l+1}} \left[q_l^{(3)}(a_i,a_j,a_k) P_l + \mathcal{LH}_l \right] . \tag{B.4.19}$$

Following Bonnet's recursion formula, we have, for $l \geq 1$, $XP_{l-1} = \frac{l}{2l-1} P_l + \mathcal{LH}_l$. We deduce

$$\frac{\cos\theta}{\rho_i\rho_j} = \sum_{l=1}^{\infty} \frac{1}{\rho^{l+1}} \left[q_{l-1}^{(2)}(a_i,a_j) \frac{l}{2l-1} P_l + \mathcal{LH}_l \right] \tag{B.4.20}$$

$$\frac{\rho\cos\theta}{\rho_i\rho_j\rho_k} = \sum_{l=1}^{\infty} \frac{1}{\rho^{l+1}} \left[q_{l-1}^{(3)}(a_i,a_j,a_k) \frac{l}{2l-1} P_l + \mathcal{LH}_l \right] \tag{B.4.21}$$

$$\frac{\cos\theta_i}{\rho_i^2} = \frac{r\cos\theta - a_i}{\rho_i^3} = \sum_{l=1}^{\infty} \frac{1}{\rho^{l+1}} \left[q_{l-1}^{(3)}(1,1,1) \frac{l}{2l-1} a_i^{l-1} P_l + \mathcal{LH}_l \right] . \tag{B.4.22}$$

Thus, we deduce the expansions $D_l[f_i^{(m)}]$, $D_l[f_{ij}^{(m)}]$ and $D_l[f_{ijk}^{(m)}]$, which in turn, provide the mass multipoles from (B.4.11):

$$\begin{aligned}
4\tilde{M}_l =& \, l_1^\infty l_2^\infty l_3^\infty Q_0 {a_0}^l + h\frac{|\varepsilon_{IJK}|}{2} l_I^\infty l_J^\infty \sum_{j=0}^{n} Q_K^{(j)} {a_j}^l + hQ_0 \sum_{J\neq K} \frac{l_J^\infty l_K^\infty}{2} \sum_{j,k=1}^{n} k_J^{(j)} k_K^{(k)} \frac{q_l^{(2)}(a_j,a_k)}{a_j a_k} \\
&- 2m_\infty \sum_{j=0}^{n} m^{(j)} {a_j}^l - 2m_\infty \sum_{j=0}^{n} \alpha_j \, l {a_j}^{l-1} - m_\infty h l_I^\infty \sum_{j=1}^{n} k_I^{(j)} {a_j}^l \\
&- m_\infty Q_0 \sum_{j=1}^{n} Q_I^{(j)} k_I^{(j)} \frac{4^{l-1}}{\binom{2(l-1)}{l-1}} \frac{l}{2l-1} {a_j}^{l-2} \\
&- 2m_\infty Q_0 \sum_{i=0}^{n} \sum_{j=1, j\neq i}^{n} Q_I^{(i)} k_I^{(j)} \left(\frac{q_l^{(2)}(a_i,a_j)}{2a_j\,(a_i-a_j)} - \frac{l}{2l-1} \frac{q_{l-1}^{(2)}(a_i,a_j)}{a_i-a_j} \right) \\
&- 2m_\infty {Q_0}^2 \sum_{1\leq i,j,k\leq n} k_1^{(i)} k_2^{(j)} k_3^{(k)} \frac{l}{2l-1} \frac{q_{l-1}^{(3)}(a_i,a_j,a_k)}{a_i a_j a_k} \,.
\end{aligned} \tag{B.4.23}$$

The position of the Taub-NUT center is fixed at $a_0 = 0$, and ${a_0}^l = \delta_{l,0}$. The binomial coefficient in the third line of (B.4.23) is not defined for $l = 0$ but, as it is multiplied by l, one can set this term to be

zero for $l=0$ and extend the formula (B.4.23) for all $l\in\mathbb{N}$. In particular,

$$\begin{aligned}4\tilde{M}_0 =& l_1^\infty l_2^\infty l_3^\infty Q_0 + h\frac{|\varepsilon_{IJK}|}{2} l_I^\infty l_J^\infty \sum_{j=0}^n Q_K^{(j)} + hQ_0 \sum_{J\neq K} \frac{l_J^\infty l_K^\infty}{2} \sum_{j,k=1}^n k_J^{(j)} k_K^{(k)} \frac{1}{a_j a_k} \\ & - 2m_\infty \sum_{j=0}^n m^{(j)} - m_\infty h l_I^\infty \sum_{j=1}^n k_I^{(j)} - m_\infty Q_0 \sum_{i=0}^n \sum_{j=1,j\neq i}^n Q_I^{(i)} k_I^{(j)} \frac{1}{a_j(a_i-a_j)}\,.\end{aligned} \tag{B.4.24}$$

and

$$\begin{aligned}4\tilde{M}_1 =& h\frac{|\varepsilon_{IJK}|}{2} l_I^\infty l_J^\infty \sum_{j=1}^n Q_K^{(j)} a_j + hQ_0 \sum_{J\neq K} \frac{l_J^\infty l_K^\infty}{2} \sum_{j,k=1}^n k_J^{(j)} k_K^{(k)} \frac{a_j+a_k}{a_j a_k} \\ & - 2m_\infty \sum_{j=1}^n m^{(j)} a_j - 2m_\infty \sum_{j=0}^n \alpha_j - m_\infty h l_I^\infty \sum_{j=1}^n k_I^{(j)} a_j - m_\infty Q_0 \sum_{j=1}^n Q_I^{(j)} k_I^{(j)} \frac{1}{a_j} \\ & - 2m_\infty Q_0 \sum_{i=0}^n \sum_{j=1,j\neq i}^n Q_I^{(i)} k_I^{(j)} \left(\frac{a_i+a_j}{2a_j(a_i-a_j)} - \frac{1}{a_i-a_j} \right) - 2m_\infty {Q_0}^2 \sum_{1\leq i,j,k\leq n} \frac{k_1^{(i)} k_2^{(j)} k_3^{(k)}}{a_i a_j a_k}\,.\end{aligned} \tag{B.4.25}$$

In the scaling limit, we scale the intercenter distances $a_i \to \lambda d_i$, with $d_i \sim \mathcal{O}(1)$, and we keep the charges $\hat{\kappa}_I^{(j)} \equiv k_I^{(j)}/a_j$ fixed, according to (4.4.8). The last term of (B.4.24) naively scales like $-\lambda^{-1} m_\infty Q_0 \sum_{i=0}^n \sum_{j=1,j\neq i}^n Q_I^{(i)} \hat{\kappa}_I^{(j)} (d_i-d_j)^{-1}$. However, using the regularity constraint (B.3.19), the scaling limit of the mass multipole $M_0 = \tilde{M}_0$ has no λ^{-1} term and is in fact of the form

$$\tilde{M}_0 = \tilde{M}_0^{(0)} + \lambda \tilde{M}_0^{(1)}\,. \tag{B.4.26}$$

We see from (B.4.23) that in the scaling limit, the dominant term in $\tilde{M}_l$ is of order λ^{l-1} for $l\geq 1$.

B.4.3 Current multipoles

To get the expression of the current multipoles $\tilde{S}_l$ defined in (4.2.5), we need to determine the $\sin^2\theta P_l'(\cos\theta)$ expansions in $1/\rho^l$ ($l\leq 0$) of $\varpi \equiv \omega_\phi\, d\phi$ in (B.3.12)

$$\begin{aligned}\omega_\phi =& \sum_j l_I^\infty k_I^{(j)} \left(h\,\tau_j^{(1)} + Q_0\,\tau_j^{(2)} \right) + \sum_j Q_I^{(j)} k_I^{(j)} \left(h\,\tau_j^{(3)} + Q_0\,\tau_j^{(5)} \right) \\ & + \sum_{i=0}^n \sum_{j=1,j\neq i}^n Q_I^{(i)} k_I^{(j)} \left(h\,\tau_{ij}^{(4)} + Q_0\,\tau_{ij}^{(6)} \right) + \frac{C_{IJK}}{6} \sum_{i,j,k} k_I^{(i)} k_J^{(j)} k_K^{(k)} \left(h^2\,\tau_{ijk}^{(7)} + {Q_0}^2\,\tau_{ijk}^{(8)} + hQ_0\,\tau_{ijk}^{(9)} \right) \\ & + \tau^{(10)}\,,\end{aligned} \tag{B.4.27}$$

where the one-forms $\tau^{(m)} d\phi \equiv t^{(m)}$ are given in equations (B.3.10) and (B.3.9).

The additional difficulty in the computation of the current multipoles with respect to the mass multipoles is that in order to check that the the metric is AC-∞ in its $g_{t\phi}$ part, one needs to be

able to factorize by $\sin^2\theta$ in the multipole development of $g_{t\phi}$. To do this, we consider ω_ϕ as a polynomial in $X \equiv \cos\theta$, before doing any expansion in $\frac{1}{\rho^l}$. The charges and the poles a_i satisfy the regularity constraints in the like of (B.3.19) to avoid Dirac-Misner strings on the z-axis, that is to say $\omega_\phi(\cos\theta = 1) = 0$ and $\omega_\phi(\cos\theta = -1) = 0$. Therefore ω_ϕ is divisible by $(1-X)(1+X) = 1-X^2 = \sin^2\theta$.

We can now read off all the current multipoles simply by looking at the coefficient in front of the dominant term, X^{l+1}. Any polynomial of degree l or less is then counted among the the lower harmonics. For instance,

$$\frac{\rho^2}{\rho_i\rho_j} = \sum_{l=0}^{\infty} \frac{1}{\rho^l}\left[q_l^{(2)}(a_i,a_j)P_l + \mathcal{LH}_l\right] \tag{B.4.28}$$

is counted among the lower harmonics $\mathcal{LH}_{l+1}$ and does not contribute to the current multipole. It is easy to see that a generic function of the form

$$\frac{\rho^n\cos^m\theta}{\rho_{i_1}\cdots\rho_{i_p}} = \sum_{l=p-n}^{\infty} \frac{1}{\rho^l}\left[q^{(p)}_{l+n-p}(a_{i_1},\ldots,a_{i_p})X^m P_{l+n-p} + \mathcal{LH}_{l+n+m-p}\right] \tag{B.4.29}$$

contributes to a polynomial of degree $l+(n+m-p)$ in the $\frac{1}{\rho^l}$-expansion. (In practice, $m=1$ or $m=2$.) The dominant multipole is a polynomial of degree $l+1$, which is achieved when $n+m-p=1$.

The last paragraph shows that in the expression $g_{t\phi} = -2\mathcal{Q}^{-1/2}\omega_\phi$, $\mathcal{Q}^{-1/2}$ does not contribute to the current multipoles. Indeed, because $\mathcal{Q}_\infty = 1$, we can write $\mathcal{Q} = 1+\mathcal{R}$, where $\mathcal{R}$ comprises only functions of the form (B.4.29) with $n+m-p \leq -1$. Thus, the same applies to $\mathcal{Q}^{-1/2}$, and the functions of $\mathcal{R}$ are absorbed in the lower harmonics of ω_ϕ, whose highest harmonic generating functions verifiy $n+m-p=1$.

The relation between P_n and P_n'

$$\frac{X^2-1}{n}P_n' = XP_n - P_{n-1} \tag{B.4.30}$$

ensures that

$$X^m P_{l+n-p} = (X^2-1)\frac{c_{l+n-p}}{c_{l+n-p+m-1}}\frac{1}{l+n-p+m-1}P'_{l+n-p+m-1} + \mathcal{LH}_{l+n+m-p}\,, \tag{B.4.31}$$

where $c_n = \frac{1}{2^n}\binom{2n}{n}$ is the coefficient of the leading order X^n in P_n. In practice, the functions that contribute to the dominant current multipole can be developed as

$$\begin{aligned}
\frac{\rho^p\cos\theta}{\rho_{i_1}\cdots\rho_{i_p}} &= \cos\theta + \sum_{l=1}^{\infty}\frac{1}{\rho^l}\left[(X^2-1)\frac{1}{l}q_l^{(p)}(a_{i_1},\ldots,a_{i_p})P_l' + \mathcal{LH}_{l+1}\right]\,,\\
\frac{\rho^{p-1}\cos^2\theta}{\rho_{i_1}\cdots\rho_{i_p}} &= \sum_{l=1}^{\infty}\frac{1}{\rho^l}\left[(X^2-1)\frac{1}{2l-1}q_{l-1}^{(p)}(a_{i_1},\ldots,a_{i_p})P_l' + \mathcal{LH}_{l+1}\right]\,.
\end{aligned} \tag{B.4.32}$$

Notice that $XP_0 = X = \cos\theta$ is not divisible by X^2-1, so it cannot contribute to any current multipole.

Using (B.4.32), one can derive the expansion of the functions appearing in ϖ involving a degree $l+1$ polynomial, and by linearity, the expansion of ω_ϕ itself. Finally, factorizing $g_{t\phi} = -2\mathcal{Q}^{-1/2}\omega_\phi$ by

$\sin^2\theta$, one deduces the current multipoles from (4.2.5)

$$\begin{aligned}\tilde{S}_l =& \frac{h}{4}\sum_{j=1}^{n} l_I^{\infty} k_I^{(j)}\, {a_j}^l - \frac{Q_0}{4}\sum_{j=1}^{n} Q_I^{(j)} k_I^{(j)} \frac{l}{2l-1}\frac{4^{l-1}}{\binom{2(l-1)}{l-1}} {a_j}^{l-2} \\ &- \frac{Q_0}{2}\sum_{i=0}^{n}\sum_{j=1,j\neq i}^{n} Q_I^{(i)} k_I^{(j)} \left(\frac{l}{2l-1}\frac{q_{l-1}^{(2)}(a_i,a_j)}{a_j-a_i} - \frac{q_l^{(2)}(a_i,a_j)}{2a_j(a_j-a_i)}\right) \\ &- \frac{{Q_0}^2}{2}\sum_{1\leq i,j,k\leq n} k_1^{(i)} k_2^{(j)} k_3^{(k)} \frac{l}{2l-1}\frac{q_{l-1}^{(3)}(a_i,a_j,a_k)}{a_i a_j a_k} - \frac{1}{2}\sum_{j=0}^{n} m^{(j)} {a_j}^l - \frac{1}{2}\sum_{j=0}^{n}\alpha_j\, l\, {a_j}^{l-1}\,.\end{aligned} \tag{B.4.33}$$

It is easy to check that in the scaling limit, one gets the equality

$$\tilde{M}_1 = m_\infty \tilde{S}_1\,, \tag{B.4.34}$$

which is consistent with equations (4.3.8) and (4.3.9) for the almost-BPS black hole (4.3.4) with a parameter α.

B.4.4 Multipole ratios

As it was shown in [118,120], if one wants to calculate *ratios of vanishing multipoles* for certain black holes, there exist two methods: the *indirect* and the *direct* one. In this section we review these methods and apply them briefly to almost-BPS black holes, as a proof of concept that the analysis of [118,120] for supersymmetric black holes and their multicentered microstates can be straightforwardly generalized to the almost-BPS case (albeit only for $h = 1$).

Brief overview of *indirect* and *direct* methods

In the *indirect* method, we consider a generic STU black hole in maximal ungauged supergravity [132]; these black holes are characterized by 10 parameters: a non-extremality parameter, m, a rotation parameter, a, and four electric and four magnetic charge parameters, δ_I, γ_I. For such a generic STU black hole, *all* of the multipoles M_ℓ, S_ℓ are non-zero, and so any multipole ratio, which we can generically denote as $\mathcal{M}$, is well-defined. Then, one can take the limit of $\mathcal{M}$ as we go from the generic STU black hole to the black hole in question. Defined in this way as a limit, any ratio of vanishing multipoles, $\mathcal{M}$, becomes well-defined for any black hole. For example, in [118,120] it was found that:

$$\frac{M_2 S_2}{M_3 S_1} = 1, \tag{B.4.35}$$

for *any* black hole; this includes the Kerr black hole for which this ratio is strictly speaking undefined (since $S_2 = M_3 = 0$ for Kerr). The multipoles of a generic STU black hole can be seen as functions of four variables: the mass, M, the angular momentum, J, the rotation parameter, a, and the dipole moment, M_1.[4] The *indirect* method of calculating a ratio of vanishing multipoles, $\mathcal{M}$, for a black hole

[4]Note that we are using a slightly different parameterization than in [120], where $D = M_1/a$ was used instead; the one we use here is more natural for almost-BPS black holes and microstate geometries.

with parameters $(M_0, J_0, (M_1)_0, a_0)$ can then be summarized as:

$$\mathcal{M}^{\text{ind}}\left(M_0, J_0, (M_1)_0, a_0\right) = \lim_{(M,J,M_1,a)\to(M_0,J_0,(M_1)_0,a_0)} \mathcal{M}\left(M, J, M_1, a\right). \tag{B.4.36}$$

For further discussion, see [120] (and especially appendix B therein for the subtleties of this *indirect* method).

The *direct* method instead uses scaling microstate geometries which tend to the black hole geometry in the scaling limit $\lambda \to 0$. This method calculates the ratios of vanishing multipoles, $\mathcal{M}$, by considering the multipole ratios of microstate geometries as one takes the scaling limit:

$$\mathcal{M}^{\text{dir}} = \lim_{\lambda\to 0} \mathcal{M}(\lambda). \tag{B.4.37}$$

It was shown in [118, 120] that ratios of vanishing multipoles can be computed in this way for supersymmetric black holes, in which all all multipole moments (except M_0) vanish.

Almost-BPS multipole ratios at $h = 1$

The Chow-Compere STU black holes [132] and thus the *indirect* method [118, 120] are only defined for the family of our almost-BPS black holes and microstates when we take the 4D modulus $h = 1$.[5] We therefore restrict ourself to these solutions; as mentioned above in section 4.4.2, this implies $M_\ell \sim \mathcal{O}(\lambda^\ell)$ and $S_\ell \sim \mathcal{O}(\lambda^{\ell-1})$ for microstate geometries in the scaling limit $\lambda \to 0$.

The generic underrotating limit (to which the almost-BPS black hole belongs) of the generic STU black hole family with parameters (M, J, M_1, a) corresponds to the $a \to 0$ limit keeping M, M_1, J finite. However, as we saw in (4.3.10), our almost-BPS black hole with $h = 1$ has *all* multipoles vanishing except M_0 and S_1. Thus, the *indirect* limit for our almost-BPS black hole family involves also taking the limit $M_1 \to 0$, which we will always consider taking *after* the underrotating limit.

Note that, precisely because all multipoles (except M_0, S_1) vanish for our almost-BPS black holes with $h = 1$, any multipole ratio that involves two monomials in M_ℓ, S_ℓ is a non-trivial quantity that we can compute and compare using both the *direct* and *indirect* method. This is similar to the analysis of the difference between the *indirect* and *direct* calculations of multipole ratios for supersymmetric black holes, which was discussed in detail in [118, 120]. There, it was found that the two methods only gave (closely) matching results for certain classes of (SUSY) black holes.

As an example, let us consider the following three multipole ratios:

$$\mathcal{M}_{(A)} \equiv \frac{M_2 M_4}{M_3 M_3}, \qquad \mathcal{M}_{(B)} \equiv \frac{S_2 S_4}{S_3 S_3}, \qquad \mathcal{M}_{(C)} \equiv \frac{M_2 S_2}{M_3 S_1}. \tag{B.4.38}$$

These have simple values when calculated with the *indirect* method:

$$\mathcal{M}^{\text{ind}}_{(A)} \equiv \lim_{M_1\to 0} \lim_{a\to 0} \frac{M_2 M_4}{M_3 M_3} = \frac{3}{4}, \qquad \mathcal{M}^{\text{ind}}_{(B)} = \frac{8}{9}, \qquad \mathcal{M}^{\text{ind}}_{(C)} = 1. \tag{B.4.39}$$

Note that these *indirect* ratios are pure numbers and do not depend on the charges of the black hole; this is a general feature of *indirect* ratios for the almost-BPS black hole we consider here. However,

[5] This can be seen for example by comparing the asymptotic values of the matrices of scalar couplings (B.1.18)-(B.1.19) for our ansatz to that of the STU black hole in [132].

the same ratios calculated in the *direct* method *do* depend on the specifics of the microstate. As an illustration, in fig. B.1 we consider the three ratios $\mathcal{M}_{(A,B,C)}$ for the family of microstates defined by (4.4.30) with varying x (and $h = 1$).

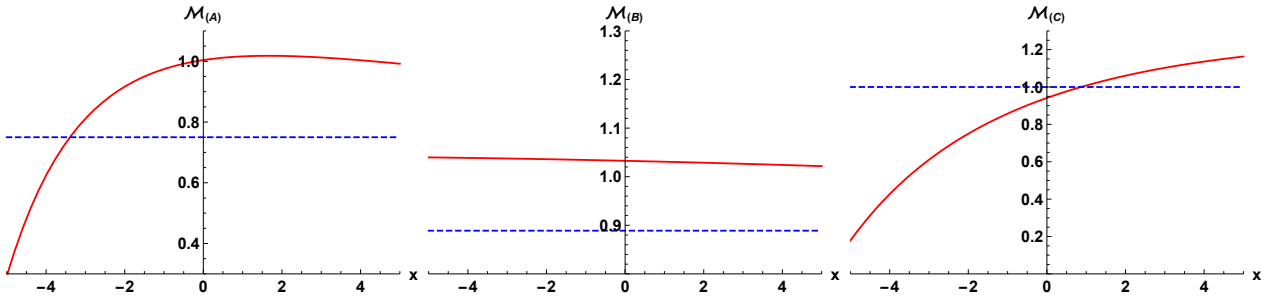

(a) $\mathcal{M}_{(A)}$ (b) $\mathcal{M}_{(B)}$ (c) $\mathcal{M}_{(C)}$

Figure B.1 – Plots of the *direct* method ratios $\mathcal{M}^{\text{dir}}_{(A,B,C)}$ (red lines) for the microstate family (4.4.30) with $h = 1$ as a function of x. The blue dashed lines indicate the *indirect* method values given in (B.4.39).

Clearly, the *indirect* and *direct* methods do not necessarily agree with their predictions for the values of multipole ratios of the almost-BPS black hole. It would be interesting to conduct an analysis similar to [118, 120] to understand if there is a certain condition that the black hole must satisfy in order for the two methods to give similar answers; we leave this for future work.

Appendix C

Appendix for Chapter 6

C.1 Chain of dualities

In this appendix we present the explicit solutions for the intermediate steps in the two duality chains that we discussed in section 6.3. In the first part we present the steps (6.3.7) that lead from the F1-P system with a non-trivial profile (6.3.5) to the NS5-P system with local D0-D4 charges (6.3.8). In the second subsection we then present the chain of dualities (6.3.11) which is used to write the latter solution in the D1-D5 frame of [199]. This allows us to consistently add a D1-brane charge which corresponds to adding an F1 charge in the F1-NS5 frame.

C.1.1 Generating the NS5-P-(D0-D4) solution

F1-P

The starting point is the F1-P configuration in Type IIB theory depicted in figure 6.2: Take the fundamental string to wrap the $S^1(y)$ circle and have a non-trivial profile $F(v)$ along one of the directions of the T^4, which we call z_9. Add momentum along the y direction and distribute (smear) the string charge along the four-torus while keeping all the charge localized at a point in $\mathbb{R}^4$. The supergravity solution corresponding to such a configuration is given by [196, 197]

$$ds^2 = -\frac{2}{H_5}\,dv\left[du - \frac{\dot{F}^2(v)}{2}\,(H_5-1)\,dv + \dot{F}(v)\,(H_5-1)\,dz^9\right] + dx^i\,dx^i + dz^a\,dz^a\,, \quad \text{(C.1.1a)}$$

$$B = -\left(1-\frac{1}{H_5}\right)\left[du\wedge dv + \dot{F}(v)\,dv\wedge dz^9\right]\,, \qquad e^{2\phi} = \frac{1}{H_5}\,, \quad \text{(C.1.1b)}$$

with all other fields vanishing. In the above, u and v are null coordinates (6.3.3) and H_5 is a harmonic function associated with the F1-string and is given by (6.3.6).

S-duality to D1-P

The next step is to perform an S-duality (C.2.8) which yields

$$ds^2 = -\frac{2}{\sqrt{H_5}}\,dv\left(du + \frac{\dot{F}^2(v)}{2}\,(1-H_5)\,dv - \dot{F}(v)\,(1-H_5)\,\dot{F}(v)\,dz^9\right) + \sqrt{H_5}\left(dx^i\,dx^i + dz^a\,dz^a\right)\,, \tag{C.1.2a}$$

$$B = 0\,, \qquad e^{2\phi} = H_5\,, \tag{C.1.2b}$$

$$C_0 = 0\,, \tag{C.1.2c}$$

$$C_2 = \left(1-\frac{1}{H_5}\right)du\wedge dv + \dot{F}(v)\left(1-\frac{1}{H_5}\right)dv\wedge dz^9\,, \tag{C.1.2d}$$

$$C_4 = 0\,, \tag{C.1.2e}$$

$$C_6 = \gamma\wedge\left(\dot{F}(v)\,dv\wedge dz^6\wedge dz^7\wedge dz^8 + \widehat{\mathrm{vol}}_4\right)\,, \tag{C.1.2f}$$

where we have introduced a two-form γ such that

$$d\gamma \equiv *_4 dH\,, \tag{C.1.3}$$

and used the volume form of the T^4

$$\widehat{\mathrm{vol}}_4 \equiv dz^6\wedge dz^7\wedge dz^8\wedge dz^9\,. \tag{C.1.4}$$

This solution describes a D1-brane wrapping the $S^1(y)$ circle and carrying momentum along that direction. The D1-brane is smeared along the T^4, with a non-trivial profile along the z_9, while being located at the origin or the base space. We use the democratic formalism (see Appendix C.2), which we have used to determine C_6 by imposing the duality condition between F_3 and F_7.

T-dual along z_9 to D2-P with local D0-F1 charges

Next we perform T-dualities (C.2.14) along all four directions of the torus, and we begin with the "special" direction z_9. When performing this duality, following Figure 6.3, the decomposition of the local charges into those along the y and the z_9 direction become important. The result is a configuration in Type IIA theory: a D2-brane (wrapping the y and z_9 directions) with a momentum along y, on which we find D0 and F1 charges (the latter wrapping the z_9 direction), which have varying densities along the y direction. The corresponding supergravity solution is

$$ds^2 = -\frac{2}{\sqrt{H_5}}\,dv\left[du - \frac{\dot{F}^2(v)}{2}\left(1-\frac{1}{H_5}\right)dv\right] + \sqrt{H_5}\left(dx^i\,dx^i + \sum_{a=6}^{8} dz^a\,dz^a\right) + \frac{1}{\sqrt{H_5}}\left(dz^9\right)^2\,, \tag{C.1.5a}$$

$$B_2 = \dot{F}(v)\left(1-\frac{1}{H_5}\right)dv\wedge dz^9\,, \qquad e^{2\phi} = \sqrt{H_5}\,. \tag{C.1.5b}$$

$$C_1 = \dot{F}(v)\left(1-\frac{1}{H_5}\right)dv\,, \tag{C.1.5c}$$

$$C_3 = \left(1 - \frac{1}{H_5}\right) du \wedge dv \wedge dz^9 \,, \tag{C.1.5d}$$

$$C_5 = \gamma \wedge dz^6 \wedge dz^7 \wedge dz^8 \,, \tag{C.1.5e}$$

$$C_7 = \frac{\dot{F}(v)}{H_5} \gamma \wedge dv \wedge \widehat{\text{vol}}_4 \,. \tag{C.1.5f}$$

In the above solution, the y-, or more appropriately v-, dependent distribution of D0 and F1 charges is seen in the dependence on $\dot{F}(v)$ that appears in B_2, which is sourced by fundamental strings, and C_1 (C_7) which is electrically (magnetically) sourced by D0-branes. On the other hand, C_3 and C_5, which are sourced by D2-branes, are independent of $\dot{F}(v)$.

T-dualities along z_8, z_7 and z_6 to the D5-P with local D3-F1 charges

The three T-dualities along z_8, z_7, and z_6 (in that order) are very similar and thus we perform them together. The final result is a configuration in Type IIB theory where the D2-brane now becomes a D5-brane wrapping the $S^1(y)$ circle and all four directions of the T^4, while the $\dot{F}(v)$ dependent fields are now sourced by local D3 and F1 charges:

$$ds^2 = -\frac{2}{\sqrt{H_5}} dv \left[du - \frac{\dot{F}^2(v)}{2}\left(1 - \frac{1}{H_5}\right) dv\right] + \sqrt{H_5} dx^i \, dx^i + \frac{1}{\sqrt{H_5}} dz^a \, dz^a \,, \tag{C.1.6a}$$

$$B_2 = \dot{F}(v)\left(1 - \frac{1}{H_5}\right) dv \wedge dz^9 \,, \qquad e^{2\phi} = \frac{1}{H_5} \,, \tag{C.1.6b}$$

$$C_0 = 0 \,, \tag{C.1.6c}$$

$$C_2 = \gamma \,, \tag{C.1.6d}$$

$$C_4 = -\frac{\dot{F}(v)}{H_5} \gamma \wedge dv \wedge dz^9 - \dot{F}(v)\left(1 - \frac{1}{H_5}\right) dv \wedge dz^6 \wedge dz^7 \wedge dz^8 \,, \tag{C.1.6e}$$

$$C_6 = \left(1 - \frac{1}{H_5}\right) du \wedge dv \wedge \widehat{\text{vol}}_4 \,, \tag{C.1.6f}$$

$$C_8 = 0 \,. \tag{C.1.6g}$$

S-duality to NS5-P with local D3-D1 charges

Since our aim is to obtain a solution corresponding to a configuration with NS5-P charges, we continue with another S-duality. Essentially, this only exchanges the D5-brane for an NS5-brane and the D1 local charges with F1 charge distribution:

$$ds^2 = -2dv \left[du - \frac{\dot{F}^2(v)}{2}\left(1 - \frac{1}{H_5}\right) dv\right] + H_5 \, dx^i \, dx^i + \, dz^a \, dz^a \,, \tag{C.1.7a}$$

$$B_2 = \gamma \,, \qquad e^{2\phi} = H_5 \,, \tag{C.1.7b}$$

$$C_0 = 0 \,, \tag{C.1.7c}$$

$$C_2 = -\dot{F}(v)\left(1 - \frac{1}{H_5}\right) dv \wedge dz^9 \,, \tag{C.1.7d}$$

$$C_4 = -\dot{F}(v)\,\gamma \wedge dv \wedge dz^9 - \dot{F}(v)\left(1 - \frac{1}{H_5}\right) dv \wedge dz^6 \wedge dz^7 \wedge dz^8\,, \tag{C.1.7e}$$

$$C_6 = -\dot{F}(v)\,\gamma \wedge dv \wedge dz^6 \wedge dz^7 \wedge dz^8\,, \tag{C.1.7f}$$

$$C_8 = 0\,. \tag{C.1.7g}$$

T-duality to NS5-P with local D0-D4 charges

Finally, we perform another T-duality along z_9, which lands us in the desired configuration: an NS5-brane with momentum along the y-direction with D0- and D4-brane charges which vary along the $S^1(y)$ circle

$$ds^2 = -2dv\left[du - \frac{\dot{F}(v)^2}{2}\left(1 - \frac{1}{H_5}\right) dv\right] + H\,dx^i\,dx^i + dz^a\,dz^a\,, \tag{C.1.8a}$$

$$B_2 = \gamma\,, \qquad e^{2\phi} = H_5\,, \tag{C.1.8b}$$

$$C_1 = -\dot{F}(v)\left(1 - \frac{1}{H_5}\right) dv\,, \tag{C.1.8c}$$

$$C_3 = -\dot{F}(v)\,\gamma \wedge dv\,, \tag{C.1.8d}$$

$$C_5 = -\dot{F}(v)\left(1 - \frac{1}{H_5}\right) dv \wedge \widehat{\text{vol}}_4 = C_1 \wedge \widehat{\text{vol}}_4\,, \tag{C.1.8e}$$

$$C_7 = -\dot{F}(v)\,\gamma \wedge dv \wedge \widehat{\text{vol}}_4 = C_3 \wedge \widehat{\text{vol}}_4\,, \tag{C.1.8f}$$

which is the solution (6.3.8) presented in the main text. Unlike any of the previous solutions presented in this appendix, (C.1.8) depends on the T^4 only through its volume form (C.1.4).

C.1.2 Adding F1 charge by using a Gibbons-Hawking base

The solution (C.1.8) (or equivalently (6.3.8) of the main text) is asymptotically a two-charge solution. To make contact with the microstate geometries programme, we would like to construct a solution which has three charges. We choose to add to the configuration an additional fundamental string that wraps the $S^1(y)$ circle and is smeared along the T^4.

We do so in a roundabout way: We write the four-dimensional flat metric in Gibbons-Hawking form and T-dualize along the Gibbons-Hawking fiber. If we then perform an S-duality, the resulting configuration should be described in terms of the complete ansatz for the D1-D5 system constructed in [199]. Adding a source corresponding to a D1-brane in this duality frame is equivalent to adding a fundamental string in the NS5-P frame, only that in the former frame we know all fields which get excited as a consequence of adding a new object into the configuration.

Begin by writing the flat base space metric in (C.1.8) as[1]

$$dx^i\, dx^i = \frac{1}{V}(d\psi + A)^2 + V\, ds_3^2\,, \tag{C.1.10}$$

where ds_3^2 denotes the flat metric on $\mathbb{R}^3$. Recall that we need to impose the following constraints on the function V and one-form A

$$*_3 dA = dV\,, \quad \Longrightarrow \quad *d*dV = 0\,, \qquad d*dA = 0\,, \tag{C.1.11}$$

which also means that the warp factor, V, is a harmonic function in $\mathbb{R}^3$. The metric (C.1.10) is invariant under a simultaneous rescaling of the coordinates, the function V, and one-form A, which we can fix by setting the periodicity of ψ to be 4π.

Now assume that ψ denotes an isometry direction of the solution. Then one can decompose

$$*_4 dH_5 = (d\psi + A) \wedge *_3 dH_5\,, \tag{C.1.12}$$

and[2]

$$\gamma \equiv -\,(d\psi + A) \wedge \gamma^{(1)} + \gamma^{(2)}\,, \tag{C.1.13}$$

where the one-form $\gamma^{(1)}$ and the two-form $\gamma^{(2)}$ are determined from the definition (6.3.9) by

$$d\gamma^{(1)} = *_3 dH_5\,, \qquad d\gamma^{(2)} = *_3 dV \wedge \gamma^{(1)}\,. \tag{C.1.14}$$

T-duality along the Gibbons-Hawking fiber

We now use the T-duality rules to dualize along the Gibbons-Hawking fiber ψ. However, after performing the transformation, we need to change the sign of ψ

$$\psi \to -\psi\,, \tag{C.1.15}$$

to obtain

$$ds^2 = -2\, dv \left[du - \frac{\dot{F}^2(v)}{2}\left(1 - \frac{1}{H_5}\right) dv\right] + V\left[\frac{1}{H_5}\left(d\psi + \gamma^{(1)}\right)^2 + H_5\, ds_3^2\right] + ds_4^2\,, \tag{C.1.16a}$$

[1] In what follows we do not specify the coordinates used in the Gibbons-Hawking ansatz. However, one can introduce spherical coordinates for $\mathbb{R}^4$ whose metric can be written as

$$ds_4^2 = dr^2 + r^2\left(d\theta^2 + \sin^2\theta\, d\varphi_1^2 + \cos^2\theta\, d\varphi_2^2\right).$$

To rewrite this metric in the Gibbons-Hawking form, we introduce new coordinates as $r \equiv 2\sqrt{\rho}$, $\tilde{\theta} \equiv 2\theta$, $\psi \equiv \varphi_1 + \varphi_2$, and $\phi \equiv \varphi_2 - \varphi_1$, where the ranges of various coordinates are taken to be $\varphi_{1,2} \in [0, 2\pi)$, $\psi \in [0, 4\pi)$, and $\phi \in [0, 2\pi)$, while r and ρ are both taken to be non-negative. The metric becomes

$$ds_4^2 = \rho\,(d\psi + \cos\tilde{\theta}\, d\phi)^2 + \frac{1}{\rho}\left(d\rho^2 + \rho^2\left(d\tilde{\theta}^2 + \sin^2\tilde{\theta}\, d\phi^2\right)\right)\,, \tag{C.1.9}$$

and one can read off that $V = \rho^{-1}$ and $A = \cos\tilde{\theta}\, d\phi$. Furthermore $H_5 = 1 + \frac{Q_5}{4\rho}$, and is thus harmonic even in $\mathbb{R}^3$.

[2] For example, in spherical coordinates (see footnote 1) $\gamma^{(1)} = \frac{1}{4}\, Q_5\, \cos\tilde{\theta}\, d\phi$ and $\gamma^{(2)} = 0$.

$$B_2 = A \wedge d\psi + \gamma^{(2)}\,, \qquad e^{2\phi} = V\,, \tag{C.1.16b}$$

$$C_0 = 0\,, \tag{C.1.16c}$$

$$C_2 = \dot{F}(v)\left(1 - \frac{1}{H_5}\right) dv \wedge (d\psi + \gamma^{(1)}) - \dot{F}\, dv \wedge \gamma^{(1)}\,, \tag{C.1.16d}$$

$$C_4 = \dot{F}(v)\, dv \wedge \left(d\psi + \gamma^{(1)}\right) \wedge \gamma^{(2)}\,, \tag{C.1.16e}$$

where the sign flip (C.1.15) ensures that the first equation of (C.1.14) now serves as the constraint between the one-form and scalar function in the new Gibbons-Hawking base-space metric.

S-duality to the D1-D5 frame

S-dualizing the above solution puts us in the D1-D5 frame, and the resulting configuration fits within the ansatz of [199]. In this transformation, and only in this transformation alone, we choose $b = -c = -1$ when performing the S-duality (C.2.8). This allows us to compare the resulting solution with the complete ansatz of [199] without changing the signs of the fields and furthermore, when transforming back to the NS5-P system we can take $b = -c = 1$ which is the inverse transformation. We find

$$ds^2 = -\frac{2}{\sqrt{V}}\, dv \left[du - \frac{\dot{F}^2(v)}{2}\left(1 - \frac{1}{H_5}\right) dv\right] + \sqrt{V}\left[\frac{1}{H_5}\left(d\psi + \gamma^{(1)}\right)^2 + H_5\, ds_3^2\right] + \frac{1}{\sqrt{V}}\, d\hat{s}_4^2\,, \tag{C.1.17a}$$

$$B_2 = \dot{F}(v)\left[\left(1 - \frac{1}{H_5}\right)\left(d\psi + \gamma^{(1)}\right) - \gamma^{(1)}\right] \wedge dv\,, \qquad e^{2\phi} = \frac{1}{V}\,, \tag{C.1.17b}$$

$$C_0 = 0\,, \tag{C.1.17c}$$

$$C_2 = A \wedge \left(d\psi + \gamma^{(1)}\right) + \gamma^{(2)} - A \wedge \gamma^{(1)}\,, \tag{C.1.17d}$$

$$C_4 = -\dot{F}(v)\left[\frac{1}{H_5}\left(d\psi + \gamma^{(1)}\right) \wedge \left(\gamma^{(2)} - A \wedge \gamma^{(1)}\right) + \gamma^{(1)} \wedge \gamma^{(2)}\right] \wedge dv\,. \tag{C.1.17e}$$

At this point one can recombine the Gibbons-Hawking decomposition of the base space (including the forms), compare the solution (C.1.17) with the complete ansatz of [199] and read off the ansatz quantities,[3] however, this is not central to our analysis.

Adding a D1 charge

What is important for us is that the harmonic function corresponding to D1-brane sources is precisely known in the complete ansatz [199].[4] Thus denoting this harmonic function with H_1

[3] Once this is done, one can check that the read-off quantities solve the BPS equations [210, 199].

[4] In the notation commonly used in the microstate geometries literature dealing with the D1-D5 system [210, 221, 50, 52] (see also appendix E.7 of [199]), this is the scalar function Z_1. Note that in addition one would need to turn on a contribution to the gauge field C_6, which would ensure, in the democratic formalism, appropriate self-duality properties of the gauge field strengths. However, we will determine higher-order gauge fields only after the last duality transformation.

(see (6.3.13)), we find that the new solution is given by

$$ds^2 = -\frac{2}{\sqrt{V\,H_1}}\,dv\left[du - \frac{\dot{F}^2(v)}{2}\left(1-\frac{1}{H_5}\right)dv\right] + \sqrt{V\,H_1}\left[\frac{1}{H_5}\left(d\psi+\gamma^{(1)}\right)^2 + H_5\,ds_3^2\right] + \sqrt{\frac{H_1}{V}}\,d\hat{s}_4^2\,, \tag{C.1.18a}$$

$$B_2 = \dot{F}(v)\left[\left(1-\frac{1}{H_5}\right)\left(d\psi+\gamma^{(1)}\right) - \gamma^{(1)}\right]\wedge dv\,, \qquad e^{2\phi} = \frac{H_1}{V}\,, \tag{C.1.18b}$$

$$C_0 = 0\,, \tag{C.1.18c}$$

$$C_2 = -\frac{1}{H_1}du\wedge dv + A\wedge\left(d\psi+\gamma^{(1)}\right) + \gamma^{(2)} - A\wedge\gamma^{(1)}\,, \tag{C.1.18d}$$

$$C_4 = -\dot{F}(v)\left[\frac{1}{H_5}\left(d\psi+\gamma^{(1)}\right)\wedge\left(\gamma^{(2)} - A\wedge\gamma^{(1)}\right) + \gamma^{(1)}\wedge\gamma^{(2)}\right]\wedge dv\,. \tag{C.1.18e}$$

It is straightforward to check that this supersymmetric torus-independent D1-D5-frame solution (C.1.18) solves the equations governing all such solutions [199].

S-dual to F1-NS5 frame in Type IIB

To return to the NS5-P system, we need to first perform an S-duality and then a T-duality along ψ. Using $b = -c = 1$, which ensures that this is the inverse transformation of the one used to arrive at (C.1.17), we obtain

$$ds^2 = -\frac{2}{H_1}\,dv\left[du - \frac{\dot{F}^2(v)}{2}\left(1-\frac{1}{H_5}\right)dv\right] + V\left[\frac{1}{H_5}\left(d\psi+\gamma^{(1)}\right)^2 + H_5\,ds_3^2\right] + ds_4^2\,, \tag{C.1.19a}$$

$$B_2 = -\frac{1}{H_1}du\wedge dv + A\wedge d\psi + \gamma^{(2)}\,, \qquad e^{2\phi} = \frac{V}{H_1}\,, \tag{C.1.19b}$$

$$C_0 = 0\,, \tag{C.1.19c}$$

$$C_2 = -\dot{F}(v)\left[\left(1-\frac{1}{H_5}\right)\left(d\psi+\gamma^{(1)}\right) - \gamma^{(1)}\right]\wedge dv\,, \tag{C.1.19d}$$

$$C_4 = -\dot{F}(v)\left(d\psi+\gamma^{(1)}\right)\wedge\gamma^{(2)}\wedge dv\,. \tag{C.1.19e}$$

T-dual to the F1-NS5 system in Type IIA

To return to the original system we perform a final T-duality along the ψ direction, which has to be again followed by a sign flip (C.1.15). Furthermore, in order to compare the final solution

to the two-charge case (C.1.8), we also exchange $\dot{F}(v) \to -\dot{F}(v)$. Then one finds

$$ds^2 = -\frac{2}{H_1} dv \left[du - \frac{\dot{F}(v)^2}{2} \left(1 - \frac{1}{H_5}\right) dv \right] + H_5 \, dx^i \, dx^i + dz^a \, dz^a \,, \tag{C.1.20a}$$

$$B_2 = -\frac{1}{H_1} \, du \wedge dv + \gamma \,, \qquad e^{2\phi} = \frac{H_5}{H_1} \,, \tag{C.1.20b}$$

$$C_1 = -\dot{F}(v) \left(1 - \frac{1}{H_5}\right) dv \,, \tag{C.1.20c}$$

$$C_3 = -\dot{F}(v) \, \gamma \wedge dv \,, \tag{C.1.20d}$$

where we have recombined the decompositions along the Gibbons-Hawking fiber. After the remaining RR gauge fields are computed, this solution matches the one presented in the main text in Equation (6.3.12).

C.2 Conventions

Democratic formalism

When dealing with brane sources it is useful to introduce the democratic formalism [198] which effectively doubles the number of gauge fields in the theory, but introduces self-duality constraints on the field strengths so that the number of degrees of freedom remains unchanged. This democracy is imposed only on the Ramond-Ramond gauge fields C_p, while we keep only one NS-NS gauge field B, with a three-form field strength

$$H_3 = dB \,. \tag{C.2.1}$$

The RR field strengths are defined as

$$F_p \equiv dC_{p-1} - H_3 \wedge C_{p-3} \,, \tag{C.2.2}$$

which satisfy modified Bianchi identities $dF_p = H_3 \wedge F_{p-2}$.

In each of the Type II theories, we introduce additional RR gauge field potentials, so that for Type IIA we consider $\{C_1, C_3, C_5, C_7\}$ and $\{C_0, C_2, C_4, C_6, C_8\}$ for Type IIB. However, the number of degrees of freedom is kept constant by imposing

$$(IIA): \qquad F_2 = *F_8 \,, \quad F_4 = - * F_6 \,, \quad F_6 = *F_4 \,, \quad F_8 = - * F_2 \,, \tag{C.2.3a}$$

$$(IIB): \qquad F_1 = *F_9, \quad F_3 = - * F_7, \quad F_5 = *F_5, \quad F_7 = - * F_3, \quad F_9 = *F_1 \,, \tag{C.2.3b}$$

which imply that the field strengths F_p and F_{10-p} essentially convey the same information. Note that we follow the conventions of [199], where the Hodge dual of a k-form in a D-dimensional spacetime is given by

$$*X_k \equiv \frac{1}{k!(D-k)!} \, \epsilon_{m_1 \ldots m_{D-k}, n_{D-k+1} \ldots n_D} \, X^{n_{D-k+1} \ldots n_D} \, e^{m_1} \wedge \ldots e^{m_{D-k}} \,. \tag{C.2.4}$$

Furthermore, we choose the orientation

$$\epsilon^{+-12346789} = \epsilon^{1234} = 1 \,. \tag{C.2.5}$$

S-duality

Define a complex field as a combination of the axion field and the dilaton and combine the two-form gauge potentials into a vector

$$\lambda \equiv C_0 + i\, e^{-\phi}\,, \qquad T = \begin{pmatrix} B_2 \\ C_2 \end{pmatrix}\,. \tag{C.2.6}$$

Type IIB theories are invariant under a transformation generated by $U \in SL(2,\mathbb{R})$

$$U = \begin{pmatrix} a & b \\ c & d \end{pmatrix}\,, \quad \text{with} \quad a\,d - b\,c = 1\,, \tag{C.2.7}$$

such that

$$\lambda \to \tilde{\lambda} = \frac{a\lambda + b}{c\lambda + d}\,, \qquad T \to \tilde{T} = U\,T\,, \tag{C.2.8}$$

while the five-form gauge field strength, F_5, and the ten-dimensional metric in the Einstein frame are invariant.

In the main text we consider only a $\mathbb{Z}_2$ subgroup of $SL(2,\mathbb{R})$ transformations where

$$a = d = 0\,, \qquad b = -c = \pm 1. \tag{C.2.9}$$

Unless explicitly stated otherwise, we choose $b = -c = 1$ whenever we perform an S-duality transformation. In addition, in all of the solutions considered, the axion field C_0 is vanishing. Then the effect of such a transformation, with either choice of sign for b and c, results in the inversion of the dilaton field

$$\tilde{\phi} = -\phi\,, \tag{C.2.10}$$

and the following change of the metric in the string frame

$$\tilde{G}_{\mu\nu} = e^{-\phi}\, G_{\mu\nu}\,. \tag{C.2.11}$$

Furthermore, the two-form gauge fields are interchanged up to a minus sign

$$\tilde{B}_2 = \pm C_2\,, \qquad\qquad \tilde{C}_2 = \mp B_2\,, \tag{C.2.12}$$

where the upper (lower) sign corresponds to $b = +1$ ($b = -1$). For either sign, the invariance of F_5 implies that the four-form gauge field transforms as

$$\tilde{C}_4 = C_4 - B_2 \wedge C_2\,. \tag{C.2.13}$$

Higher-form gauge fields can be calculated by using the duality rules of the democratic formalism (C.2.3) and (C.2.2). The effect of this particular transformation is thus to effectively exchange the two-form gauge potentials.

T-duality

For performing T-duality transformations we use the conventions of [116], which are convenient when one works in the democratic formalism. Assume that we are performing a T-duality along an isometry direction coordinatized by y. Rewrite the initial string frame metric and gauge fields as

$$ds^2 = G_{yy}\,(dy + A_\mu\,dx^\mu)^2 + \widehat{g}_{\mu\nu}\,dx^\mu\,dx^\nu \tag{C.2.14a}$$

$$B_2 = B_{\mu y} dx^\mu \wedge (dy + A_\mu\,dx^\mu) + \widehat{B}_2\,, \tag{C.2.14b}$$

$$C_p = C^y_{p-1} \wedge (dy + A_\mu\,dx^\mu) + \widehat{C}_p\,, \tag{C.2.14c}$$

where the forms $\widehat{B}_2$, $\widehat{C}_p$ and $\widehat{C}^y_{p-1}$ do not have any legs along y. After applying the rules of a T-duality transformation [222, 223], the new fields (denoted with the tilde) are

$$d\widetilde{s}^2 = G^{-1}_{yy}\,(dy - B_{\mu y}\,dx^\mu)^2 + \widehat{g}_{\mu\nu}\,dx^\mu\,dx^\nu \tag{C.2.15a}$$

$$\widetilde{B}_2 = -A_\mu dx^\mu \wedge dy + \widehat{B}_2\,, \tag{C.2.15b}$$

$$\widetilde{C}_p = \widehat{C}_{p-1} \wedge (dy - B_{\mu y}\,dx^\mu) + C^y_p\,, \tag{C.2.15c}$$

$$e^{2\widetilde{\phi}} = G^{-1}_{yy}\,e^{2\phi}\,. \tag{C.2.15d}$$

Bibliography

[1] S. W. Hawking, "Gravitational radiation from colliding black holes," *Phys. Rev. Lett.* **26** (1971) 1344–1346.

[2] J. M. Bardeen, B. Carter, and S. Hawking, "The Four laws of black hole mechanics," *Commun. Math. Phys.* **31** (1973) 161–170.

[3] J. D. Bekenstein, "Black holes and the second law," *Lett. Nuovo Cim.* **4** (1972) 737–740.

[4] J. D. Bekenstein, "Black holes and entropy," *Phys. Rev.* **D7** (1973) 2333–2346.

[5] S. W. Hawking, "Particle Creation by Black Holes," *Commun. Math. Phys.* **43** (1975) 199–220. Erratum: [Commun. Math. Phys. **46**, 206 (1976)].

[6] I. Bena, S. El-Showk, and B. Vercnocke, "Black Holes in String Theory," *Springer Proc. Phys.* **144** (2013) 59–178.

[7] S. D. Mathur, "The fuzzball proposal for black holes: An elementary review," *Fortsch. Phys.* **53** (2005) 793–827, arXiv:hep-th/0502050.

[8] K. Skenderis and M. Taylor, "The fuzzball proposal for black holes," *Phys. Rept.* **467** (2008) 117–171, arXiv:0804.0552 [hep-th].

[9] S. D. Mathur, "The information paradox: A pedagogical introduction," *Class. Quant. Grav.* **26** (2009) 224001, arXiv:0909.1038 [hep-th].

[10] I. Bena, E. J. Martinec, S. D. Mathur, and N. P. Warner, "Snowmass White Paper: Micro- and Macro-Structure of Black Holes," arXiv:2203.04981 [hep-th].

[11] I. Bena, E. J. Martinec, S. D. Mathur, and N. P. Warner, "Fuzzballs and Microstate Geometries: Black-Hole Structure in String Theory," arXiv:2204.13113 [hep-th].

[12] S. G. Avery, B. D. Chowdhury, and S. D. Mathur, "Emission from the D1D5 CFT," *JHEP* **10** (2009) 065, arXiv:0906.2015 [hep-th].

[13] I. Bena and N. P. Warner, "Black holes, black rings and their microstates," *Lect. Notes Phys.* **755** (2008) 1–92, arXiv:hep-th/0701216.

[14] N. P. Warner, "Lectures on Microstate Geometries," arXiv:1912.13108 [hep-th].

[15] P. Heidmann, *Black-Hole Microstates in String Theory: Black is the Color but Smooth are the Geometries?* PhD thesis, Orsay, 2019.

[16] Y. Li, "Black holes and the swampland: the deep throat revelations," *JHEP* **06** (2021) 065, arXiv:2102.04480 [hep-th].

[17] Y. Li, "An Alliance in the Tripartite Conflict over Moduli Space," arXiv:2112.03281 [hep-th].

[18] I. Bah, I. Bena, P. Heidmann, Y. Li, and D. R. Mayerson, "Gravitational Footprints of Black Holes and Their Microstate Geometries," arXiv:2104.10686 [hep-th].

[19] N. Ceplak, S. Hampton, and Y. Li, "A Helix Down the Throat: Internal Tidal Effects," arXiv:2106.03841 [hep-th].

[20] I. Bena, N. Ceplak, S. Hampton, Y. Li, D. Toulikas, and N. P. Warner, "Resolving Black-Hole Microstructure with New Momentum Carriers," arXiv:2202.08844 [hep-th].

[21] J. D. Bekenstein, "Generalized second law of thermodynamics in black hole physics," *Phys. Rev.* **D9** (1974) 3292–3300.

[22] S. W. Hawking, "Breakdown of Predictability in Gravitational Collapse," *Phys. Rev.* **D14** (1976) 2460–2473.

[23] S. W. Hawking, "The Unpredictability of Quantum Gravity," *Commun. Math. Phys.* **87** (1982) 395.

[24] A. Almheiri, T. Hartman, J. Maldacena, E. Shaghoulian, and A. Tajdini, "The entropy of Hawking radiation," arXiv:2006.06872 [hep-th].

[25] D. N. Page, "Information in black hole radiation," *Phys. Rev. Lett.* **71** (1993) 3743–3746, arXiv:hep-th/9306083.

[26] D. N. Page, "Time Dependence of Hawking Radiation Entropy," *JCAP* **1309** (2013) 028, arXiv:1301.4995 [hep-th].

[27] A. Sen, "Extremal black holes and elementary string states," *Mod. Phys. Lett.* **A10** (1995) 2081–2094, arXiv:hep-th/9504147.

[28] A. Strominger and C. Vafa, "Microscopic Origin of the Bekenstein-Hawking Entropy," *Phys. Lett.* **B379** (1996) 99–104, arXiv:hep-th/9601029.

[29] S. R. Das and S. D. Mathur, "Excitations of D-strings, Entropy and Duality," *Phys. Lett.* **B375** (1996) 103–110, arXiv:hep-th/9601152.

[30] J. M. Maldacena and L. Susskind, "D-branes and Fat Black Holes," *Nucl. Phys.* **B475** (1996) 679–690, arXiv:hep-th/9604042.

[31] E. J. Martinec, S. Massai, and D. Turton, "Little Strings, Long Strings, and Fuzzballs," *JHEP* **11** (2019) 019, arXiv:1906.11473 [hep-th].

[32] N. Seiberg, "New theories in six-dimensions and matrix description of M theory on T**5 and T**5 / Z(2)," *Phys. Lett. B* **408** (1997) 98–104, arXiv:hep-th/9705221.

[33] D. Kutasov, "Introduction to little string theory," *ICTP Lect. Notes Ser.* **7** (2002) 165–209.

[34] I. Bena and P. Kraus, "Three Charge Supertubes and Black Hole Hair," *Phys. Rev.* **D70** (2004) 046003, arXiv:hep-th/0402144.

[35] S. D. Mathur, "Tunneling into fuzzball states," *Gen. Rel. Grav.* **42** (2010) 113–118, arXiv:0805.3716 [hep-th].

[36] P. Kraus and S. D. Mathur, "Nature abhors a horizon," *Int. J. Mod. Phys. D* **24** no. 12, (2015) 1543003, arXiv:1505.05078 [hep-th].

[37] I. Bena, D. R. Mayerson, A. Puhm, and B. Vercnocke, "Tunneling into Microstate Geometries: Quantum Effects Stop Gravitational Collapse," *JHEP* **07** (2016) 031, arXiv:1512.05376 [hep-th].

[38] A. Almheiri, D. Marolf, J. Polchinski, and J. Sully, "Black Holes: Complementarity or Firewalls?," *JHEP* **1302** (2013) 062, arXiv:1207.3123 [hep-th].

[39] I. Bena and N. P. Warner, "Resolving the Structure of Black Holes: Philosophizing with a Hammer," arXiv:1311.4538 [hep-th].

[40] I. Bena and N. P. Warner, "Bubbling supertubes and foaming black holes," *Phys. Rev.* **D74** (2006) 066001, arXiv:hep-th/0505166.

[41] I. Bena, C.-W. Wang, and N. P. Warner, "The foaming three-charge black hole," *Phys. Rev.* **D75** (2007) 124026, arXiv:hep-th/0604110.

[42] J. Breckenridge, R. C. Myers, A. Peet, and C. Vafa, "D-branes and spinning black holes," *Phys.Lett.* **B391** (1997) 93–98, arXiv:hep-th/9602065 [hep-th].

[43] I. Bena, C.-W. Wang, and N. P. Warner, "Mergers and Typical Black Hole Microstates," *JHEP* **11** (2006) 042, arXiv:hep-th/0608217.

[44] B. Bates and F. Denef, "Exact solutions for supersymmetric stationary black hole composites," *JHEP* **1111** (2011) 127, arXiv:hep-th/0304094 [hep-th].

[45] K. Behrndt, D. Lust, and W. A. Sabra, "Stationary solutions of N=2 supergravity," *Nucl. Phys. B* **510** (1998) 264–288, arXiv:hep-th/9705169.

[46] F. Denef, "Supergravity flows and D-brane stability," *JHEP* **0008** (2000) 050, arXiv:hep-th/0005049 [hep-th].

[47] D. Mateos and P. K. Townsend, "Supertubes," *Phys. Rev. Lett.* **87** (2001) 011602, arXiv:hep-th/0103030.

[48] R. Emparan, D. Mateos, and P. K. Townsend, "Supergravity supertubes," *JHEP* **07** (2001) 011, arXiv:hep-th/0106012.

[49] I. Bena, J. de Boer, M. Shigemori, and N. P. Warner, "Double, Double Supertube Bubble," *JHEP* **10** (2011) 116, arXiv:1107.2650 [hep-th].

[50] I. Bena, S. Giusto, R. Russo, M. Shigemori, and N. P. Warner, "Habemus Superstratum! A constructive proof of the existence of superstrata," *JHEP* **05** (2015) 110, arXiv:1503.01463 [hep-th].

[51] I. Bena, S. Giusto, E. J. Martinec, R. Russo, M. Shigemori, D. Turton, and N. P. Warner, "Smooth horizonless geometries deep inside the black-hole regime," *Phys. Rev. Lett.* **117** no. 20, (2016) 201601, arXiv:1607.03908 [hep-th].

[52] I. Bena, S. Giusto, E. J. Martinec, R. Russo, M. Shigemori, D. Turton, and N. P. Warner, "Asymptotically-flat supergravity solutions deep inside the black-hole regime," *JHEP* **02** (2018) 014, arXiv:1711.10474 [hep-th].

[53] M. Shigemori, "Superstrata," *Gen. Rel. Grav.* **52** no. 5, (2020) 51, arXiv:2002.01592 [hep-th].

[54] I. Bena, M. Shigemori, and N. P. Warner, "Black-Hole Entropy from Supergravity Superstrata States," *JHEP* **1410** (2014) 140, arXiv:1406.4506 [hep-th].

[55] M. Shigemori, "Counting Superstrata," *JHEP* **10** (2019) 017, arXiv:1907.03878 [hep-th].

[56] D. R. Mayerson and M. Shigemori, "Counting D1-D5-P microstates in supergravity," *SciPost Phys.* **10** no. 1, (2021) 018, arXiv:2010.04172 [hep-th].

[57] D. Bufalini, S. Iguri, N. Kovensky, and D. Turton, "Worldsheet Correlators in Black Hole Microstates," arXiv:2203.13828 [hep-th].

[58] R. J. Glauber, "Coherent and incoherent states of the radiation field," *Phys. Rev.* **131** (1963) 2766–2788.

[59] O. Lunin and S. D. Mathur, "AdS/CFT duality and the black hole information paradox," *Nucl. Phys.* **B623** (2002) 342–394, arXiv:hep-th/0109154.

[60] O. Lunin, J. M. Maldacena, and L. Maoz, "Gravity solutions for the D1-D5 system with angular momentum," arXiv:hep-th/0212210.

[61] M. Taylor, "General 2 charge geometries," *JHEP* **03** (2006) 009, arXiv:hep-th/0507223.

[62] I. Kanitscheider, K. Skenderis, and M. Taylor, "Fuzzballs with internal excitations," *JHEP* **06** (2007) 056, arXiv:0704.0690 [hep-th].

[63] S. Raju and P. Shrivastava, "A Critique of the Fuzzball Program," arXiv:1804.10616 [hep-th].

[64] J. de Boer, S. El-Showk, I. Messamah, and D. Van den Bleeken, "Quantizing N=2 Multicenter Solutions," *JHEP* **05** (2009) 002, arXiv:0807.4556 [hep-th].

[65] I. Bena, A. Puhm, O. Vasilakis, and N. P. Warner, "Almost BPS but still not renormalized," *JHEP* **1309** (2013) 062, arXiv:1303.0841 [hep-th].

[66] I. Bena, G. Dall'Agata, S. Giusto, C. Ruef, and N. P. Warner, "Non-BPS Black Rings and Black Holes in Taub-NUT," *JHEP* **06** (2009) 015, arXiv:0902.4526 [hep-th].

[67] I. Bena, S. Giusto, C. Ruef, and N. P. Warner, "Multi-Center non-BPS Black Holes - the Solution," *JHEP* **11** (2009) 032, arXiv:0908.2121 [hep-th].

[68] I. Bena, P. Heidmann, and D. Turton, "AdS_2 holography: mind the cap," *JHEP* **12** (2018) 028, arXiv:1806.02834 [hep-th].

[69] H. Ooguri and C. Vafa, "On the Geometry of the String Landscape and the Swampland," *Nucl. Phys. B* **766** (2007) 21–33, arXiv:hep-th/0605264.

[70] T. W. Grimm, E. Palti, and I. Valenzuela, "Infinite Distances in Field Space and Massless Towers of States," *JHEP* **08** (2018) 143, arXiv:1802.08264 [hep-th].

[71] D. Lüst, E. Palti, and C. Vafa, "AdS and the Swampland," *Phys. Lett. B* **797** (2019) 134867, arXiv:1906.05225 [hep-th].

[72] B. S. DeWitt, "Quantum Theory of Gravity. 1. The Canonical Theory," *Phys. Rev.* **160** (1967) 1113–1148.

[73] P. Candelas and X. de la Ossa, "Moduli Space of Calabi-Yau Manifolds," *Nucl. Phys. B* **355** (1991) 455–481.

[74] Q. Bonnefoy, L. Ciambelli, D. Lüst, and S. Lüst, "Infinite Black Hole Entropies at Infinite Distances and Tower of States," *Nucl. Phys. B* **958** (2020) 115112, arXiv:1912.07453 [hep-th].

[75] E. Witten, "Interacting Field Theory of Open Superstrings," *Nucl. Phys. B* **276** (1986) 291–324.

[76] C. Crnkovic, "Symplectic Geometry of the Covariant Phase Space, Superstrings and Superspace," *Class. Quant. Grav.* **5** (1988) 1557–1575.

[77] J. B. Gutowski and H. S. Reall, "General supersymmetric AdS(5) black holes," *JHEP* **04** (2004) 048, arXiv:hep-th/0401129.

[78] I. Bena and N. P. Warner, "One ring to rule them all ... and in the darkness bind them?," *Adv. Theor. Math. Phys.* **9** (2005) 667–701, arXiv:hep-th/0408106.

[79] P. Berglund, E. G. Gimon, and T. S. Levi, "Supergravity microstates for BPS black holes and black rings," *JHEP* **0606** (2006) 007, arXiv:hep-th/0505167 [hep-th].

[80] I. Bena, C.-W. Wang, and N. P. Warner, "Plumbing the Abyss: Black Ring Microstates," *JHEP* **07** (2008) 019, arXiv:0706.3786 [hep-th].

[81] J. Michelson and A. Strominger, "Superconformal multiblack hole quantum mechanics," *JHEP* **09** (1999) 005, arXiv:hep-th/9908044 [hep-th].

[82] F. Denef, "Quantum quivers and Hall / hole halos," *JHEP* **0210** (2002) 023, arXiv:hep-th/0206072 [hep-th].

[83] M. Abreu, "Kahler geometry of toric manifolds in symplectic coordinates," *arXiv Mathematics e-prints* (Apr, 2000) math/0004122, arXiv:math/0004122 [math.DG].

[84] V. Guillemin, "Kaehler structures on toric varieties," *J. Differential Geom.* **40** no. 2, (1994) 285–309. https://doi.org/10.4310/jdg/1214455538.

[85] S.-J. Lee, W. Lerche, and T. Weigand, "Tensionless Strings and the Weak Gravity Conjecture," *JHEP* **10** (2018) 164, arXiv:1808.05958 [hep-th].

[86] D. Klaewer and E. Palti, "Super-Planckian Spatial Field Variations and Quantum Gravity," *JHEP* **01** (2017) 088, arXiv:1610.00010 [hep-th].

[87] N. Gendler and I. Valenzuela, "Merging the Weak Gravity and Distance Conjectures Using BPS Extremal Black Holes," arXiv:2004.10768 [hep-th].

[88] D. Andriot, N. Cribiori, and D. Erkinger, "The web of swampland conjectures and the TCC bound," *JHEP* **07** (2020) 162, arXiv:2004.00030 [hep-th].

[89] E. J. Martinec and B. E. Niehoff, "Hair-brane Ideas on the Horizon," *JHEP* **11** (2015) 195, arXiv:1509.00044 [hep-th].

[90] E. J. Martinec and S. Massai, "String Theory of Supertubes," *JHEP* **07** (2018) 163, arXiv:1705.10844 [hep-th].

[91] E. J. Martinec, S. Massai, and D. Turton, "String dynamics in NS5-F1-P geometries," *JHEP* **09** (2018) 031, arXiv:1803.08505 [hep-th].

[92] E. J. Martinec, S. Massai, and D. Turton, "Stringy Structure at the BPS Bound," arXiv:2005.12344 [hep-th].

[93] S. Giusto, S. D. Mathur, and A. Saxena, "Dual geometries for a set of 3-charge microstates," *Nucl. Phys.* **B701** (2004) 357–379, arXiv:hep-th/0405017.

[94] S. Giusto, S. D. Mathur, and A. Saxena, "3-charge geometries and their CFT duals," *Nucl. Phys.* **B710** (2005) 425–463, arXiv:hep-th/0406103.

[95] S. Giusto and S. D. Mathur, "Geometry of D1-D5-P bound states," *Nucl. Phys.* **B729** (2005) 203–220, arXiv:hep-th/0409067.

[96] S. Giusto, O. Lunin, S. D. Mathur, and D. Turton, "D1-D5-P microstates at the cap," *JHEP* **1302** (2013) 050, arXiv:1211.0306 [hep-th].

[97] W. G. Ritter, "Geometric quantization," arXiv:math-ph/0208008.

[98] A. Echeverria-Enriquez, M. C. Munoz-Lecanda, N. Roman-Roy, and C. Victoria-Monge, "Mathematical foundations of geometric quantization," *Extracta Math.* **13** (1998) 135–238, arXiv:math-ph/9904008.

[99] D. S. Berman and G. Cardoso, "Geometric Quantization: Particles, Fields and Strings," arXiv:2201.00349 [hep-th].

[100] L. Maoz and V. S. Rychkov, "Geometry quantization from supergravity: The Case of 'Bubbling AdS'," *JHEP* **08** (2005) 096, arXiv:hep-th/0508059.

[101] V. S. Rychkov, "D1-D5 black hole microstate counting from supergravity," *JHEP* **01** (2006) 063, arXiv:hep-th/0512053.

[102] R. C. Ferrell and D. M. Eardley, "Slow motion scattering and coalescence of maximally charged black holes," *Phys. Rev. Lett.* **59** (1987) 1617.

[103] N. Manton, "A remark on the scattering of bps monopoles," *Physics Letters B* **110** no. 1, (1982) 54–56. https://www.sciencedirect.com/science/article/pii/0370269382909509.

[104] M. R. Douglas, J. Polchinski, and A. Strominger, "Probing five-dimensional black holes with D-branes," *JHEP* **12** (1997) 003, arXiv:hep-th/9703031.

[105] D. M. Kaplan and J. Michelson, "Scattering of several multiply charged extremal D = 5 black holes," *Phys. Lett. B* **410** (1997) 125–130, arXiv:hep-th/9707021.

[106] J. Michelson, "Scattering of four-dimensional black holes," *Phys. Rev. D* **57** (1998) 1092–1097, arXiv:hep-th/9708091.

[107] O. Gil-Medrano and P. W. Michor, "The riemannian manifold of all riemannian metrics," 1992.

[108] F. Baume and E. Palti, "Backreacted Axion Field Ranges in String Theory," *JHEP* **08** (2016) 043, arXiv:1602.06517 [hep-th].

[109] J. M. Maldacena, J. Michelson, and A. Strominger, "Anti-de Sitter fragmentation," *JHEP* **02** (1999) 011, arXiv:hep-th/9812073 [hep-th].

[110] **LIGO Scientific, Virgo** , B. P. Abbott *et al.*, "Observation of Gravitational Waves from a Binary Black Hole Merger," *Phys. Rev. Lett.* **116** no. 6, (2016) 061102, arXiv:1602.03837 [gr-qc].

[111] **LIGO Scientific** , B. P. Abbott *et al.*, "LIGO: The Laser interferometer gravitational-wave observatory," *Rept. Prog. Phys.* **72** (2009) 076901, arXiv:0711.3041 [gr-qc].

[112] EHT Collaboration, "First M87 Event Horizon Telescope Results. I. The Shadow of the Supermassive Black Hole," *ApJL* **875** no. 1, (Apr., 2019) L1.

[113] **LISA** , P. Amaro-Seoane *et al.*, "Laser Interferometer Space Antenna," arXiv:1702.00786 [astro-ph.IM].

[114] M. Punturo *et al.*, "The Einstein Telescope: A third-generation gravitational wave observatory," *Class. Quant. Grav.* **27** (2010) 194002.

[115] K. Goldstein and S. Katmadas, "Almost BPS black holes," *JHEP* **05** (2009) 058, arXiv:0812.4183 [hep-th].

[116] G. Dall'Agata, S. Giusto, and C. Ruef, "U-duality and non-BPS solutions," *JHEP* **02** (2011) 074, arXiv:1012.4803 [hep-th].

[117] O. Vasilakis and N. P. Warner, "Mind the Gap: Supersymmetry Breaking in Scaling, Microstate Geometries," *JHEP* **1110** (2011) 006, arXiv:1104.2641 [hep-th].

[118] I. Bena and D. R. Mayerson, "Multipole Ratios: A New Window into Black Holes," *Phys. Rev. Lett.* **125** no. 22, (2020) 22, arXiv:2006.10750 [hep-th].

[119] M. Bianchi, D. Consoli, A. Grillo, J. F. Morales, P. Pani, and G. Raposo, "Distinguishing fuzzballs from black holes through their multipolar structure," *Phys. Rev. Lett.* **125** no. 22, (2020) 221601, arXiv:2007.01743 [hep-th].

[120] I. Bena and D. R. Mayerson, "Black Holes Lessons from Multipole Ratios," *JHEP* **03** (2021) 114, arXiv:2007.09152 [hep-th].

[121] M. Bianchi, D. Consoli, A. Grillo, J. F. Morales, P. Pani, and G. Raposo, "The multipolar structure of fuzzballs," *JHEP* **01** (2021) 003, arXiv:2008.01445 [hep-th].

[122] D. R. Mayerson, "Fuzzballs and Observations," *Gen. Rel. Grav.* **52** no. 12, (2020) 115, arXiv:2010.09736 [hep-th].

[123] V. Cardoso and P. Pani, "The observational evidence for horizons: from echoes to precision gravitational-wave physics," arXiv:1707.03021 [gr-qc].

[124] V. Cardoso and P. Pani, "Testing the nature of dark compact objects: a status report," *Living Rev. Rel.* **22** no. 1, (2019) 4, arXiv:1904.05363 [gr-qc].

[125] H. A. Buchdahl, "General Relativistic Fluid Spheres," *Phys. Rev.* **116** (1959) 1027.

[126] V. Dimitrov, T. Lemmens, D. R. Mayerson, V. S. Min, and B. Vercnocke, "Gravitational Waves, Holography, and Black Hole Microstates," arXiv:2007.01879 [hep-th].

[127] G. Bossard, "Octonionic black holes," *JHEP* **05** (2012) 113, arXiv:1203.0530 [hep-th].

[128] G. Bossard and C. Ruef, "Interacting non-BPS black holes," *Gen. Rel. Grav.* **44** (2012) 21–66, arXiv:1106.5806 [hep-th].

[129] G. Bossard and S. Katmadas, "Duality covariant non-BPS first order systems," *JHEP* **09** (2012) 100, arXiv:1205.5461 [hep-th].

[130] E. Cremmer, C. Kounnas, A. Van Proeyen, J. P. Derendinger, S. Ferrara, B. de Wit, and L. Girardello, "Vector Multiplets Coupled to N=2 Supergravity: SuperHiggs Effect, Flat Potentials and Geometric Structure," *Nucl. Phys. B* **250** (1985) 385–426.

[131] M. J. Duff, J. T. Liu, and J. Rahmfeld, "Four-dimensional string-string-string triality," *Nucl. Phys. B* **459** (1996) 125–159, arXiv:hep-th/9508094.

[132] D. D. K. Chow and G. Compère, "Black holes in N=8 supergravity from SO(4,4) hidden symmetries," *Phys. Rev. D* **90** no. 2, (2014) 025029, arXiv:1404.2602 [hep-th].

[133] K. S. Thorne, "Multipole Expansions of Gravitational Radiation," *Rev. Mod. Phys.* **52** (1980) 299–339.

[134] V. Cardoso, C. F. B. Macedo, P. Pani, and V. Ferrari, "Black holes and gravitational waves in models of minicharged dark matter," *JCAP* **05** (2016) 054, arXiv:1604.07845 [hep-ph]. [Erratum: JCAP 04, E01 (2020)].

[135] B. Ripperda, J. Davelaar, H. Olivares, D. R. Mayerson, F. Bacchini, B. Vercnocke, and T. Hertog, "Can we detect signatures of dark matter and hidden dimensions in black-hole shadows?," 2021. in preparation.

[136] G. Bozzola and V. Paschalidis, "General relativistic simulations of the quasi-circular inspiral and merger of charged black holes: Gw150914 and fundamental physics implications," 2020.

[137] T. P. Sotiriou and T. A. Apostolatos, "Corrected multipole moments of axisymmetric electrovacuum spacetimes," *Class. Quant. Grav.* **21** (2004) 5727–5733, arXiv:gr-qc/0407064.

[138] S. Babak, J. Gair, A. Sesana, E. Barausse, C. F. Sopuerta, C. P. L. Berry, E. Berti, P. Amaro-Seoane, A. Petiteau, and A. Klein, "Science with the space-based interferometer LISA. V: Extreme mass-ratio inspirals," *Phys. Rev. D* **95** no. 10, (2017) 103012, arXiv:1703.09722 [gr-qc].

[139] L. Barack and C. Cutler, "Using LISA EMRI sources to test off-Kerr deviations in the geometry of massive black holes," *Phys. Rev. D* **75** (2007) 042003, arXiv:gr-qc/0612029.

[140] J. R. Gair, M. Vallisneri, S. L. Larson, and J. G. Baker, "Testing General Relativity with Low-Frequency, Space-Based Gravitational-Wave Detectors," *Living Rev. Rel.* **16** (2013) 7, arXiv:1212.5575 [gr-qc].

[141] E. Barausse *et al.*, "Prospects for Fundamental Physics with LISA," *Gen. Rel. Grav.* **52** no. 8, (2020) 81, arXiv:2001.09793 [gr-qc].

[142] P. V. P. Cunha, C. A. R. Herdeiro, and E. Radu, "Isolated black holes without $\mathbb{Z}_2$ isometry," *Phys. Rev. D* **98** no. 10, (2018) 104060, arXiv:1808.06692 [gr-qc].

[143] G. Raposo, P. Pani, and R. Emparan, "Exotic compact objects with soft hair," *Phys. Rev. D* **99** no. 10, (2019) 104050, arXiv:1812.07615 [gr-qc].

[144] H. C. D. L. Junior, L. C. B. Crispino, P. V. P. Cunha, and C. A. R. Herdeiro, "Mistaken identity: can different black holes cast the same shadow?," arXiv:2102.07034 [gr-qc].

[145] C.-Y. Chen, "Rotating black holes without $\mathbb{Z}_2$ symmetry and their shadow images," *JCAP* **05** (2020) 040, arXiv:2004.01440 [gr-qc].

[146] I. Bena, N. Bobev, C. Ruef, and N. P. Warner, "Supertubes in Bubbling Backgrounds: Born-Infeld Meets Supergravity," *JHEP* **07** (2009) 106, arXiv:0812.2942 [hep-th].

[147] I. Bena, N. Bobev, and N. P. Warner, "Spectral Flow, and the Spectrum of Multi-Center Solutions," *Phys. Rev.* **D77** (2008) 125025, arXiv:0803.1203 [hep-th].

[148] I. Bena, S. Giusto, C. Ruef, and N. P. Warner, "Supergravity Solutions from Floating Branes," *JHEP* **03** (2010) 047, arXiv:0910.1860 [hep-th].

[149] K. Fransen and D. R. Mayerson, "On Detecting Equatorial Symmetry Breaking with LISA," arXiv:2201.03569 [gr-qc].

[150] F. Bacchini, D. R. Mayerson, B. Ripperda, J. Davelaar, H. Olivares, T. Hertog, and B. Vercnocke, "Fuzzball Shadows: Emergent Horizons from Microstructure," arXiv:2103.12075 [hep-th].

[151] T. Ikeda, M. Bianchi, D. Consoli, A. Grillo, J. F. Morales, P. Pani, and G. Raposo, "Black-hole microstate spectroscopy: ringdown, quasinormal modes, and echoes," arXiv:2103.10960 [gr-qc].

[152] J. M. Maldacena, "The large N limit of superconformal field theories and supergravity," *Adv. Theor. Math. Phys.* **2** (1998) 231–252, arXiv:hep-th/9711200.

[153] N. Čeplak, R. Russo, and M. Shigemori, "Supercharging Superstrata," *JHEP* **03** (2019) 095, arXiv:1812.08761 [hep-th].

[154] P. Heidmann and N. P. Warner, "Superstratum Symbiosis," *JHEP* **09** (2019) 059, arXiv:1903.07631 [hep-th].

[155] P. Heidmann, D. R. Mayerson, R. Walker, and N. P. Warner, "Holomorphic Waves of Black Hole Microstructure," *JHEP* **02** (2020) 192, arXiv:1910.10714 [hep-th].

[156] D. R. Mayerson, R. A. Walker, and N. P. Warner, "Microstate Geometries from Gauged Supergravity in Three Dimensions," *JHEP* **10** (2020) 030, arXiv:2004.13031 [hep-th].

[157] A. Houppe and N. P. Warner, "Supersymmetry and Superstrata in Three Dimensions," arXiv:2012.07850 [hep-th].

[158] A. Tyukov, R. Walker, and N. P. Warner, "Tidal Stresses and Energy Gaps in Microstate Geometries," *JHEP* **02** (2018) 122, arXiv:1710.09006 [hep-th].

[159] I. Bena, E. J. Martinec, R. Walker, and N. P. Warner, "Early Scrambling and Capped BTZ Geometries," *JHEP* **04** (2019) 126, arXiv:1812.05110 [hep-th].

[160] I. Bena, A. Houppe, and N. P. Warner, "Delaying the Inevitable: Tidal Disruption in Microstate Geometries," *JHEP* **02** (2021) 103, arXiv:2006.13939 [hep-th].

[161] I. Bena, P. Heidmann, R. Monten, and N. P. Warner, "Thermal Decay without Information Loss in Horizonless Microstate Geometries," *SciPost Phys.* **7** no. 5, (2019) 063, arXiv:1905.05194 [hep-th].

[162] I. Bena, F. Eperon, P. Heidmann, and N. P. Warner, "The Great Escape: Tunneling out of Microstate Geometries," *JHEP* **04** (2021) 112, arXiv:2005.11323 [hep-th].

[163] E. J. Martinec and N. P. Warner, "The Harder They Fall, the Bigger They Become: Tidal Trapping of Strings by Microstate Geometries," *JHEP* **04** (2021) 259, arXiv:2009.07847 [hep-th].

[164] S. G. Avery, "Using the D1D5 CFT to Understand Black Holes," arXiv:1012.0072 [hep-th].

[165] B. Guo and S. Hampton, "A freely falling graviton in the D1D5 CFT," arXiv:2107.11883 [hep-th].

[166] B. Guo and S. Hampton, "The Dual of a Tidal Force in the D1D5 CFT," arXiv:2108.00068 [hep-th].

[167] M. Blau, J. M. Figueroa-O'Farrill, and G. Papadopoulos, "Penrose limits, supergravity and brane dynamics," *Class. Quant. Grav.* **19** (2002) 4753, arXiv:hep-th/0202111.

[168] I. Bena, D. Turton, R. Walker, and N. P. Warner, "Integrability and Black-Hole Microstate Geometries," *JHEP* **11** (2017) 021, arXiv:1709.01107 [hep-th].

[169] S. Rawash and D. Turton, "Supercharged AdS_3 Holography," arXiv:2105.13046 [hep-th].

[170] S. G. Avery, B. D. Chowdhury, and S. D. Mathur, "Deforming the D1D5 CFT away from the orbifold point," *JHEP* **06** (2010) 031, arXiv:1002.3132 [hep-th].

[171] S. G. Avery, B. D. Chowdhury, and S. D. Mathur, "Excitations in the deformed D1D5 CFT," *JHEP* **06** (2010) 032, arXiv:1003.2746 [hep-th].

[172] Z. Carson, S. Hampton, S. D. Mathur, and D. Turton, "Effect of the twist operator in the D1D5 CFT," *JHEP* **1408** (2014) 064, arXiv:1405.0259 [hep-th].

[173] Z. Carson, S. Hampton, S. D. Mathur, and D. Turton, "Effect of the deformation operator in the D1D5 CFT," *JHEP* **01** (2015) 071, arXiv:1410.4543 [hep-th].

[174] Z. Carson, S. D. Mathur, and D. Turton, "Bogoliubov coefficients for the twist operator in the D1D5 CFT," *Nucl.Phys.* **B889** (2014) 443–485, arXiv:1406.6977 [hep-th].

[175] J. R. David, G. Mandal, and S. R. Wadia, "Microscopic formulation of black holes in string theory," *Phys. Rept.* **369** (2002) 549–686, arXiv:hep-th/0203048.

[176] G. T. Horowitz and J. Polchinski, "A correspondence principle for black holes and strings," *Phys. Rev.* **D55** (1997) 6189–6197, arXiv:hep-th/9612146.

[177] T. Damour and G. Veneziano, "Selfgravitating fundamental strings and black holes," *Nucl. Phys.* **B568** (2000) 93–119, arXiv:hep-th/9907030 [hep-th].

[178] Y. Chen, J. Maldacena, and E. Witten, "On the black hole/string transition," arXiv:2109.08563 [hep-th].

[179] G. Gibbons and N. Warner, "Global structure of five-dimensional fuzzballs," *Class.Quant.Grav.* **31** (2014) 025016, arXiv:1305.0957 [hep-th].

[180] S. D. Mathur, "Fuzzballs and the information paradox: A Summary and conjectures," arXiv:0810.4525 [hep-th].

[181] I. Bena, E. Martinec, D. Turton, and N. P. Warner, "M-theory Superstrata and the MSW String," *JHEP* **06** (2017) 137, arXiv:1703.10171 [hep-th].

[182] S. Giusto, M. R. Hughes, and R. Russo, "The Regge limit of AdS_3 holographic correlators," arXiv:2007.12118 [hep-th].

[183] N. Ceplak and M. R. R. Hughes, "The Regge limit of AdS_3 holographic correlators with heavy states: towards the black hole regime," *JHEP* **07** (2021) 021, arXiv:2102.09549 [hep-th].

[184] B. Ganchev, A. Houppe, and N. Warner, "Q-Balls Meet Fuzzballs: Non-BPS Microstate Geometries," arXiv:2107.09677 [hep-th].

[185] B. Ganchev, A. Houppe, and N. P. Warner, "New Superstrata from Three-Dimensional Supergravity," arXiv:2110.02961 [hep-th].

[186] I. Kanitscheider, K. Skenderis, and M. Taylor, "Holographic anatomy of fuzzballs," *JHEP* **04** (2007) 023, arXiv:hep-th/0611171.

[187] M. Taylor, "Matching of correlators in AdS(3) / CFT(2)," *JHEP* **06** (2008) 010, arXiv:0709.1838 [hep-th].

[188] S. Giusto, E. Moscato, and R. Russo, "AdS_3 holography for 1/4 and 1/8 BPS geometries," *JHEP* **11** (2015) 004, arXiv:1507.00945 [hep-th].

[189] A. Bombini, A. Galliani, S. Giusto, E. Moscato, and R. Russo, "Unitary 4-point correlators from classical geometries," arXiv:1710.06820 [hep-th].

[190] S. Giusto, S. Rawash, and D. Turton, "Ads_3 holography at dimension two," *JHEP* **07** (2019) 171, arXiv:1904.12880 [hep-th].

[191] J. Garcia i Tormo and M. Taylor, "One point functions for black hole microstates," *Gen. Rel. Grav.* **51** no. 7, (2019) 89, arXiv:1904.10200 [hep-th].

[192] B. Ganchev, S. Giusto, A. Houppe, and R. Russo, "AdS_3 holography for non-BPS geometries," arXiv:2112.03287 [hep-th].

[193] O. Lunin and S. D. Mathur, "Metric of the multiply wound rotating string," *Nucl. Phys.* **B610** (2001) 49–76, arXiv:hep-th/0105136.

[194] F. Chen, B. Michel, J. Polchinski, and A. Puhm, "Journey to the Center of the Fuzzball," *JHEP* **02** (2015) 081, arXiv:1408.4798 [hep-th].

[195] B. E. Niehoff and N. P. Warner, "Doubly-Fluctuating BPS Solutions in Six Dimensions," *JHEP* **1310** (2013) 137, arXiv:1303.5449 [hep-th].

[196] C. G. Callan, J. M. Maldacena, and A. W. Peet, "Extremal Black Holes As Fundamental Strings," *Nucl. Phys.* **B475** (1996) 645–678, arXiv:hep-th/9510134.

[197] A. Dabholkar, J. P. Gauntlett, J. A. Harvey, and D. Waldram, "Strings as Solitons & Black Holes as Strings," *Nucl. Phys.* **B474** (1996) 85–121, arXiv:hep-th/9511053.

[198] E. Bergshoeff, R. Kallosh, T. Ortin, D. Roest, and A. Van Proeyen, "New formulations of D = 10 supersymmetry and D8 - O8 domain walls," *Class. Quant. Grav.* **18** (2001) 3359–3382, arXiv:hep-th/0103233 [hep-th].

[199] S. Giusto, L. Martucci, M. Petrini, and R. Russo, "6D microstate geometries from 10D structures," *Nucl.Phys.* **B876** (2013) 509–555, arXiv:1306.1745 [hep-th].

[200] G. W. Gibbons and S. W. Hawking, "Gravitational Multi - Instantons," *Phys. Lett. B* **78** (1978) 430.

[201] A. A. Tseytlin, "Harmonic superpositions of M-branes," *Nucl. Phys. B* **475** (1996) 149–163, arXiv:hep-th/9604035.

[202] R. C. Myers and M. Perry, "Black Holes in Higher Dimensional Space-Times," *Annals Phys.* **172** (1986) 304.

[203] D. Bufalini, S. Iguri, N. Kovensky, and D. Turton, "Black hole microstates from the worldsheet," *JHEP* **08** (2021) 011, arXiv:2105.02255 [hep-th].

[204] I. Bena, S. F. Ross, and N. P. Warner, "On the Oscillation of Species," *JHEP* **1409** (2014) 113, arXiv:1312.3635 [hep-th].

[205] F. C. Eperon, H. S. Reall, and J. E. Santos, "Instability of supersymmetric microstate geometries," *JHEP* **10** (2016) 031, arXiv:1607.06828 [hep-th].

[206] D. Marolf, B. Michel, and A. Puhm, "A rough end for smooth microstate geometries," *JHEP* **05** (2017) 021, arXiv:1612.05235 [hep-th].

[207] E. J. Martinec, "AdS3's with and without BTZ's," arXiv:2109.11716 [hep-th].

[208] J. de Boer, F. Denef, S. El-Showk, I. Messamah, and D. Van den Bleeken, "Black hole bound states in AdS3 x S2," *JHEP* **11** (2008) 050, arXiv:0802.2257 [hep-th].

[209] M. Cariglia and O. A. P. Mac Conamhna, "The General form of supersymmetric solutions of N=(1,0) U(1) and SU(2) gauged supergravities in six-dimensions," *Class. Quant. Grav.* **21** (2004) 3171–3196, arXiv:hep-th/0402055 [hep-th].

[210] I. Bena, S. Giusto, M. Shigemori, and N. P. Warner, "Supersymmetric Solutions in Six Dimensions: A Linear Structure," *JHEP* **1203** (2012) 084, arXiv:1110.2781 [hep-th].

[211] N. Čeplak, S. Hampton, and N. P. Warner, "Linearizing the BPS Equations with Vector and Tensor Multiplets," arXiv:2204.07170 [hep-th].

[212] E. Bakhshaei and A. Bombini, "Three-charge superstrata with internal excitations," arXiv:1811.00067 [hep-th].

[213] P. Heidmann, "Non-BPS Floating Branes and Bubbling Geometries," arXiv:2112.03279 [hep-th].

[214] H. Nishino and E. Sezgin, "Matter and Gauge Couplings of N=2 Supergravity in Six-Dimensions," *Phys. Lett. B* **144** (1984) 187–192.

[215] S. Ferrara, F. Riccioni, and A. Sagnotti, "Tensor and vector multiplets in six-dimensional supergravity," *Nucl. Phys.* **B519** (1998) 115–140, arXiv:hep-th/9711059 [hep-th].

[216] J. B. Gutowski, D. Martelli, and H. S. Reall, "All supersymmetric solutions of minimal supergravity in six dimensions," *Class. Quant. Grav.* **20** (2003) 5049–5078, arXiv:hep-th/0306235.

[217] P. de Lange, D. R. Mayerson, and B. Vercnocke, "Structure of Six-Dimensional Microstate Geometries," *JHEP* **09** (2015) 075, arXiv:1504.07987 [hep-th].

[218] I. Antoniadis, S. Ferrara, and T. R. Taylor, "N=2 heterotic superstring and its dual theory in five-dimensions," *Nucl. Phys.* **B460** (1996) 489–505, arXiv:hep-th/9511108 [hep-th].

[219] M. Gunaydin, G. Sierra, and P. K. Townsend, "The Geometry of N=2 Maxwell-Einstein Supergravity and Jordan Algebras," *Nucl. Phys.* **B242** (1984) 244–268.

[220] M. Gunaydin, G. Sierra, and P. K. Townsend, "Gauging the d = 5 Maxwell-Einstein Supergravity Theories: More on Jordan Algebras," *Nucl. Phys.* **B253** (1985) 573. [,573(1984)].

[221] S. Giusto and R. Russo, "Superdescendants of the D1D5 CFT and their dual 3-charge geometries," *JHEP* **1403** (2014) 007, arXiv:1311.5536 [hep-th].

[222] T. H. Buscher, "Path Integral Derivation of Quantum Duality in Nonlinear Sigma Models," *Phys. Lett. B* **201** (1988) 466–472.

[223] T. H. Buscher, "A Symmetry of the String Background Field Equations," *Phys. Lett. B* **194** (1987) 59–62.